# PROTEOGLYCANS IN NEURULATION

By

Wai Cheong George Yip

*A thesis submitted for the degree of Doctor of Philosophy*

*University of London*

*2001*

Developmental Biology Unit

Institute of Child Health

University College London

30 Guilford Street

London

WC1N 1EH

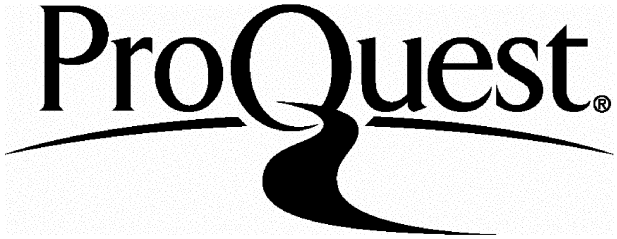

# ABSTRACT

Glycosaminoglycans are made up of repeating disaccharide subunits consisting of a hexosamine and a hexose or hexuronic acid. They occur freely or as carbohydrate side chains in proteoglycans. Although widely distributed, their importance in embryogenesis is incompletely understood. This thesis investigates their roles in neurulation and neural crest migration.

Primary neurulation occurs between E8.5 and E10.5 in the mouse embryo. Neural tube closure in the spinal region is accomplished by bending at the median hinge point and at paired dorsolateral hinge points. Histochemical and immunohistochemical studies show that sulphated glycosaminoglycans are present in the basement membrane of the closing neural tube, as well as elsewhere in the embryo.

Culturing E8.5 *CD1* mouse embryos in the presence of chlorate, a competitive inhibitor of glycosaminoglycan sulphation, suppressed median hinge point formation. This was associated with increased bending at the dorsolateral hinge points, resulting in accelerated posterior neuropore closure. Suppression of median hinge point formation was prevented by addition of heparan sulphate, but not chondroitin sulphate, de-N- or de-O-sulphated heparan sulphate, to the culture medium. This may be due to the requirement for heparan sulphate in Sonic hedgehog induction of median hinge point formation.

Chondroitin sulphate also influenced posterior neuropore closure. Chondroitinase treatment of *CD1* mouse embryos in culture retarded

closure of the neuropore, whereas exogenous chondroitin sulphate accelerated closure. However, the median and dorsolateral hinge points were unaffected. The mechanism of action of chondroitin sulphate is unknown and requires further investigation.

Besides their role in neurulation, chondroitin sulphate proteoglycans are known to inhibit cell migration. *Splotch* mouse mutants, where mutations in *Pax-3* result in deficiencies of neural crest derived structures, have been shown by *in situ* hybridisation to over-express versican mRNA. To determine whether the glycosaminoglycan component was increased, chondroitin sulphate was quantified in E9.5 *splotch* embryos photospectroscopically using a 1,9-dimethylmethylene blue binding assay. It was found that mutants contained larger amounts of chondroitin sulphate than wild type embryos. On the other hand, there was no difference in the net synthetic rate, as determined by $^{35}S$-labelling of chondroitin sulphate in cultured *splotch* embryos. This suggests that the defect may lie in the mutants' ability to degrade chondroitin sulphate, resulting in its accumulation and inhibition of neural crest migration.

These experiments underline the importance of sulphated glycosaminoglycans in mouse development and raise the possibility that these molecules may contribute to development of neural tube defects and neurocristopathies in humans.

# ACKNOWLEDGEMENTS

I would like to take this opportunity to express my heartfelt thanks to the many people who helped in the production of this thesis.

Firstly, I am very grateful to my supervisors, Andy Copp and Patrizia Ferretti, for their generosity, inspiration and guidance throughout the course of my studies in London. I would also like to thank my first supervisor, the late Peter Thorogood, who introduced me to the function of heparan sulphate in embryonic development. Although this project has taken a substantial change in direction from the one we planned initially, I am sure he would have enjoyed reading this thesis.

I would like to show my appreciation for the many past and present members of the Developmental Biology and Neural Development Units who have been very helpful and who have made my stay in London so enjoyable. I would like to specially thank Patricia Cogram for sharing her tips on embryo culture; Carlos Gaston, Jason Neil-Dwyer, Anita Petiot, Viccy Reed and Patricia Ybot-Gonzalez for showing me the various practical aspects of Molecular Biology and for sharing reagents; Rachel Moore, Paul O'Neill and Sarah Reid for practical protocols and help with microscopy and immunohistochemistry; Joe Chan for his computer expertise; and Melanie MacKay and Fang Zhang for stimulating discussions. I am also grateful to Dave Stanton for his help with the scintillating counter and Angie Wade for her expert advice on statistical data analysis.

I would like to thank the National University of Singapore for the award of an Overseas Graduate Scholarship for my studies, as well as Professors E A Ling and S K Leong, Associate Professors S S W Tay and B H Bay, and my other friends and colleagues in the Department of Anatomy, National University of Singapore for their kind support.

Last, but not least, I would like to express my deepest gratitude to my parents for their love, kindness and encouragement over the years.

Thank you very much!

# CONTENTS

# LIST OF FIGURES

# LIST OF TABLES

# ABBREVIATIONS

| | |
|---|---|
| Ab | antibody |
| AEC | 3-amino-9-ethylcarbazole |
| ANP | anterior neuropore |
| APS | adenosine 5'-phosphosulphate |
| ATP | adenosine 5'-triphosphate |
| BCA | bicinchoninic acid |
| BCIP | 5-bromo-4-chloro-3-indolyl phosphate |
| BMP | bone morphogenetic protein |
| bp | base pair |
| BSA | bovine serum albumin |
| CHO | Chinese hamster ovary |
| $ClO_3$ | chlorate |
| cm | centimetre |
| cpm | counts per minute |
| CS | chondroitin sulphate |
| CTP | cytidine 5'-triphosphate |
| DAB | 3,3'-diaminobenzidine tetrahydrochloride |
| DEPC | diethylpyrocarbonate |
| De-N-HS | de-N-sulphated heparan sulphate |
| De-O-HS | de-O-sulphated heparan sulphate |
| DePX | dextropropoxyphene |
| DIG | digoxigenin |
| DMEM | Dulbecco's modified Eagle's medium |
| DNA | deoxyribonucleic acid |
| DNase I | deoxyribonuclease I |

| | |
|---|---|
| dNTP | deoxyribonucleoside 5'-triphosphate |
| dpm | disintegrations per minute |
| DTT | dithiothreitol |
| EDTA | ethylenediaminetetraacetic acid |
| FCS | foetal calf serum |
| FGF | fibroblast growth factor |
| FGFR | fibroblast growth factor receptor |
| GAG | glycosaminoglycan |
| Gal | galactose |
| GalNAc | N-acetylgalactosamine |
| GlcA | glucuronate |
| GlcNAc | N-acetylglucosamine |
| GPI | glycosylphosphatidylinositol |
| GTP | guanosine 5'-triphosphate |
| HEPES | N-(2-hydroxyethyl)piperazine-N'-(2-ethanesulphonic acid) |
| HRP | horseradish peroxidase |
| HS | heparan sulphate |
| htx-HS | heparitinase-treated heparan sulphate |
| IdoA | iduronate |
| Ig | immunoglobulin |
| kb | kilobase |
| LB Agar | Lennox L Agar |
| LB Broth | Lennox L Broth |
| LP | long PCR products |
| MARCKS | myristoylated, alanine-rich C kinase substrate |
| mes | mesoderm |
| mg | milligram |
| ml | millilitre |

| | |
|---|---|
| mm | millimetre |
| MOPS | 3-(N-morpholino)propanesulphonic acid |
| mRNA | messenger ribonucleic acid |
| μCi | microcurie |
| μg | microgram |
| μl | microlitre |
| μm | micrometre |
| μS | microsiemen |
| NBT | nitroblue tetrazolium |
| nc | notochord |
| N-CAM | neural cell adhesion molecule |
| NDST | N-deacetylase N-sulphotransferase |
| neb | neuroepithelial basement membrane |
| nm | nanometre |
| NTMT | sodium chloride/Tris/magnesium chloride/Tween buffer |
| NTP | ribonucleoside 5'-triphosphate |
| OST | O-sulphotransferase |
| PAPC | 3'-phosphoadenosine 5'-phosphochlorate |
| PAPS | 3'-phosphoadenosine 5'-phosphosulphate |
| PBS | phosphate buffered saline |
| PBT | PBS/Tween buffer |
| PCR | polymerase chain reaction |
| PFA | paraformaldehyde |
| PNP | posterior neuropore |
| RNA | ribonucleic acid |
| RNase A | ribonuclease A |
| SA | streptavidin |
| SDS | sodium dodecyl sulphate |

| | |
|---|---|
| $SO_4$ | sulphate |
| STP | short target PCR products |
| SSC | sodium chloride/sodium citrate buffer |
| TAE | Tris/acetic acid/EDTA buffer |
| TBS | Tris buffered saline |
| TE | Tris/EDTA buffer |
| TESPA | 3-aminopropyltriethoxysilane |
| TGF-β | transforming growth factor-β |
| Tris | tris(hydroxymethyl)aminomethane |
| TTP | thymidine 5'-triphosphate |
| UDP | uridine 5'-diphosphate |
| UTP | uridine 5'-triphosphate |
| Xyl | xylose |

# *Chapter 1*

# GENERAL

# INTRODUCTION

## 1.1 Introduction

Glycosaminoglycans are widely distributed molecules in the animal kingdom, and are found in organisms ranging from *Drosophila* to mammals. They are present in many different tissues and organs, and are involved in cellular functions such as proliferation, differentiation, adhesion and migration. These molecules play vital roles in many physiological and pathological processes, including embryonic development, tumourigenesis and inflammation. The importance of the sulphated glycosaminoglycans in neurulation and neural crest cell migration during mouse embryonic development is examined in this thesis.

## 1.2 Glycosaminoglycans and proteoglycans

### *1.2.1 Glycosaminoglycans*

Glycosaminoglycans are large polyanionic molecules, consisting of long, unbranched chains of repeating disaccharide subunits. The disaccharide subunits are made up of a hexosamine, which is either glucosamine or galactosamine, and a hexuronic acid (Varki et al, 1999).

Glycosaminoglycans are divided into two main groups, based on the presence of sulphate groups in the disaccharide subunit. The commonest example of non-sulphated glycosaminoglycans is hyaluronan, which consists of repeats of N-acetylglucosamine (GlcNAc) and glucuronate (GlcA). Unlike other glycosaminoglycans, it is not

covalently linked to a protein core to form a proteoglycan (Varki et al, 1999).

The sulphated glycosaminoglycans are further divided into three groups: heparan sulphate/heparin, chondroitin sulphate/dermatan sulphate, and keratan sulphate. Heparan sulphate/heparin consists of repeating disaccharide subunits of N-acetylglucosamine and either iduronate (IdoA) or glucuronate (Figures 1.1A to D). The glucosamine, iduronate and glucuronate residues are modified by the addition of variable numbers of sulphate groups at the C2, C3 and C6 positions (Figures 1.1A, C).

The subunit in chondroitin sulphate comprises N-acetylgalactosamine (GalNAc) and glucuronate (Figures 1.1E, F). The galactosamine residues are variably modified by the addition of sulphate groups at the C4 and C6 positions (Figure 1.1E). In dermatan sulphate, some of the glucuronate residues are epimerised to form iduronate residues.

Keratan sulphate distinguishes itself from the other sulphated glycosaminoglycans in the lack of a hexuronic acid. The disaccharide subunit is made up of N-acetylglucosamine and galactose residues.

At the time of neurulation in the rodent embryo, the main sulphated glycosaminoglycans synthesised are heparan sulphate and chondroitin sulphate (Solursh and Morriss, 1977; Copp and Bernfield, 1988a). Hence, these two molecules form the focus of the remainder of this thesis.

A. Heparan sulphate: $[GlcA \rightarrow GlcNAc]_n$

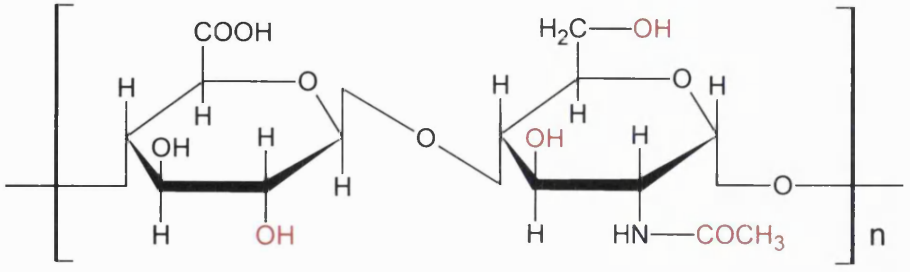


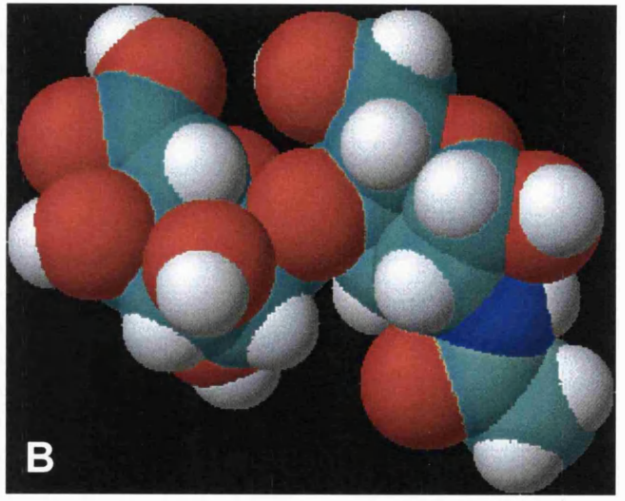


C. Heparan sulphate: $[IdoA \rightarrow GlcNAc]_n$

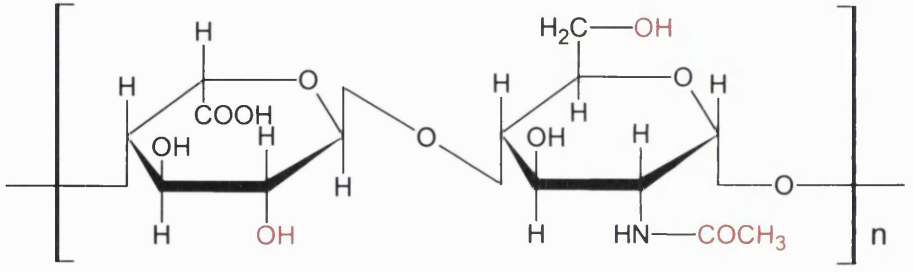


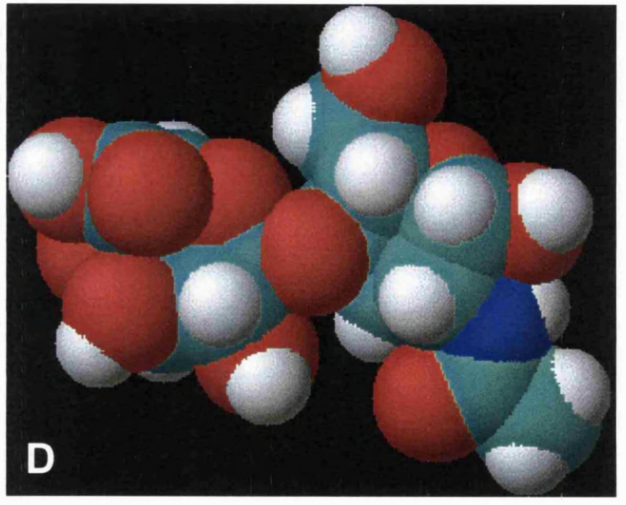

**E. Chondroitin sulphate: [GlcA→GalNAc]$_n$**

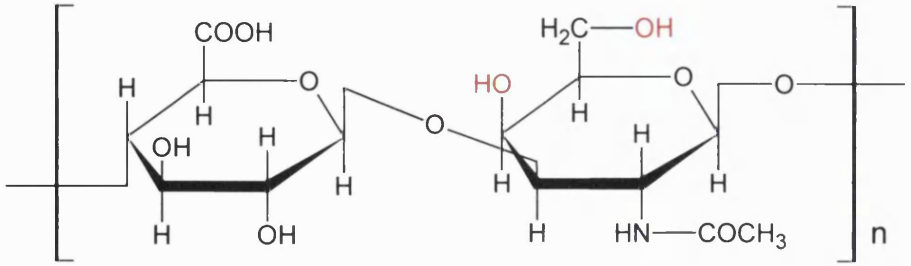


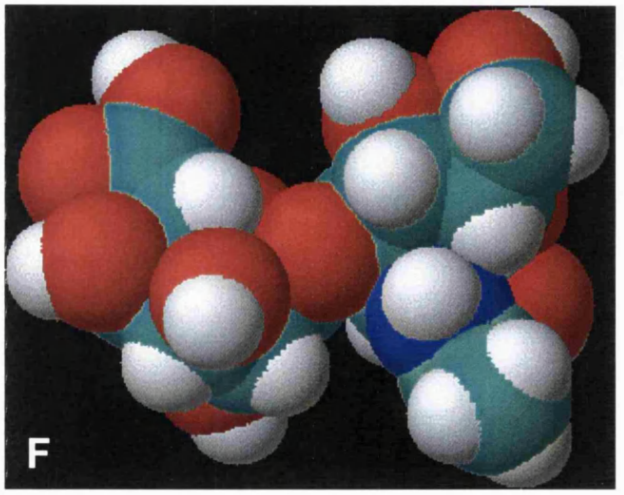




**Figure 1.1 Disaccharide subunits of heparan sulphate and chondroitin sulphate.** (A) and (C) show the chemical structures of heparan sulphate disaccharide subunits, and (E) shows the chondroitin sulphate subunit. Groups that are variably modified by sulphation during glycosaminoglycan biosynthesis are shown in red. (B), (D) and (F) are space filling models of the structures in (A), (C) and (E) respectively. Note the three-dimensional conformational change in the heparan sulphate subunit when the glucuronate residue in (B) is epimerised to form iduronate in (D). Abbreviations: GalNAc, N-acetylgalactosamine; GlcA, glucuronate; GlcNAc, N-acetylglucosamine; IdoA, iduronate. Colour code for space filling model: blue, nitrogen; cyan, carbon; red, oxygen; white, hydrogen. (A), (C) and (E) were modified after Prydz and Dalen (2000). (B), (D) and (F) were generated using ChemSketch Version 4.01 (see Chapter 2).

#### 1.2.1.1 Differences between heparan sulphate and heparin

Although both heparan sulphate and heparin are made up of repeating subunits of glucosamine and glucuronate/iduronate, there are important physicochemical and biological differences between the two molecules.

Heparin has an average of 2.5 sulphate groups per disaccharide unit, making it the most negatively charged glycosaminoglycan known. It is highly modified by deacetylation, sulphation and epimerisation of the glucuronate residues to iduronate residues (Conrad, 1998; Varki et al, 1999). The 3-O sulphate group on the glucosamine residue is critical for its anticoagulant activity.

In contrast, heparan sulphate only contains about one sulphate group per disaccharide subunit. The molecule is less extensively modified by deacetylation, sulphation and epimerisation. There are approximately equal amounts of N-sulphated and N-acetylated glucosamine residues present, and the ratio of O-sulphate to N-sulphate groups is one or less (Gallagher and Walker, 1985). Short segments, which are highly modified and sulphated, are dispersed among the less sulphated sequences in heparan sulphate, resulting in a structure that is much more complex compared with heparin (Turnbull et al, 2001).

These differences between heparan sulphate and heparin are reflected in their physicochemical properties. The average molecular weight, solubility in 2 M potassium acetate, number of bands on isoelectric focusing in polyacrylamide gels, and susceptibility to degradation by heparinase I differ between the two molecules (Linhardt, 1995; Conrad,

1998; Varki et al, 1999). Functionally, heparin is capable of binding bioactive molecules, such as growth factors, with a higher affinity and avidity than heparan sulphate due to its higher negative charge. This affects the availability of these signalling molecules to their cellular receptors.

Heparin is synthesised in mast cells on its core protein, serglycin. It is stored in secretory granules and released during inflammation (Matsumota et al, 1995). Recently, heparin is also discovered to be synthesised by oligodendrocyte-type-2-astrocyte progenitor cells, which are precursors of oligodendrocytes and type-2 astrocytes (Stringer et al, 1999). Upon differentiation into oligodendrocytes and astrocytes, these cells switch from the expression of heparin to heparan sulphate.

In contrast, heparan sulphate is synthesised on a distinct series of core proteins (see below) and secreted continually by most animal cells. Hence, heparan sulphate, rather than heparin, is the species that is encountered by most of the cells in an organism.

The biological significance of the differences between heparan sulphate and heparin is highlighted by comparing mutant mice that are deficient in heparan sulphate with those that are deficient in heparin. Mice that lack heparin are viable and fertile (Forsberg et al, 1999; Humphries et al, 1999). On the other hand, mice that are deficient in heparan sulphate have a wide range of abnormalities, depending on which part of the heparan sulphate biosynthetic pathway is affected. These abnormalities range from gastrulation defects (Lin et al, 2000), abnormalities of the kidney, eye and skeletal system (Bullock et al,

1998), to neonatal death from severe respiratory distress syndrome (Ringvall et al, 2000; Fan et al, 2000).

## *1.2.2 Proteoglycans*

Proteoglycans are formed by the covalent attachment of glycosaminoglycan chains to the serine residues of core proteins via a linkage region that consists of xylose-galactose-galactose-glucuronate. Proteoglycans are found on cell surfaces, in the basement membranes and in the extracellular matrix. The expression pattern of proteoglycans is developmentally regulated. Proteoglycans are classified by either the core protein or the predominant glycosaminoglycan species attached.

### 1.2.2.1 Syndecans

Syndecans are transmembrane core proteins. Four members of the syndecan family are currently known, named syndecan-1 to 4 (Bernfield et al, 1992; Salmivirta and Jalkanen, 1995). Syndecans contain an extracellular domain, a transmembrane domain, and a short cytoplasmic tail. Glycosaminoglycan chains are attached to the extracellular domain. The transmembrane and cytoplasmic regions are highly conserved, as are the glycosaminoglycan attachment sites and the proteolytic cleavage sites in the extracellular domain. Syndecans are expressed in a developmentally regulated manner in tissues derived from all three germ layers (David et al, 1993; Kim et al, 1994; Gould et al, 1995). Although classified as heparan sulphate proteoglycans, syndecan-1 and 4 are known to carry chondroitin sulphate chains in addition to heparan sulphate chains. The relative abundance of

heparan sulphate and chondroitin sulphate on each core protein varies among different tissues (Kokenyesi and Bernfield, 1994).

### 1.2.2.2 Glypicans

Glypicans are heparan sulphate proteoglycans that are anchored to the cell surface by a glycosylphosphatidylinositol (GPI) linkage (Conrad, 1998). The family consists of six known members, named glypican-1 to 6. Like syndecans, the presence of glypicans in a wide variety of tissues is developmentally regulated (Stipp et al, 1994; Watanabe et al, 1995; Saunders et al, 1997; Litwack et al, 1998; Paine-Saunders et al, 2000).

### 1.2.2.3 Basement membrane proteoglycans

The major proteoglycans in the basement membrane are perlecan, agrin and bamacan (Iozzo, 1998). Perlecan and agrin are heparan sulphate proteoglycans. Both of them contain laminin-like modules. Perlecan is expressed in the embryo as early as the pre-implantation stage. The distribution of fibroblast growth factor-2 (FGF-2) in the basement membrane parallels that of perlecan in the mouse embryo, suggesting that perlecan might play a role in regulating FGF-2 signalling (Aviezer et al, 1994). Agrin is important for the development of neuromuscular function. Bamacan is a chondroitin sulphate proteoglycan and helps in maintaining the stability of the basement membrane.

#### 1.2.2.4 Hyalectans

The chondroitin sulphate proteoglycans aggrecan, versican, neurocan and brevican are members of the hyalectan family, based on their common ability to interact with hyaluronan at their N-terminal and with lectins at their C-terminal (Iozzo, 1998). These proteoglycans exhibit alternative splicing, and several variants of them are found in the extracellular matrix in distinct spatial and temporal patterns during development (Oohira et al, 2000). In addition, a short isoform of brevican is known which attaches to the plasma membrane by a glycosylphosphatidylinositol anchor.

#### 1.2.2.5 Other proteoglycans

Many other proteoglycans are known which carry heparan sulphate and/or chondroitin sulphate chains. Examples of these include collagen XVIII (heparan sulphate), collagen IX (chondroitin sulphate), phosphacan (chondroitin sulphate) and betaglycan (both heparan sulphate and chondroitin sulphate). The term 'part-time proteoglycan' has been applied to some of them, such as betaglycan, because variants of the core proteins exist which do not carry any glycosaminoglycan side chains (David, 1993; Erickson and Couchman, 2000).

### *1.2.3 Biosynthesis*

The biosynthesis of proteoglycans involves several cellular compartments (Prydz and Dalen, 2000). The proteoglycan core protein is made in the rough endoplasmic reticulum. This is then transported to

the Golgi apparatus where synthesis of the glycosaminoglycan chains takes place. Sugar residues are activated by attachment to uridine 5'-triphosphate (UTP) in the cytoplasm before they are transported to the Golgi apparatus for elongation of the glycosaminoglycan chains. Similarly, the sulphate group donor, 3'-phosphoadenosine 5'-phosphosulphate (PAPS), is first synthesised in the cytoplasm from inorganic sulphate and adenosine 5'-triphosphate. The reaction is catalysed by a bifunctional enzyme named 3'-phosphoadenosine 5'-phosphosulphate synthase. The donor is then transported to the Golgi apparatus.

#### 1.2.3.1 Linkage region

Synthesis of the linkage region takes place in the endoplasmic reticulum/*cis*-Golgi network. This begins with the addition of xylose to the serine residue of the core protein (Figure 1.2). Thereafter, galactose and glucuronate are sequentially added by their respective transferases. Although different core proteins are found in heparan sulphate proteoglycans and chondroitin sulphate proteoglycans, the same set of hexose transferases is used for synthesis of the linkage region in both groups. Mutant Chinese hamster ovary (CHO) cells that lack xylosyl transferase and galactosyltransferase I are unable to synthesise both heparan sulphate and chondroitin sulphate (Esko et al, 1987).

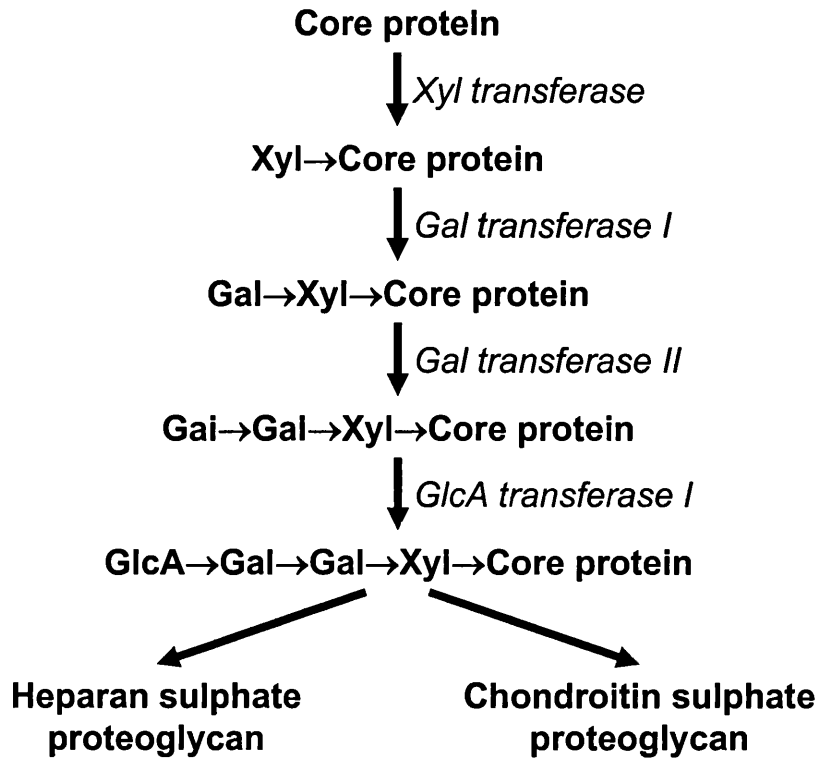


**FIgure 1.2 Biosynthesis of the proteoglycan linkage regIon.** Proteoglycan synthesis begins with formation of the core protein chain. This is followed by the sequential addition of components of the linker tetrasaccharide, which consists of xylose, galactose and glucuronate, by the respective transferases shown above. The same set of transferase enzymes is used in synthesis of heparan sulphate and chondroitin sulphate proteoglycans. Once synthesis of the linkage region is completed, the biochemical pathway diverges to form either heparan sulphate or chondroitin sulphate proteoglycan. Abbreviations: Gal, galactose; GlcA, glucuronate; Xyl, xylose.

### 1.2.3.2 Glycosaminoglycan chain

The first carbohydrate residue that is attached to the linkage region determines the identity of the glycosaminoglycan chain that is to be made. In the synthesis of heparan sulphate, GlcNAc-transferase I adds the first N-acetylglucosamine residue to the glucuronate residue of the linkage region (Figure 1.3). Chain elongation then proceeds through the alternate addition of glucuronate and N-acetylglucosamine residues. This is catalysed by heparan sulphate copolymerase, a hetero-oligomeric enzyme complex. The enzyme complex is encoded by the *EXT1*/*EXT2* tumour suppressor genes, which are the mammalian homologues of the *Drosophila tout-velu* gene. Synthesis of the heparan sulphate chain occurs in the *cis*-, *medial*- and *trans*- Golgi cisternae (Prydz and Dalen, 2000). A variable amount of sequential modification of the heparan sulphate chain occurs through deacetylation, epimerisation, and N- and O-sulphation (Figure 1.3).

In chondroitin sulphate synthesis, the enzyme GalNAc-transferase I attaches the first N-acetylgalactosamine residue to the linkage region (Figure 1.4). The chain is then elongated by alternate additions of glucuronate and N-acetylgalactosamine residues. Finally, the chondroitin sulphate chain is variably modified by the action of 4- and 6-O sulphotransferases. Synthesis of chondroitin sulphate occurs in the *trans*-Golgi network (Prydz and Dalen, 2000).

Further processing of the core protein has been described, which involves the attachment of either N- or O-linked oligosaccharides to the arginine and serine residues respectively of the protein backbone (Kjellen and Lindahl, 1991).

**Figure 1.3 Biosynthesis of heparan sulphate.** Synthesis of heparan sulphate begins with addition of the first N-acetylglucosamine residue to the linker tetrasaccharide by GlcNAc transferase I, which is encoded by the tumour suppressor gene *EXTL2*. Elongation of the heparan sulphate chain follows, with alternate addition of glucuronate and N-acetylglucosamine. This reaction is catalysed by a hetero-oligomeric heparan sulphate copolymerase enzyme complex that possesses both glucuronate transferase and N-acetylglucosamine transferase activity. The enzyme complex is the gene product of *EXT1/EXT2*, the mammalian homologues of the *Drosophila tout-velu* gene. The N-acetyl group on N-acetylglucosamine is then removed and replaced by a sulphate group. Both reactions are carried out by the same bifunctional enzyme, N-deacetylase N-sulphotransferase. Some glucuronate residues are epimerised to form iduronate by glucuronate epimerase. Finally, sulphate groups are added to C2, C3 and C6 positions of the carbohydrate residues by the respective action of 2-O, 3-O and 6-O sulphotransferases. The modification reactions do not proceed to completion, resulting in a complex heparan sulphate structure where highly modified and sulphated segments are dispersed among less modified sequences. Abbreviations: GlcA, glucuronate; GlcNAc, N-acetylglucosamine; IdoA, iduronate; NDST, N-deacetylase N-sulphotransferase; OST, O-sulphotransferase.

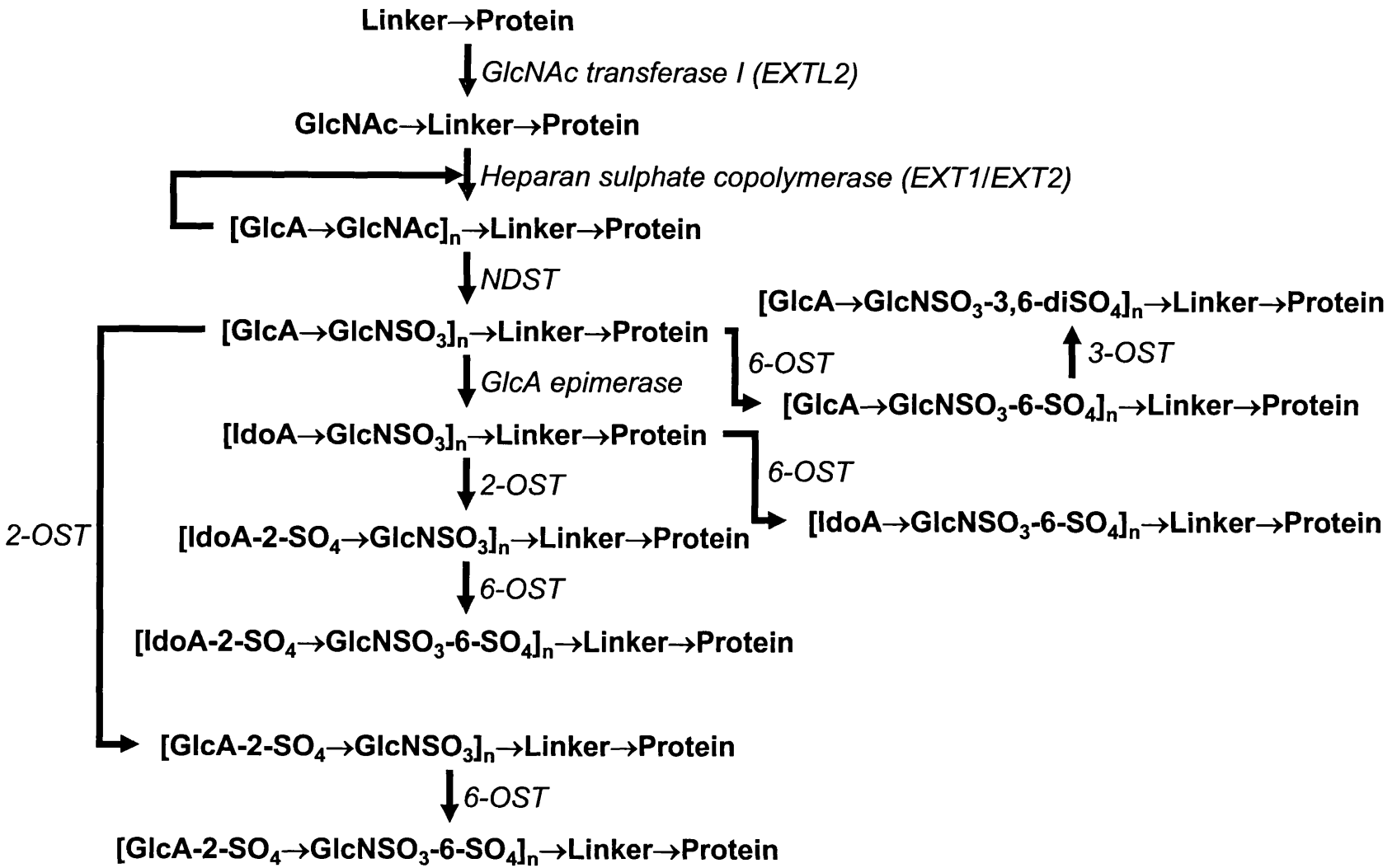
Linker→Protein
GlcNAc transferase I (EXTL2)
GlcNAc→Linker→Protein
Heparan sulphate copolymerase (EXT1/EXT2)
[GlcA→GlcNAc]n→Linker→Protein
NDST
[GlcA→GlcNSO3]n→Linker→Protein
[GlcA→GlcNSO3-3,6-diSO4]n→Linker→Protein
6-OST
3-OST
GlcA epimerase
[GlcA→GlcNSO3-6-SO4]n→Linker→Protein
[IdoA→GlcNSO3]n→Linker→Protein
6-OST
2-OST
[IdoA→GlcNSO3-6-SO4]n→Linker→Protein
2-OST
[IdoA-2-SO4→GlcNSO3]n→Linker→Protein
6-OST
[IdoA-2-SO4→GlcNSO3-6-SO4]n→Linker→Protein
[GlcA-2-SO4→GlcNSO3]n→Linker→Protein
6-OST
[GlcA-2-SO4→GlcNSO3-6-SO4]n→Linker→Protein

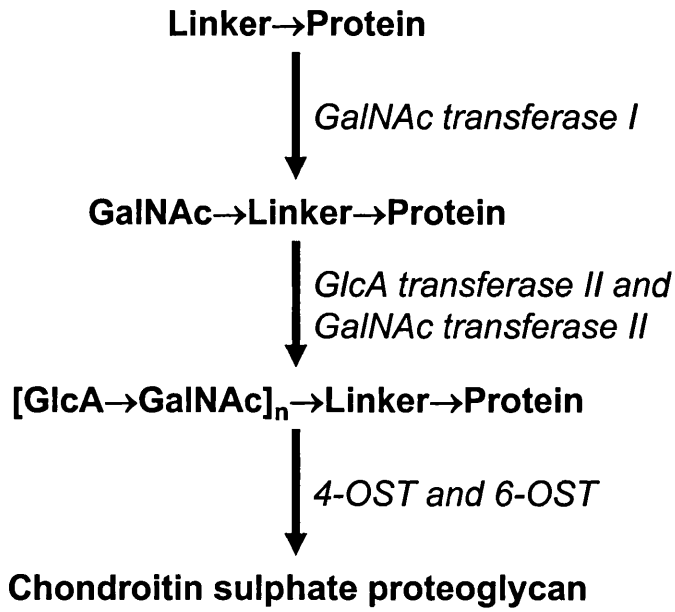


**Figure 1.4 Biosynthesis of chondroitin sulphate.** Synthesis of chondroitin sulphate begins with attachment of N-acetylgalactosamine to the terminal glucuronate of the linker tetrasaccharide by GalNAc transferase I. The chondroitin sulphate chain elongates by the alternate addition of glucuronate and N-acetylgalactosamine. These reactions are catalysed by GlcA transferase II and GalNAc transferase II respectively. The glycosaminoglycan chain is then subjected to variable amounts of sulphation by the 4-O and 6-O sulphotransferases. Abbreviations: GalNAc, N-acetylgalactosamine; GlcA, glucuronate; OST, O-sulphotransferase.

### 1.2.3.3 Regulation of proteoglycan biosynthesis

The glycosaminoglycan attachment site on the core protein is characterised by serine and glycine- containing sequences that are flanked by acidic amino acids and adjacent tryptophan residues (Zhang and Esko, 1994; Zhang et al, 1995). These serine-glycine sequences tend to be clustered together in heparan sulphate proteoglycans. In chondroitin sulphate proteoglycans, the sequences tend to be isolated.

Other factors, which are not well understood, help to determine the type of glycosaminoglycan chain that is attached. For example, the syndecan-1 core protein is identical regardless of the tissue of origin, but the ratio of attached heparan sulphate to chondroitin sulphate varies from one tissue to another (Kokenyesi and Bernfield, 1994). The glycosaminoglycan chains on a core protein influence the location of the proteoglycan on the cell surface. For example, glypicans are usually found on the basolateral surface of epithelial cells. Removal of the heparan sulphate chains results in apical transport of the core protein (Mertens et al, 1996). On the other hand, the presence of chondroitin sulphate chains might promote apical secretion of the proteoglycan (Kolset et al, 1999).

The fine structure of a glycosaminoglycan chain, including the amount of sulphation, deacetylation and epimerisation, appears to be cell type specific rather than core protein-specific (Kato et al, 1991; Kato et al, 1994). Developmentally regulated expression of multiple isoforms of the glycosaminoglycan biosynthetic enzymes has been postulated to contribute to the fine structure (Kitagawa et al, 1997; Fan et al, 1999; Habuchi, 2000). The glycosaminoglycan fine structure helps determine

which bioactive molecules are able to bind to the proteoglycan and the biological effect of this interaction (Guimond et al, 1993; Ishihara, 1994; Bernfield et al, 1999). For example, heparan sulphate is capable of binding to and potentiating the activity of fibroblast growth factors. When neural precursor cells switch from a proliferative to a differentiative state, there is an accompanying change in the sulphation pattern of heparan sulphate, which switches the potentiating activity of the glycosaminoglycan from FGF-2 to FGF-1 (Nurcombe et al, 1993; Brickman et al, 1998).

Growth factors and other biologically active molecules influence both the amount and type of proteoglycans that are associated with a cell. Examples of these bioactive molecules include FGF-2, TGF-β, inositol and retinoic acid (Elenius et al, 1992; Morriss-Kay and Mahmood, 1992; Grässel et al, 1995; Schmidt et al, 1995). For example, rat aortic smooth muscle cells synthesise both syndecan-1 and 2, the relative proportion of which is altered by different growth factors (Cizmeci-Smith et al, 1993). TGF-β upregulates expression of syndecan-2 and versican in smooth muscle cells.

Control of the quantity of proteoglycan associated with a cell occurs not just at the transcriptional level but post-transcriptionally as well (Bernfield et al, 1999). For example, a ten-fold increase in the amount of syndecan-1 is seen in kidney mesenchymal cells during development without an appreciable change in the mRNA level. In contrast, abundant transcripts of *syndecan-3* are found in the developing rat heart, but the proteoglycan itself is hardly detectable.

### *1.2.4 Turnover*

Proteoglycans can be secreted directly into the extracellular environment. This is seen in the case of the basement membrane proteoglycans and the hyalectans. Proteoglycans can also be shed from the cell surface by enzymatic action. Transmembrane proteoglycans such as syndecans are shed by proteolytic cleavage, while glycosylphosphatidylinositol-linked proteoglycans such as glypicans are shed by the action of phospholipase C. Proteoglycans removed by endocytosis are degraded by endo- and exo-glycosidases and sulphatases in the lysosomes (Yanagishita and Hascall, 1992; David, 1993). However, not all endocytosed proteoglycans are degraded. Some endocytosed glypicans are modified and then re-secreted by the cell (Edgren et al, 1997). Transport of heparan sulphate to the cell nuclei has also been reported (Margolis et al, 1976; Fedarko and Conrad, 1986).

The turnover of proteoglycans is very rapid. In steady state radiolabelling of heparan sulphate in cell cultures, turnover occurs between three and eight hours (Bienkowski and Conrad, 1984). Thus, glycosaminoglycans can rapidly adapt to different requirements during embryonic development (Nurcombe et al, 1993; Brickman et al, 1998).

#### 1.2.4.1 Mucopolysaccharidoses

Mucopolysaccharidoses are a group of inherited disorders where there is abnormal accumulation of glycosaminoglycans due to deficiencies in certain lysosomal enzymes (Varki et al, 1999). The severity of the clinical signs and symptoms varies widely. Patients with less severe

Hunter syndrome, where a lack of iduronate-2-sulphatase leads to the accumulation of heparan sulphate and dermatan sulphate, can have normal intelligence and survive up to 60 years of age. On the other hand, *in utero* or neonatal death from hydrops foetalis is seen in Sly syndrome, where a β-glucuronidase deficiency results in an inability to degrade heparan sulphate, chondroitin sulphate and dermatan sulphate.

### 1.2.5 Biological function

Proteoglycans are capable of binding to over one hundred molecules (Conrad, 1998; Bernfield et al, 1999; Oohira et al, 2000). These molecules include several classes of signalling molecules that are vital to embryonic development, such as the fibroblast growth factor and receptor family, the Wnt proteins, and the Hedgehog proteins. Binding occurs via the glycosaminoglycan chains of the proteoglycan, the core protein, or both. In the last case, the glycosaminoglycan chains and core protein may act synergistically to increase the affinity of the proteoglycan for the signalling molecule (Herndon et al, 1999).

Specific binding is seen between glycosaminoglycans and signalling molecules. The signalling molecule usually contains one or more binding sequences that are rich in basic amino acids and hydropathic amino acids (Cardin and Weintraub, 1989). These bind to specific sequences on the glycosaminoglycan chain, such as the one found in heparan sulphate to which FGF-2 binds (Habuchi et al, 1992; Turnbull et al, 1992). The ligand-binding ability of a glycosaminoglycan is enhanced by the presence of multiple closely arrayed charged sulphate and carboxyl groups, which allows for polyvalent association with

positively charged domains on the surface of a specific ligand. For example, the sulphate groups on heparan sulphate influence the ability of the glycosaminoglycan chain to bind to different members of the fibroblast growth factor family (Guimond et al, 1993; Ishihara, 1994). Rotation at the glycosidic linkages of the glycosaminoglycan chain helps to present these negatively charged groups to the signalling molecule (Conrad, 1998). It has been postulated that the proteoglycan core protein facilitates binding of glycosaminoglycan chains to the signalling molecules by tethering multiple chains together and positioning them in an optimal position for ligand attachment. Positively charged metal ions in the vicinity of this molecular interaction can also affect the binding affinity and avidity (Kan et al, 1996).

The binding of fibroblast growth factors to heparan sulphate has been extensively studied. Fibroblast growth factors bind to high affinity fibroblast growth factor receptors, leading to dimerisation and mutual tyrosine phosphorylation of these receptors. Heparan sulphate acts as a low affinity co-receptor, facilitating the binding of the growth factor with its high affinity receptor (Spivak et al, 1994; Schlessinger et al, 1995). Binding of FGF-2 to heparan sulphate helps to concentrate the growth factor at the cell surface, and protects it from being degraded (Rosengart et al, 1988). The growth factor can also be internalised while bound to heparan sulphate (Murono et al, 1993). FGF-2 induces syndecan-1 expression, and this has been postulated as a mechanism by which FGF-2 regulates its own activity (Bernfield et al, 1999).

Besides directly helping signalling molecules to activate their receptors, heparan sulphate is able to influence signalling in other ways. In the case of the Hedgehog proteins, heparan sulphate helps to propagate

the signal from the producing cells to the receiving cells, as has been shown in *Drosophila* (Bellaiche et al, 1998; The et al, 1999) and in mice (Lin et al, 2000). In addition, heparan sulphate potentiates the activity of TGF-β1 and β2 by binding to the growth factors and preventing them from being inactivated by $\alpha_2$-macroglobulin (Lyon et al, 1997).

Changes in the amount of heparan sulphate proteoglycan are associated with different phases of the cell cycle. Synthesis of the glycosaminoglycan chain is reduced four fold during mitosis compared with interphase (Preston et al, 1985). Smooth muscle cells synthesise and secrete the proteoglycan in $G_1$- and $G_2$-phases, but stop at the beginning of the S-phase and during mitosis (Breton et al, 1986). Addition of exogenous heparin blocks the cell cycle in the late $G_1$-phase (Reilly et al, 1989). In addition, the rate of cell division is inversely correlated with the amount of nuclear heparan sulphate (Fedarko and Conrad, 1986; Ishihara et al, 1986).

Syndecans are found on the basolateral surface of epithelial cells, colocalised with and bound to actin and other components of the cytoskeleton (Carey et al, 1994; Fernandez-Borja et al, 1995; Carey et al, 1996). This helps to stabilise both intercellular and cell-extracellular matrix adhesions (Bernfield et al, 1999). Syndecans play a role in maintaining the epithelial phenotype and prevent epitheliomesenchymal transformation from occurring. Syndecans are also involved in the transfer of signals from the extracellular matrix into the cell and the coupling of cytosolic downstream signalling molecules. For example, the binding of syndecan-4 to the extracellular matrix enables its cytoplasmic domain to bind to and activate the catalytic domain of protein kinase C (Bernfield et al, 1999). Abolition of the cytoplasmic tail

of syndecan-4 prevents syndecan-4 dependent augmentation of responses to FGF-2 signalling (Volk et al, 1999).

Chondroitin sulphate proteoglycans are involved in development of the skeletal, cardiovascular and nervous systems. They are important in neuronal development, and affect neurite outgrowth, cellular adhesion and axonal pathfinding in a cell type specific manner (Iozzo, 1998; Oohira et al, 2000; Bovolenta and Fernaud-Espinosa, 2000). For example, phosphacan promotes neurite outgrowth from mesencephalic and hippocampal neurons, but inhibits neuritogenesis of explants of the dorsal root ganglion. Chondroitin sulphate has been reported at glial boundaries in the developing mammalian nervous system, and is found in tissues that constrain growth of spinal cord motor axons to their target. Since heparan sulphate proteoglycans are able to promote neurite outgrowth, it has been suggested that the balance of different proteoglycan types encountered by a cell could help determine its behaviour.

Chondroitin sulphate proteoglycans also help to regulate cell migration. They are involved in the control of epiblast cell movement during gastrulation in the chick embryo, and prevent ingression of ectopic epiblast cells (Canning et al, 2000).

Versican, a chondroitin sulphate proteoglycan, is found in developing heart tissues (Henderson et al, 1997). It plays a role in directing neural crest cell migration (Perissinotto et al, 2000). In its absence, the endocardial cushions of the conotruncal region of the heart, which are derived from cranial neural crest cells, fail to develop (Mjaatvedt et al,

1998). The role of chondroitin sulphate in neural crest cell migration is described further later.

Aggrecan is the major chondroitin sulphate proteoglycan found in cartilage. Chains of aggrecan molecules are non-covalently linked with hyaluronan. This results in a hydrated and highly viscous matrix that functions as a shock absorber in cartilage and intervertebral discs.

### *1.2.6 Mutations involving proteoglycan synthesis*

Several *Drosophila* and mouse mutants with defects in proteoglycan biosynthesis are known. These mutants have highlighted the specific requirement for proteoglycans during embryonic development, as well as the importance of the different sulphate groups on these proteoglycans (Tables 1.1, 1.2 and 1.3).

#### 1.2.6.1 Heparan sulphate proteoglycans

The requirement for heparan sulphate in propagation of the Hedgehog signal has been revealed by analysis of the *Drosophila tout-velu* mutant. The *tout-velu* gene is homologous to the mammalian *EXT* gene family, and encodes heparan sulphate copolymerase, the enzyme used in heparan sulphate chain elongation during biosynthesis (Bellaiche et al, 1998; The et al, 1999). The *tout-velu* mutant embryo has a segment polarity phenotype that resembles the phenotype of the *hedgehog* mutant. Immunostaining of the imaginal discs in mutant embryos

**Table 1.1. Mutations involving heparan suiphate proteoglycan synthesis in *Drosophila***

| MUTANT | GENE | GENE PRODUCT | SIGNALLING PATHWAY DISRUPTED | REF[a] |
|---|---|---|---|---|
| Dally-like | *dlp* | Novel glypican | Wingless | 1 |
| Division abnormally delayed | *dally* | Glypican | Decapentaplegic; Wingless | 2 |
| Sugarless | *sgl* | UDP-glucose dehydrogenase | Fibroblast growth factor; Wingless | 3 |
| Sulfateless | *sfl* | N-deacetylase N-sulphotransferase | Fibroblast growth factor; Hedgehog; Wingless | 4 |
| Tout-velu | *ttv* | Heparan sulphate copolymerase | Hedgehog | 5 |

[a]References: 1, Khare and Baumgartner, 2000; Baeg et al, 2001; 2, Nakato et al, 1995; Jackson et al, 1997; Tsuda et al, 1999; 3, Häcker et al, 1997; Binari et al, 1997; Haerry et al, 1997; 4, Lin et al, 1999; Lin and Perrimon, 1999; The et al, 1999; 5, Bellaiche et al, 1998; The et al, 1999.

**Table 1.2. Mutations involving heparan sulphate proteoglycan synthesis in the mouse**

| MUTANT | GENE | GENE PRODUCT | PHENOTYPE | REF[a] |
|---|---|---|---|---|
| EXT1 | *EXT-1* | Heparan sulphate copolymerase | Gastrulation defect | 1 |
| Ndst1 | *Ndst1* | N-deacetylase N-sulphotransferase 1 | Lung defect | 2 |
| Ndst2 | *Ndst2* | N-deacetylase N-sulphotransferase 2 | Lack of heparin granules in mast cells | 3 |
| 2-OST | *Hs2st* | 2-O-sulphotransferase | Eye, kidney and skeletal defects | 4 |

[a]References: 1, Lin et al, 2000; 2, Ringvall et al, 2000; Fan et al, 2000; 3, Forsberg et al, 1999; Humphries et al, 1999; 4, Bullock et al, 1998.

**Table 1.3. Mutations involving chondroitin sulphate proteoglycan synthesis in the mouse**

| MUTANT | GENE | GENE PRODUCT | PHENOTYPE | REF[a] |
|---|---|---|---|---|
| Cartilage matrix deficient | *Cspg1* | Aggrecan | Skeletal defect | 1 |
| Heart defect | *Cspg2* | Versican | Heart defect | 2 |

[a]References: 1, Watanabe et al, 1994; Watanabe et al, 1997; 2, Mjaatvedt et al, 1998.

shows that the Hedgehog protein is present in the cells of production in the posterior compartment. However, the signal is unable to pass across a domain of eight to ten cells in the anterior compartment that respond to it. Structural analysis of the glycosaminoglycans from these mutants shows a highly reduced level of heparan sulphate (Toyoda et al, 2000a). It has been postulated that heparan sulphate interacts with the transmembrane protein, Dispatched, in releasing Hedgehog from the producing cells and propagating the signal through the tissues (Burke et al, 1999). The absence of FGF and Wg signalling defects shows that the necessity for heparan sulphate in different signalling pathways is highly specific.

A requirement for heparan sulphate in Hedgehog signalling has also been shown in the mouse. Expression of the *EXT* genes is developmentally regulated in the mouse during embryogenesis (Stickens et al, 2000). *EXT1*-deficient homozygous mice fail to gastrulate and are dead by E8.5 (Lin et al, 2000). Immunohistochemical staining for the Hedgehog protein is absent, although the mRNA transcript is detected. A similar lack of staining for the Hedgehog protein is seen in wild type tissues that have been pre-treated with heparitinase I to remove heparan sulphate. This suggests that heparan sulphate is needed for localisation and propagation of the Hedgehog signal.

Two *Drosophila* mutants, *sugarless* and *sulfateless*, demonstrate the importance of heparan sulphate and its sulphate group in the FGF signalling pathway (Häcker et al, 1997; Binari et al, 1997; Haerry et al, 1997; Lin et al, 1999; Lin and Perrimon, 1999). The *sugarless* gene, also known as *kiwi* or *suppenkasper*, encodes UDP-glucose

dehydrogenase (Häcker et al, 1997; Binari et al, 1997; Haerry et al, 1997). This enzyme catalyses the synthesis of UDP-glucuronate, which is the glucuronate donor in the biosynthesis of heparan sulphate and chondroitin sulphate. As expected, the *Drosophila sugarless* mutant contains reduced levels of both heparan sulphate and chondroitin sulphate (Toyoda et al, 2000b). The *sulfateless* gene encodes the N-deacetylase N-sulphotransferase enzyme, which removes the acetyl group from the glucosamine residue in heparan sulphate and adds a sulphate group to it. Heparan sulphate produced by the *sulfateless* mutant is under-sulphated. In contrast, neither the amount nor the composition of chondroitin sulphate is affected (Toyoda et al, 2000b). Both the *sugarless* and *sulfateless* mutants have mesodermal and tracheal cell migration defects. These are reminiscent of the defects seen in the *Drosophila heartless* and *breathless* mutants, where tissue-specific fibroblast growth factor receptors are absent. Although the Heartless and Breathless receptors are intact in the *Drosophila sugarless* and *sulfateless* mutants, no downstream intracellular signal transduction by these receptors is detected (Lin et al, 1999).

Besides a defect in FGF signalling, Wg signalling in the *Drosophila sugarless* and *sulfateless* mutants is also disrupted. Both mutants resemble the *wg* null mutant in having a loss of the naked cuticle associated with mirror-image duplication of the denticle belts (Häcker et al, 1997; Binari et al, 1997; Haerry et al, 1997). The amount of Armadillo protein, a downstream product of Wg signalling, is reduced (Haerry et al, 1997).

The mammalian homologue of the *Drosophila sulfateless* gene is the *Ndst* gene family. The *Ndst1* null mice die neonatally from severe

respiratory distress syndrome, due to pulmonary hypoplasia and lung atelectasis (Ringvall et al, 2000; Fan et al, 2000). There is an increase in the number of immature type II pneuomocytes present.

Tissue specific effects of defective sulphation of heparan sulphate are also seen when the *Hs2st* gene is mutated in the mouse (Bullock et al, 1998). *Hs2st* encodes the heparan sulphate 2-O-sulphotransferase enzyme, which catalyses the addition of a sulphate group to the glucuronate/iduronate residue during heparan sulphate synthesis. Disruption of this gene results in bilateral renal agenesis with failure of ureteric bud branching and renal mesenchymal condensation. There are also defects of the eye and skeletal system.

The *Drosophila dally* (*division abnormally delayed*) mutant demonstrates that there is a tissue specific and signalling pathway specific requirement for heparan sulphate during embryonic development. The *dally* gene encodes glypican, a heparan sulphate proteoglycan (Nakato et al, 1995). Both Wg and Decapentaplegic signalling are disrupted in the *dally* mutant, with effects on development of the eye, antenna, genitalia and wing (Jackson et al, 1997; Lin and Perrimon, 1999; Tsuda et al, 1999). In the developing genitalia, Decapentaplegic but not Wg signalling is affected. On the other hand, Wg signalling is disrupted in patterning of the embryonic epidermis, but the Decapentaplegic pathway is unaffected. Recently, the *dally-like* (*dlp*) gene, which encodes a novel glypican molecule, has been discovered (Khare and Baumgartner, 2000; Baeg et al, 2001). Both *dally* and *dlp* function in Wg signalling. Absence of both gene products results in a more severe phenotype than when only one gene is affected.

The human homologue of the *Drosophila dally* gene is *GPC3*, which codes for glypican-3. Mutations of this gene have been found in patients with Simpson-Golabi-Behmel dysmorphia, an overgrowth and tumour-susceptibility X-linked syndrome (Pilia et al, 1996). Besides tissue overgrowth, these patients are predisposed to Wilm's tumour of the kidney and neuroblastomas as well as heart and skeletal defects. Knockout of the *Gpc3* gene in the mouse also results in tissue overgrowth and renal defects (Cano-Gauci et al, 1999).

### 1.2.6.2 Chondroitin sulphate proteoglycans

Tissue specific defects in mouse embryogenesis are also seen when the synthesis of chondroitin sulphate proteoglycans is affected. The mouse *Cspg2* gene encodes versican, a chondroitin sulphate proteoglycan. *Cspg2* is disrupted in the heart defect (*hdf*) mutant mouse (Mjaatvedt et al, 1998). The condition is recessively lethal, and affected embryos die *in utero* at E10.5. The right ventricle and conotruncal region fail to develop, and the endocardial cushions of the atrioventricular and conotruncal regions are absent.

The cartilage matrix deficient (*cmd*) mutant mouse has a defect in the *aggrecan* gene (Watanabe et al, 1994; Watanabe et al, 1997). Aggrecan is the main chondroitin sulphate proteoglycan found in cartilage. These mutant mice are slightly dwarfed at birth, show age-related hyperlordosis and develop spastic gait within 19 months of age due to misalignment of the cervical spine. Herniation and degeneration of the intervertebral discs are very common.

Skeletal abnormalities have also been described in humans where there is defective sulphation of chondroitin sulphate. This leads to the development of spondyloepiphyseal dysplasia tarda and mild dwarfism associated with corneal opacities. The urinary glycosaminoglycans show a high proportion of non-sulphated chondroitin sulphate (Mourao et al, 1981).

## 1.3 Neurulation

Neurulation is the embryonic process by which the neural tube is formed. It is divided into two events, primary and secondary neurulation (Copp et al, 1990; Smith and Schoenwolf, 1997). Primary neurulation begins with inductive formation of the neural plate from the embryonic ectoderm. This is followed by a series of morphogenetic events, involving changes in the shape of the neural plate and elevation and apposition of the neural folds. Finally, the neural folds fuse to form the neural tube. This is followed by secondary neurulation in the region of the tail bud. The neural tube that arises from both primary and secondary neurulation gives rise to the central nervous system.

### *1.3.1 Primary neurulation*

The neural plate is formed from the embryonic ectoderm (Copp et al, 1990). In this process, multipotent stem cells in the dorsal midline region of the ectodermal layer form a pseudostratified columnar layer, which constitutes the neural plate. Cells lying lateral to the neural plate assume a squamous morphology. These give rise to the surface ectoderm. Neural induction is regulated by interaction between the dorsal embryonic ectoderm and the underlying notochord in the midline and the paraxial mesoderm.

Shaping of the neural plate occurs after it is formed (Jacobson and Gordon, 1976; Schoenwolf and Alvarez, 1989; Smith and Schoenwolf, 1997; Sausedo et al, 1997). In this process, the neural plate lengthens along the longitudinal axis of the embryo and narrows transversely. The

neuroepithelial cells intercalate with each other in the transverse plane, and cell divisions are oriented such that daughter cells are positioned along the longitudinal axis rather than transversely.

Elevation of the two sides of the neural plate gives rise to the neural groove in the midline. This extends along the longitudinal axis of the embryo, and lies dorsal to the notochord. In the cranial region, the two sides of the neural plate bulge outwards in a dorsolateral direction, resulting in the formation of a biconvex shape (Morriss-Kay, 1981). This is associated with an increase in the amount of mesenchyme underlying the convex cranial neural folds. The neural folds then bend medially to become V-shaped and converge in the midline. This is accompanied by a progressive change in the neuroepithelium from a columnar to cuboidal to pseudostratified layer.

In the spinal region, there is no initial bulging of the neural plate. Instead, continuous elevation of the neural folds brings them into apposition in the dorsal midline.

Apposition of the left- and right-sided neural folds is followed by their fusion to form a closed neural tube. The lumen of the neural tube is thus no longer exposed to the external environment dorsally. The two sides of the surface ectoderm fuse across the midline to form a complete ectodermal layer. Midline fusion of the two sides of the neural folds results in a continuous dorsal neuroepithelial layer beneath the surface ectoderm. In the forebrain region, the neural folds contact each other on the neuroepithelial surface initially. In the midbrain, the point of first contact occurs on the ectodermal surface. Contact occurs at the tips of the neural folds in both the hindbrain and spinal regions (Sadler,

1978; Geelen and Langman, 1979). Cells lying in the transition zone between the neural fold and the surface ectoderm have numerous protrusions and lamellipodia that project outwards. These, and the associated surface layer of carbohydrate-rich material, might play a role in fusion of the neural folds (Waterman, 1976; Sadler, 1978; O'Shea and Kaufman, 1980). Removal of the carbohydrate-rich material by treatment with phospholipase C in mouse embryo cultures leads to a failure of fusion of the normally elevated neural folds.

Closure of the neural tube consists of three types of events. The first type, *de novo* initiation of closure, occurs at a site where the neural folds both immediately cranial and caudal to it have yet to fuse together (Figure 1.5). *De novo* initiation of closure is seen at the level of the cervical spine (closure 1), at the forebrain/midbrain boundary (closure 2), and at the extreme anterior end of the neural tube (closure 3). Closure 1 occurs at the four- to seven-somite stage embryo, while closures 2 and 3 occur at the 11- to 12-somite stage. Variations in the site of closure 2 at the forebrain/midbrain boundary due to mouse strain differences have been reported (Juriloff et al, 1991; Fleming and Copp, 2000). *De novo* initiation of closure results in the formation of neuropores in the cranial and caudal regions of the embryo where the neural folds have yet to come together.

The second type of closure, continuation of closure, occurs after *de novo* closure initiation has occurred. This proceeds in a zippering manner in the cranial and/or caudal direction, resulting in progression of neural fold fusion along the longitudinal axis of the embryo. The neuropore size is reduced by this zippering continuation of closure.

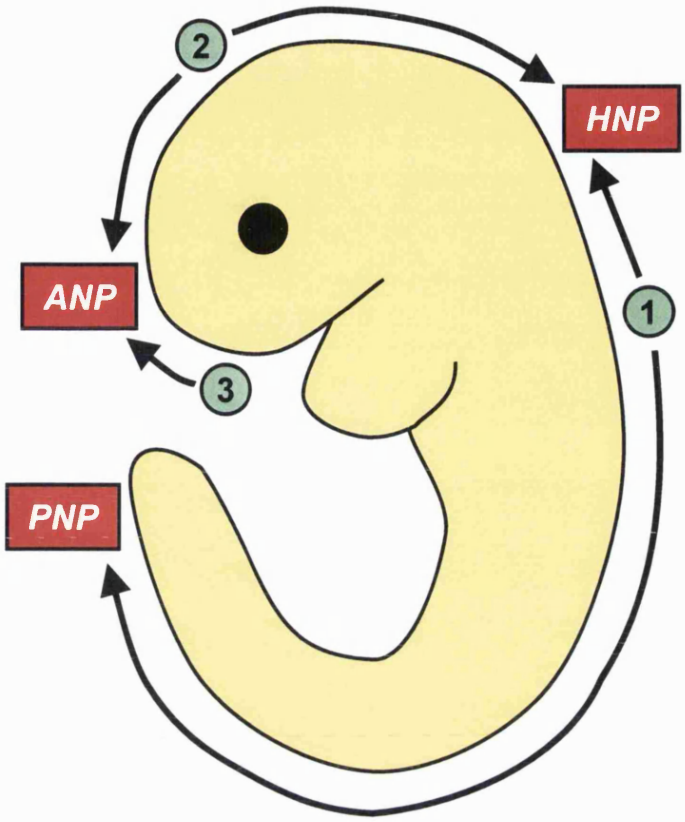


**Figure 1.5 Neural tube closure.** Diagram to show sites of de *novo* initiation of closure at the cervical-hindbrain boundary (closure 1), forebrain-midbrain boundary (closure 2), and rostral extremity of the forebrain (closure 3). Continuation of closure proceeds in a zippering manner, from the three sites of closure initiation, along the neuraxis in the direction indicated by the arrows. The anterior neuropore lies between closure points 2 and 3, the hindbrain neuropore between 1 and 2, and the posterior neuropore lies caudal to closure point 1. Abbreviations: ANP, anterior neuropore; HNP, hindbrain neuropore; PNP, posterior neuropore.

Final closure involves closure of the neuropores in the cranial and caudal regions of the embryo. The anterior, hindbrain and posterior neuropores are closed at the 16-, 17- and 29-somite stages respectively.

### 1.3.2 Secondary neurulation

Secondary neurulation takes place in the lower sacral and caudal regions of the spine. In the mouse, secondary neurulation contributes about half of the spinal cord. On the other hand, secondary neurulation contributes to only a relatively minor proportion of the caudal neural tube in humans. In this process, mesenchymal cells that have recently emerged from the primitive streak remnant condense to form the medullary cord. The medullary cord then canalises to form the neural tube. Fusion of the cranial end of the neural tube formed in secondary neurulation with the caudal end of the neural tube formed in primary neurulation gives rise to a continuous structure (Schoenwolf, 1984; Shum and Copp, 1996).

### 1.3.3 Hinge points in neurulation

Although neural fold elevation and neural tube closure are continuous processes in the spinal region of the mouse embryo, regional morphological differences have been described (Shum and Copp, 1996). Mode 1 closure occurs in the early stages of spinal neurulation, between the eight- and fifteen-somite stages. Bending of the neuroepithelium overlying the notochord results in the formation of a median hinge point (Figure 1.6). This is associated with elevation and

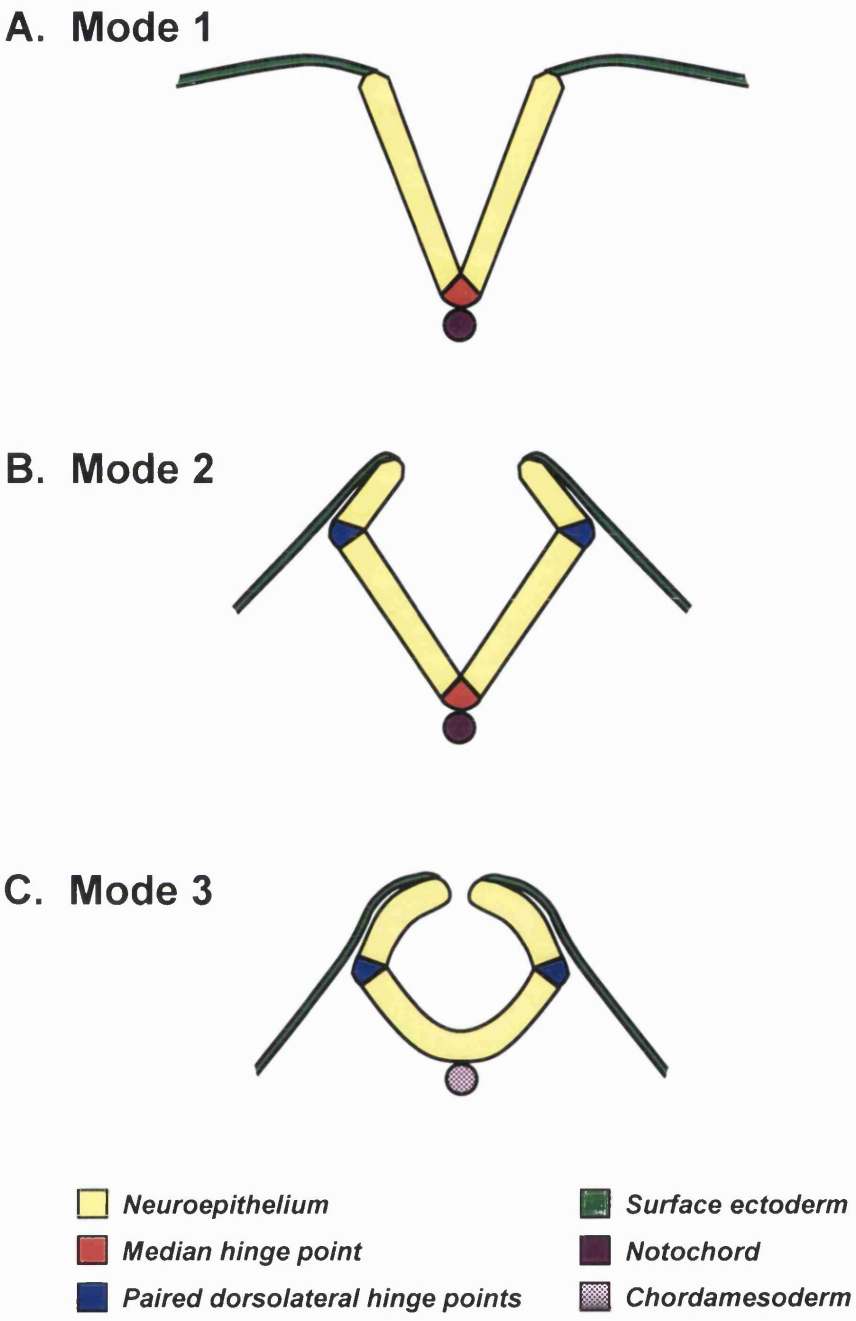


**Figure 1.6 Modes of neural tube closure in spinal neurulation.** Diagrams of transverse sections through the posterior neuropore region to illustrate (A) Mode 1, (B) Mode 2, and (C) Mode 3 neurulation.

medial apposition of the neural folds to produce a slit-like lumen in the neural tube.

Mode 2 closure occurs between the 16- and 23-somite stages, and is seen from the mid-thoracic level downwards. In this mode, the median hinge point is seen together with paired dorsolateral hinge points on the left- and right-sided neural folds. The dorsolateral hinge points serve to bring the neural fold apices towards the midline, resulting in a neural tube with a diamond shaped lumen.

Mode 3 closure is seen from the 24-somite stage onwards. The median hinge point is not formed in this mode. Bending of the entire neuroepithelium occurs along the transverse axis, resulting in a circular lumen in the neural tube. The generalised curvature of the neuroepithelium masks the presence of paired dorsolateral hinge points in transverse sections of the neural tube (Ybot-Gonzalez and Copp, 1999).

Formation of the median and paired dorsolateral hinge points is associated with cell shape changes in the neuroepithelial cells at these hinge points. In a flat neural plate, the neuroepithelial cells are arranged in a pseudostratified layer and have, on average, a uniform height. Most of these cells are spindle shaped, while the rest are wedge shaped. These two types of cells are randomly intermixed throughout the neuroepithelium (Schoenwolf and Franks, 1984; Schoenwolf, 1985; Smith et al, 1994). However, in the process of formation of the median and paired dorsolateral hinge points, most cells within the hinge points become wedge shaped.

Wedging of the cells in the median hinge point depends on induction by the notochord (Smith and Schoenwolf, 1989; Figure 1.7). Sonic hedgehog (Shh) is produced by the notochord. The level of expression of *Sonic hedgehog* decreases along the rostrocaudal axis of the neural tube, and this correlates with the reduction in cell wedging in the median hinge point along the neuraxis (Ybot-Gonzalez and Copp, unpublished). On the other hand, bone morphogenetic proteins (BMP) produced by the dorsal ectoderm appear to be required for formation of the paired dorsolateral hinge points, an effect that is antagonised by Sonic hedgehog. Thus, in the rostral part of the spinal neural tube, the paired dorsolateral hinge points are not formed due to the inhibitory activity of a high level of Sonic hedgehog. More caudally, where the expression of *Sonic hedgehog* is reduced or absent, these dorsolateral hinge points are present.

### 1.3.4 Mechanisms of neural tube closure

Although the morphological changes that occur during neural fold elevation are known, the forces that drive these changes are not well understood. These forces are postulated to arise either from the neuroepithelium itself (intrinsic forces) or from the surrounding tissues (extrinsic forces).

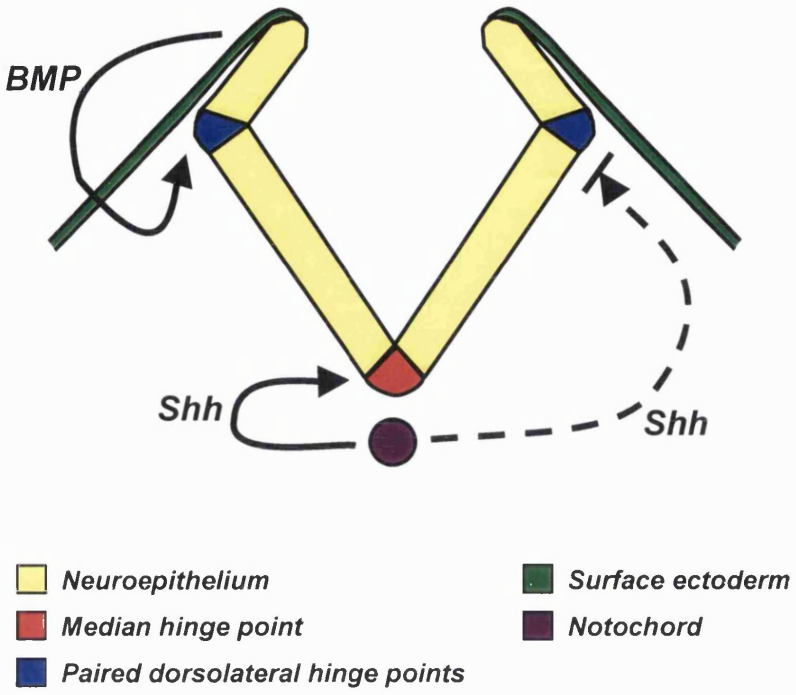


**Figure 1.7 Hypothesis on hinge point formation in spinal neurulation.** Diagram of transverse section through the posterior neuropore region to illustrate hypothesis on formation of the median and paired dorsolateral hinge points (Ybot-Gonzalez and Copp, unpublished). Shh produced by the notochord induces formation of the median hinge point in the overlying neuroepithelium and inhibits dorsolateral hinge point formation. On the other hand, BMP produced by the surface ectoderm stimulates dorsolateral hinge point formation in the elevating neural folds. Solid arrow, stimulation; dotted arrow, inhibition. Abbreviations: BMP, Bone morphogenetic protein; Shh, Sonic hedgebog.

#### 1.3.4.1 Intrinsic forces

Cells of the neural plate contain apically-arranged microfilament bundles (Baker and Schroeder, 1967; Karfunkel, 1974; Morriss and New, 1979; Nagele and Lee, 1980; Sadler et al, 1982; Morriss-Kay and Tuckett, 1985; Ybot-Gonzalez and Copp, 1999). The distribution of the actin-binding protein, spectrin, has also been correlated with the appearance of the microfilaments (Sadler et al, 1986; Thomas, 2001). Contraction of these microfilament bundles could theoretically reduce the apical surface area of the cells in a purse-string manner, leading to cell wedging and the formation of hinge points (Karfunkel, 1974). This theory has been tested by culturing rat embryos in the presence of cytochalasin D, which causes depolymerisation of microfilaments (Morriss-Kay and Tuckett, 1985). The treated embryos show collapse of the convex cranial neural folds, suggesting that actin microfilaments do play a role in cranial neurulation. This finding has also been reported in the mouse, in which cytochalasin D treatment inhibited closure of the cranial folds and the initiation of spinal neurulation (Ybot-Gonzalez and Copp, 1999). Furthermore, actin is found to be necessary for maintaining the rigidity of the neural folds. However, actin does not appear to be essential for the formation of either the median or the paired dorsolateral hinge points in the spinal region. In addition, closure of the posterior neuropore is not abolished by cytochalasin D treatment. These findings suggest that different mechanisms might be acting in closure of the neural tube at different axial levels.

Changes in cell shape have been correlated with the different phases of the cell cycle. Interkinetic nuclear migration results in the cell nucleus occupying a basal position during S- and early $G_2$-phases of the cell

cycle, and this is accompanied by the adoption of a wedge shape by the cell. At mitosis, the nucleus moves towards the apical region, and the cell becomes an inverted wedge shape. At other time points during the cell cycle, the cell assumes a spindle shape, with the nucleus lying in the middle of the cell. Hence, formation of the hinge points and elevation of the neural folds could be explained by alterations in the cell cycle. It has been shown in the chick embryo that more cells are in $G_2$-phase in the median hinge point than in non-bending regions of the neural plate, and that these cells have a prolonged cell cycle (Smith and Schoenwolf, 1987; Smith and Schoenwolf, 1988). In the mouse embryo, cells in the median hinge point have been demonstrated to have a lower mitotic index than elsewhere in the neuroepithelium (Gerrelli and Copp, 1997).

Rapid cell proliferation has also been suggested as a possible cause of neural fold elevation. Since the cells are tethered to the basement membrane, cell proliferation would initially lead to the cells adopting a tall and narrow shape in order to accommodate the increase in cell numbers. Once the maximum ability of the cell to elongate has been exceeded, the neuroepithelium would curl up.

A fourth hypothesis suggests that an increase in the strength of intercellular adhesion between adjacent cells in the neural plate might play a part in neural fold elevation. Assuming that there is no change in the volume of each cell, and that the basal surface of the cell is tethered to the basement membrane, an increase in intercellular adhesive strength would increase the area of cell-cell contact, resulting in bending of the neural plate. The cell adhesion molecules N-CAM and N-cadherin are expressed in the neuroepithelium at the time of neurulation

(Kintner and Melton, 1987, Detrick et al, 1990), and they might be responsible for this postulated increase in intercellular adhesion. Treatment of chick embryos with blocking antibodies to N-cadherin and N-CAM results in an open neural tube in the former group, but not in the latter (Bronner-Fraser et al, 1992). However, neither the N-CAM nor N-cadherin mutant mouse has neural tube closure defects (Cremer et al, 1994; Radice et al, 1997). Furthermore, over-expression of *N-cadherin* transcripts and N-CAM with abnormal sialylation have been reported in the *splotch* mouse mutant, which does have neural tube defects (Moase and Trasler, 1991; Neale and Trasler, 1994; Bennett et al, 1998). The role of these adhesion molecules in neural fold elevation is not currently clear.

### 1.3.4.2 Extrinsic forces

Forces external to the neuroepithelium have been suggested to be responsible for elevation of the cranial neural folds. The neural plate lies dorsal to the underlying mesoderm. An expansion of the extracellular spaces in the mesoderm could result in passive elevation of the cranial neural folds (Morriss and Solursh, 1978; Morris-Wiman and Brinkley, 1990). Such an expansion could be due to the accumulation of hyaluronan in the extracellular matrix of the cranial mesenchyme, leading to an increase in tissue hydration. Bending at the median hinge point could be explained by tethering of the neuroepithelium to the notochord in the midline. Similarly, the basal lamina that connects the ectodermal epithelium with the neuroepithelium has been suggested to act as anchorage for the formation of the paired dorsolateral hinge points (Martins-Green, 1988). However, cranial neural tube closure is not inhibited after degradation of

hyaluronan by *Streptomyces* hyaluronidase treatment of cultured rat embryos, despite the presence of a compact mesenchyme (Morriss-Kay et al, 1986). Furthermore, mutant mice that lack the enzymes for biosynthesis of hyaluronan do not have neural tube defects (Camenisch et al, 2000).

Mesenchymal swelling is not likely to be important in closure of the spinal neural tube. Depending on the stage of development, the neural folds in this region are flanked either by presomitic mesoderm (earlier stage) or by epithelial somites (later stage). In both cases, the mesodermal cells are packed relatively closely together. However, somites have been proposed to act as an external closure factor in forcing the neural folds to elevate during the initial period of closure 1 in the cervical region (van Straaten et al, 2000).

The epidermal ectoderm has also been proposed to provide an extrinsic force for elevation and bending of the neural folds (Alvarez and Schoenwolf, 1992). Part of this force has been ascribed to an increase in width of the epidermal ectoderm cells by their conversion from a low cuboidal shape to a squamous shape during neurulation, and the medial migration of these cells (Schoenwolf and Alvarez, 1991). An additional contribution comes from the preferential rostrocaudal and transverse orientation of the mitotic spindles of the epidermal ectoderm cells (Sausedo et al, 1997). The transversely oriented mitotic spindles result in the medial localisation of daughter cells, which help to elevate and converge the neural folds.

The growth in length of the embryo that occurs during neurulation has been suggested to exert a stretch force on the neural plate along its

longitudinal axis. This could then lead to dorsal buckling of the neural plate, giving rise to elevation of the neural folds (Jacobson and Gordon, 1976).

#### 1.3.4.3 Combination of forces

Evidence for the importance of the intrinsic forces comes from the observation that non-neural tissues appear not to be essential for wedging of the cells in the median hinge point and formation of the neural groove in the chick embryo. These two events are not aborted by isolation of the neural plate from the lateral tissues (Schoenwolf, 1988). In addition, the posterior neuropore is able to close normally in mouse neural tube explants, where the neuroepithelium has been separated from all adjacent non-neural tissues (van Straaten et al, 1993). These results suggest that intrinsic forces are sufficient for neurulation to occur.

On the other hand, other studies have pointed to the requirement for extrinsic forces in neurulation. When the neural plate is isolated from the more lateral tissues, the lateral edges of the neural plate fail to elevate and converge (Schoenwolf, 1988). Furthermore, when the median hinge point, underlying notochord, and some of the lateral neuroepithelial cells are removed, the neural folds still undergo elevation, convergence and fusion (Smith and Schoenwolf, 1991). Thus, the median hinge point appears to be neither essential nor sufficient for neural fold elevation and convergence. The surface ectoderm appears to be necessary for bending of the neural plate (Alvarez and Schoenwolf, 1992; Hackett et al, 1997). Neural fold

elevation and convergence continue to occur, even when the underlying mesoderm, endoderm and extracellular matrix have been removed.

It is likely that both intrinsic and extrinsic forces contribute to closure of the neural tube, and that different mechanisms are important at different axial levels. The histology of the neural plate and underlying tissues varies along the longitudinal axis of the embryo (Morriss-Kay, 1981; Shum and Copp, 1996). A difference exists between the sexes in the incidence of cranial versus caudal neural tube defects. Females are more prone to exencephaly, whereas the incidence of spina bifida is roughly equal between the two sexes (Copp et al, 1990). Different mutations in the mouse give rise to cranial and/or caudal neural tube defects (Copp et al, 1990; Harris and Juriloff, 1997; Juriloff and Harris, 2000). Experimental disruption of neurulation has differential effects on cranial versus spinal neural tube closure (Morriss-Kay and Tuckett, 1985; Ybot-Gonzalez and Copp, 1999). Furthermore, qualitatively, *de novo* closure requires the establishment of a new set of conditions, wherein previously separated neural folds are brought towards each other. On the other hand, continuation of closure and neuropore closure occur at sites where the adjacent neural folds have already been brought together. Thus, only a duplication of the pre-existing conditions in these adjacent tissues is required.

### 1.3.5 Developmental events associated with neurulation

Neurulation occurs at a time when other developmental events are happening in adjacent tissues, and these could affect closure of the

neural tube. These other developmental events include bending of the longitudinal axis of the embryo, and the development of the gut and the neural crest.

During neurulation, the development of the cranial flexure brings the longitudinal axis of the forebrain to lie perpendicularly to the axis of the neural tube. This ventral curvature might oppose the dorsal elevation of the neural folds and account for the relatively late closure of the neural tube fold in the midbrain region (Jacobson and Tam, 1982). Closure of the posterior neuropore can similarly be delayed by excessive ventral curvature of the longitudinal body axis (Copp et al, 1988a; Brook et al, 1991).

The developing gut is located ventral to the neural plate. During the initial stages of cranial neurulation, the foregut invagination lies beneath the cranial neural folds. However, this relationship between the forebrain and foregut is lost with development of the cranial flexure. On the other hand, the hindgut invagination is closely associated with the spinal neural plate throughout development, the two being separated only by the notochord. This close relationship between the hindgut and notochord is disrupted only at the end of neurulation, when the paired dorsal aortae come to lie between the two structures. Thus, a defect in gut development might lead to a secondary effect on neural tube closure (Copp et al, 1988a; Brook et al, 1991). This is seen in the *curly tail* (*ct*) mouse mutant, where abnormal proliferation of the gut endoderm results in the development of spina bifida (see later).

The neural crest cells are derived from cells lying at the boundary between the neural plate and surface ectoderm. In the cranial region,

these cells start to emigrate after initial bulging of the neural plate has occurred, before the neural folds have fused. Emigration of the cranial neural crest cells has been suggested to assist in medial bending of the cranial neural folds by increasing their flexibility (Morriss and New, 1979). Inhibition of cranial neural crest cell emigration from the neural epithelium is associated with a delay in, or failure of, cranial neural tube closure (Morriss and New, 1979; Morriss-Kay and Tuckett, 1989b). However, in the trunk region, the crest cells only begin to emigrate after neurulation is completed, when a cell-free space is detected over the dorsal surface of the neural tube (Erickson and Weston, 1983). Hence, emigration of neural crest cells probably does not play an important role in neural tube closure in this region.

### *1.3.6 Glycosaminoglycans and neurulation*

Both sulphated (heparan sulphate and chondroitin sulphate) and non-sulphated (hyaluronan) glycosaminoglycans are found in the region of the developing neural tube (Solursh and Morriss, 1977; Morriss and Solursh, 1978; Morriss-Kay et al, 1986; O'Shea, 1987; Copp and Bernfield, 1988a; Morriss-Kay and Tuckett, 1989b). These molecules are located in the mesodermal extracellular matrix, in the neuroepithelial basement membrane, as well as around the notochord. They have been implicated in the expansion of the mesodermal extracellular spaces during cranial neurulation (Morriss-Kay et al, 1986). Furthermore, chondroitin sulphate appears to be necessary for the emigration of the cranial neural crest cells (Morriss-Kay and Tuckett, 1989b).

Neurulation defects have been observed when the synthesis of heparan sulphate proteoglycan is disrupted, or when heparan sulphate is degraded. The chemical β-D-xyloside acts as a substitute for the core protein linkage region in proteoglycan biosynthesis. In its presence, glycosaminoglycans chains are attached to this chemical instead of the proteoglycan core protein, resulting in the production of free glycosaminoglycan chains. This drug has been used to demonstrate the requirement for proteoglycans in conversion of the convex cranial neural folds to a concave morphology in cultured rat embryos (Morriss-Kay and Crutch, 1982). Failure of cranial neural tube closure has been reported with heparitinase treatment in cultured rat embryos (Tuckett and Morriss-Kay, 1989a). Degradation of heparan sulphate by this enzyme prevents the convex cranial folds from becoming concave in shape. Failure of cranial neural tube closure is also seen when either β-D-xyloside or sodium chlorate is administered to pregnant female mice intraperitoneally (Kubota et al, 1999). Chlorate inhibits the sulphation of glycosaminoglycans by competitively blocking the synthesis of the sulphate donor, 3'-phosphoadenosine 5'-phosphosulphate. The presence of cranial neural tube defects in the chlorate-treated group of mice suggests that sulphation of heparan sulphate is important for cranial neural tube closure.

Chondroitin sulphate and hyaluronan have been shown to regulate the speed of neural tube closure, although they may not be essential for closure to occur. Degradation of chondroitin sulphate by chondroitinase treatment retarded, but did not prevent, cranial neurulation (Morriss-Kay and Tuckett, 1989b). This effect has been attributed to the reduced emigration of neural crest cells from the cranial neural folds, which helps in medial bending of the neural folds.

Similarly, cranial neural tube closure is delayed, but not inhibited, after degradation of hyaluronan by *Streptomyces* hyaluronidase (Morriss-Kay et al, 1986). Hyaluronidase treatment is associated with reduction in cell number and prolongation of cell cycle time in the cranial mesenchyme and, to a lesser extent, the neuroepithelium. The result suggests that expansion of the cranial mesenchyme by deposition of hyaluronan is not essential for cranial neural tube closure. This conclusion is supported by examination of the phenotype of the hyaluronan synthase-2 null mouse. These mice show a lack of hyaluronan, are smaller than wild type embryos, and exhibit severe cardiac and vascular abnormalities. However, no neural tube defects have been reported and, from the published figures, the cranial neural folds appear to have fused by E9.5 (Camenisch et al, 2000). Double homozygous null mutants for both hyaluronan synthase-1 and 3 have also been reported to be viable and fertile (Camenisch et al, 2000).

The *splotch* mouse mutant has a mutation of the *Pax-3* gene. The phenotype of the homozygous embryos includes cranial and caudal neural tube defects, a deficiency of neural crest derivatives, and other abnormalities (see later). Elevated levels of chondroitin sulphate proteoglycans have been reported in this mutant. This has been postulated to lead to defective neural crest migration, resulting in a lack of neural crest derivatives (Trasler and Morriss-Kay, 1991; Henderson et al, 1997). However, the part played by excess chondroitin sulphate in development of the neural tube defect is unclear.

The *curly tail* mouse mutant is prone to develop tail flexion defects and spina bifida due to reduced proliferation of the gut endoderm. The mutant has a lower amount of hyaluronan in the neuroepithelial

basement membrane and around the notochord in the region of the posterior neuropore (Copp and Bernfield, 1988b). However, it is not clear if this is responsible for the reduced cellular proliferation or if it is a secondary effect.

### 1.3.7 Neural tube defects

Neural tube defects result from either the failure of neural tube closure or the re-opening of a previously closed neural tube. This leads to persistent exposure of the central canal of the nervous system to the external environment. Such exposure of nervous tissues to the amniotic fluid *in utero* results in their degeneration and to a disruption in the formation of the overlying bony cover.

Neural tube defects can be classified according to their location along the neuraxis, and this helps to suggest which aberrant neurulation mechanisms have led to the development of these defects (Copp et al, 1990; van Allen et al, 1993). Neural tube defect which begins in the caudal part of the midbrain and extends along the entire spine, or exencephaly which specifically affects the midbrain and also variably the forebrain and hindbrain, arises from a failure of *de novo* initiation of closure. Failure of continuation of closure is seen in exencephaly specifically affecting the hindbrain and variably involving the caudal part of the midbrain. Lumbosacral spina bifida is a result of failure of completion of closure of the posterior neuropore. Failure of more than one mechanism of neural tube closure may occur at the same time. For example, the *splotch* mouse mutant has both a hindbrain defect and spina bifida. The hindbrain defect is a result of failure of continuation of closure into the hindbrain from the cervical region where *de novo*

initiation of closure has occurred. The spina bifida is a result of failure of closure of the posterior neuropore.

#### 1.3.7.1 Mouse mutants with neural tube defects

A large number of mouse mutants with neural tube defects are known (Copp et al, 1990; Harris and Juriloff, 1997; Juriloff and Harris, 2000). The means by which these defects arise in some mutants have been discovered, and these have shed light on the normal mechanism of neurulation. However, in many other mutants, the aberrant developmental pathways that result in neural tube defects are not well understood. Some of these mutants are discussed below and summarised in Table 1.4.

The *curly tail* (*ct*) mouse mutant illustrates the effects that abnormal growth of the hindgut and excessive ventral curvature of the tail bud have on closure of the neural tube. Homozygous *curly tail* mouse mutants are prone to develop tail flexion defects. Lumbosacral spina bifida is seen in 15 – 20% of the embryos (Embury et al, 1979; Copp et al, 1982). These abnormalities are related to a delay in neural tube closure at the posterior neuropore. A moderate delay results in development of the tail flexion defect, and a severe delay causes spina bifida. The primary defect is not in the neural folds themselves, but in the reduced rate of cell proliferation in the gut endoderm and notochord. Proliferation in the neuroepithelium and the mesoderm is normal (Copp et al, 1988b). This imbalance of cell proliferation results in an increase in ventral curvature in the region of the posterior neuropore. This interferes with apposition of the neural folds and retards closure of the

## Table 1.4. Mouse mutants with neural tube defects

| MUTANT | GENE | PROTEIN FUNCTION | NTD[a] | REF[b] |
|---|---|---|---|---|
| Bent tail | *Zic3* | Transcription factor | EX + SB | 1 |
| Curly tail | *ct* | Unknown | EX + SB | 2 |
| Fibroblast growth factor receptor-1 | *Fgfr-1* | Receptor tyrosine kinase | SB | 3 |
| Laminin α5 | *Lama5* | Basement membrane component | EX | 4 |
| MARCKS-like protein | *Mlp* | Actin regulator | EX + SB | 5 |
| Myristoylated, alanine-rich C kinase substrate | *Macs* | Actin regulator | EX | 6 |
| Shroom | *Shrm* | Actin-binding protein | EX + SB | 7 |
| Splotch | *Pax-3* | Transcription factor | EX + SB | 8 |
| Vacuolated lens | *vl* | Unknown | SB | 9 |
| Zic2 | *Zic2* | Transcription factor | EX + SB | 10 |

[a]EX, exencephaly; NTD, neural tube defect; SB, spina bifida

[b]References: 1, Johnson, 1976; Klootwijk et al, 2000; Carrel et al, 2000; 2, Embury et al, 1979; 3, Deng et al, 1997; Xu et al, 1999; 4, Miner et al, 1998; 5, Chen et al, 1996; Wu et al, 1996; 6, Stumpo et al, 1995; Blackshear et al, 1996; 7, Hildebrand and Soriano, 1999; 8, Auerbach, 1954; Epstein et al, 1991; 9, Wilson and Wyatt, 1986; 10, Nagai et al, 2000.

posterior neuropore (Peeters et al, 1996; Peeters et al, 1998). The incidence of spina bifida in this mutant can be reduced by mechanically correcting the abnormal ventral curvature of the tail bud, retarding growth of the neuroepithelium, or treatment with retinoic acid at low dose (Seller and Perkins, 1982; Copp et al, 1988a; Brook et al, 1991; Chen et al, 1994). Analysis of *curly tail* mouse mutants by *in situ* hybridisation has shown deficiencies in transcripts of Wnt-5a and the retinoic acid receptors RAR-$\beta$ and RAR-$\gamma$ (Chen et al, 1995; Gofflot et al, 1998).

The importance of the basal lamina in neurulation is suggested by mouse embryos with a mutation in *Lama5*, the gene coding for $\alpha_5$ laminin (Miner et al, 1998). $\alpha_5$ laminin is expressed in the neuroepithelial and surface ectodermal basement membrane. In homozygous mutant embryos, the basal lamina of the medial strip of surface ectoderm bordering the cranial neural folds is thin and patchy, and the neural tube often fails to close, resulting in exencephaly in 60% of these embryos (Miner et al, 1998). It has been suggested that this medial strip of surface ectoderm is essential for neural fold elevation (Hackett et al, 1997). Thus, absence of $\alpha_5$ laminin in the surface ectodermal basal lamina could weaken the extrinsic force needed for elevation of the cranial neural folds (Miner et al, 1998). An alternative explanation is that the ability of the surface ectoderm to induce formation of the paired dorsolateral hinge points, which help to bring the neural fold apices together in the dorsal midline, is affected in the mutant embryo (see earlier).

Actin-related mouse mutants with neural tube defects support the *in vitro* finding of an essential role for actin in neurulation (Morriss-Kay and

Tuckett, 1985; Ybot-Gonzalez and Copp, 1999). The MARCKS (myristoylated, alanine-rich C kinase substrate) protein, encoded by the *Macs* gene, is found on the inside of the cell membrane. It is phosphorylated by activated protein kinase C and cross-links actin when unphosphorylated. Thus, it regulates the arrangement of actin molecules at the cell membrane (Blackshear et al, 1996). Cranial neural tube defects occur when *Macs* is disrupted (Stumpo et al, 1995; Blackshear et al, 1996). A similar role is played by Mlp (MARCKS-like protein, also known as MARCKS-related protein, MacMARCKS and F52) in which the knockout yields both exencephaly and spina bifida (Chen et al, 1996; Wu et al, 1996). Exencephaly and spina bifida are also seen in the *shroom* (*shrm*) mouse mutant (Hildebrand and Soriano, 1999). Shroom is a PDZ (postsynaptic density protein, disc-large, zonulin-1) domain-containing actin-binding protein that is localised to adherens junctions and the cytoskeleton and is involved in organisation of the cytoskeleton. The PDZ domain in PDZ proteins are involved in coupling of the syndecan family of heparan sulphate proteoglycans to the cytoskeleton (Grootjans et al, 1997). Abnormalities in actin microfilaments have also been reported in the *vacuolated lens* (*vl*) mouse mutant (Wilson and Wyatt, 1986; Wilson and Wyatt, 1992). Spina bifida and curling of the tail are seen in this mutant. The *vl* gene product is unknown, but ultrastructural examination of the of the caudal neuroepithelium shows that actin microfilaments are less prominent and more delicate in the mutants (Wilson and Wyatt, 1992). Other abnormalities reported in the *vl* mouse mutant include an excessively wide ventral angle in the midline of the neuroepithelium and surface blebs in the neural fold apices at the transition zone between the surface ectoderm and neuroepithelium (Wilson and Wyatt, 1988; Wilson and Wyatt, 1992).

Cranial and caudal neural tube defects and deficiencies of neural crest derivatives have been reported in the *splotch* mouse mutant (Auerbach, 1954). The mutation involves the *Pax-3* gene, which encodes a transcription factor containing both a homeodomain and a paired motif (Epstein et al, 1991). Elevated chondroitin sulphate proteoglycan content has been reported in the *splotch* mutant, and this has been suggested to contribute to the neural crest abnormalities (Trasler and Morriss-Kay, 1991; Henderson et al, 1997). Over-expression of heparan sulphate proteoglycans and transcripts of *N-cadherin* has also been detected, and N-CAM is abnormally glycosylated, in the mutant (O'Shea and Liu, 1987; Trasler and Morriss-Kay, 1991; Moase and Trasler, 1991; Neale and Trasler, 1994; Bennett et al, 1998). In addition, the cells of the neuroepithelium are loosely packed, and there is an increase in the number of gap junction vesicles (Wilson and Finta, 1979; Yang and Trasler, 1988). The neural tube defects can be prevented by supplementation with either thymidine or folate, which is involved in thymidine biosynthesis (Fleming and Copp, 1998). However, the mechanism by which the *Pax-3* mutation leads to neural tube defects, the role of abnormal amounts of heparan sulphate and chondroitin sulphate proteoglycans in the pathogenesis of these defects, and how folate supplementation reduces the incidence of these defects are unclear.

Fibroblast growth factor receptor-1 (FGFR-1) has been shown to be essential for spinal neurulation (Deng et al, 1997). FGFR-1 is a transmembrane tyrosine kinase with immunoglobulin-like domains that functions as a high affinity receptor for fibroblast growth factors. Alternative splicing results in the generation of several isoforms. The ligand-receptor interaction is facilitated by heparan sulphate, leading to

dimerisation and mutual tyrosine phosphorylation of these receptors (Spivak et al, 1994; Schlessinger et al, 1995). Homozygous mice with disrupted *Fgfr-1* gene die by E9.5 with severe growth retardation and defective mesodermal patterning (Deng et al, 1994; Yamaguchi et al, 1994). On the other hand, low degree chimeras generated by seeding wild type blastocysts with FGFR-$1^{-/-}$ cells can complete gastrulation and develop to adulthood (Deng et al, 1997). Spina bifida and tail distortion have been reported in these chimeras. Spina bifida is also seen in embryos deficient in the FGFR-1$\alpha$ isoform, where three immunoglobulin-like domains are present (Xu et al, 1999). The primary defect in FGFR-1$\alpha$-deficient embryos is a failure of axial mesoderm cell migration toward the posterior portions of the embryos during gastrulation.

The mouse *Zic* gene family encodes a group of zinc finger transcription factors and appears to be involved in regulating neurulation. *Zic* genes are homologous to the *Drosophila* pair-rule segmentation gene *odd-paired*, which is required for activation of *engrailed* and *wingless* in *Drosophila* embryos (Aruga et al, 1996). Reduced expression of mouse *Zic2* results in a delay in neurulation, leading to exencephaly and spina bifida (Nagai et al, 2000). Deletion of the *Zic3* locus is found in the *Bent tail* mouse mutant (Johnson, 1976; Klootwijk et al, 2000; Carrel et al, 2000). This X-linked mutation leads to short kinked tails and occasional exencephaly and sacral neural tube defects.

## 1.4 Neural crest

The neural crest arises at the dorsal tips of the neural folds. The cells originate from multipotent ectodermal cells located between the neural plate medially and the surface ectoderm laterally, in the region described as the transition zone (Geelen and Langman, 1979). During embryonic development, these cells undergo epitheliomesenchymal transformation, detach from their epithelial location, and migrate extensively in both ventral and lateral directions. They give rise to the spinal ganglia, the cranial ganglia of cranial nerves V, VII, IX and X, the autonomic nervous system, and Schwann cells and supporting cells of the peripheral nervous system. Other derivatives include pigment cells, the adrenal medulla and the endocardial cushions of the cardiac outflow tract. The cranial neural crest contributes to the bones of the skull and the connective tissues of the head and neck regions (Le Douarin and Kalcheim, 1999).

### *1.4.1 Neural crest cell migration*

In the mouse, migration of the cranial neural crest begins after the initial bulging of the neural plate has occurred, before the neural folds have fused, and this has been suggested to assist in medial bending of the neural folds (Morriss-Kay and Tuckett, 1989b). The neural crest cells migrate along different pathways, depending on their ultimate fates. Neural crest cells that migrate in the subectodermal region give rise to the cranial and hypobranchial skeleton. Cardiac neural crest cells, which arise from the post-otic to the third somite level, follow the path taken by the aortic arches to contribute to the aorto-pulmonary septum

in the cardiac outflow tract. Ventromedially migrating neural crest cells give rise to the enteric innervation of the pharynx and foregut, and ventrally migrating cells form the cranial sensory and superior cervical ganglia. The melanocyte precursors take a dorsolateral path. In the hindbrain region, neural crest cells emerge along the dorsal midline of all the rhombomeres, but they avoid the regions lateral to r3 and r5. Some of the neural crest cells that emigrate from r3 and r5 travel either rostrally or caudally to join other cells that exit from r2, r4 and r6, while other cells undergo apoptosis (Graham et al, 1993; Graham et al, 1994; Kulesa and Fraser, 1998).

In the trunk, neural crest cells only begin to migrate after the neural folds have fused, when a cell-free space appears between the dorsal surface of the neural tube and the overlying surface ectoderm (Erickson and Weston, 1983). Crest cells that migrate along a ventral pathway between the neural tube and the somites give rise to the sensory and sympathetic ganglia and Schwann cells. The melanocyte precursors take a dorsolateral path.

Migration of the neural crest cells is linked to the development of the somites (Loring and Erickson, 1987). In the caudal region of the embryo, before the somites are formed, the neural crest cells are found in the neuroepithelium. More rostrally, where epithelial somites have formed, the crest cells start to emigrate from the neuroepithelium and enter the dorsolateral space between the neural tube and the somite. Even further rostrally, where the somites have begun to undergo epitheliomesenchymal conversion, the crest cells either migrate ventrally towards the aorta or pass through the rostral half of the somites (Rickmann et al, 1985). Neural crest cells appear to avoid the

caudal somitic half, and so do motor axons. This segmented migration pattern leads to the metameric arrangement of the dorsal root ganglia, sympathetic ganglia, peripheral nerves and accompanying Schwann cells.

### 1.4.2 Guidance of neural crest migration

The migration of neural crest cells is regulated by the environment through which they pass. When somites are rotated about their rostrocaudal axis, migrating neural crest cells continue to avoid the previously caudal somitic halves, suggesting an autonomous distinction between anterior and posterior somitic 'compartments' (Stern et al, 1991). The direction of migration of neural crest cells follows the orientation of the extracellular matrix fibrils. A change in the orientation of these fibrils results in a corresponding change in the direction of migration (Newgreen, 1989). In addition, neural crest cells from the sacral axial level migrate into the mesentery to populate the gut, while crest cells from the thoracic level do not. When crest cells are heterotopically grafted from the sacral level to the thoracic level and vice versa, the migratory behaviour of the cells adapts to the new position (Erickson and Goins, 2000). On the other hand, ectopically transplanted notochord fragments inhibit crest cell migration in the chick embryo (Pettway et al, 1990). This inhibitory property is temporally regulated. Segmental plate mesoderm is also inhibitory to crest cell migration, but this effect is lost once the paraxial mesoderm differentiates into sclerotome (Bronner-Fraser and Stern, 1991).

### 1.4.2.1 Permissive molecules

The extracellular matrix contains numerous permissive molecules for neural crest cell migration. These are expressed along the neural crest migratory pathways and extensively support neural crest cell attachment and migration.

#### *1.4.2.1.1 Fibronectin, laminin, collagen and integrin*

Fibronectin is a glycoprotein that permits neural crest cell migration. It is expressed along the migratory pathway of neural crest cells, and migration has been observed to stop when fibronectin is no longer present (Thiery et al, 1982a; Duband et al, 1986). *In vitro*, fibronectin promotes cell attachment and dispersion (Rovasio et al, 1983; Rogers et al, 1990). Application of a blocking anti-fibronectin antibody results in abnormal neural crest migration (Poole and Thiery, 1986). Laminin and collagen types I, III, IV and VI also permit migration of neural crest cells. Like fibronectin, these molecules are expressed along the neural crest migratory pathways (Newgreen and Thiery, 1980; Tuckett and Morriss-Kay, 1986; Krotoski et al, 1986; Sternberg and Kimber, 1986; Perris, 1997). *In vitro*, they are able to mediate crest cell migration (Greenberg et al, 1981; Newgreen, 1984; Perris et al, 1989; Lallier and Bronner-Fraser, 1991; Perris et al, 1991a). Laminin at low concentration promotes neural crest migration, while at high concentration it inhibits migration (Perris et al, 1989). Micromembranes coated with laminin trigger premature neural crest migration when implanted into axolotl embryos (Olsson et al, 1996; Perris and Perissinotto, 2000).

Neural crest cells express integrin receptors, which enable the cells to recognise the above permissive molecules. Integrins bind fibronectin, laminin and other components of the extracellular matrix (Lallier and Bronner-Fraser, 1991; Perris et al, 1993a; Perris et al, 1993b). Using blocking antibodies and antisense oligonucleotides, the importance of integrins in neural crest cell migration has been demonstrated. $\beta_1$ integrin binds fibronectin, laminin and collagen. The attachment of cranial and trunk neural crest cells to these molecules is abolished by an antibody that blocks $\beta_1$ integrin function *in vitro*. In contrast, neutralisation of $\alpha_1$ integrin inhibits the attachment of trunk, but not cranial, neural crest cells to laminin and collagen type I. A blocking antibody against mouse integrin $\alpha_4$ subunit severely inhibits murine neural crest cell emigration and migration at the trunk and hindbrain levels *in vitro* (Kil et al, 1998). However, the segmental pattern of migration is unaffected. Cranial crest cell migration is also affected by injecting avian embryos with a synthetic peptide that contains the integrin $\alpha_4$ binding site in fibronectin (Kil et al, 1998). Furthermore, antisense oligonucleotides to integrins inhibit cranial neural crest cell migration in the chick embryo (Kil et al, 1996; Kil et al, 1998). Thus, different integrin heterodimers may be needed for the interaction of trunk and cranial neural crest cells with the extracellular matrix.

Embryos may only be sensitive to disturbances in the levels of integrin for a limited time during development. Blocking antibodies applied before the 10-somite stage result in neural crest migratory defects. No such defects are seen when the injection is made at a later stage (Bronner-Fraser, 1985; Bronner-Fraser, 1986). However, no abnormalities in cell migration and ganglion formation have been reported in null mutations for integrin in the mouse embryo (Yang et al,

1995; Perris, 1997). One possible reason could be functional compensation by other integrin subunits.

#### *1.4.2.1.2 Thrombospondin-1*

Recently, thrombospondin-1 has been proposed to act as an attractive factor in neural crest cell migration (Tucker et al, 1999). The thrombospondins are a family of multimeric, calcium-binding extracellular glycoproteins. They contain domains that are capable of binding heparan sulphate and other glycosaminoglycans. In the avian embryo, thrombospondin-1 is found along pathways taken by migrating neural crest cells. Using immunohistochemistry, ventrally migrating neural crest cells are seen to lie in an anti-thrombospondin-1 labelled matrix, with little or no immunoreactivity in the caudal sclerotome. The *in situ* hybridisation signal is located in the rostral somitic halves and not in the neural crest cells, suggesting that the thrombospondin-1-containing matrix is synthesised by the somites themselves. Thrombospondin-1 mRNA is detected both before and during neural crest migration. *In vitro*, somite-derived thrombospondin-1 is able to stimulate neural crest cell migration. Similar numbers of neural crest cells are attached to culture dishes coated with either thrombospondin-1 or fibronectin.

### 1.4.2.2 Non-permissive molecules

Neural crest cells migrate only in the rostral half of somites. However, except for thrombospondin-1, the other permissive molecules discussed above are not differentially distributed in the somites. In contrast, non-permissive molecules are found in regions avoided by migrating neural

crest cells, whereas they are scarce or absent along the migratory pathways. These molecules do not sustain significant neural crest cell attachment or movement, and may directly impede migration of these cells. Thus, the possibility is raised that these non-permissive molecules might inhibit neural crest migration *in vivo*. It has been postulated that these molecules help to set up barriers to neural crest migration in the caudal somitic halves and other tissues avoided by migrating neural crest cells.

#### *1.4.2.2.1 Chondroitin sulphate proteoglycans*

Chondroitin sulphate is a non-permissive molecule to neural crest migration (Oakley and Tosney, 1991; Oakley et al, 1994; Pettway et al, 1996). The molecule is initially distributed homogeneously along the entire somite. However, with the onset of neural crest migration, chondroitin sulphate becomes localised to the caudal sclerotome and dermamyotome (Perris et al, 1991b; Oakley et al, 1994). The chondroitin sulphate proteoglycans aggrecan, collagen IX and versican are all present at the time of neural crest cell migration (Ring et al, 1996; Perissinotto et al, 2000). When immobilised on culture dishes, these molecules do not support the attachment and spreading of neural crest cells, and counteract the migration-promoting activities of other matrix components (Landolt et al, 1995; Perris et al, 1996). Other highly negatively charged chondroitin sulphate proteoglycans have also been isolated from avian embryos (Kerr and Newgreen, 1997). These molecules carry chondroitin sulphate chains, and lack heparan sulphate, keratan sulphate and dermatan sulphate chains. They have physicochemical properties that differ from aggrecan and versican. *In vitro*, these chondroitin sulphate proteoglycans are more efficient in

inhibiting neural crest cell migration than aggrecan. The inhibitory effect is abolished by chondroitinase treatment.

Aggrecan is the primary chondroitin sulphate proteoglycan produced by the notochord. It is largely restricted to the perinotochordal extracellular matrix (Domowicz et al, 1995; Perissinotto et al, 2000). Deposition of aggrecan in the extracellular matrix is spatiotemporally regulated in a metameric pattern that alternates with the segmental distribution of the peripheral sensory ganglia. *In vitro*, aggrecan strongly interferes with neural crest migration on a number of motility-promoting substrates. This interference is abolished by degradation of chondroitin sulphate by either chondroitinase or testicular hyaluronidase, but not by *Streptomyces* hyaluronidase which degrades hyaluronan specifically (Newgreen et al, 1986). In addition, soluble aggrecan is able to block emigration of neural crest cells from the neural tube in a dose-dependent manner (Perris et al, 1996). *In vivo*, chick neural crest cells avoid an ectopically implanted quail notochord isolated using collagenase. However, this effect is reduced when the notochord is isolated using either trypsin or chondroitinase, suggesting that a chondroitin sulphate proteoglycan is responsible for the migration inhibitory activity (Pettway et al, 1990). Implantation of micromembranes coated with purified aggrecan into various regions of the chick embryo causes neural crest cells to stop migrating at the site of the implant (Perissinotto et al, 2000).

Collagen IX is synthesised by sclerotome cells and the notochord (Ring et al, 1996). It is immunohistochemically localised to the caudal sclerotome and other tissues avoided by migrating neural crest cells. *In vitro*, collagen IX is avoided by chick neural crest cells in stripe assays.

This avoidance is abolished by chondroitinase treatment, suggesting that the effect is mediated by chondroitin sulphate. Although the expression of collagen IX in the posterior sclerotome does not precede invasion of the somites by neural crest cells, the molecule might contribute to the inhibitory nature of this tissue.

Versican is initially distributed throughout the somite. With the onset of neural crest migration, it becomes restricted to the caudal sclerotome, early subectodermal tissues and perinotochordal mesenchyme (Landolt et al, 1995; Perris et al, 1996; Perissinotto et al, 2000). The $V_0$ and $V_1$ isoforms of versican are the prevalent versican variants present at this time. These isoforms are transcribed by tissues that line the neural crest migratory pathways and by tissues that delimit the non-permissive areas. *In vitro*, immobilised versican does not support the attachment and migration of neural crest cells and inhibits cellular interactions with fibronectin, laminin and collagen I (Yamagata et al, 1989). Thus, it has been previously postulated that versican, like other chondroitin sulphate proteoglycans, functions as a non-permissive molecule and helps to set up a barrier to neural crest migration.

However, this hypothesis has been challenged by recent studies (Perris and Perissinotto, 2000; Perissinotto et al, 2000). The redistribution of versican to the caudal sclerotome appears to be dependent on migration of neural crest cells through the rostral sclerotome and is abolished when the neural crest cells are removed. Three-dimensional reconstruction of versican distribution shows that migrating neural crest cells travel from regions that are relatively scarce in versican towards regions that are richer in this proteoglycan. *In vitro*, neural crest cells migrate along an increasing concentration of versican. This movement

is restricted when the gradient is reversed or when there is a sudden large change in versican concentration. In addition, chick neural crest cells migrate towards ectopically implanted versican *in vivo*. Orthotopic implantation of versican in axolotl embryos elicits precocious neural crest migration at the site of the graft. A lack of versican in the subectodermal region of the white axolotl mutant embryo is associated with failure of neural crest migration along the dorsolateral pathway (Stigson et al, 1997). Furthermore, the endocardial cushions of the cardiac outflow tract, which are populated by immigrating cardiac neural crest cells, are absent in mice where the *versican* gene has been disrupted (Mjaatvedt et al, 1998).

The degree of sulphation of chondroitin sulphate appears to help determine its efficiency in inhibiting neural crest cell migration (Newgreen et al, 1982). Chondroitin sulphate which is either highly or minimally sulphated is unable to retard neural crest migration. On the other hand, moderately sulphated chondroitin sulphate strongly retards neural crest migration. Thus, inhibition of sulphation of chondroitin sulphate by chlorate treatment results in migration of neural crest cells into regions that are normally avoided by them (Kubota et al, 1999). The segmental organisation of the dorsal root ganglia is lost, with ganglia appearing even in the most caudal level of the sclerotome. Immunostaining reveals an increase in the amount of non-sulphated chondroitin sulphate.

In summary, it appears that not all chondroitin sulphate proteoglycans are non-permissive to neural crest migration. Aggrecan, collagen IX, and other highly negatively charged chondroitin sulphate proteoglycans, which were isolated by Kerr and Newgreen (1997), are inhibitory to

neural crest migration. In contrast, versican appears to support neural crest migration. This difference could, at least partly, be due to a difference in the degree of sulphation of the chondroitin sulphate chains.

#### *1.4.2.2.2 F-spondin*

F-spondin is a secreted molecule containing thrombospondin-like repeats and regions that may be involved in binding to heparin and other glycosaminoglycans. The molecule is associated with the extracellular matrix. F-spondin mRNA is initially homogeneously distributed in the somites, but later becomes restricted to sites avoided by migrating neural crest cells, including the caudal half of the sclerotome, paranotochordal mesenchyme and dermamyotome. Addition of F-spondin to chick trunk explants results in a lack of crest cell migration into the sclerotome, whereas antibody neutralisation of the protein *in vivo* allows neural crest cells to migrate into otherwise inhibitory sites in the caudal somitic half (Debby-Brafman et al, 1999). Thus, F-spondin might mediate the migration inhibitory quality of the caudal somite.

#### *1.4.2.2.3 Collapsin-1*

Collapsin-1 (Sema III/Sema D) belongs to the Semaphorin family of molecules, several members of which have been implicated in the co-ordination of axon growth and guidance. Collapsin-1 has been shown to function as a selective chemorepellent for sensory neurons. It is expressed in regions bordering neural crest cell migratory pathways in both the trunk and hindbrain regions of the chick embryo, and is also selectively expressed in the caudal half of somites in the rat embryo

(Wright et al, 1995; Giger et al, 1996; Eickholt et al, 1999). Neuropilin-1, the receptor for collapsin-1, is expressed by migrating trunk and hindbrain neural crest cells. *In vitro*, collapsin-1 is avoided by explanted neural crest cells in stripe assays. However, disruption of either *collapsin-1* or *neuropilin-1* expression does not result in obvious defects in neural crest derivatives (Behar et al, 1996; Taniguchi et al, 1997; Kitsukawa et al, 1997).

#### *1.4.2.2.4 T-cadherin*

Truncated cadherin (T-cadherin) differs from known cadherins in not having cytoplasmic sequences that are highly conserved in other cadherins. T-cadherin is associated with the inhibitory pathway of neural crest migration. It is expressed in the caudal sclerotomal half, at the time when neural crest cells migrate into the rostral somitic half (Ranscht and Bronner-Fraser, 1991). Expression of T-cadherin in the caudal sclerotome is associated with an increase in cell density there. The increase occurs shortly after the initial expression of T-cadherin, and persists with somitic maturation. The metameric distribution of T-cadherin is not dependent on the presence of neural crest cells. T-cadherin inhibits neurite extension from spinal motor neurons and sympathetic neurons *in vitro*. Thus, it might act as an inhibitory substrate for neural crest migration. Alternatively, it might mechanically prevent neural crest migration by tight packing of the cells in the caudal sclerotome.

#### 1.4.2.2.5 Eph and ephrins

The Eph family of molecules has also been implicated in directing neural crest migration. The Eph family ligands are membrane bound molecules, and the Eph receptors are transmembrane receptor tyrosine kinases. In the rat embryo, EphB2 (Nuk receptor) is highly expressed in neural crest cells and the rostral sclerotome (Wang and Anderson, 1997). Complementary expression of the transmembrane ligands ephrin-B2 (HtkL) and ephrin-B1 (Lerk2) is found in the caudal somitic half and other regions avoided by migrating neural crest cells. Ephrin-B2 starts to be expressed just before neural crest cells migrate into the rostral somite. Crest cells avoid these ephrin ligands in stripe assays. However, the avoidance is not absolute, as migration can occur on a substrate that is uniformly coated with the ligand. Soluble ephrin-B1 is able to interfere with receptor function, thus allowing neural crest cells to migrate over stripes of ephrin-B1. Similarly, in whole trunk explants, soluble ephrin-B1 disrupts the metameric pattern of neural crest migration, resulting in the entry of neural crest cells into the caudal sclerotome (Krull et al, 1997). Thus, the ephrin-B proteins appear to act as repulsive cues to direct neural crest migration. However, trunk neural crest migration is normal in the ephrin-B2 null mouse (Wang et al, 1998).

#### 1.4.2.2.6 ErbB4

ErbB4, the neuregulin receptor, is a receptor tyrosine kinase. It helps to regulate branchial neural crest cell migration (Golding et al, 2000). ErbB4 is expressed in rhombomeres r3 and r5, and has not been detected in migrating neural crest cells, developing cranial ganglia or

cranial mesenchyme. In both the chick and mouse embryos, branchial neural crest cells migrate into the first three branchial arches in three streams that are separated by gaps adjacent to rhombomeres r3 and r5. Some of the neural crest cells that arise from r3 and r5 migrate either rostrally or caudally to join the streams of neural crest cells arising from r2, r4 and r6, while other cells undergo apoptosis (Graham et al, 1993; Graham et al, 1994; Kulesa and Fraser, 1998). Aberrant migration of crest cells into the paraxial mesoderm adjacent to r3 is seen in mouse embryos with a null mutation of ErbB4 (Golding et al, 2000). The effect is non-neural crest cell autonomous. Wild type neural crest cells have abnormal migratory behaviour when transplanted into the ErbB4 null mutant, whereas neural crest cells from the null mutant migrate normally when transplanted into a wild type embryo. Thus, ErbB4 appears to be indirectly needed to pattern the cranial mesoderm such that crest cells are excluded from the mesoderm adjacent to r3, perhaps by affecting the distribution of other permissive and/or non-permissive molecules.

#### 1.4.2.3 Multiple directional cues

In conclusion, it appears that the segmental patterning of neural crest cells and their derivatives require multiple directional cues (Table 1.5). Neural crest migration in the rostral somitic half occurs through a permissive mesenchyme lying between inhibitory areas in the dermamyotome and paranotochordal sclerotome. On the other hand, inhibitory signals help to set up barriers in regions avoided by the neural crest cells.

**Table 1.5 Permissive and non-permissive molecules in neural crest migration**

| PERMISSIVE MOLECULES | NON-PERMISSIVE MOLECULES |
|---|---|
| Fibronectin | Aggrecan |
| Laminin | Collagen IX |
| Collagen types I, III, IV, VI | Other highly negatively charged chondroitin sulphate proteoglycans |
| Thrombospondin-1 | F-spondin |
| Versican | Collapsin-1 |
| | T-cadherin |
| | Eph and ephrins |
| | ErbB4 (*indirect mode of action*) |

### 1.4.3 Mutations affecting the neural crest

Several animal mutants with an absence of neural crest derivatives have demonstrated the importance of glycosaminoglycans in regulating neural crest migration.

The white *Amblystoma mexicanum* mutant embryo has normally migrating neuronal precursors but the melanoblasts fail to disperse (Löfberg et al, 1989). When membranes covered with extracellular matrix material derived from the subectodermal space of normal embryos are grafted into equivalent sites of mutant embryos, neural crest cell migration is rescued along the lateral pathway. In contrast, grafting of membranes pre-coated with extracellular matrix from mutant embryos into wild type embryos results in failure of host neural crest cell migration. This inhibitory effect is stage dependent, suggesting that the defect in the extracellular matrix of the mutant embryo might be due to a transient delay in matrix maturation. The same approach has shown that the composition of the extracellular matrix of the ventral pathway is similar in both wild type and mutant embryos. The defect in the subectodermal extracellular matrix of the mutant appears to be a reduced level of the chondroitin sulphate proteoglycan versican (Stigson et al, 1997).

The *splotch* mouse mutant has a mutation in the *Pax-3* gene. Deficiencies of neural crest derivatives are seen in the mutant embryos, including reduced or absent dorsal root ganglia, diminished Schwann cell numbers, pigmentation defects, and a persistent truncus arteriosus that has been attributed to a failure of cardiac neural crest colonisation of the heart outflow tract (Chalepakis et al, 1993). Only a subset of

neural crest cells is affected, as the cranial skeleton is largely normal. An elevated amount of chondroitin sulphate has been detected in the homozygous embryos by immunohistochemistry (Trasler and Morriss-Kay, 1991). In addition, increased expression of *versican* mRNA has been found along the pathways of neural crest migration as well as in ectopic sites (Henderson and Copp, 1997; Henderson et al, 1997). It has been suggested that the excess chondroitin sulphate in the mutant embryo is responsible for the disruption of neural crest migration, leading to the absence of neural crest derivatives.

The gene for platelet-derived growth factor A receptor is deleted in the *patch* mouse mutant. This results in pigmentation abnormalities, fluid-filled blebs along the spinal cord and a persistent truncus arteriosus (Morrison-Graham and Weston, 1989; Morrison-Graham et al, 1992). Increased numbers of glycosaminoglycan-containing granules are found in the mutant embryos in the matrix between the myocardium and endocardium and in the fluid-filled blebs along the spinal cord. A profuse deposition of interstitial proteoglycans is also seen along the neural crest migratory routes. The accumulation occurs before the onset of neural crest migration, suggesting that it may contribute to the abnormalities rather than be a secondary effect.

Mutations of the *endothelin-3* and *endothelin-B receptor* genes are seen in the *lethal spotting* (*ls*/*ls*) and *piebald lethal* ($s^{l}$/$s^{l}$) mouse mutants respectively (Baynash et al, 1994; Hosoda et al, 1994). These mutants have pigmentation abnormalities and diminished innervation of the gut. An over-abundance of perlecan, proteoglycans and other extracellular matrix components is seen in the enteric basement membrane and gut mesenchyme of the aganglionic region (Payette et al, 1988; Tennyson

et al, 1990). This is postulated to be the cause of the absence of neural crest derivatives. In the *ls/ls* mouse embryos, neural crest cells do not colonise the terminal part of the gut, even when co-cultured with neural crest cell donor tissues (Morrison-Graham and Weston, 1989). The *endothelin-B receptor* gene is required between E10 and E12.5, implying that the gene product is needed for neural crest cell migration and/or survival (Shin et al, 1999).

## 1.5 Aims of the thesis

This thesis aims to study the roles played by the sulphated glycosaminoglycans, heparan sulphate and chondroitin sulphate, in the processes of neurulation and neural crest migration. The distribution of these molecules during neurulation in the region of the posterior neuropore is localised in Chapter 4 at the time of formation of the median and paired dorsolateral hinge points, using both Alcian blue histochemistry and immunohistochemical staining. The requirement for these molecules, and specifically for the sulphate group, in closure of the posterior neuropore is investigated in Chapter 5, using the method of whole embryo culture. Chapter 6 looks at the requirement for chondroitin sulphate in spinal neurulation. In Chapter 7, the part played by sulphated glycosaminoglycans in neurulation and neural crest migration is examined in the *splotch* ($Sp^{2H}$) mouse embryo. Finally, Chapter 8 summarises the major findings in this thesis and discusses the future direction of this project.

# *Chapter 2*

# MATERIALS

## 2.1 General reagents and equipment

All equipment and AnalaR grade reagents were supplied by BDH (Poole, Dorset, UK) except for those listed below. Sigma-Aldrich (Poole, Dorset, UK) provided the following: Bouin's fixative, bovine serum albumin (BSA), diethylpyrocarbonate (DEPC), dithiothreitol (DTT), ethidium bromide, foetal calf serum (FCS), formamide, hydrogen peroxide, Orange G, paraformaldehyde (PFA), sodium chlorate, tris(hydroxymethyl)aminomethane (Tris) and Tween-20.

## 2.2 Glycosaminoglycans

Sigma-Aldrich supplied the following glycosaminoglycans: Chondroitin-4-sulphate derived from bovine trachea, chondroitin-6-sulphate from shark cartilage, heparan sulphate from bovine kidney and hyaluronic acid from human umbilical cord. De-N- and de-O-sulphated heparan sulphate, prepared by chemical modification of heparan sulphate derived from bovine kidney, were obtained from Seikagaku (Chuo-ku, Tokyo, Japan).

## 2.3 Enzymes

Affinity purified protease-free chondroitinase ABC, derived from *Proteus vulgaris*, was purchased from Sigma-Aldrich. Seikagaku supplied heparitinase derived from *Flavobacterium heparinum*.

*Streptomyces* hyaluronidase and Pronase were obtained from Calbiochem-Novabiochem (Beeston, Nottingham, UK). Proteinase K was purchased from Sigma-Aldrich.

Promega (Southampton, Hampshire, UK) supplied all the restriction enzymes (*Bam*H I, *Eco*R I, *Hin*d III *and Pst* I), T3 and T7 RNA polymerases and RNasin ribonuclease inhibitor used. RNase A was obtained from Sigma-Aldrich while RNase-free DNase I was provided by Roche (Lewes, East Sussex, UK). *Taq* DNA polymerase was purchased from Qiagen (Crawley, West Sussex, UK).

## 2.4 Source of mice and rats

*CD1* and *splotch* ($Sp^{2H}$) mouse embryos were obtained from the respective mouse strains kept at the Western Laboratory (Institute of Child Health, London, UK). The mice were maintained in a 24-hour cycle period consisting of 12 hours of daylight and 12 hours of darkness. Female mice were mated with male mice overnight and the presence of copulation plugs was determined the following morning. Noon on the day of detecting a copulation plug was designated as embryonic day 0.5 (E0.5) of gestation.

Male Wistar rats used for the preparation of rat serum were also obtained from the Western Laboratory.

## 2.5 Micro-dissection

Micro-dissection was done using a Zeiss SV6 stereomicroscope (Carl Zeiss, Welwyn Garden City, Hertfordshire, UK). Dulbecco's modified Eagle's medium (DMEM), containing 25 mM HEPES and 4.5 g/l D-glucose, was supplied by Life Technologies (Paisley, UK). Scientific Laboratory Supplies (Wilford, Nottingham, UK) provided the fine-tipped Number 5 watchmaker's forceps.

## 2.6 Embryo culture

Mouse embryos were cultured in Universal tubes (Nunc, Rochester, NY, USA) using a roller incubator obtained from BTC Engineering (Milton, Cambridge, UK). CryoService (Worcester, UK) provided the gas mixtures for gassing the embryos.

## 2.7 Polymerase chain reaction

*Splotch* ($Sp^{2H}$) embryos were genotyped using the polymerase chain reaction (PCR) that was run on a PTC-100 Peltier Thermal Cycler (MJ Research, Waltham, MA, USA). PCR primers were custom synthesised by Sigma-Genosys (Pampisford, Cambridge, UK) using the sequences CCT CGG TAA GCT TCG CCC TCTG for *Pax-3b* and CAG CGC AGG AGC AGA ACC ACC TTC for *Pax-3c* (Epstein et al, 1991). Qiagen provided the deoxynucleoside triphosphate mixture.

## 2.8 Agarose gel electrophoresis

The Horizon 58 and Horizon 11-14 horizontal gel electrophoresis systems, the 11-14 gel casting system and agarose were all supplied by Life Technologies. The Apelex PS304 electrophoresis power supply was obtained from Apelex (Massy, France). The nucleic acid bands were visualised and photographed using the Alpha Imager 1200 Documentation & Analysis System (Flowgen, Ashby de la Zouch, Leicestershire, UK) running Version 3.3b of the associated AlphaEase software.

## 2.9 Molecular size markers

Hyperladder I from Bioline (London, UK) and pUC18 DNA *Msp* I digest from Sigma-Aldrich were used to size DNA. The 0.24 – 9.5 kb RNA ladder was obtained from Life Technologies.

## 2.10 Histological reagents and equipment

Glass staining troughs, racks and glass microscope slides were purchased from BDH. Raymond A Lamb (Eastbourne, East Sussex, UK) provided the glass cover slips and paraffin wax (melting point 57 - 58°C) as well as the Microm HM330 rotary microtome and disposable blades used for cutting the sections. Heraeus (Heraeus instruments, Brentwood, Essex, UK) provided the T6030 wax oven. HistoClear was obtained from National Diagnostics (Atlanta, GA, USA). Sigma-Aldrich provided the 3-aminopropyltriethoxysilane (TESPA) for coating the glass slides as well as all the histological stains (haematoxylin, eosin

and Alcian Blue 8GX) used. Slides were mounted in either dextropropoxyphene (DePX) from BDH or VectaMount from Vector (Burlingame, CA, USA).

## 2.11 Microscopy

Brightfield and phase contrast microscopy were performed on an Olympus BH2 microscope (Olympus, Southall, Middlesex, UK), using objective lenses of 4X, 10X and 20X magnification. Digital imaging was done with a Zeiss Kontron ProgRes 3012 digital camera (Imaging Associates, Thame, Oxon, UK) using Version 2.0 of the associated software. Large specimens were photographed on a Zeiss SV11 stereomicroscope using Kodak Ektachrome 64T colour reversal photographic film (Leeds Photovisual, London, UK). The images were processed using Adobe Photoshop Version 5.0 (Adobe Systems Europe, Edinburgh, UK).

## 2.12 Primary antibodies

Primary antibodies that were raised against the following antigens were used in this thesis.

### *2.12.1 Heparan sulphate*

The 10E4 mouse monoclonal IgM anti-heparan sulphate antibody (Seikagaku) is derived from a hybridoma formed from the fusion of mouse myeloma cells (SP2/O-Ag14) and spleen cells of a BALB/c mouse immunised against liposome-incorporated membrane heparan

sulphate proteoglycans (F58) from human foetal lung fibroblasts. The epitope, which is present in many types of heparan sulphate, includes an N-sulphated glucosamine residue that is critical for the reactivity of the antibody. The antibody does not react with hyaluronan, chondroitin sulphate, dermatan sulphate or DNA (David et al, 1992). Its reactivity with most heparan sulphate is almost completely abolished after heparitinase degradation of heparan sulphate. It is supplied at a concentration of 1.0 mg/ml.

### *2.12.2 Chondroitin sulphate*

The CS-56 mouse monoclonal IgM anti-chondroitin sulphate antibody (Sigma-Aldrich) is derived from a hybridoma produced by fusion of mouse myeloma cells and splenocytes from a mouse immunised using the ventral membranes of chicken gizzard fibroblasts. The antibody reacts specifically with chondroitin sulphate, and the reactivity is abolished after degradation of chondroitin sulphate using either chondroitinase ABC or chondroitinase AC (Avnur and Geiger, 1984). It is supplied at a concentration of 0.9 mg/ml.

## 2.13 Control antibodies

Monoclonal mouse IgM antibody (DAKO, Ely, Cambridgeshire, UK) raised against *Aspergillus niger* glucose oxidase (an enzyme neither present nor inducible in mammalian tissues) was used in the negative controls in immunohistochemistry.

## 2.14 Reagents for detection

Zymed (South San Francisco, CA, USA) provided the HistoMouse-SP kit for the detection of mouse primary antibodies on mouse tissue samples. Roche supplied the alkaline phosphatase-conjugated sheep anti-digoxigenin antibody, Fab fragment, for detection of digoxigenin-labelled riboprobes. The chromogen 3,3'-diaminobenzidine tetrahydrochloride (DAB) was purchased from Vector while nitroblue tetrazolium (NBT) and 5-bromo-4-chloro-3-indolyl phosphate (BCIP) were obtained from Roche.

## 2.15 Bacterial plasmids

The mouse *Patched* plasmid was kindly provided by M P Scott (Goodrich et al, 1996) and the *Sonic hedgehog* plasmid was obtained from A P McMahon (Echelard et al, 1993). The pBluescript vectors are shown in Figures 2.1 and 2.2. The restriction maps of the two plasmids are shown in Figures 2.3 and 2.4.

## 2.16 Transformation of bacteria

DH5$\alpha$ competent cells, Miller's LB Agar and LB Broth Base were obtained from Life Technologies. Ampicillin was purchased from Sigma-Aldrich. The cells were grown in the INFORS-HT RFI-125 incubator shaker (INFORS, Wigan, Lancashire, UK).

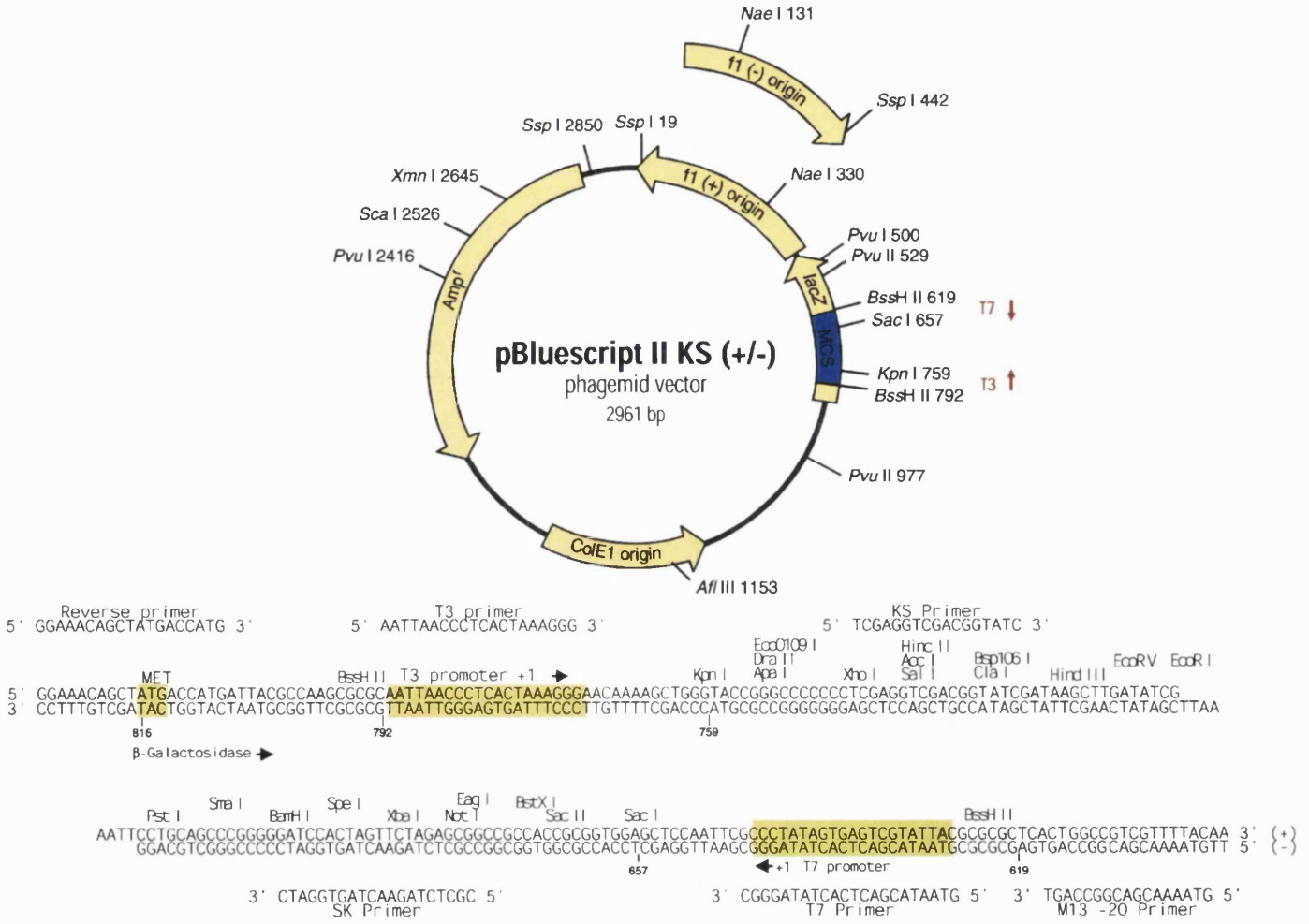


**Figure 2.1 Vector map of plasmid pBluescript II KS+.** Modified from Stratagene (La Jolla, CA, USA).

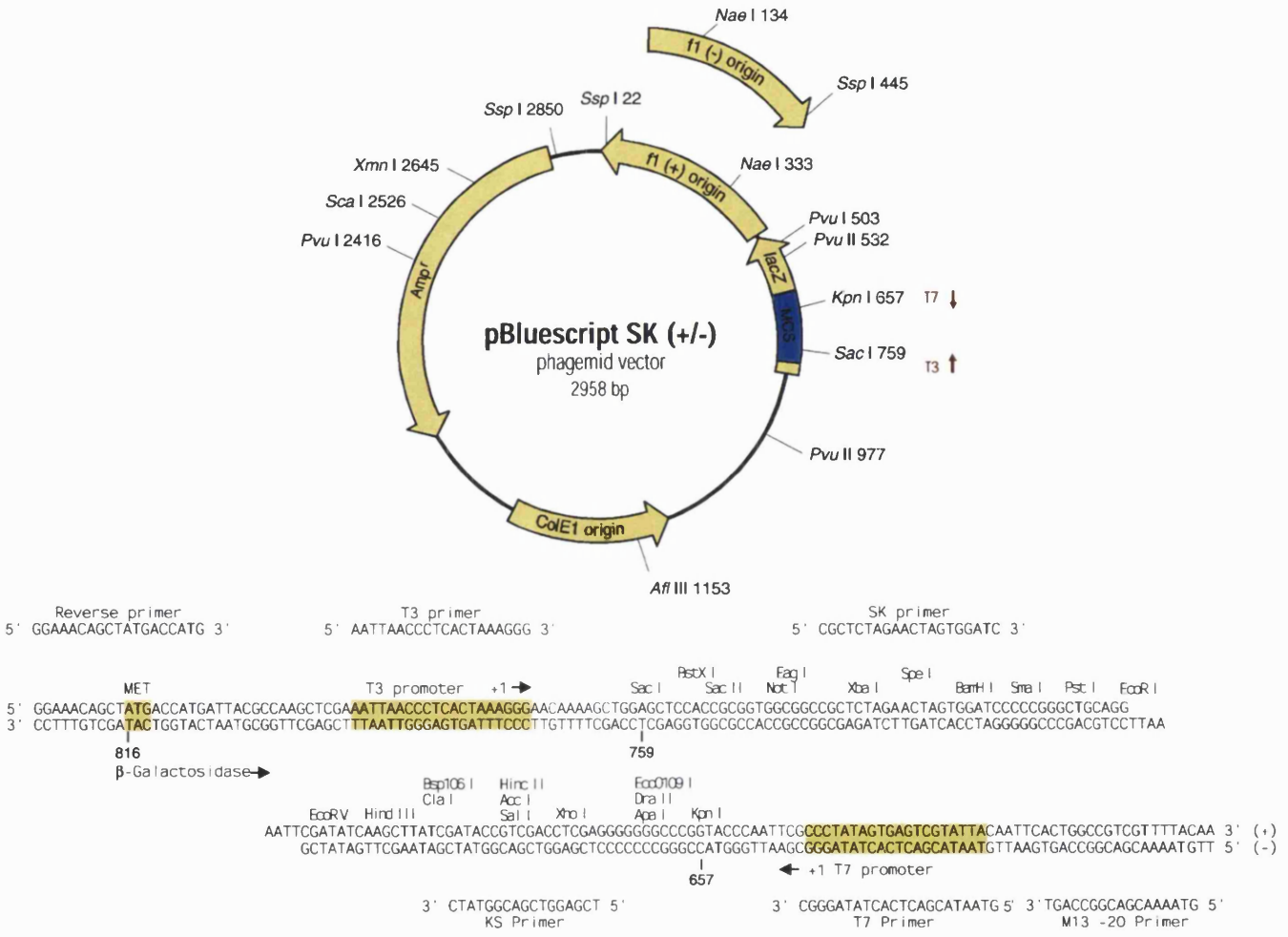


**Figure 2.2 Vector map of plasmid pBluescript SK-.** Modified from Stratagene.

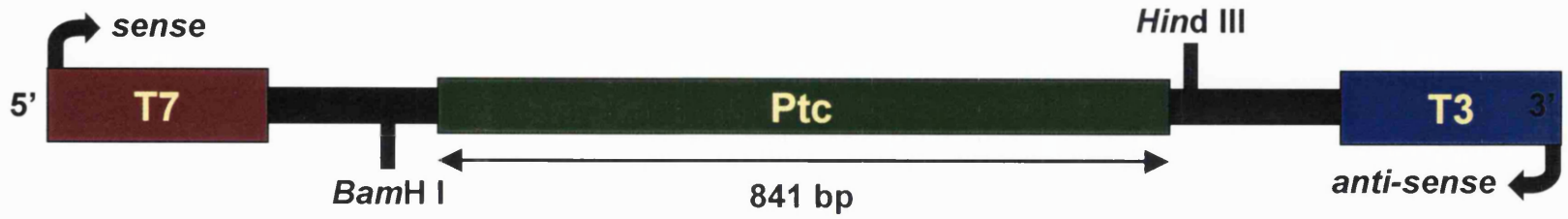


**Figure 2.3 Restriction map of mouse *Patched* plasmid.** Sequence was cloned into the *Eco*R I site of the pBluescript II KS+ vector.



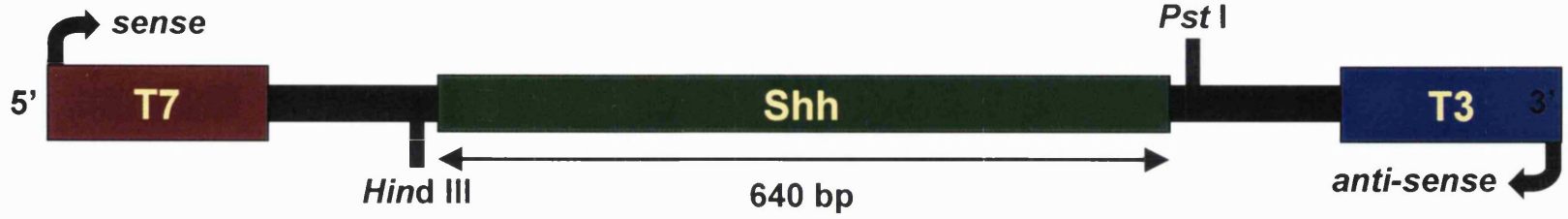


**Figure 2.4 Restriction map of mouse *Sonic hedgehog* plasmid.** Sequence was cloned into the *Eco*R I site of the pBluescript SK- vector.

## 2.17 RNA labelling

RNA was labelled by *in vitro* transcription of DNA using the DIG RNA labelling mix from Roche.

## 2.18 Radiolabelling of glycosaminoglycans

Carrier-free $^{35}$S-sulphur in the form of neutral sodium sulphate solution (chemical concentration of 15 – 17 μM) was obtained from Amersham Pharmacia. The radioactivity level was measured with a Wallac 1410 liquid scintillation counter (Wallac, Turku, Finland) using Version 1.52 of the associated software. ICN (Basingstoke, Hampshire, UK) provided the liquid scintillation cocktail, Universol. Scintillation vials were purchased from BDH.

## 2.19 Anion exchange chromatography

Anion exchange chromatography was performed using 0.5 cm X 5 cm (internal diameter X height) glass Econo-Column chromatography columns from Bio-Rad (Hemel Hempstead, Hertfordshire, UK). The columns were packed with DE52, a pre-swollen micro-granular weakly basic anion exchanger based on diethylaminoethyl (DEAE) cellulose with tertiary amine functional groups, purchased from Whatman (Maidstone, Kent, UK). Amersham Pharmacia (Little Chalfont, Buckinghamshire, UK) supplied the peristaltic pump (P-1) and the fraction collector (FRAC-100). The gradient maker was obtained from Hoefer Scientific Instruments (San Francisco, CA, USA). The

conductivity of the eluted fractions was measured using a Hanna Conmet 1 conductivity meter purchased from Sigma-Aldrich.

## 2.20 Quantification of glycosaminoglycans

The Ultrospec III ultraviolet/visible light spectrophotometer was supplied by Amersham Pharmacia. The Blyscan Assay Kit, containing 1,9-dimethylmethylene blue for quantifying sulphated glycosaminoglycans, was purchased from Biocolor (Belfast, Northern Ireland).

## 2.21 Quantification of proteins

The protein content of the collected samples was determined using the Pierce BCA Protein Assay Kit purchased from Pierce & Warriner (Chester, UK).

## 2.22 Statistical analysis

Statistical analysis of the experimental results was performed using GraphPad Prism Version 2.01 (GraphPad Software, San Diego, CA, USA).

## 2.23 Molecular modelling

Molecular modelling of glycosaminoglycans was done using ChemSketch Version 4.01 (Advanced Chemistry Development, Toronto, ON, Canada).

## 2.24 Other equipment

The MSE Soniprep 150 ultrasonic disintegrator was obtained from Sanyo Gallenkamp (Loughborough, UK).

Grant Instruments provided the QBT4 heater blocks and the W28 water baths. Heraeus supplied the T6030 ovens. The KT1930 refrigerator and the GS801 non-self-defrosting freezer were purchased from Liebherr (Ochsenhausen, Germany) while the U570-85 ultra low freezer was obtained from New Brunswick Scientific (Hartfield, Hertfordshire, UK).

Kinematica (Littau-Lucerne, Switzerland) supplied the RCT S23 magnetic stirrer. The orbital shaker SO3 was obtained from Stuart Scientific (Redhill, Surrey, UK). Scientific Industries (Bohemia, NY, USA) supplied the Vortex-Genie 2 vortex mixer. The Ohaus G1200-SO weighing machine was purchased from Ohaus Scale Corp (Florham Park, NJ, USA).

Samples were centrifuged either in an IEC Centra-7R refrigerated centrifuge (International Equipment Company, Needham Heights, MA, USA) or a Sigma 1-15 microfuge (Sigma, Osterode, Germany).

The Corning 220 pH meter was obtained from Corning Incorporated Life Sciences (Acton, MA, USA).

The Milli-Q Ultrapure Water System was provided by Millipore (Watford, Hertfordshire, UK). Pall Gelman (Portsmouth, Hampshire, UK) supplied the 0.45 μm Acrodisc syringe filters.

# *Chapter 3*

# METHODS

## 3.1 Culture of intact embryos

The technique of culturing intact embryos in a rotating tube with intermittent gassing, which has been described for rat and mouse embryos (New et al, 1973; Sadler and New, 1981), was used in this thesis. It allows experimental studies to be done on rodent embryos during the process of neurulation.

### *3.1.1 Preparation of rat serum*

Specially prepared, immediately centrifuged rat serum was used in the whole embryo cultures. Haemolysis of the blood is to be avoided as the haemoglobin released into the serum can affect the quality of the culture (Copp et al, 2000).

Healthy adult Wistar rats were anaesthetised by inhalation of ether (Cockroft, 1990). After cleaning the rat skin with 70% ethanol, the abdominal cavity was opened and whole blood was collected via arterial puncture of the abdominal aorta using a sterile 21G needle, care being taken to avoid haemolysis by pulling gently on the plunger of the syringe. The collected blood was immediately centrifuged at 1000 *g* for four minutes and the sample was left to stand to allow coagulation to take place. The fibrin plug was then squeezed, using a clean pair of forceps, to release the serum and the sample re-centrifuged to sediment the blood cells. The serum was pipetted into fresh centrifuge tubes and centrifuged again to ensure removal of all remaining red blood cells. Any serum that was not clear and pale straw coloured was discarded. The sera obtained from the bleeding session were pooled

and heat-inactivated in a water bath at 56°C for 30 minutes before being aliquoted and stored at -20°C until required.

### *3.1.2 Collection of embryos*

Mice were maintained in a 24-hour cycle period consisting of 12 hours of daylight and 12 hours of darkness. Female mice were mated with male mice overnight and the presence of copulation plugs was determined the following morning. Noon on the day of detecting a copulation plug was designated as embryonic day 0.5 of gestation (E0.5).

At the time of harvesting the embryos, the pregnant female mice were killed by cervical dislocation. The uterus was removed and placed in sterile dissection medium in petri dishes, consisting of 10% heat-inactivated FCS in DMEM, pre-warmed to 38°C. Under a dissecting microscope and using flame-sterilised precisely-sharpened fine Number 5 watchmaker's forceps, a hole was made in the uterine wall and gently enlarged until it was large enough for the decidual swelling to be 'milked' out of the uterus. Beginning at one end of the uterine horn, the process was repeated along the uterus, until all the decidual swellings had been taken out. The decidual swellings were then transferred to a fresh Petri dish of dissection medium and opened from the mesometrial (fluffy-looking) end. Using watchmaker's forceps, the decidual tissue was separated from the conceptus, and the underlying trophoblast and Reichert's membrane removed, care being taken not to damage the yolk sac and its blood vessels.

### 3.1.3 Culture and assessment of the embryos

The specially prepared rat serum was first filtered through a 0.45 μm syringe filter, warmed to 38°C and gassed to remove any remaining traces of ether before starting the culture. Embryos were put into 30 ml Universal tubes containing 1 ml of rat serum per embryo. The inside rim of the tubes was lightly smeared with silicone grease to produce a gas-tight seal. Culturing was done in a roller incubator maintained at 38°C. The embryos were gassed initially and then six hourly with a mixture of 5% oxygen, 5% carbon dioxide and 90% nitrogen for embryos between E8.5 and E9.5 while a mixture of 20% oxygen, 5% carbon and 75% nitrogen was used for embryos between E9.5 and E10.5.

At the end of the culture period, the status of the yolk sac circulation and the embryonic heart rate were determined. Embryos were considered healthy if there was a vigorous flow of blood in the yolk sac circulation and the embryonic heart rate was regular and above 100 per minute. Embryos that exhibited signs of ill health, such as an expanded pericardial cavity, irregularity of the most caudal somites, waviness of the neural tube and sub-epidermal fluid-filled blebs were not used for subsequent analysis (Copp et al, 2000). The somite number was counted and the crown-rump length, head length and posterior neuropore length were measured using an eyepiece graticule fitted to the dissecting stereomicroscope. The posterior neuropore length was measured from the rostral end of the posterior neuropore to the tip of the tail. Each embryo was also assessed using the Brown and Fabro Morphological Scoring System, as shown in Table 3.1 (Brown and Fabro, 1981). The presence of any gross morphological abnormalities such as neural tube defects was noted.

**Table 3.1 Brown and Fabro Morphological Scoring System.** From Brown and Fabro (1981).

| SCORE / FEATURE | 0 | 1 | 2 | 3 | 4 | 5 |
|---|---|---|---|---|---|---|
| YOLK SAC CIRCULATION | No visible or scattered blood vessels | Corona of blood islands with or without anastomoses | Vitelline vessels with few yolk sac vessels | Full yolk sac plexus of vessels | Yolk stalk obliterated, vitelline artery and vein well separated | |
| ALLANTOIS | Allantois free in exocoelom | Allantois fused with chorion | Umbilical vessels | Separate aortic origins of umbilical and vitelline vessels | | |
| FLEXION | Ventrally convex | Turning | Dorsally convex | Dorsally convex with spiral torsion | | |
| HEART | Endocardial rudiment not visible, or visible but not beating | Beating 'S' shaped cardiac tube | Convoluted cardiac tube | Bulbs cordis, atrium commune and ventriculus communis | Dividing atrium commune | |
| CAUDAL NEURAL TUBE | Neural plate or neural folds | Closing, but unfused neural folds (groove) | Neural folds fused at level of somites 4/5 | Posterior neuropore formed, but open | Posterior neuropore closed | |
| HIND BRAIN | Neural plate | Rhombomeres A and B | Fusing folds | Completely fused | Pronounced pontine flexure with transparent roof of 4th ventricle | |
| MID BRAIN | Neural plate | Mesencephalic brain folds | Fusing folds | Completely fused | Visible division between mesencephalon and diencephalon | |

| | | | | | | |
|---|---|---|---|---|---|---|
| **FORE BRAIN** | Neural plate or no visible prosencephalon | Prosencephalic brain folds | Completely fused prosencephalon | Visible telencephalic evaginations | Well elevated telencephalic hemispheres | |
| **OTIC SYSTEM** | No sign of otic development | Flattened or indented otic primordium | Otic pit | Otocyst | Otocyst with dorsal recess | Otocyst with endolymphatic duct |
| **OPTIC SYSTEM** | No sign of optic development | Sulcus opticus | Elongated optic primordium | Primary optic vesicle with open optic stalk | Indented lens plate | Lens pocket or lens vesicle |
| **OLFACTORY SYSTEM** | No sign of olfactory development | Olfactory plate | Olfactory plate with rim | Distinct olfactory ridges | Lateral nasal process and medial rim | |
| **BRANCHIAL BARS** | None visible | I visible | I and II visible | I, II and III visible | II overgrowing and obscuring III | |
| **MAXILLARY PROCESS** | No visible separation of maxilla and bar I | Maxillary process demarcated visible cleft anterior to bar I | Maxillary process fused with nasal process | | | |
| **MANDIBULAR PROCESS** | Medial edges of bar I less than 5% fused | First branchial bars fused and forming mandibular process | | | | |
| **FORE LIMB** | No sign of fore limb development | Distinct evagination of wolfian crest at level of somites 7 – 11 | Fore limb bud | Paddle shaped fore limb bud | Distinct apical ridge on fore limb bud | |
| **HIND LIMB** | No sign of hind limb development | Distinct evagination of wolfian crest at level of somites 26 – 30 | Hind limb bud | Paddle shaped hind limb bud | | |
| **SOMITES** | 0 – 6 | 7 – 13 | 14 – 20 | 21 – 27 | 28 – 34 | 35 - 41 |

## 3.2 Genotyping of *splotch* ($Sp^{2H}$) embryos

The *splotch* ($Sp^{2H}$) embryos were genotyped using the polymerase chain reaction (PCR), as shown in Figure 3.1 (Saiki et al, 1985). This technique produces multiple copies of the segment of DNA of interest that is flanked by the two primers. The genomic DNA is first denatured by heat. The primers are then allowed to bind to the single stranded DNA by specific base pairing. Thereafter, thermostable *Taq* DNA polymerase is used to synthesise the complementary strands of DNA in a 5' $\rightarrow$ 3' direction. The whole procedure is repeated, usually between 25 and 40 times, resulting in the amplification of the desired DNA sequence. Excessive cycles are not desirable as this could lead to a higher background and reduce the yield of specific products from the reaction.

In *splotch* ($Sp^{2H}$) mutants, there is a 32-base pair deletion in the *Pax-3* gene. The sequence for the *Pax-3b* primer is CCT CGG TAA GCT TCG CCC TCTG while the sequence for the *Pax-3c* primer is CAG CGC AGG AGC AGA ACC ACC TTC (Epstein et al, 1991). Using these primers in the polymerase chain reaction, wild type embryos show a 125-base pair band, homozygous *splotch* ($Sp^{2H}$) embryos a 93-base pair band, while heterozygous embryos yield both bands.

**Figure 3.1 Genotyping *splotch* ($Sp^{2H}$) embryos using the poiymerase chain reaction.** Genomic DNA is first denatured by heating. The *Pax-3b* and *Pax-3c* primers (which flank the ends of the target region) are then allowed to anneal to the two single stranded DNA which act as templates for *Taq* DNA polymerase. Polymerisation proceeds in a 5' → 3' direction, forming long PCR products (LP) capped at the 5' end with the respective *Pax-3* primer used. In the second cycle, these LPs also act as templates for *Taq* polymerase, resulting in the formation of short 'target' products (STP) corresponding to the target region of interest. At the end of 33 cycles, millions of copies of STPs are formed and these can easily be detected under ultraviolet light after electrophoresis on an agarose gel.

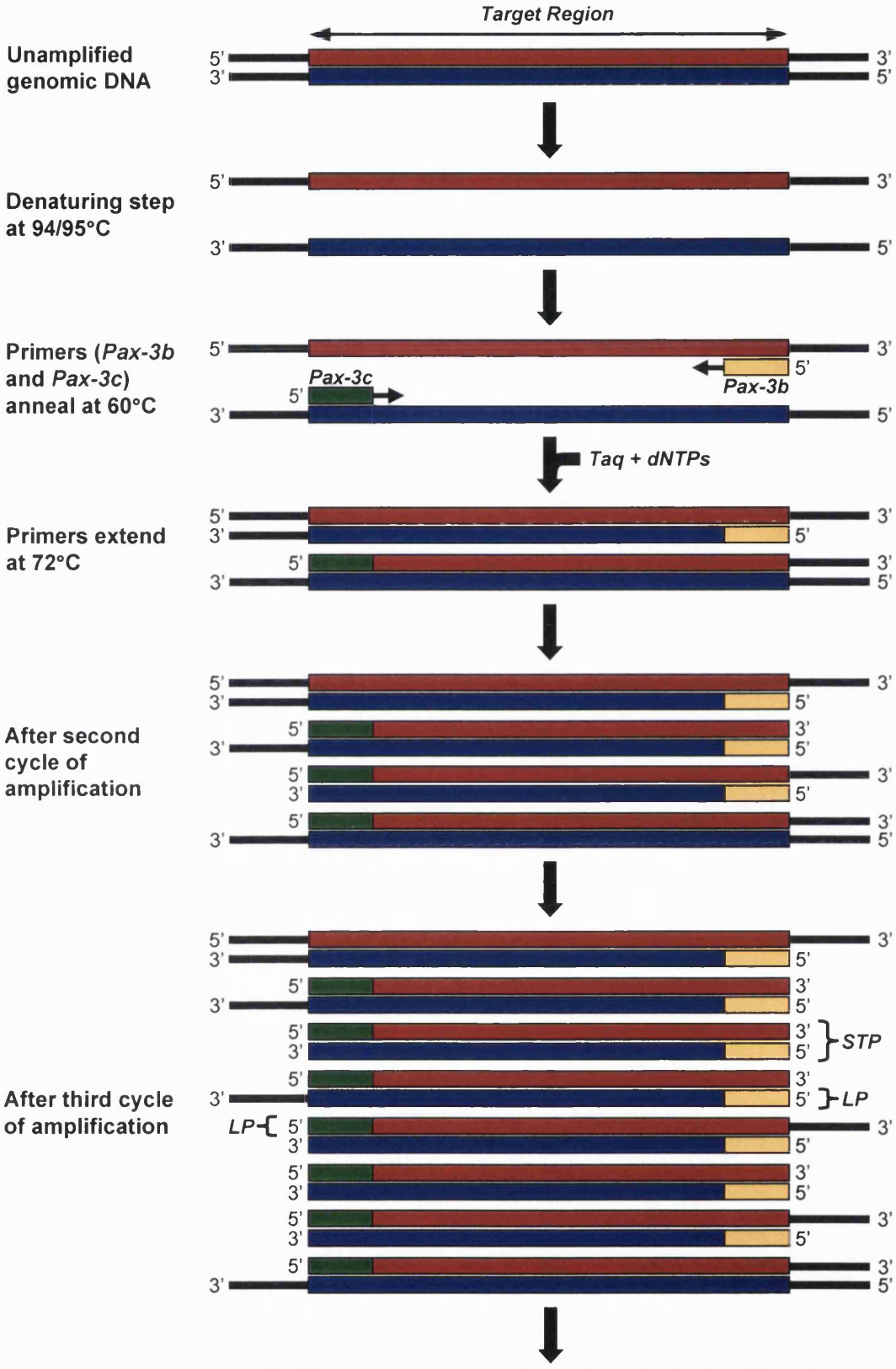
Target Region
Unamplified genomic DNA
Denaturing step at 94/95°C
Primers (Pax-3b and Pax-3c) anneal at 60°C
Pax-3c
Pax-3b
Taq + dNTPs
Primers extend at 72°C
After second cycle of amplification
After third cycle of amplification
STP
LP
LP
Multiple copies of short 'target' product after 33 cycles

### 3.2.1 Polymerase chain reaction

Yolk sacs and amniotic membranes from the collected *splotch* ($Sp^{2H}$) embryos were digested with 100 μg of Proteinase K in 100 μl PBS at 55°C overnight. The enzyme was inactivated by boiling for five minutes. After spinning down the undigested material, 2 μl of the supernatant was added to the polymerase chain reaction mixture containing 2.5 μl of buffer solution (100 mM Tris, pH 8.0; 15 mM potassium chloride; 500 mM magnesium chloride), 2 μl of dNTPs (2 mM each of dATP, dCTP, dGTP and dTTP), 0.25 μl of *Taq* DNA polymerase (5 units/μl) and 17.6 μl of de-ionised water. *Pax-3b* and *Pax-3c* primers (0.33 μl each of 100 μg/ml stock solutions) were then added. The reaction mixture was overlaid with 40 μl of mineral oil to prevent loss of volume through evaporation at the high temperatures used. Tubes for both positive and negative controls were set up for every PCR run, using genomic DNA extracted from heterozygous animals and PBS respectively.

The PCR program comprised an initial genomic DNA denaturing step at 95°C for five minutes. This was followed by 33 cycles consisting of 94°C for 30 seconds, 60°C for a minute and 72°C for 30 seconds. Finally, the samples were kept at 72°C for 10 minutes.

### 3.2.2 Agarose gel electrophoresis

A 2.5% agarose gel was prepared by adding 2.5 g of agarose to 100 ml of TAE buffer (40 mM Tris, pH 7.2; 0.114% v/v glacial acetic acid; 1 mM EDTA). This was heated in a microwave oven with intermittent agitation until all the agarose had dissolved. After cooling, 2.5 μl of ethidium

bromide (10 mg/ml stock solution) was added and the agarose left to solidify at room temperature for an hour in a gel casting tray with inserted combs. The combs were then removed and the gel was transferred to an electrophoresis tank. This was filled with TAE buffer containing 25 μl of ethidium bromide per litre of buffer.

Orange G (loading buffer, 2 μl) was mixed with 10 μl of the PCR product. This was then loaded into the gel well and electrophoresed at 80 V until the dye front approached the edge of the gel. The bands were visualised on an ultraviolet transilluminator and photographed. The pUC18 DNA *Msp* I digest was used for sizing the DNA.

## 3.3 Histochemistry

Microscopic examination of wax embedded tissue sections is a simple method by which much information about tissue structure and organisation can be obtained. By making use of dyes with different staining properties, it is possible to study the distribution of various molecules in the specimen.

The first step in preparing a sample for such a study is fixation, whereby a fixative such as paraformaldehyde is used to preserve the tissue architecture and prevent metabolic breakdown of the specimen. Thereafter, the sample is progressively dehydrated and thoroughly permeated with wax for embedding. The specimen can then be sectioned and stained for examination under the microscope (Bancroft and Stevens, 1996).

### 3.3.1 Fixation and wax embedding

Embryos were dissected out in ice-cold DMEM containing 10% FCS. After two washes in ice-cold PBS, the tissues were fixed overnight, with gentle rocking, in either 4% paraformaldehyde at 4°C or Bouin's fixative at room temperature. The tissues were then washed twice in PBS and dehydrated through half-hourly changes of 50%, 70% (twice), 85%, 95% and 100% (twice) ethanol. Thereafter, the tissues were placed in two changes of HistoClear for half an hour each before being transferred to a 1:1 HistoClear:paraffin wax mixture at 60°C for 20 minutes. Finally, three 20-minute changes of wax at 60°C were made to ensure adequate penetration of wax into the tissues. The specimens were then placed in warm glass moulds filled with wax and oriented using heated fine needles. The wax was left to set at room temperature overnight and the tissue blocks stored at 4°C until required.

### 3.3.2 TESPA coating of slides

In order to increase the adherence of tissue sections to glass slides, several different materials have been used for coating the slides, including albumin, gelatin, poly-L-lysine and aminoalkylsilanes such as TESPA (Maddox and Jenkins, 1987). The latter acts by forming a covalent bond with the hydroxyl group of glass, thus linking the aminoalkyl groups to the glass and increasing the adhesion between the glass and the tissue sections.

Clean glass slides were washed in acetone for two minutes to remove all traces of oil and water before use. After air-drying, the slides were coated in a 2% TESPA solution in acetone for two minutes, and then

washed briefly in two changes of de-ionised water. The slides were left to dry overnight at 37°C and stored at room temperature until required.

### 3.3.3 Sectioning

Excess wax on the tissue block was trimmed using a razor blade and the block was mounted on to a wooden cube using melted wax. After leaving overnight at 4°C for the wax to completely solidify, 6 μm thick sections were cut using a microtome. The tissue sections were then floated on de-ionised water on horizontally placed TESPA coated slides. These were incubated at 40°C on a hot plate until all the creases had disappeared. The excess water was removed and the slides dried overnight at 37°C. They were stored at 4°C until required.

### 3.3.4 De-waxing and re-hydration

Paraffin wax embedded sections have to be de-waxed and re-hydrated before further histological procedures are done. This was achieved by leaving the sections in two changes of HistoClear for 10 minutes each, followed by five-minute changes of 100% (twice), 90%, 75% and 50% ethanol and finally PBS.

### 3.3.5 Haematoxylin and eosin staining

Haematoxylin, a basic dye, stains cell nuclei dark blue in colour while eosin, an acidic dye, stains the cytoplasm pink. They are frequently used in routine histology for staining tissue sections.

Sections were de-waxed and re-hydrated as described above and then placed in Mayer's haematoxylin solution for five minutes. After a five-minute wash in water, the slides were briefly dipped in 1% acid alcohol (1% hydrochloric acid in 70% ethanol) for differentiation and left to "blue" for five minutes in a 250 mM sodium bicarbonate solution. They were then rinsed in water, stained in 1% aqueous eosin for a minute and rapidly dehydrated through 50%, 70% and 90% ethanol before being left in 100% ethanol (twice) and HistoClear (twice) for five minutes each. The slides were mounted in DePX, cover slipped and left to dry in a fume hood overnight.

### *3.3.6 Alcian blue staining*

Alcian blue, a cationic dye, stains glycosaminoglycans blue in colour. At pH 2.5, both sulphated and non-sulphated glycosaminoglycans are stained. At pH 1, only sulphated glycosaminoglycans, which are highly negatively charged, are stained.

De-waxed and re-hydrated tissue sections were placed in 1% Alcian blue 8GX solution at pH 1 for half an hour. The slides were blotted dry, washed briefly in 95% ethanol and left in 100% ethanol (twice) and HistoClear (twice) for five minutes each. They were then mounted in DePX as described above.

## 3.4 Immunohistochemistry

The specific binding of antibodies to antigens is made use of in the well established technique of immunohistochemistry to study the distribution

of these antigens in tissue sections. Amplification procedures, such as the labelled streptavidin method (Shi et al, 1988), enable small amounts of antigens to be detected. In this method, after binding of the primary antibody to the antigen has occurred, a biotinylated secondary antibody, which has been raised against the primary antibody, is applied. The attached biotin then binds to streptavidin, which has been conjugated to the enzyme horseradish peroxidase. By adding a chromogen, such as DAB or AEC, which is a substrate for the enzyme, the amount and distribution of the antigen can be visualised and compared among different specimens. False positive results can arise from the presence of endogenous peroxidase and charged proteins in the specimens. Furthermore, the use of primary antibodies of mouse origin on mouse tissues can lead to erroneous findings due to the secondary antibody cross-reacting with endogenous immunoglobulins. Both of these problems can be resolved by blocking steps, as illustrated in Figure 3.2.

### *3.4.1 Pre-treatment*

Tissue sections were de-waxed and re-hydrated and incubated at room temperature in 3% hydrogen peroxide in PBS for 15 minutes to block the activity of endogenous peroxidase. The sections were then washed in three changes of PBS for five minutes each. Excess saline was drained off and hydrophobic circles were then drawn around the sections using a PAP pen. Two drops of blocking solution 1A from the HistoMouse-SP kit were added to each section and the specimens were incubated at room temperature for 30 minutes in a moist chamber. After briefly washing the sections in de-ionised water, they were incubated with two drops of blocking solution 1B at room temperature

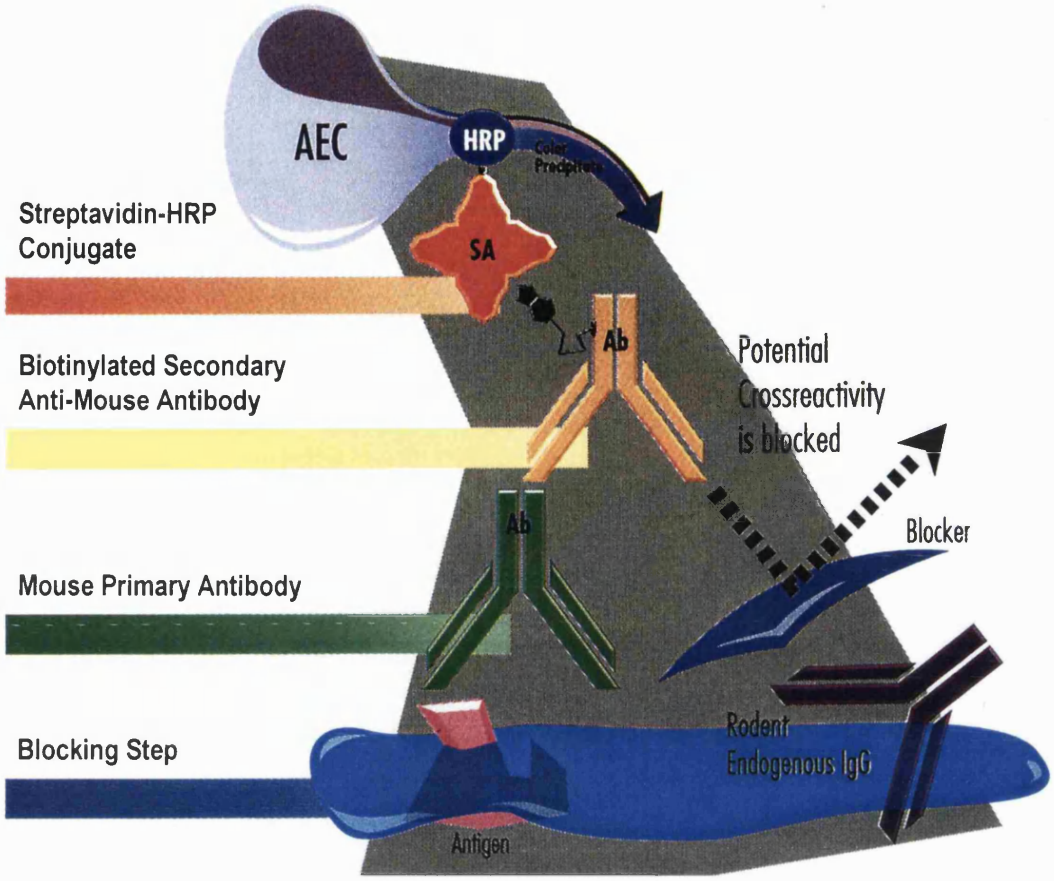


**Figure 3.2 Immunohistochemical detection of mouse antigen using mouse primary antibody.** This consists of an initial blocking step to block endogenous peroxidase and non-specific binding of the primary antibody (Ab). A second block prevents potential cross-reactivity between the secondary antibody and the rodent endogenous IgG in the tissue section. After the mouse primary antibody has bound to the antigen of interest, the biotinylated secondary antibody is applied. Biotin binds to streptavidin (SA), which has been conjugated to horseradish peroxidase (HRP). This allows colour detection of the antigen via the use of a chromogen such as AEC or DAB. The figure illustrates the use of the HistoMouse kit for this purpose (modified from Zymed).

for 10 minutes. The sections were then rinsed with de-ionised water and three changes of PBS for two minutes each before applying the primary antibody.

### 3.4.2 Binding of primary antibodies

The anti-heparan sulphate and anti-chondroitin sulphate antibodies were used at a dilution of 1:150. The antibodies were diluted using 10% FCS and 1% BSA in PBS.

Each section was incubated with 100 μl of diluted primary antibody at room temperature for an hour in a moist chamber. At the end of this period, the sections were washed in three changes of 0.5% Tween-20 in PBS for two minutes each in order to reduce background staining. They were then briefly rinsed in PBS to remove excess detergent. Negative controls were run on adjacent sections in all the experiments using isotype-matched control antibodies that had been diluted to the same concentration as the respective primary antibodies. These control antibodies were derived from mice that had been immunised against *Aspergillus niger* glucose oxidase (an enzyme neither present nor inducible in mammalian tissues). A complete list of all the antibodies used is given in Chapter 2.

### 3.4.3 Signal amplification and detection

Two drops of Reagent 1C (biotinylated secondary antibody) were added to each section and left to incubate at room temperature for 10 minutes in order for the secondary antibody to bind to the primary antibody. The slides were then washed in three changes of 0.5% Tween-20 in PBS for

two minutes each to remove the excess unbound secondary antibody. This was followed by a rinse in PBS for two minutes.

Two drops of Reagent 2 (streptavidin-horseradish peroxidase conjugate) were then added to each section. The sections were again incubated at room temperature for 10 minutes to allow the streptavidin to bind to the biotin on the secondary antibody. The sections were then washed in three changes of 0.5% Tween-20 in PBS for two minutes each, followed by a rinse in PBS.

The signal was detected by adding 200 μl of DAB solution to each section and allowing colour development to proceed for two minutes. The amount of brown precipitate formed was monitored under a microscope. The reaction was stopped by rinsing the sections in de-ionised water for a minute followed by PBS for another minute. The sections were then dehydrated and mounted in DePX as described above.

## 3.5 Non-radioactive *in situ* hybridisation

The technique of *in situ* hybridisation enables studies to be done on the expression patterns of various genes at different stages of development. The use of a non-radioactive label such as digoxigenin eliminates the risk of exposure to radiochemicals yet retains high sensitivity for detection of low levels of mRNA (Tautz and Pfeiffle, 1989; Breitschopf et al, 1992).

Since the method involved working with RNA, special care was taken to avoid contamination of reagents and equipment with RNases.

Disposable gloves were worn at all times. Glassware was baked overnight at 180°C before use. All de-ionised water and solutions, besides those containing Tris or amines or those which cannot be autoclaved, were treated with 0.1% DEPC overnight and autoclaved the next morning prior to use (Sambrook et al, 1989). DEPC inactivated RNases and was broken down to ethanol and carbon dioxide by autoclaving. Solutions were made from chemicals that had been put aside specially for RNA work.

## *3.5.1 Transformation of DNA into bacteria*

Transformation of plasmids into bacterial cells enables large amounts of plasmid DNA to be produced. These can then be used for the synthesis of digoxigenin-labelled riboprobes by *in vitro* transcription.

### 3.5.1.1 Preparation of Miller's LB Agar and LB Broth

Miller's LB Agar was prepared by dissolving 37 g of the agar powder in 1 l of de-ionised water. The agar was autoclaved at 121°C for 20 minutes and left to cool to 50°C. Ampicillin was then added to a final concentration of 50 μg/ml. The agar was dispensed into sterile petri dishes and left to harden overnight. The agar plates were then stored at 4°C until required.

LB Broth was prepared by dissolving 20 g of the broth base powder in 1 l of de-ionised water. The broth was sterilised by autoclaving.

### 3.5.1.2 Transformation of competent cells

Competent DH5α cells were first thawed on ice before the addition of 3 μl of plasmid (containing 50 ng of DNA) to 100 μl of these cells in a pre-cooled eppendorf tube. The cells were incubated on ice for 20 minutes and then heat-shocked in a water bath at 42°C for 90 seconds followed by immediate cooling on ice for two minutes. After this, the cells were kept at 37°C for 20 minutes with 1 ml of LB Broth that had been pre-warmed to 37°C. Following the incubation step, the cells were pelleted by centrifugation at 3000 *g* for 30 seconds. Most of the supernatant was then removed, leaving only 100 μl for re-suspending the cells. The transformed cells were plated onto LB plates containing ampicillin using a flame-sterilised glass spreader and left to incubate at 37°C overnight. The presence of ampicillin in the plate selected for transformed bacteria containing the plasmid carrying the ampicillin resistance gene.

## *3.5.2 Small scale isolation of plasmid DNA*

An isolated white bacterial colony was picked from the agar plate using a sterile pipette tip and transferred to 4 ml of LB medium containing 50 μg/ml ampicillin in a sterile 25 ml Universal tube. The lid was loosely replaced and the bacteria incubated at 37°C for 16 hours in a shaker incubator.

The cells were pelleted by centrifugation at 1000 *g* for 10 minutes. The supernatant was then removed, and the cells re-suspended in 500 μl of Solution I (25 mM Tris, pH 8.0; 10 mM EDTA; 100 μg/ml DNase-free RNase A). The RNase A was used to digest the RNA that was

released from the cells in the subsequent steps, hence ensuring that there would not be RNA contamination of the purified plasmid DNA.

The cells were then lysed by adding 500 μl of Solution II (1% sodium dodecyl sulphate; 0.2 mM sodium hydroxide). The tube contents were gently mixed by inversion in order to avoid shearing of the genomic DNA and then left to incubate for five minutes at room temperature. The lysate became clear and viscous at this point. This timing must not be exceeded, as prolonged incubation may result in the formation of irreversibly denatured plasmid.

After incubation, the solution was neutralised by the addition of 500 μl of Solution III (3 M potassium acetate, pH 4.8). The tubes were mixed by inversion and left to incubate on ice for five minutes. A fine white precipitate was formed and this was pelleted by centrifuging at 18,000 *g* for five minutes.

The supernatant was removed and divided equally between two clean eppendorf tubes. DNA was then precipitated by adding 500 μl of isopropanol to each tube and the tubes were centrifuged again at 18,000 *g* for five minutes. After removal of the isopropanol, each pellet of DNA was re-dissolved in 200 μl of $TE_1$ buffer (10 mM Tris, pH 8.0; 1 mM EDTA) and the samples were pooled together. The contents were mixed with 500 μl of phenol/chloroform and then centrifuged at 18,000 *g* for five minutes. The upper phase, containing plasmid DNA, was transferred into a fresh tube. The DNA was precipitated by the addition of 1 ml of 100% ethanol. The specimen was again centrifuged at 18,000 *g* for five minutes. The supernatant was then removed and the

pellet washed with 500 μl of 70% ethanol. The DNA was then air-dried and re-dissolved in 100 μl of $TE_1$ buffer.

## *3.5.3 Preparation of riboprobes*

Before using the isolated plasmid DNA for synthesis of digoxigenin-labelled riboprobes, it is important to confirm that the plasmids do contain the correct inserts by cutting them out using restriction enzymes and checking their sizes using agarose gel electrophoresis. The bands of DNA can be detected visually after electrophoresis as ethidium bromide intercalates between the bases of DNA and fluoresces under ultraviolet light.

After this confirmation, the plasmid DNA can be linearised with the appropriate enzymes and used as templates for synthesis of the riboprobes by *in vitro* transcription (Figure 3.3).

### 3.5.3.1 Restriction digestion

The gene inserts were cut out of the plasmid by digestion with *Eco*R I. For a 20μl reaction volume, 2 μl of plasmid was added to 14 μl of DEPC-treated water, 2 μl of 10X enzyme buffer (0.9 M Tris, pH 7.5; 0.1 M magnesium chloride; 0.5 M sodium chloride), and 2 μl of restriction enzyme. The reaction mixture was incubated at 37°C for two hours.

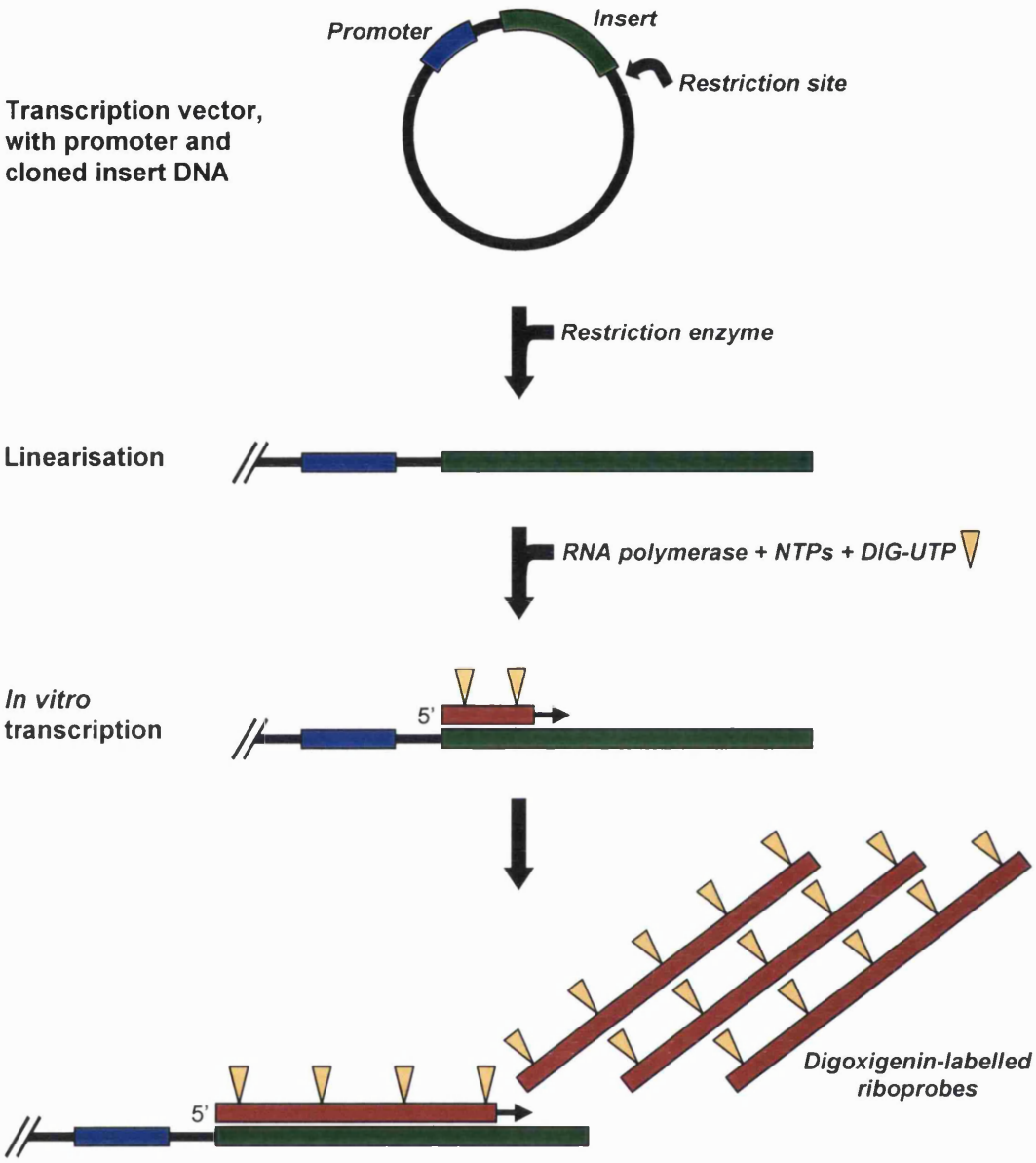


**Figure 3.3 Digoxigenin-labelling of RNA by *in vitro* transcription.** The plasmid containing the cloned insert DNA is first linearised with the appropriate restriction enzyme. Under the influence of the promoter region, RNA polymerase synthesises the riboprobes (red bars), incorporating DIG-UTP which acts as a substrate and is base-paired complementarily with adenine in the template.

### 3.5.3.2 Electrophoresis

The products of the restriction digestion were separated by electrophoresis on a 1% agarose gel as described above. Hyperladder I was used as the molecular weight marker.

### 3.5.3.3 Plasmid iinearisation

After confirming that the plasmid DNA contained the correct inserts, the plasmids were linearised for use as templates for *in vitro* transcription. The restriction enzymes used for linearisation of the *Patched* plasmid were *Bam*H I (for synthesis of the anti-sense probe) and *Hin*d III (for the sense probe; Figure 2.3). With regard to the *Sonic hedgehog* plasmid, the restriction enzymes used were *Hin*d III (for the anti-sense probe) and *Pst* I (for the sense probe; Figure 2.4). The 10X enzyme buffer for *Pst* I contained 0.9 M Tris (pH 7.5), 0.1 M magnesium chloride and 0.5 M sodium chloride while the 10X buffer for *Bam*H I and *Hin*d III contained 60 mM Tris (pH 7.5), 60 mM magnesium chloride, 1 M sodium chloride and 10 mM DTT.

The reaction mixture for restriction digestion was prepared as described above, except that the volume of plasmid DNA used was increased to 5 μl while the amount of DEPC-treated water used was decreased to 11 μl. After incubation, the linear template DNA was purified using phenol/chloroform extraction and ethanol precipitation (see earlier) and the pellet re-suspended in 10 mM Tris buffer (pH 8.0). To check that linearisation of the plasmid was complete, 1 μl was removed and electrophoresed on a 1% agarose gel.

### 3.5.3.4 Synthesis of digoxigenin-labelled probes

Synthesis of the riboprobes was done by *in vitro* transcription. Digoxigenin-labelled UTP was incorporated at approximately every 20$^{th}$ to 25$^{th}$ position in the transcripts. About 10 μg of full-length RNA transcripts could be produced in a two-hour incubation period, starting from 1 μg of template DNA.

For a 20 μl reaction volume, 4 μl of the transcription-optimised 5X buffer (200 mM Tris, pH 7.5; 30 mM magnesium chloride; 10 mM spermidine; 50 mM sodium chloride) was added to 8 μl of DEPC-treated water. The following reagents were then added in sequence: 2 μl of 100 mM DTT, 1 μl of RNase inhibitor, 2 μl of digoxigenin-labelling mix (10 mM each of ATP, CTP and GTP; 6.5 mM UTP; 3.5 mM DIG-UTP), 2 μl of linearised plasmid DNA and 1 μl of RNA polymerase (T3 RNA polymerase for synthesis of the anti-sense probes; T7 RNA polymerase for the sense probes; see Figures 2.3 and 2.4). The reaction mixture was incubated at 37°C for two hours.

After incubation, 1 μl of the mixture was electrophoresed on a 1% formaldehyde/agarose gel (see below) to check that the RNA probe had been synthesised. The DNA template was removed by adding 1 μl of RNase-free DNase I to the remaining reaction mix and incubating at 37°C for 15 minutes.

After incubation, 70 μl of DEPC-treated water, 10 μl of 3 M sodium acetate and 300 μl of 100% ethanol were added to the reaction mixture and the RNA was allowed to precipitate overnight at -20°C. The precipitate was collected by centrifugation at 18,000 *g* for 30 minutes at

4°C, washed in 100 μl of 70% ethanol, air-dried and dissolved in 100 μl of DEPC-treated water. To check that the DNA template had been completely removed, 5 μl was taken and run on a 1% formaldehyde/agarose gel. The digoxigenin-labelled probes were stored at -70°C until required.

### 3.5.3.5 Agarose/formaldehyde gel electrophoresis

A 1% agarose gel was prepared by adding 0.3 g of agarose to 24 ml of DEPC-treated water. This was boiled in a microwave oven until all the agarose had dissolved. The solution was allowed to cool to 55°C and 3 ml of 10X MOPS buffer (0.2 M MOPS, pH 7.0; 50 mM sodium acetate; 10 mM EDTA) and 3 ml of formaldehyde (37% stock solution) were added. The agarose was left to solidify for an hour. After setting, the gel combs were removed and the gel covered with MOPS buffer containing 3.7% formaldehyde.

Each 5 μl of RNA sample was mixed with 14 μl of RNA denaturing loading buffer. The RNA loading buffer was prepared by mixing 750 μl of formamide with 240 μl of formaldehyde, 200 μl of glycerol, 80 μl of 1% bromophenol blue and 150 μl of MOPS buffer. The RNA sample was then denatured at 70°C for 10 minutes before being immediately cooled on ice. Ethidium bromide (1 μl of 1 mg/ml stock solution) was added and the sample loaded into the gel well. Electrophoresis was carried out at 60 V and the RNA bands visualised as described above. The 0.24 – 9.5 kb RNA ladder was used as the molecular size marker.

### 3.5.4 Specimen preparation

The specimens were fixed overnight at 4°C in 4% paraformaldehyde in PBS. These were then washed twice in PBT (0.1% Tween-20 in PBS) and dehydrated through a graded series of methanols. The embryos were stored in 100% methanol at -20°C until the pre-hybridisation step.

### 3.5.5 Pre-hybridisation

The specimens were re-hydrated through a graded series of methanols and washed twice in PBT. They were then incubated in 6% hydrogen peroxide in PBT for one hour and washed thrice in PBT before being treated with Proteinase K (10 μg/ml) for two minutes. The reaction was stopped by rinsing the specimens once in freshly prepared glycine (2 mg/ml) and twice in PBT. The tissues were re-fixed in 0.2% glutaraldehyde and 4% paraformaldehyde in PBS for 20 minutes, and then rinsed twice in PBT.

### 3.5.6 Hybridisation

The embryos were transferred to 1 ml pre-hybridisation mix (50% formamide; 5X SSC [1X SSC solution contains 150 mM sodium chloride; 15 mM sodium citrate, pH 4.5]; 50 μg/ml yeast RNA; 1% sodium dodecyl sulphate; 50 μg/ml heparin) and incubated at 70°C for two hours. The specimens were then placed in the hybridisation mix, in which digoxigenin-labelled anti-sense riboprobes were diluted 1:100 in pre-hybridisation mix, and incubated at 70°C overnight.

### 3.5.7 Post-hybridisation washes

The embryos were washed twice at 70°C for 30 minutes each in Solution 1 (50% formamide; 5X SSC; 1% sodium dodecyl sulphate) and twice at 65°C for 30 minutes each in Solution 2 (50% formamide; 2X SSC). They were then rinsed thrice at room temperature for 5 minutes each in TBS (140 mM sodium chloride; 3 mM potassium chloride; 25 mM Tris, pH 7.5).

### 3.5.8 Detection of digoxigenin-labelled riboprobes

The digoxigenin-labelled riboprobes were detected using an anti-digoxigenin antibody. To prevent non-specific binding of the antibody to the embryos, the specimens were pre-blocked by incubating the tissues in 10% heat-inactivated sheep serum in TBS for 90 minutes at room temperature. In addition, the antibody was pre-absorbed with embryo powder (see below) to reduce non-specific binding. This was done by adding the embryo powder to 1 ml TBS and incubating this at 70°C for 30 minutes. After cooling, 10 μl sheep serum and 2 μl anti-digoxigenin antibody were added and the powder was incubated at 4°C for 1 hour. The powder was pelleted by centrifugation at 1,500 *g* for 10 minutes. The supernatant was diluted to a final volume of 4 ml using 1% sheep serum in TBS and this was filtered with a 0.45-μm syringe filter. The specimens were then added to this pre-absorbed antibody solution and incubated at 4°C overnight. The next day, the specimens were washed extensively with eight changes of TBS to remove unbound antibody and then left in TBS overnight. On the following day, the specimens were

rinsed in three changes of NTMT (100 mM sodium chloride; 50 mM magnesium chloride; 1 mM levamisole; 0.1% Tween-20; 100 mM Tris, pH 9.5) for 10 minutes each. Colour development was achieved by incubating the embryos in NBT/BCIP solution (4.5 μl of 100 mg/ml nitroblue tetrazolium; 3.5 μl of 50 mg/ml 5-bromo-4-chloro-3-indolyl phosphate; 1 ml NTMT) in the dark for about an hour. The reaction was stopped by washing twice in PBT before the appearance of background staining.

### *3.5.9 Preparation of embryo powder*

Mouse embryo powder was prepared by homogenising E12.5 to E14.5 mouse embryos in a minimum volume of PBS. This was then mixed with four volumes of ice-cold acetone and incubated on ice for 30 minutes. The suspension was centrifuged at 10,000 *g* for 10 minutes and the supernatant was discarded. The pellet was washed with ice-cold acetone and then re-pelleted by centrifugation. Finally, the pellet was finely ground on a sheet of filter paper, air-dried and stored in an air-tight tube at 4 °C.

## 3.6 Radiolabelling of glycosaminoglycans

Newly synthesised sulphated glycosaminoglycans can be labelled by culturing embryos in the presence of small doses of $^{35}$S-sulphate for a short period (Solursh and Morriss, 1977; Copp and Bernfield, 1988b). Sulphur-containing proteins, which may also incorporate the $^{35}$S-radiolabel, can be removed by protease degradation. After purification, the sulphated glycosaminoglycans can be separated out using anion

exchange chromatography. The amount of incorporated $^{35}$S-radiolabel can then be quantified using a scintillation counter. Using this method, the net rate of synthesis of different sulphated glycosaminoglycans can be compared between different groups of embryos.

### 3.6.1 Radioactive embryo culture

The basic culture technique has been described above. After being explanted from the uterus, the embryos were first stabilised for three hours in the roller incubator. Neutral carrier-free $^{35}$S-sulphate solution (chemical concentration of 15 – 17 μM) was then added to the culture medium to a final concentration of 100 μCi/ml (Copp and Bernfield, 1988b). The cultures were continued for a further five hours after re-gassing the embryos. At the end of the culture period, the embryos were washed using four changes of ice-cold dissection medium (10% FCS in DMEM) and four changes of ice-cold PBS to remove unincorporated $^{35}$S-radiolabel. The embryos were then examined under a stereomicroscope and the growth parameters measured (see earlier). Each embryo was stored in 100 μl of $TE_2$ buffer (50 mM Tris, pH 7.5; 2 mM EDTA) at -70°C until required.

### 3.6.2 Purification of glycosaminoglycans

Each embryo was sonicated on ice for 30 seconds and 20 μl was removed for scintillation counting and protein quantification. To facilitate precipitation of the labelled glycosaminoglycans, 20 μl of a solution of carrier hyaluronic acid and chondroitin-6-sulphate (each at a concentration of 2.5 mg/ml) was added to the remaining sample. The

sample was boiled for 10 minutes, cooled to room temperature and three volumes of 1.3% potassium acetate in 95% ethanol were added. The glycosaminoglycans were allowed to precipitate out overnight at -20°C. The sample was then centrifuged at 14,000 *g* for 15 minutes and the ethanol supernatant removed for scintillation counting. After drying, the pellet was re-suspended in 180 μl of de-ionised water and treated with 2 mg of Pronase at 55°C for six hours. A further 2 mg of Pronase was then added and left overnight to complete the protein degradation.

On the following morning, Pronase was inactivated by boiling for 10 minutes. The sample was then centrifuged and the supernatant decanted into a fresh eppendorf tube. The glycosaminoglycans were again precipitated overnight at -20°C using three volumes of 1.3% potassium acetate in 95% ethanol. Finally, the sample was centrifuged, the supernatant was removed for scintillation counting and the pellet was air-dried. This was then re-dissolved in 300 μl of de-ionised water for anion exchange chromatography and 30 μl was taken for scintillation counting.

### *3.6.3 Separation of glycosaminoglycans*

Anion exchange chromatography was used to separate the different sulphated glycosaminoglycans that had been labelled with $^{35}$S-sulphate. The highly negatively charged glycosaminoglycans were first allowed to bind to the DEAE cellulose in the anion exchange column. Then, by using a linearly increasing concentration of sodium chloride solution for elution, the different sulphated glycosaminoglycans were displaced from

the column at characteristic salt concentrations, thus permitting their separation (Copp and Bernfield, 1988a).

### 3.6.3.1 Preparation of anion exchange column

DEAE cellulose was allowed to equilibrate with three changes of 10 times its volume of 50 mM Tris buffer (pH 7.5) over 24 hours at 4°C. The slurry was then re-suspended in twice its volume of Tris buffer and packed into the glass anion exchange column. Excess buffer was drained and additional slurry was added until the column bed was 5 cm in height. Care was taken throughout the process to ensure that the column bed was not disturbed and that the column did not dry out.

### 3.6.3.2 Anion exchange chromatography

The anion exchange column was first flushed with 10 ml of 50 mM Tris buffer (pH 7.5). The sample was then carefully loaded without agitating the resin bed. A further wash with 10 ml of Tris buffer removed the non-negatively charged molecules which did not bind to the column. Elution was carried out using 50 mM Tris buffer (pH 7.5) with a linearly increasing gradient of sodium chloride (from 0 to 0.7 M) generated using a gradient maker that was placed horizontally on a magnetic stirrer. The flow rate was maintained at 15 ml/hr using a peristaltic pump and the total elution volume was 25 ml. Fractions were collected at two-minute intervals for scintillation counting and conductivity measurement.

### 3.6.4 Scintillation counting

Using a vortex mixer, 0.3 ml of each of the collected fractions was thoroughly mixed with 3 ml of scintillant fluid in a scintillation vial. The vials were then loaded on to a scintillation counter and the counts per minute (cpm) determined for each fraction. The disintegrations per minute (dpm) for the samples was calculated from the counting efficiency of the scintillation counter, which was determined using a $^{35}S$-standard with a known rate of disintegration.

### 3.6.5 Identification of glycosaminoglycans

Polysaccharide lyases are enzymes that cleave specific glycosidic linkages in glycosaminoglycans. They work through an eliminase mechanism, resulting in the formation of double bonds.

These lyases can be used for the identification of different glycosaminoglycans. The sample was divided into three aliquots. One aliquot was digested with heparitinase (which degraded heparan sulphate), the second aliquot was digested with chondroitinase ABC (which degraded chondroitin sulphate), and the third aliquot was treated with buffer alone. By passing the treated samples though the anion exchange column and comparing the eluted fractions, it was possible to ascertain the identity of the glycosaminoglycans present in the different fractions.

The commercial preparation of heparitinase used in this thesis contains trace amounts of chondroitin lyase activity (Seikagaku data sheet; Linhardt, 1995). To avoid potential problems in correct identification of

the radiolabelled glycosaminoglycans, "cold" carrier chondroitin sulphate was added to the reaction mixture when using heparitinase in order to block the action of the contaminating chondroitin lyases (Linhardt, 1995). Furthermore, only small amounts of heparitinase were used in the reactions and the incubation period was kept intentionally short.

### 3.6.5.1 Degradation by heparitinase

The reaction mixture consisted of 270 μl of the first aliquot of purified labelled glycosaminoglycans, 30 μl of 10X enzyme buffer (500 mM dibasic sodium phosphate, pH 7.6), and 50 μg each of "cold" chondroitin-4-sulphate and chondroitin-6-sulphate. After adding 30 μl of heparitinase (1 U/ml stock solution in 1X enzyme buffer), the reaction mixture was incubated at 37°C for three hours. The enzyme was then inactivated by boiling for 10 minutes.

### 3.6.5.2 Degradation by chondroitinase ABC

The reaction mixture comprised 270 μl of the second aliquot of purified glycosaminoglycans, 30 μl of 10X enzyme buffer (500 mM Tris, pH 8.0; 600 mM sodium acetate), and 30 μl of chondroitinase ABC (2 U/ml stock solution in 1X enzyme buffer). This was incubated at 37°C for three hours. The enzyme was then heat-inactivated.

## 3.7 Quantification of sulphated glycosaminoglycans

The sulphated glycosaminoglycan content of *splotch* ($Sp^{2H}$) embryos was determined using the cationic dye, 1,9-dimethylmethylene blue, which binds sulphated glycosaminoglycans at an acidic pH (Farndale et al, 1986). After binding, the dye exhibits a metachromatic colour change from blue to pinkish purple and the dye-glycosaminoglycan complex precipitates out of solution. Excess unbound dye can easily be removed by centrifugation. After dissociating the dye-glycosaminoglycan precipitate, the amount of dye present can be determined spectrophotometrically and the sulphated glycosaminoglycan content can be determined from a standard curve. The main sulphated glycosaminoglycans synthesised by the rodent embryo at the time of neurulation are heparan sulphate and chondroitin sulphate (Solursh and Morriss, 1977; Copp and Bernfield, 1988a). Thus, the chondroitin sulphate content in a sample can be determined by dividing the sample into two aliquots, treating one of them with chondroitinase ABC and the other with enzyme buffer alone, and calculating the difference in absorbance between the two aliquots. The amount of heparan sulphate present can be calculated from the absorbance of the enzyme-treated aliquot.

### *3.7.1 Pre-treatment of samples*

At the stage of development that was being studied, each embryo contained only small amounts of sulphated glycosaminoglycans. Hence, four embryos were pooled together for each run of the

quantification assay. The embryos were grouped according to genotype and the somite number, crown-rump length and head length were matched as closely as possible.

Each embryo was placed in 100 μl $TE_2$ buffer. The embryos were sonicated on ice and 10 μl was removed for protein quantification. The remaining sample was divided equally into two aliquots and digested overnight at 55°C with 5 μl of Proteinase K (10 mg/ml stock solution). Both aliquots were then treated sequentially with 5 μl of RNase A (10 mg/ml stock solution) and DNase I (10 U/μl stock solution) for five hours each at 37°C. After every treatment, the enzyme was heat-inactivated before addition of the next enzyme. This pre-treatment removed proteins, RNA and DNA that might interfere with the dye-binding assay.

The first aliquot was then mixed with 20 μl of 10X enzyme buffer (500 mM Tris, pH 8.0, 600 mM sodium acetate) and 20 μl of chondroitinase ABC (2 U/ml stock solution), while 40 μl of buffer solution alone was added to the second aliquot. The tubes were incubated at 37°C overnight and then boiled for 10 minutes on the following morning.

### *3.7.2 Dye-binding assay*

Each sample was thoroughly mixed with 1 ml of Blyscan dye reagent (1,9-dimethylmethylene blue) for 30 minutes using a vortex mixer to allow the dye to bind to and form a precipitate with the sulphated glycosaminoglycans. The precipitate was then packed to the bottom of the tube by centrifugation at 9000 *g* for 10 minutes. After carefully pouring out the dye solution, 0.5 ml of dissociation reagent (containing a chaotropic salt in an aqueous propan-1-ol solution) was added and the

contents mixed for 20 minutes to allow the precipitate to dissolve. Each sample was then transferred to a quartz micro cuvette and the absorbance at 656 nm measured on a spectrophotometer that had been zeroed against water. The reagent blank reading was subtracted from the test sample readings and the sulphated glycosaminoglycan content was determined from the standard curve, plotted using known concentrations of chondroitin-4-sulphate.

## 3.8 Protein quantification

The protein content of the samples was determined colorimetrically using the BCA Protein Assay Kit. This kit utilises the well-known biuret reaction, where the peptide bonds in proteins reduce cupric ions in an alkaline medium to cuprous ions. Each cuprous ion is then chelated with two molecules of bicinchoninic acid to form a purple soluble complex, the amount of which can be determined spectrophotometrically (Smith et al, 1985). As this is not a true end-point method, colour development continues after incubation, but this is sufficiently slowed by cooling the samples down to room temperature so that no significant errors are introduced if all the absorbance readings are done within 10 minutes. The protein content is then read off a standard curve.

The kit's working reagent was prepared by mixing 50 parts of Reagent A (containing bicinchoninic acid) with one part of Reagent B (containing 4% cupric sulphate). Each 50 μl of the test sample was thoroughly mixed with 1 ml of the working reagent and incubated at 60°C for 30 minutes. The samples were then cooled to room temperature and

transferred to plastic disposable semi-micro cuvettes. The absorbance at 562 nm was measured using a spectrophotometer that had been zeroed against water. The reagent blank reading was subtracted from the readings for the test samples and the protein content was then determined using the standard curve plotted using known concentrations of BSA.

*Chapter 4*

# DISTRIBUTION OF SULPHATED GLYCOSAMINOGLYCANS

## 4.1 Introduction

The murine central nervous system arises from the neural tube, which is formed in the embryonic process of neurulation (Copp et al, 1990; Smith and Schoenwolf, 1997). Primary neurulation gives rise to the cranial and upper spinal neural tube. This process involves inductive formation of the neural plate from the embryonic ectoderm by the underlying tissues. Shaping of the neural plate, elevation and convergence of the neural folds, and finally fusion of the neural folds give rise to a closed neural tube. In contrast, secondary neurulation occurs by cavitation of the medullary cord in the tail bud to form the distal neural tube.

Although neural fold elevation and fusion in spinal neurulation is a continuous process, regional variation in the morphology of the neuroepithelium has been described in three different strains of mouse, namely CBA/Ca, C57BL/6 and the mutant *curly tail* (Shum and Copp, 1996). Mode 1 closure occurs in the cervical and upper thoracic regions, between the eight- and fifteen-somite stages (Figure 1.6). The neuroepithelium bends at the median hinge point, which lies dorsal to the notochord. The straight neural folds elevate and converge in the midline like a closing book. Mode 2 closure is seen from the mid-thoracic level downwards, between the 16- and 23-somite stages. In this mode, both median and paired dorsolateral hinge points are present, resulting in a neural tube with a diamond shaped lumen. Mode 3 closure takes place from the 24-somite stage onwards. The median hinge is no longer formed, although the paired dorsolateral hinge points are still present (Ybot-Gonzalez and Copp, 1999). Instead, generalised

curvature of the neuroepithelium results in a neural tube with a circular lumen.

Glycosaminoglycans are long, unbranched, polyanionic molecules that are involved in many cellular processes, such as proliferation, differentiation, adhesion and migration (reviewed in Chapter 1). The expression of glycosaminoglycans is spatiotemporally regulated during development (Iozzo, 1998; Conrad, 1998; Bernfield et al, 1999; Oohira et al, 2000). At the time of neurulation in the mammalian embryo, the main non-sulphated glycosaminoglycan that is synthesised is hyaluronan, while the main sulphated glycosaminoglycans synthesised are heparan sulphate and chondroitin sulphate (Solursh and Morriss, 1977; Copp and Bernfield, 1988a). It has been suggested that these molecules are involved in regulating neural tube closure (Copp and Bernfield, 1988a; Tuckett and Morriss-Kay, 1989a; Morriss-Kay and Tuckett, 1989b). Although the distribution of glycosaminoglycans during murine spinal neurulation has been studied in the past (O'Shea, 1987; Copp and Bernfield, 1988a), the expression pattern of heparan sulphate and chondroitin sulphation in the posterior neuropore region during the three modes of closure has not been systematically examined.

This chapter examines the distribution of heparan sulphate and chondroitin sulphate in the region of the posterior neuropore during the three modes of spinal neurulation. It provides a baseline for the subsequent studies in the thesis where glycosaminoglycan content and sulphation are experimentally altered (Chapters 5 and 6), and where glycosaminoglycan synthesis and accumulation are measured in the *splotch* mouse mutant, which has both neurulation and neural crest abnormalities (Chapter 7). The distribution of heparan sulphate and

chondroitin sulphate is studied using Alcian blue histochemistry and antibody localisation. Alcian blue 8GX is a cationic dye, and is widely used in histochemistry for the localisation of glycosaminoglycans (Bancroft and Stevens, 1996). At pH 2.5, it stains both non-sulphated and sulphated glycosaminoglycans. In contrast, at pH 1, non-sulphated glycosaminoglycans are not bound by the dye. Heparan sulphate is localised using the mouse monoclonal antibody 10E4, and chondroitin sulphate is detected using the monoclonal antibody CS-56. Both antibodies have been previously shown to bind specifically to their respective glycosaminoglycans, and have been used in localisation of heparan sulphate and chondroitin sulphate in embryonic tissues (Avnur and Geiger, 1984; Morriss-Kay and Tuckett, 1989b; David et al, 1992; Bai et al, 1994; Sorrell et al, 1996).

## 4.2 Results

### *4.2.1 Regional morphological differences during spinal neurulation*

To determine whether morphological variations are present during spinal neurulation in the *CD1* mouse strain, the morphology of the posterior neuropore region was examined at various time points between E8.5 and E10.0.

Mode 1 closure is seen at E8.5/E9.0 (Figure 4.1A). The neural plate is bent at the median hinge point, which lies dorsal to the notochord in the midline. The lateral portions of the neural folds are elevated and the dorsal tips of the folds converge towards the midline. The region of the neural fold lying between the apex and the median hinge point is straight.

Mode 2 closure is seen at E9.0/E9.5 (Figure 4.1B). In addition to the median hinge point, paired dorsolateral hinge points are seen in the neural folds. Although bending of the neural folds at the median hinge point is less acute at this stage compared with Mode 1 closure, the neural fold apices are brought to the midline by additional bends at the paired dorsolateral hinge points. The neural fold regions between the median and dorsolateral hinge points, and between the dorsolateral hinge points and neural fold apices, are straight.


**Figure 4.1 Haematoxylin and eosin stained transverse sections through the posterior neuropore region.** Sections illustrate Mode 1 (10-somite stage; Panel A), Mode 2 (19-somite stage; Panel B) and Mode 3 (25-somite stage; Panel C) closures. The median hinge point (star) is seen in both Modes 1 and 2, but is absent in Mode 3. Paired dorsolateral hinge points (arrows) are clearly seen in Mode 2, but are masked by the generalised curvature of the neuroepithelium in Mode 3. Abbreviations: da, dorsal aorta; nc, notochord. Scale bar, 100 μm.

Mode 3 closure is seen at E9.5/E10.0 (Figure 4.1C). The median hinge point is no longer present. Instead, the neural plate curves along its transverse axis, elevating the sides of the neural plate and bringing the neural fold apices towards the dorsal midline. The paired dorsolateral hinge points are not obvious as they are masked by the generalised curvature of the neural plate, but can be revealed by treatment of embryos with cytochalasin D (Ybot-Gonzalez and Copp, 1999).

### 4.2.2 Alcian blue histochemistry

To determine the expression pattern of sulphated glycosaminoglycans in relation to the different modes of spinal neurulation, the posterior neuropore region of *CD1* mouse embryos was stained with Alcian blue 8GX at pH 1 between E8.5 and E10.0.

In Mode 1 neurulation, moderately strong staining is seen in the basement membrane of the neuroepithelium, the surface ectoderm, the gut endoderm and the endothelium of the paired dorsal aortae (Figures 4.2A and B). Strong staining is present along the base of the neuroepithelium in its medial region, where the neural plate contacts the paraxial mesoderm. In contrast, in the lateral region, where the neuroepithelium lies adjacent to the surface ectoderm, staining is much less intense. Alcian blue is also present in an incomplete layer around the notochord, with especially strong staining in the region adjacent to the median hinge point, but weaker staining on the surface of the notochord adjacent to the gut endoderm. The apical surface of the neuroepithelium and the entire paraxial mesoderm are very weakly stained.

**Figure 4.2 Alcian blue staining of transverse sections through the posterior neuropore region.** Sections taken at Mode 1 (10-somite stage; Panel A), Mode 2 (19-somite stage; Panel C) and Mode 3 (25-somite stage; Panel E) closures. (B) and (D) are magnified views of (A) and (C) respectively. The specimen in (D) has been rotated anti-clockwise by 90°. In general, the intensity of staining increases with progression of posterior neuropore closure. Staining of the neuroepithelial basement membrane is stronger medially in Mode 1 and Mode 2, and is reduced in regions where the neuroepithelium is in close apposition with the overlying surface ectoderm. Transition zone between the two regions is marked by the arrowhead. Arrows, paired dorsolateral hinge points; star, median hinge point. Abbreviations: da, dorsal aorta; neb, neuroepithelial basement membrane; nc, notochord. Scale bar, 100 μm (A, C, E); 50 μm (B, D).

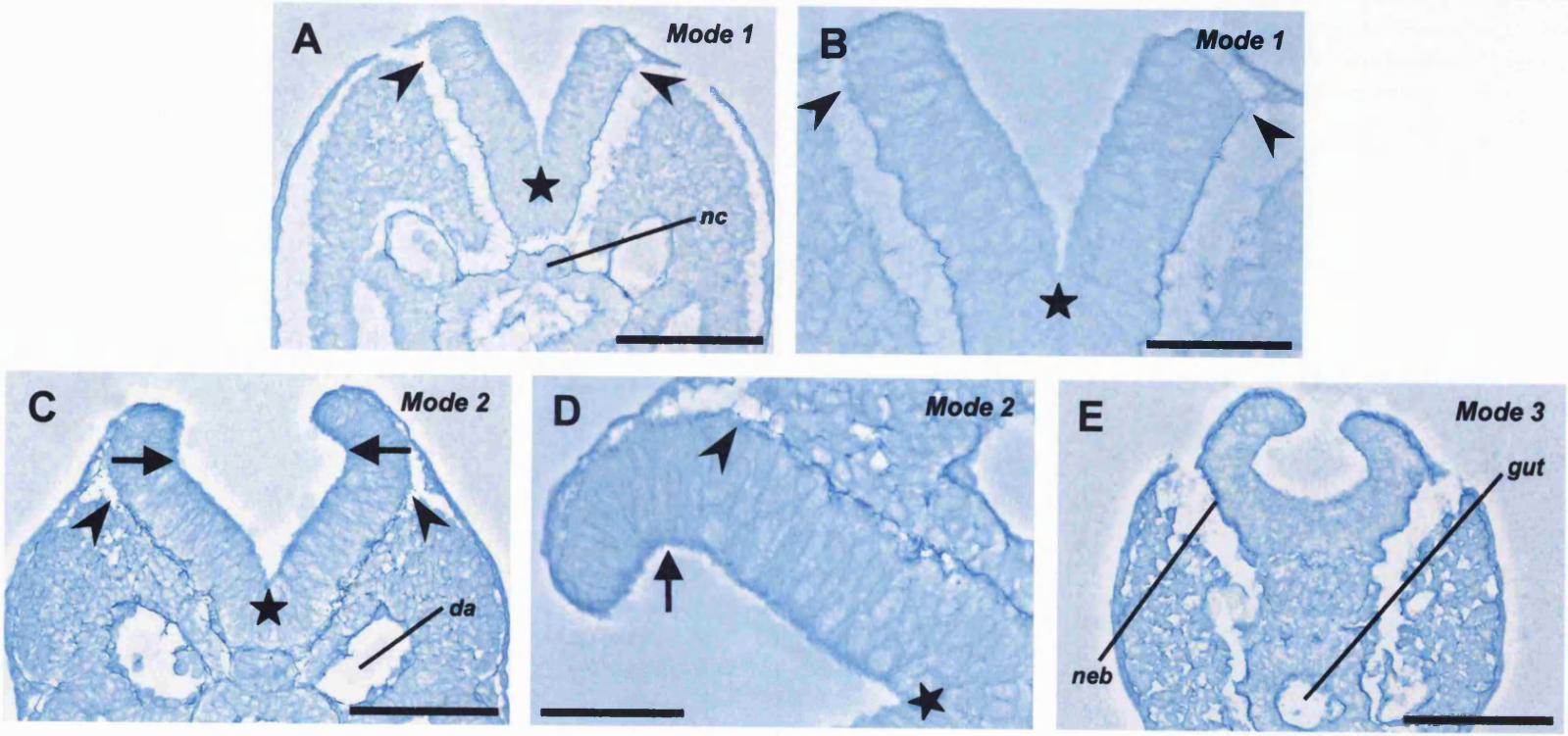
A
Mode 1
nc
B
Mode 1
C
Mode 2
da
D
Mode 2
E
Mode 3
gut
neb

The staining pattern in Mode 2 neurulation is largely similar to that seen in Mode 1, but with a stronger intensity of staining in most areas (Figures 4.2C and D). The neuroepithelial basement membrane between the median and dorsolateral hinge points is strongly stained. In contrast, staining is lighter in the region between the dorsolateral hinge point and the neural fold apex, where the neuroepithelium is in close apposition with the surface ectoderm. The transition region where this change from a less intensely stained to a more intensely stained area occurs corresponds to the location of the dorsolateral hinge point.

In Mode 3 neurulation, unlike Modes 1 and 2, strong staining of the neuroepithelial basement is seen to extend into the tips of the neural folds, despite the close apposition of the neuroepithelium and surface ectoderm in the lateral region of the neural folds (Figure 4.2E). In contrast, staining of the neuroepithelial basement membrane is relatively weak and patchy in the midline, where the neuroepithelium appears not to be clearly demarcated from the underlying chordamesoderm. The staining pattern of the other tissues resembles that seen in Mode 2.

## *4.2.3 Immunohistochemistry*

### 4.2.3.1 Antigen recognition

To confirm that the anti-heparan sulphate antibody and the anti-chondroitin sulphate antibody recognise their respective glycosaminoglycans, tissue sections were pre-incubated with either heparitinase (to degrade heparan sulphate), chondroitinase (to degrade

chondroitin sulphate), or buffer solution before applying the primary antibodies.

When tissue sections were pre-treated with buffer solution, strong immunostaining is seen with both the anti-heparan sulphate antibody (Figure 4.3A) and the anti-chondroitin sulphate antibody (Figure 4.3C). In both instances, the stain is strongly localised to the basement membrane of the neural tube, surface ectoderm and gut endoderm. Strong staining is also seen around the notochord, on the apical surface of the gut endoderm and in the material lying within the lumen of the gut.

In contrast, when heparan sulphate in the tissue sections was first degraded with heparitinase, the immunostaining is very much reduced (Figure 4.3B). A similar reduction in staining for chondroitin sulphate is observed when the tissue is pre-treated with chondroitinase to degrade chondroitin sulphate (Figure 4.3D). However, in both cases, the intensity of staining of the gut contents and the apical surface of the gut endoderm is unaffected by the enzyme treatment. This is borne in mind when interpreting the results of the subsequent experiments.

#### 4.2.3.2 Antibody titration

To determine the optimal concentration of primary antibody for use in immunolocalisation of heparan sulphate and chondroitin sulphate, a series of titrations was done for each antibody on adjacent tissue sections.

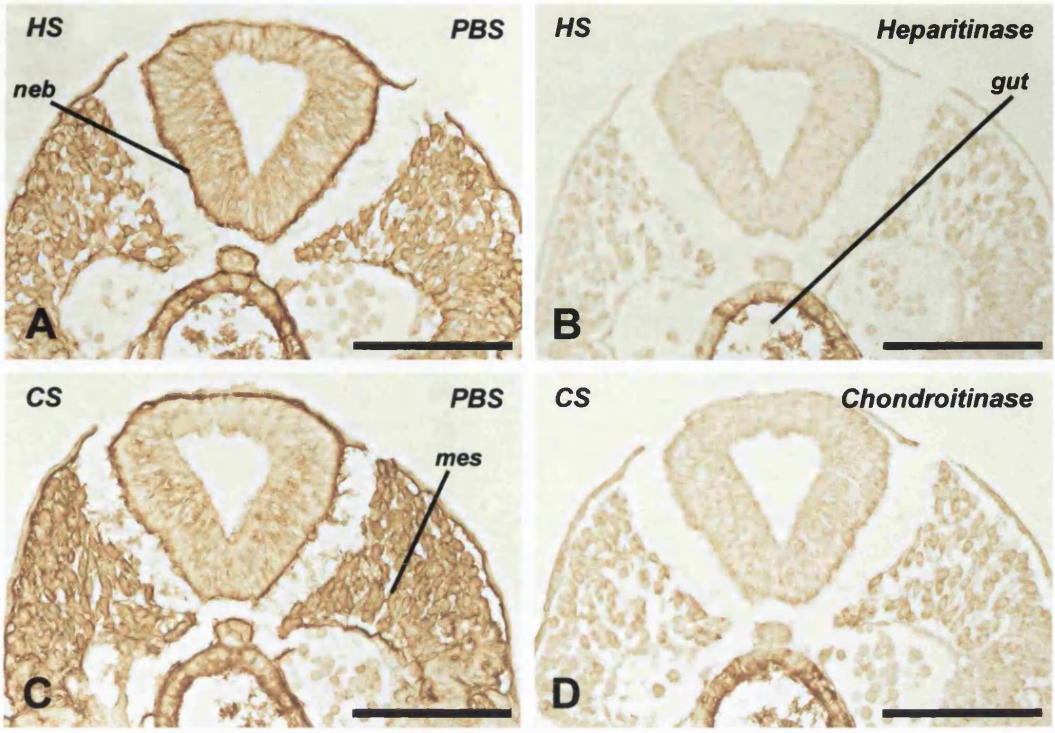


**Figure 4.3 Antibody recognition of heparan sulphate and chondroitin sulphate.** Sections were first incubated with either phosphate buffered saline (A, C), heparitinase (B) or chondroitinase (D). They were then immunostained for either heparan sulphate (A, B) or chondroitin sulphate (C, D). Note the decrease in staining intensity by the primary antibodies after enzymatic glycosaminoglycan degradation (compare A and C with B and D respectively). Non-specific staining of the gut contents and the apical surface of the gut endoderm is present. This is resistant to the enzymatic treatment. Abbreviations: CS, chondroitin sulphate; HS, heparan sulphate; mes, mesoderm; neb, neuroepithelial basement membrane; PBS, phosphate buffered saline. Scale bar, 100 μm.

Figures 4.4A, B and C show the titration series for 10E4 (anti-heparan sulphate antibody) at a concentration of 1:150, 1:100 and 1:50 respectively. The staining intensity increases from 1:150 dilution to 1:100 dilution, but does not increase further when the antibody is used at the increased titre of 1:50. Thus, a dilution factor of 1:100 was used for this antibody in subsequent studies.

Figures 4.4D, E and F show the titration series for CS-56 (anti-chondroitin sulphate antibody). As in the case for 10E4, the staining intensity increases from a 1:150 dilution to a 1:100 dilution. No significant increase in staining intensity is seen at a concentration of 1:50. This antibody was used at a 1:100 dilution in subsequent experiments.

An isotype matched mouse IgM, raised against *Aspergillus niger* glucose oxidase (an enzyme neither present nor inducible in mammalian tissues), was used as a negative control instead of the anti-glycosaminoglycan antibodies. No staining is seen at a concentration that is equivalent to a 1:100 dilution of the anti-glycosaminoglycan antibodies (Figure 4.4G). Figure 4.4H shows the tissue architecture of the section in Figure 4.4G, viewed under phase contrast microscopy.

#### 4.2.3.3 Expression pattern of heparan sulphate

In Mode 1 neurulation, moderately strong staining is seen in the basement membrane of the surface ectoderm, whereas the apical surface of the neuroepithelium, the neuroepithelial basement

**Figure 4.4 Titration of primary antibody concentration.** A titration series was performed for the anti-heparan sulphate antibody (A - C) and the anti-chondroitin sulphate antibody (D - F). The dilution factor for each antibody is shown in the upper right hand corner of each panel. For both antibodies, the intensity of staining increases when the antibody dilution is reduced from 1:150 to 1:100. Further reduction in antibody dilution did not result in a significant increase in the staining intensity. No staining is seen in the negative control (G), where an isotype matched mouse IgM, raised against *Aspergillus niger* glucose oxidase (an enzyme neither present nor inducible in mammalian tissues), was used as the primary antibody at a concentration equivalent to a 1:100 dilution of the anti-glycosaminoglycan antibody. The section in (G) is shown under phase contrast microscopy in (H). Abbreviations: CS, chondroitin sulphate; HS, heparan sulphate; mes, mesoderm; neb, neuroepithelial basement membrane. Scale bar, 100 μm.

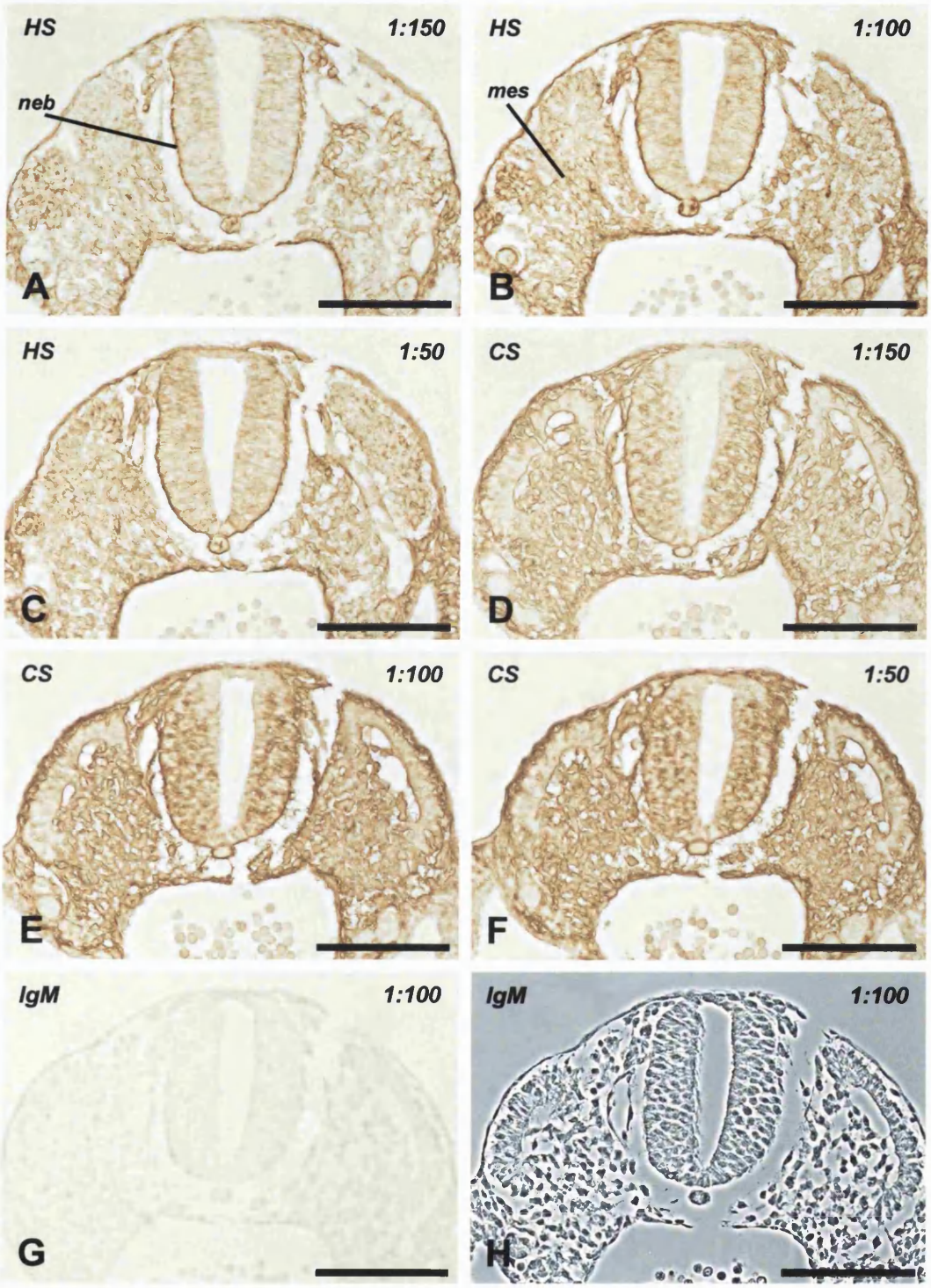
HS
1:150
neb
A
HS
1:100
mes
B
HS
1:50
C
CS
1:150
D
CS
1:100
E
CS
1:50
F
IgM
1:100
G
IgM
1:100
H

membrane and the paraxial mesoderm are all very weakly stained (Figure 4.5A). Non-specific staining of the gut contents is present, as discussed above.

In Mode 2 neurulation, moderately strong staining is seen in the neuroepithelial basement membrane (Figure 4.5B). The staining intensity varies along the basal surface of the medial part of the neuroepithelium, with areas of moderately strong staining dispersed between less strongly stained regions. Moderately strong staining is also present on the apical surface of the neuroepithelium and around the cells of the mesoderm.

The staining pattern in Mode 3 neurulation is largely similar to that seen in Mode 2, but with a higher intensity (Figure 4.5C). Strong staining is seen in the basement membrane of the neuroepithelium, surface ectoderm and gut endoderm. In the midline where the neuroepithelium appears not to be well demarcated from the underlying chordamesoderm, staining of the neuroepithelial basement membrane is discontinuous.

#### 4.2.3.4 Expression pattern of chondroitin sulphate

In Mode 1 neurulation, moderately strong staining for chondroitin sulphate is seen in the basement membrane of the surface ectoderm, gut endoderm and endothelium of the paired dorsal aortae (Figures 4.6A and B). The neuroepithelial basement membrane is also moderately stained, but the intensity of staining is reduced at the lateral margins of the neuroepithelium where the neural plate contacts the

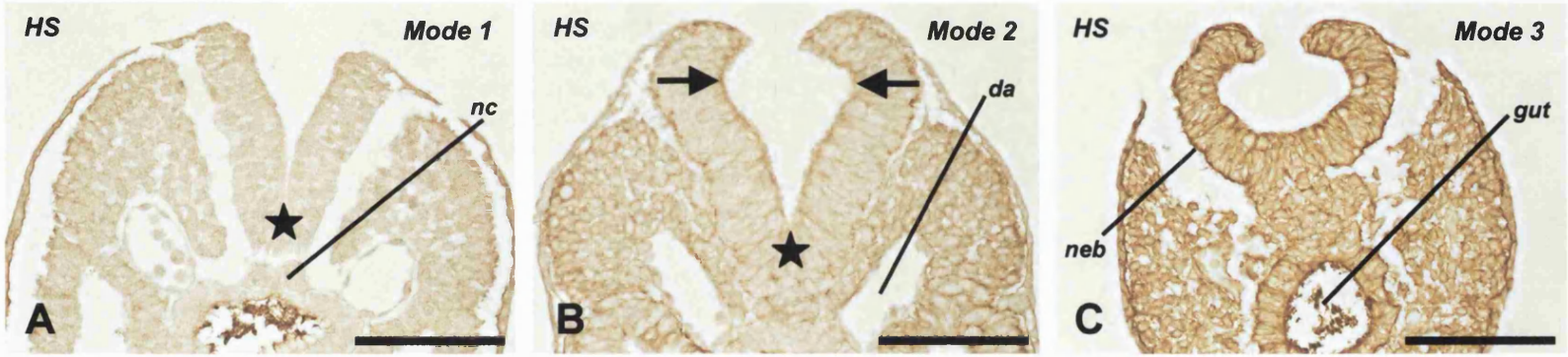


**Figure 4.5 Immunostaining for heparan sulphate in transverse sections through the posterior neuropore region.** Sections taken at Mode 1 (10-somite stage; Panel A), Mode 2 (19-somite stage; Panel B) and Mode 3 (25-somite stage; Panel C) closures. Staining intensity increases generally with progression of posterior neuropore closure. Arrows, paired dorsolateral hinge points; star, median hinge point. Abbreviations: da, dorsal aorta; HS, heparan sulphate; neb, neuroepithelial basement membrane; nc, notochord. Scale bar, 100 μm.

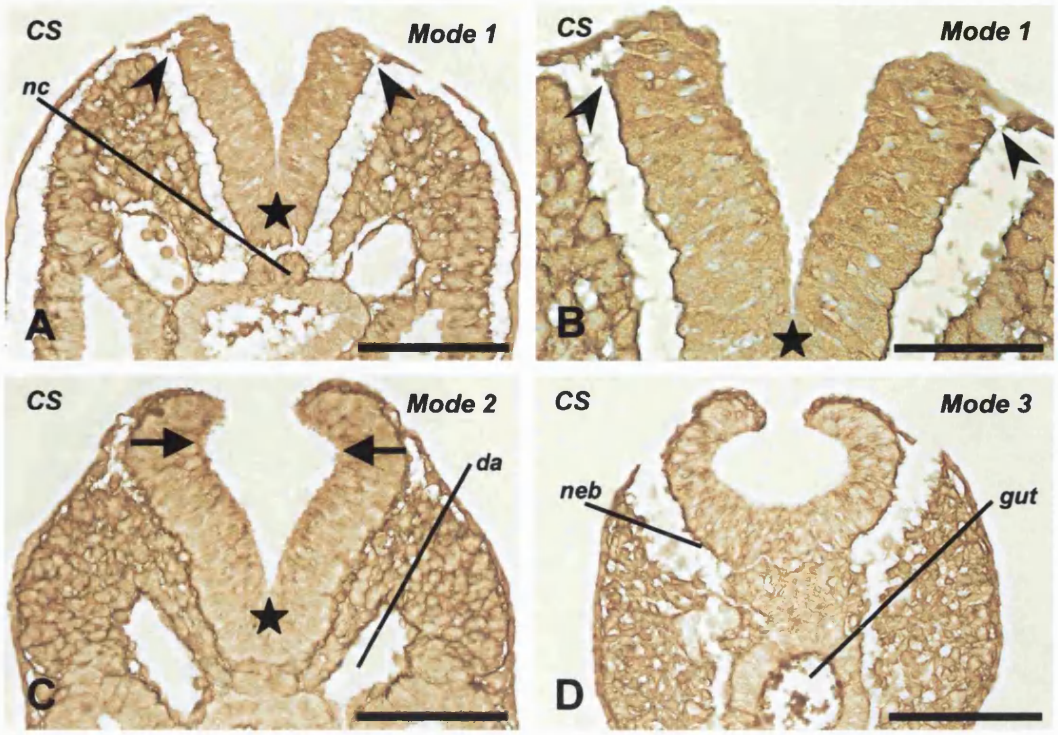


**Figure 4.6 Immunostaining for chondroitin sulphate in transverse sections through the posterior neuropore region.** Sections taken at Mode 1 (10-somite stage; Panel A), Mode 2 (19-somite stage; Panel C) and Mode 3 (25-somite stage; Panel D) closures. (B) is a higher magnification of (A). In general, there is no marked change in staining intensity with progression of posterior neuropore closure. In Mode 1, the lateral neuroepithelial basement membrane, where the neuroepithelium lies adjacent to the surface ectoderm, stains less intensely than the medial region. The transition zone between the two regions is marked by the arrowhead. Arrows, paired dorsolateral hinge points; star, median hinge point. Abbreviations: CS, chondroitin sulphate; da, dorsal aorta; neb, neuroepithelial basement membrane; nc, notochord. Scale bar, 100 μm (A, C, D); 50 μm (B).

surface ectoderm. In addition, the dorsal and lateral sides of the notochord, as well as the area around the mesodermal cells, are moderately strongly stained. Non-specific staining of the gut contents is present.

The staining patterns in Modes 2 and 3 neurulation are similar to that seen in Mode 1, and there is no marked difference in staining intensity between the three modes (Figures 4.6C and D). In both Modes 2 and 3, strong staining of the neuroepithelial basement membrane is seen, and this extends laterally into the apices of the neural folds in contrast to Mode 1. In the midline, where the neuroepithelium appears not to be clearly distinct from the underlying chordamesoderm, staining of the neuroepithelial basement membrane is weaker and tends to form a discontinuous layer. The area around the cells in the mesoderm is well stained.

## 4.3 Discussion

In this chapter, the presence of regional variation in the morphology of the neuroepithelium of *CD1* mouse embryo during spinal neurulation is confirmed. The modes of neural fold elevation and closure are similar to those described in other mouse strains. Mode 1 closure entails the formation of a median hinge point, Mode 2 closure contains both median and paired dorsolateral hinge points, and Mode 3 closure involves paired dorsolateral hinge points and a generalised curvature of the neuroepithelium (Shum and Copp, 1996; Ybot-Gonzalez and Copp, 1999). Progression through the three closure modes is associated with an increase in the amount of sulphated glycosaminoglycans laid down in the neuroepithelial basement membrane as well as the surrounding tissues of the posterior neuropore region. Regional differences in the expression pattern of these glycosaminoglycans are seen in the neuroepithelial basement membrane.

### *4.3.1 Sulphated glycosaminoglycans and spinal neurulation*

This study shows that both heparan sulphate and chondroitin sulphate are present in the neuroepithelial basement membrane during spinal neurulation. In general, the main basement membrane heparan sulphate proteoglycans are perlecan and agrin, and the main basement membrane chondroitin sulphate proteoglycan is bamacan (Iozzo, 1998). These glycosaminoglycans, together with other components of the neuroepithelial basement membrane, may function to support the neuroepithelium during spinal neurulation. It has been suggested that

extrinsic forces pushing on the neuroepithelium might be primarily involved in elevation and convergence of the neural folds in Modes 1 and 2 neurulation (Schoenwolf, 1988; Alvarez and Schoenwolf, 1992; Shum and Copp, 1996). In this hypothesis, bending at the median hinge point is explained by tethering of the medial part of the neural plate to the underlying notochord. The neuroepithelial basement membrane may help to maintain the neural folds in a straight and rigid manner during Modes 1 and 2 neurulation. Indeed, bending at the paired dorsolateral hinge points in Mode 2 neurulation occurs at the lateral regions of the neuroepithelium where a smaller amount of sulphated glycosaminoglycans is present in the basement membrane. Maintenance of the rigidity of the neuroepithelium is likely to involve not just the basement membrane but the cytoskeleton of the neuroepithelium as well. Disassembly of actin microfilaments by cytochalasin D treatment leads to a loss of this rigidity (Ybot-Gonzalez and Copp, 1999). Members of the syndecan family of heparan sulphate proteoglycan colocalise with actin, are able to interact with these microfilaments through their cytoplasmic domain, and help in the organisation of the cytoskeleton (Carey et al, 1996; Bernfield et al, 1999).

It has been proposed that spinal neurulation involves not just mechanistic elevation and convergence of the neural folds but a progressive delamination of the surface ectoderm and neuroepithelium as well (Martins-Green, 1988). It is suggested that the dorsal third of the neural tube forms by the delamination of these two epithelia, resulting in a transient period where there is an incomplete basement membrane underlying the two epithelia. The lack of sulphated glycosaminoglycans in the lateral regions of the neural folds in Modes 1

and 2 neurulation supports this hypothesis. However, in Mode 3 neurulation, sulphated glycosaminoglycans in the neuroepithelial basement membrane extend into the apices of the neural folds. This suggests that a different neurulation mechanism might be working at this time. Indeed, intrinsic forces appear to be sufficient for neural tube closure in Mode 3 neurulation (van Straaten et al, 1993). Closure of the posterior neuropore occurs normally in mouse neural tube explants, in which the neuroepithelium has been completely separated from adjacent non-neural tissues. Since neural fold elevation and fusion occur through curvature of the neural plate rather than delamination of the neuroepithelium and surface epithelium in Mode 3 neurulation, the sulphated glycosaminoglycans form a complete layer underlying both epithelia.

Besides having a structural role, sulphated glycosaminoglycans might regulate neurulation by interacting with signalling molecules that are involved in the neurulation process. An example of such a signalling molecule is Sonic hedgehog, which is involved in formation of the median hinge point (Ybot-Gonzalez and Copp, unpublished). Heparan sulphate is required for the localisation and propagation of Hedgehog signalling (Bellaiche et al, 1998; The et al, 1999; Lin et al, 2000). This is further investigated in Chapter 5.

In summary, the sulphated glycosaminoglycans are expressed at the right time and in the right place to be involved in spinal neurulation. Regional variation in the expression pattern of these molecules exists, and this appears to correlate with the different modes of neurulation and the relative importance of extrinsic and intrinsic forces at different stages of spinal neurulation.

### 4.3.2 Sulphated glycosaminoglycans and neural crest migration

Emigration of neural crest cells from the neural tube requires the presence of locomotory ability in the cells and a suitable substrate for migration, as well as an absence of migratory barriers and adhesion between cells (Newgreen and Gibbins, 1982). The basal lamina has been shown to be impenetrable to neural crest cells, and might act as a barrier to the initiation of neural crest migration (Erickson, 1987). There is a smaller amount of sulphated glycosaminoglycans in the lateral neuroepithelial basement membrane than in the medial region during Modes 1 and 2 neurulation. This might be due to an incomplete basal lamina in the lateral part of the neuroepithelium, which would then allow neural crest cells to emigrate from the neuroepithelium. Indeed, it has been shown that a continuous basal lamina does not form over the dorsal neural tube until emigration of neural crest cells is complete (Martins-Green and Erickson, 1986). However, in Mode 3 neurulation, the presence of a complete basal lamina is suggested by the continuous layer of sulphated glycosaminoglycans in the neuroepithelial basement membrane, which extends into the neural fold apices. Emigration of the neural crest cells from the neuroepithelium at this stage might depend on remodelling of the extracellular matrix by proteases secreted by the neural crest (Menoud et al, 1989).

Immunostaining for chondroitin sulphate shows strong staining in the neuroepithelium basement membrane and around the mesoderm cells in all three modes of neurulation. This molecule is thus well positioned to influence neural crest cell emigration and migration. Indeed,

chondroitin sulphate has been shown to regulate emigration of cranial neural crest cells from the neuroepithelium (Morriss-Kay and Tuckett, 1989b). In the cranial region, degradation of chondroitin sulphate results in an inhibition of neural crest cell emigration. In addition, different chondroitin sulphate proteoglycans have been implicated in guiding neural crest migration (Henderson and Copp, 1997; Perris and Perissinotto, 2000). For example, aggrecan appears to be strongly inhibitory to migration of neural crest cells whereas these cells tend to move along an increasing concentration gradient of versican (Perissinotto et al, 2000). The role of chondroitin sulphate in neural crest migration is further investigated in Chapter 7.

### *4.3.3 Comparison between Alcian blue staining and immunostaining*

Alcian blue staining and immunohistochemistry complement each other in the localisation of sulphated glycosaminoglycans. When the Alcian blue solution is adjusted to pH 1, the dye stains all sulphated glycosaminoglycans (Bancroft and Stevens, 1996). On the other hand, immunostaining allows localisation of specific epitopes on sulphated glycosaminoglycans and provides stronger staining and better morphological detail (Daugaard et al, 1991; this chapter). However, care must be taken when interpreting the results of immunostaining of complex molecules such as heparan sulphate. An absence of staining with a monoclonal antibody, such as the 10E4 antibody used in this thesis, only implies that the epitope recognised by this antibody is absent. It does not necessarily mean that heparan sulphate is not expressed in the tissue being studied. Indeed, immunostaining of rat

kidneys with five different anti-heparan sulphate antibodies reveals five different expression patterns (van Kuppevelt et al, 1998). This suggests that the heparan sulphate structure varies in different tissues, and this is likely to have a biological significance. Furthermore, the structure of heparan sulphate that is expressed by a tissue changes with the stage of development. For example, heparan sulphate binds to and potentiates the activity of fibroblast growth factors. When neural precursor cells switch from a proliferative to a differentiative state, there is an accompanying change in the sulphation pattern of heparan sulphate, which switches the potentiating activity of the glycosaminoglycan from FGF-2 to FGF-1 (Nurcombe et al, 1993; Brickman et al, 1998).

Bearing the above points in mind, a comparison of the expression pattern of sulphated glycosaminoglycan, as revealed by Alcian blue staining, is made with the expression patterns determined using the monoclonal anti-heparan sulphate and anti-chondroitin sulphate antibodies. At first sight, the pattern of Alcian blue staining appears to largely correspond to the anti-chondroitin sulphate immunostaining in all the three modes of neurulation (compare Figure 4.2 with Figure 4.6). However, there is an obvious difference in the staining patterns produced by the two methods in the neuroepithelial basement membrane in Mode 2 neurulation (compare Figures 4.2C and D with Figure 4.6C). Strong Alcian blue staining is present in the medial region of the neuroepithelial basement membrane between the paired dorsolateral hinge points, but the staining is less intense between the dorsolateral hinge point and the neural fold apex (Figures 4.2C and D). In contrast, using the anti-chondroitin sulphate antibody, strong staining is seen throughout the neuroepithelial basement membrane including

the neural fold apices, except in the midline where the neuroepithelium abuts the underlying notochord (Figure 4.6C). A less marked difference is the presence of moderately stained alcianophilic material on the neuroepithelial apical surface, which is not particularly well stained with either the anti-heparan sulphate or the anti-chondroitin sulphate antibodies (compare Figures 4.2C and D, Figure 4.5B and Figure 4.6C). In addition, the areas around the mesodermal cells are quite well stained for chondroitin sulphate, even in Modes 1 and 2, whereas these areas do not take up much Alcian blue stain (compare Figures 4.2A to D with Figures 4.6A to C). These discrepancies are not due to variation between embryos, since adjacent sections from each embryo were used for Alcian blue staining and immunohistochemistry, and correlation of staining patterns is always made using sections taken from the same embryo.

One explanation for these discrepancies is that the embryo produces one or more heparan sulphate species that are not recognised by the 10E4 antibody. In this hypothesis, the moderate Alcian blue staining seen in Mode 2 neurulation at the base of the neuroepithelium, between the dorsolateral hinge points and the neural fold apices (Figures 4.2C and D), represents the sum of the chondroitin sulphate and heparan sulphate present in this region (Figures 4.5B and 4.6C). Similarly, the relatively weak Alcian blue staining seen around the mesodermal cells (Figures 4.2A to D) represents the sum of the two sulphated glycosaminoglycans detected with immunohistochemistry (Figures 4.5A and B; Figures 4.6A to C). Additional heparan sulphate species, which are not recognised by antibody 10E4, are located in the medial neuroepithelial basement membrane between the median hinge point and the lateral part of the basement membrane (indicated by the

arrowheads in Figures 4.2A to D). The relatively strong Alcian blue staining seen in this region is thus accounted for by the concomitant presence of chondroitin sulphate and at least two species of heparan sulphate. It is unlikely that the relative lack of staining for heparan sulphate is due to interference by colocalised chondroitin sulphate, since chondroitin sulphate has been shown not to interfere with the binding of the 10E4 anti-heparan sulphate antibody to its epitope on heparan sulphate (David et al, 1992).

Support for the presence of more than one heparan sulphate species comes from biochemical analysis of the accumulation of sulphated glycosaminoglycans during neurulation. In both early and later stages of spinal neurulation, radiolabelling of glycosaminoglycans suggests that the average rate of heparan sulphate accumulation is similar to the rate of chondroitin sulphate accumulation in the caudal region of the embryo (Solursh and Morriss, 1977; Copp and Bernfield, 1988a). This is not in agreement with the change in immunostaining intensity for heparan sulphate (Figure 4.5) and chondroitin sulphate (Figure 4.6). Progressing from Mode 1 to Mode 3 neurulation, there is a no marked increase in staining for chondroitin sulphate. The increase in Alcian blue staining is also relatively gradual. In contrast, a large increase in the intensity of immunostaining for heparan sulphate is present as Mode 1 progresses to Mode 3. This can be explained by the presence of a second heparan sulphate species that is not recognised by the 10E4 antibody. As Mode 1 progresses to Mode 3, the structure of the heparan sulphate that is produced changes from one that is not recognised by 10E4 to one that is recognised. Furthermore, Sonic hedgehog, which is produced in the notochord, induces formation of the median hinge point during neurulation (Ybot-Gonzalez and Copp,

unpublished). It has been shown that heparan sulphate is required for localisation and propagation of the Hedgehog signal (Bellaiche et al, 1998; The et al, 1999; Lin et al, 2000). The presence of a heparan sulphate species that is not recognised by antibody 10E4 would account for the propagation of the Sonic hedgehog signal from the notochord to the neuroepithelium, despite the apparent lack of immunostaining for heparan sulphate in the notochord and the median hinge point using the 10E4 antibody.

It is interesting to postulate that these two heparan sulphate species might have different Sonic hedgehog-binding avidities. Thus, species 1 (not recognised by 10E4) might bind Sonic hedgehog and help to propagate the signal from the notochord to the overlying neuroepithelium to induce median hinge point formation. Production of heparan sulphate species 1 might decrease with progression from Mode 1 to Mode 3 of spinal neurulation. In contrast, species 2 (recognised by 10E4) might not bind Sonic hedgehog, and the synthesis of species 2 might increase with progression of spinal neurulation. This could account for the induction of median hinge point formation in Modes 1 and 2 closure, and the absence of the median hinge point in Mode 3 closure.

### *4.3.4 Critique of fixative used*

The fixatives used in this thesis for the study of heparan sulphate and chondroitin sulphate are 4% paraformaldehyde and Bouin's solution. Both of them are formalin-based fixatives. In a systematic study of the effect of different fixatives on the preservation of embryonic material that is stainable by Alcian blue at pH 2.5, an acetic acid/ethanol-based

fixative (Sainte-Marie's solution) is found to provide a strong and reproducible staining pattern with good preservation of tissue structure (Tuckett and Morriss-Kay, 1988). Alcian blue at pH 2.5 stains both non-sulphated (mainly hyaluronan) and sulphated glycosaminoglycans. It has recently been suggested that the preservation of Alcian blue stainable material is due to the generation of a semi-solid, poorly water-soluble gel from hyaluronan in the presence of ethanol and acid (Lin et al, 1997). However, the preservation of sulphated glycosaminoglycans, such as heparan sulphate and chondroitin sulphate, that are covalently linked to proteoglycan core proteins appears to be satisfactory in formalin-fixed tissues (Lin et al, 1997). When Alcian blue staining of tissues fixed in an acetic acid/ethanol fixative were compared with tissues fixed in formalin alone, there was only a very slight decrease in staining intensity after hyaluronan degradation by *Streptomyces* hyaluronidase (Lin et al, 1997). Thus, heparan sulphate and chondroitin sulphate appear to be indirectly but adequately fixed by formaldehyde through the reaction of formaldehyde with the proteoglycan core proteins.

# *Chapter 5*

# HEPARAN SULPHATE

# AND

# SPINAL NEURULATION

## 5.1 Introduction

The neural tube is the primordium of the central nervous system. Closure of the neural tube involves a series of morphogenetic events in which the neural folds are elevated and the neural fold apices are brought to converge in the dorsal midline (Copp et al, 1990; Smith and Schoenwolf, 1997; reviewed in Chapter 1). Fusion of the neuroepithelium across the midline closes the neural tube off to the external environment dorsally. This is accompanied by fusion of the two sides of the surface ectoderm to form a continuous ectodermal layer overlying the neural tube. In spinal neurulation, elevation and midline apposition of the neural folds are accompanied by the formation of hinge points in the neuroepithelium (Shum and Copp, 1996; Chapter 4). Mode 1 neurulation occurs early in spinal neurulation, and this is accompanied by the formation of a median hinge point in the midline of the neural plate. In Mode 2 neurulation, paired dorsolateral hinge points are formed on the lateral sides of the neural folds in addition to the median hinge point in the midline. Mode 3 neurulation, which occurs from the 24-somite stage onwards, involves a generalised curvature of the neuroepithelium together with bending at the paired dorsolateral hinge points (Ybot-Gonzalez and Copp, 1999). The median hinge point is not present at this stage.

The sulphated glycosaminoglycans are large polyanionic molecules that are attached to specific core proteins to form proteoglycans (Varki et al, 1999). Expression of the different glycosaminoglycans is developmentally regulated. Sulphated glycosaminoglycans bind to and modulate the action of signalling molecules during development, and

this interaction is affected by the fine structure of the glycosaminoglycans, such as the degree of sulphation, acetylation and epimerisation (Guimond et al, 1993; Ishihara, 1994; Bernfield et al, 1999; Oohira et al, 2000).

The main sulphated glycosaminoglycans synthesised at the time of neurulation in the rodent embryo are heparan sulphate and chondroitin sulphate (Solursh and Morriss, 1977; Copp and Bernfield, 1988a). These molecules are present in the basement membrane of the neuroepithelium and surface ectoderm, as well as in the adjacent tissues of the posterior neuropore region (Chapter 4). The expression pattern of the sulphated glycosaminoglycans correlates with the progression from Mode 1 to Mode 3 in spinal neurulation. These molecules are thus well positioned to influence spinal neurulation. Heparan sulphate appears to be essential for cranial neurulation. Both degradation of heparan sulphate by heparitinase treatment and inhibition of heparan sulphate attachment to the proteoglycan core protein by exposure to β-D-xyloside result in inhibition of cranial neural tube closure (Morriss-Kay and Crutch, 1982; Tuckett and Morriss-Kay, 1989a). On the other hand, chondroitin sulphate seems to indirectly affect the speed of cranial neural tube closure by its influence on neural crest emigration from the cranial neuroepithelium (Morriss-Kay and Tuckett, 1989b).

Although sulphated glycosaminoglycans are needed for cranial neurulation, their role in spinal neurulation has not been systematically studied. For example, it is not known whether these molecules are required for formation of the median and paired dorsolateral hinge points, and whether the sulphate group on these molecules is important.

This chapter aimed to answer these questions by inhibiting the sulphation of glycosaminoglycans. This was done by exposing *CD1* mouse embryos in culture to chlorate treatment at the time of formation of the median and paired dorsolateral hinge points.

Chlorate is a competitive inhibitor in the sulphation of glycosaminoglycans, and is useful for examining the importance of the sulphate group in glycosaminoglycan function (Greve et al, 1988; Conrad, 1998). The sulphate donor for glycosaminoglycan sulphation is 3'-phosphoadenosine 5'-phosphosulphate (PAPS). This is synthesised by two sequential enzymatic reactions. First, inorganic sulphate is transferred to adenosine 5'-triphosphate (ATP) to form adenosine 5'-phosphosulphate (APS) by the enzyme ATP sulphurylase. This is followed by the transfer of a phosphate group to APS by the enzyme APS kinase. In animals, the bifunctional enzyme PAPS synthetase catalyses both reactions. Chlorate acts as a sulphate analogue and competes with sulphate in the synthesis of PAPS, resulting in the production of 3'-phosphoadenosine 5'-phosphochlorate (PAPC) instead of PAPS. PAPC itself is either unstable, or it may produce glycosaminoglycans with unstable chlorate groups that are spontaneously hydrolysed. Concentrations of chlorate up to 30 mM have been used in both cell and organ cultures to inhibit sulphation with no other apparent effect on glycosaminoglycan or protein synthesis or on cell viability (Greve et al, 1988; Davies et al, 1995; Miao et al, 1996; Conrad, 1998).

## 5.2 Results

### *5.2.1 Titration of chlorate concentration*

To obtain a chlorate concentration that would affect posterior neuropore closure without generalised toxic effects on embryonic growth and development, a titration series was done using increasing chlorate concentrations in whole embryo cultures of *CD1* mouse embryos. Embryos were explanted from the uterus between the 10- and 14-somite stages, stabilised in culture, and then treated with different concentrations of chlorate for 14 hours (Figures 5.1A and B). At the end of the culture period, the embryos were examined and considered healthy if there was vigorous blood flow in the yolk sac circulation, and if the heart rate was regular and above 100 per minute. The embryos were also assessed by their crown-rump length, head length, somite number, protein content and the Brown and Fabro Morphological Scoring System (Brown and Fabro, 1981; Table 3.1).

All embryos cultured in the presence of chlorate concentrations of 30 mM or less (treatment group) or phosphate buffered saline (control group) were healthy according to the above criteria. Both groups had vigorous yolk sac circulation and regular heartbeats of over 100 per minute. All embryos had between 19 and 23 pairs of somites. No obvious difference in gross morphology was found between the treatment group and the control group (Figures 5.1C to F), except in the posterior neuropore length which was measured from the rostral end of the posterior neuropore to the tip of the tail bud (see later). In both

**Figure 5.1 Titration of chlorate concentration.** (A) *CD1* mouse embryos explanted at E8.5 for culture. In (B), the yolk sac and amniotic membrane have been removed to show the open anterior and posterior neuropores. (C) shows an embryo treated with phosphate buffered saline in culture, and (E) shows an embryo that was treated with 30 mM chlorate. (D) and (F) are close-up views of (C) and (E) respectively to illustrate the posterior neuropore. The caudal region has been displaced to the left of the embryo for the purpose of photography. (G) and (H) show embryos with sub-epidermal fluid-filled blebs and a wavy neural tube after exposure to 40 mM chlorate in culture. Abbreviations: ANP, anterior neuropore; $ClO_3$, chlorate; PBS, phosphate buffered saline; PNP, posterior neuropore. Scale bar, 1 mm.

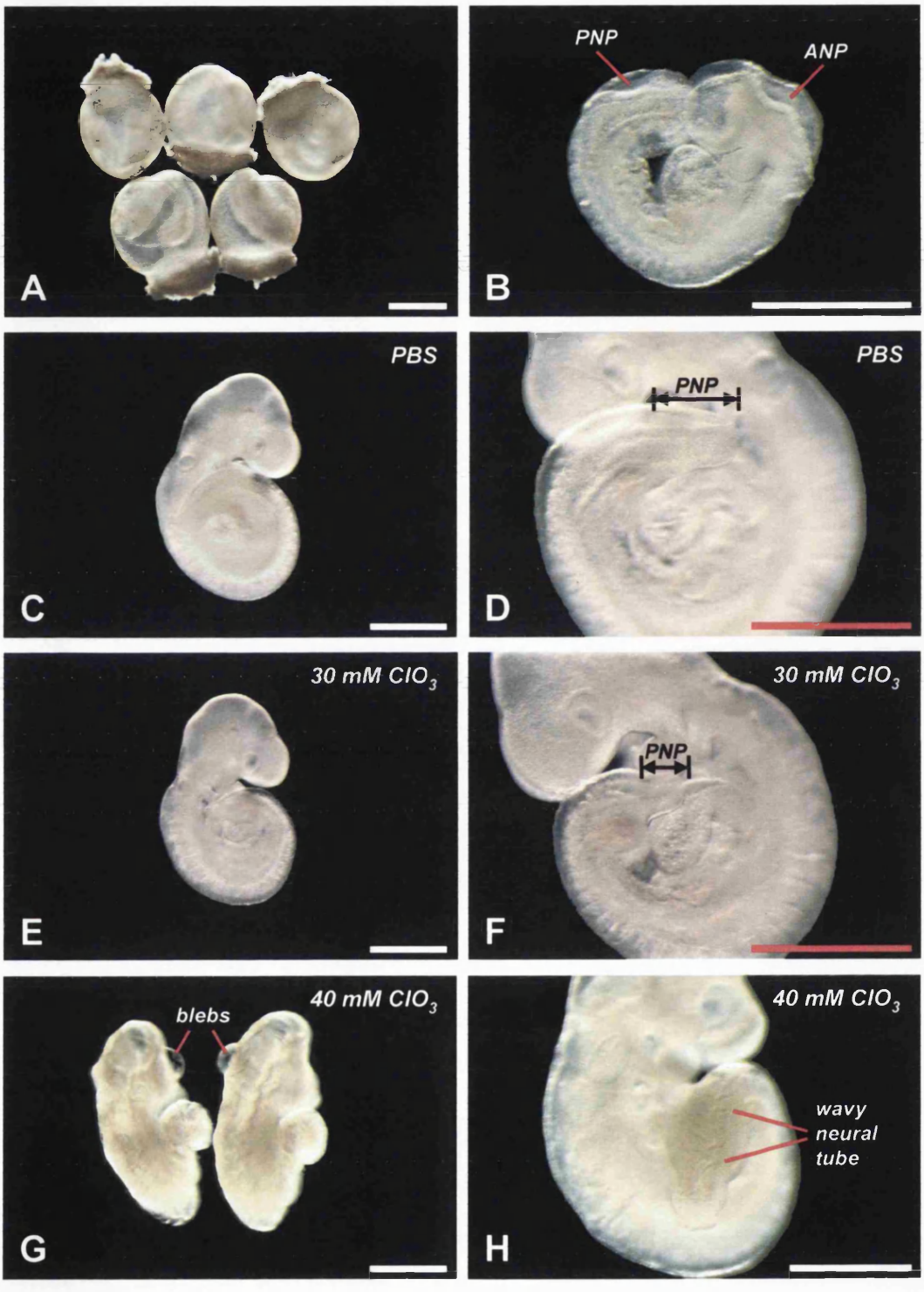
A
B
PNP
ANP
C
PBS
D
PBS
PNP
E
30 mM ClO3
F
30 mM ClO3
PNP
G
40 mM ClO3
blebs
H
40 mM ClO3
wavy
neural
tube

groups of embryos, closure of the cranial neural folds was completed by the time the cultures were stopped. Comparison of the crown-rump length, head length and Brown and Fabro morphological score among embryos exposed to 0, 10, 20 and 30 mM chlorate showed no statistically significant difference between these groups (Figures 5.2 and 5.3). There was also no difference in the embryonic protein content between embryos exposed to 30 mM chlorate and those exposed to buffer alone (Figure 5.4). In contrast, embryos that were exposed to chlorate concentrations of 40 mM and above had signs of ill health, including poor yolk sac circulation, sub-epidermal fluid-filled blebs and waviness of the neural tube (Figures 5.1G, H). Thus, chlorate was used at a concentration of 30 mM in the subsequent experiments unless otherwise specified.

### 5.2.2 Inhibition of glycosaminoglycan sulphation results in accelerated posterior neuropore closure

To determine if the sulphate group on glycosaminoglycans has an effect on closure of the posterior neuropore, the posterior neuropore length was compared among embryos exposed to different concentrations of chlorate (Figure 5.5). No statistically significant difference in the posterior neuropore length was detected among embryos exposed to 0, 10 and 20 mM chlorate. In contrast, embryos exposed to 30 mM chlorate showed a 34.2% reduction in posterior neuropore length compared to embryos that were not exposed to chlorate in culture ($p < 0.01$). This suggests that inhibition of glycosaminoglycan sulphation results in early closure of the posterior neuropore.

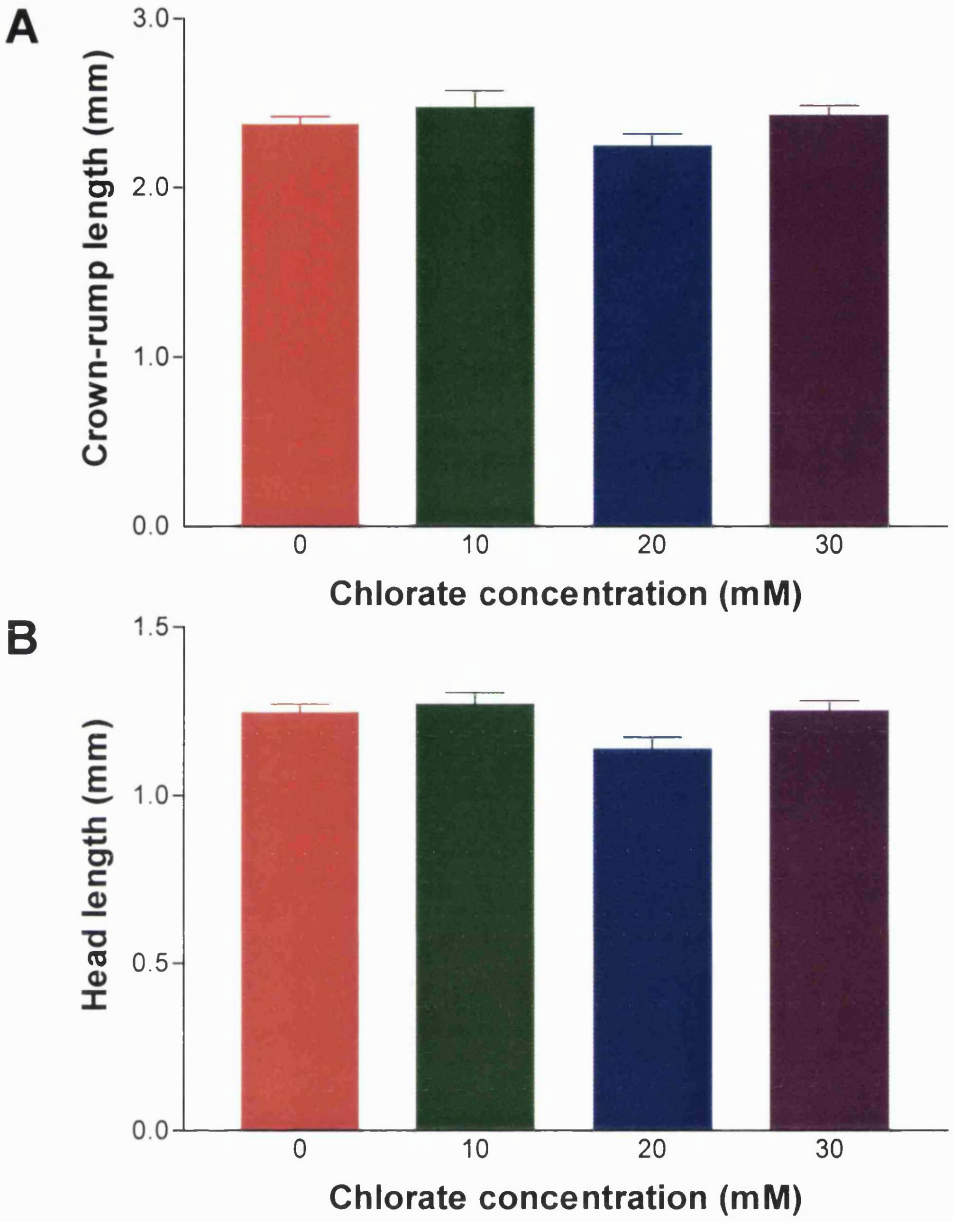


**Figure 5.2 Effect of chlorate on embryonic growth parameters.** (A) shows the crown-rump length and (B) shows the head length of embryos treated with 0, 10, 20 and 30 mM chlorate in culture. Statistical comparison using one-way ANOVA gives a *p* value of 0.3071 and 0.1783 in (A) and (B) respectively. Line above each bar represents standard error. There are at least nine embryos in each group.

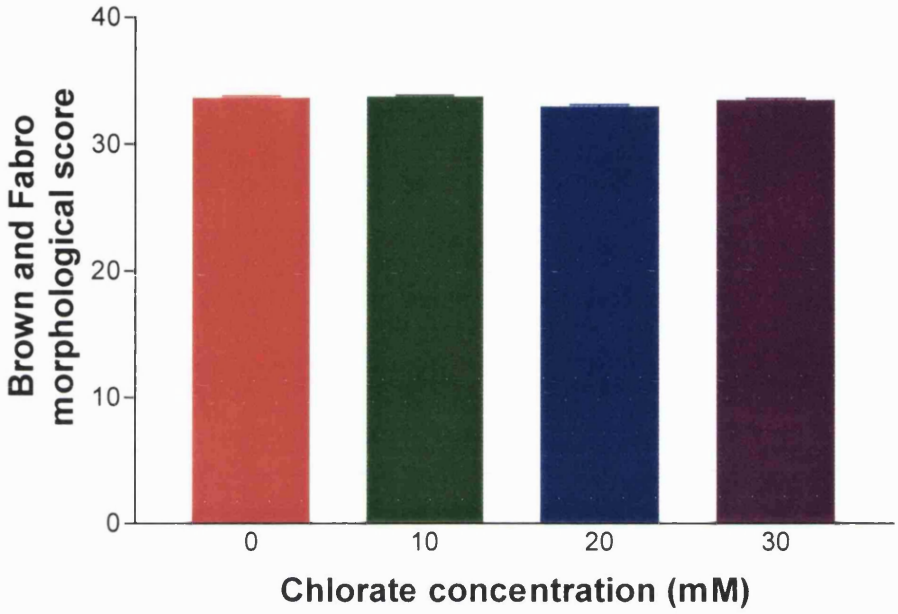


**Figure 5.3 Effect of chlorate on Brown and Fabro morphological score.** Embryos were treated with 0, 10, 20 and 30 mM chlorate in culture. Statistical comparison using one-way ANOVA gives a *p* value of 0.3076. Line above each bar represents standard error. There are at least nine embryos in each group.

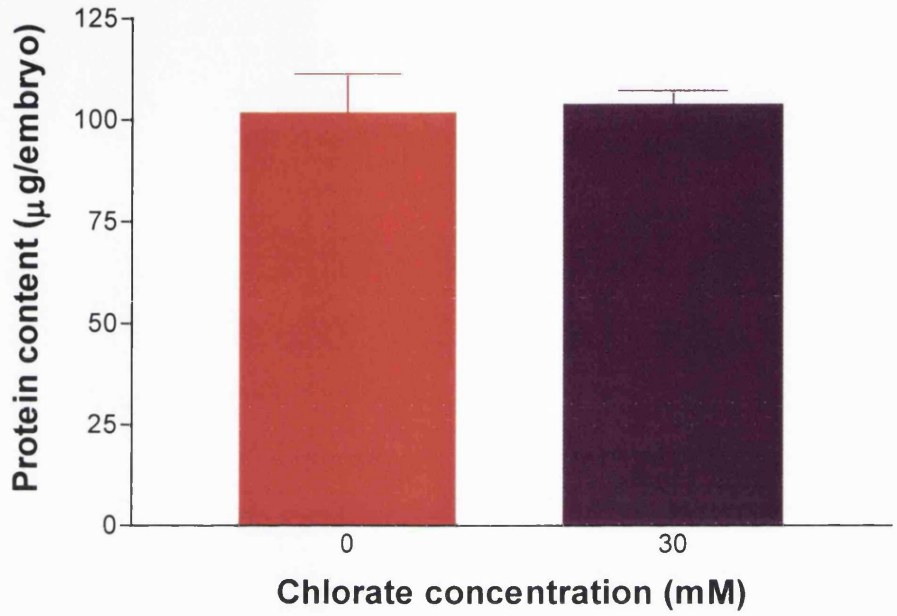


**Figure 5.4 Effect of chlorate on embryonic protein content.** The protein content of embryos treated with 0 and 30 mM chlorate in culture was determined using the BCA Protein Assay Kit. Statistical comparison using Student's t-test gives a *p* value of 0.8539. Line above each bar represents standard error. There are at least five embryos in each group.

A

| Number of somites | Posterior neuropore length (mm) | | | |
|---|---|---|---|---|
| | 0 mM $ClO_3$ | 10 mM $ClO_3$ | 20 mM $ClO_3$ | 30 mM $ClO_3$ |
| 19 | 0.46 | 0.52 | 0.34 | 0.18 |
| | 0.48 | | 0.40 | 0.28 |
| | | | | 0.22 |
| 20 | 0.50 | 0.40 | 0.54 | 0.20 |
| | 0.44 | 0.54 | 0.36 | 0.20 |
| | 0.52 | | | 0.28 |
| 21 | 0.40 | 0.28 | 0.42 | 0.30 |
| | 0.46 | | 0.32 | 0.44 |
| | 0.40 | | | |
| 22 | 0.54 | 0.36 | 0.40 | 0.30 |
| | 0.44 | 0.36 | 0.34 | |
| 23 | 0.40 | 0.42 | 0.40 | 0.28 |
| | 0.36 | 0.34 | | 0.30 |
| | | 0.38 | | |

B

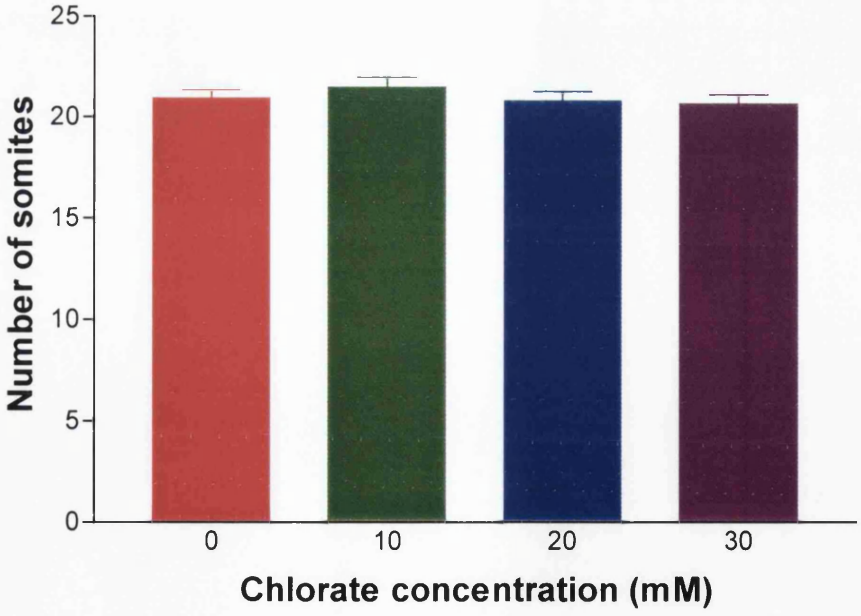

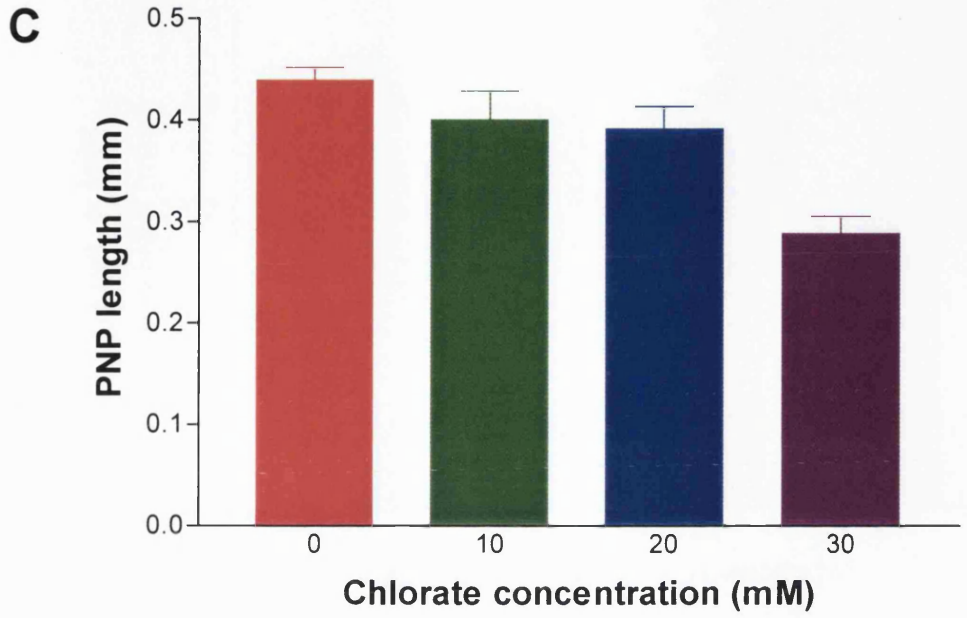


**Figure 5.5 Effect of chlorate on closure of the neural tube.** Embryos were cultured in the presence of 0, 10, 20 or 30 mM chlorate. Data for the embryos are shown in (A). Comparison of the number of somites (B) and the posterior neuropore length (C) among the four groups using one-way ANOVA gives a *p* value of 0.6413 and less than 0.0001 respectively. Dunnett's multiple comparison test shows that the posterior neuropore length is significantly shorter in the group treated with 30 mM chlorate compared with the 0 mM group ($p < 0.01$). Treatment with 10 mM and 20 mM chlorate did not significantly reduce the posterior neuropore length compared with the 0 mM group ($p > 0.05$ in each case). Line above each bar represents standard error. Abbreviations: $ClO_3$, chlorate; PNP, posterior neuropore.

To confirm that accelerated posterior neuropore closure is due to competitive inhibition of glycosaminoglycan sulphation by chlorate, embryos were cultured in the presence of chlorate, chlorate and sulphate, or phosphate buffered saline. Chlorate competitively inhibits glycosaminoglycan sulphation by acting as a sulphate analogue (Conrad, 1998). If the chlorate-induced premature posterior neuropore closure were due to competitive inhibition of glycosaminoglycan sulphation, exogenous sulphate in the culture medium is predicted to compete out the effect of chlorate. This would result in the production of 'normally-sulphated' glycosaminoglycans and a 'normal' posterior neuropore length. On the other hand, if the early neuropore closure from chlorate treatment were not due to inhibition of glycosaminoglycan sulphation, exogenous sulphate in the culture medium would not be expected to block the effect of chlorate.

Figure 5.6 shows the result of this experiment. The length of the posterior neuropore was shortened in embryos that were treated with chlorate. This chlorate-induced effect was blocked by exogenous sulphate ($p < 0.01$). There was no difference in the posterior neuropore length between embryos treated with both chlorate and sulphate and those treated with phosphate buffered saline ($p > 0.05$). This result suggests that acceleration of posterior neuropore closure is due to competitive inhibition of glycosaminoglycan sulphation.

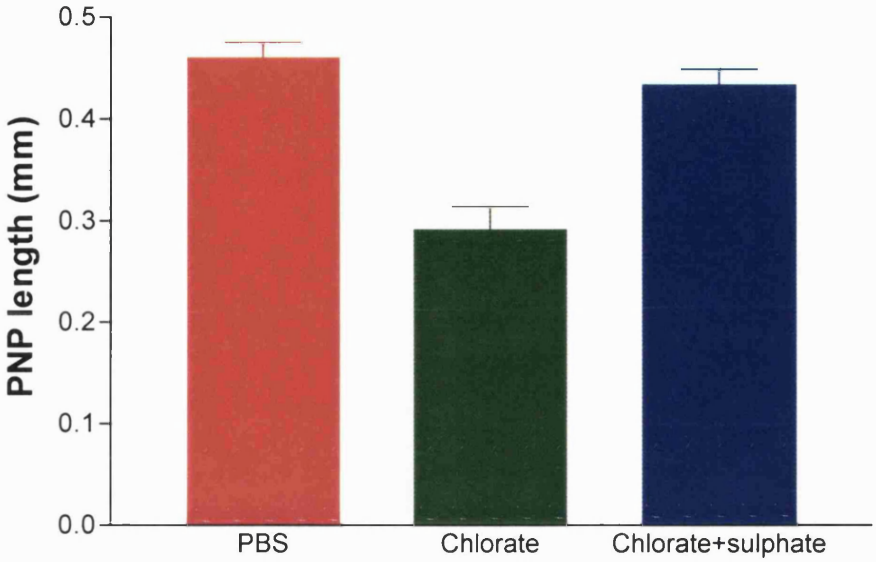


**Figure 5.6 Exogenous sulphate prevents chlorate-induced premature posterior neuropore closure.** Embryos were treated with phosphate buffered saline, 30 mM chlorate, or 30 mM chlorate and 10 mM exogenous sulphate in culture. Statistical comparison of the posterior neuropore length using one-way ANOVA gives a *p* value of less than 0.0001. Dunnett's multiple comparison test shows that treatment with chlorate alone significantly shortened the posterior neuropore length compared with the buffer treated group ($p < 0.01$). Embryos treated with both chlorate and exogenous sulphate did not differ significantly from the buffer treated group in posterior neuropore length ($p > 0.05$). Line above each bar represents standard error. There are at least 12 embryos in each group. Abbreviations: PBS, phosphate buffered saline; PNP, posterior neuropore.

### *5.2.3 Effect of chlorate on glycosaminoglycan sulphation*

To confirm that chlorate inhibits glycosaminoglycan sulphation in whole embryo culture, glycosaminoglycans were labelled by culturing embryos in the presence of $^{35}$S-sulphate. The $^{35}$S-labelled glycosaminoglycans were then analysed using anion exchange chromatography. Glycosaminoglycans were eluted using a linearly increasing concentration of sodium chloride. The concentration of the sodium chloride solution was determined using the standard conductivity curve (Figure 5.7). Variations in the scintillation counts from decay of the $^{35}$S-radioisotope (half life of 87.4 days) were corrected using the standard radioactivity decay curve (Figure 5.8). Comparison of the radioactivity level among different embryos was done by standardising the level to the protein content of each embryo. The protein content was determined from the standard curve obtained using the BCA Protein Assay Kit (Figure 5.9).

#### 5.2.3.1 Elution profile of 'normally-sulphated' glycosaminoglycans

A typical elution profile of $^{35}$S-labelled sulphated glycosaminoglycans extracted from control embryos (not exposed to chlorate) is shown in Figure 5.10. The elution profile contains two peaks. The first peak, Peak HS, eluted at a sodium chloride concentration of 0.33 M ± 0.01 (mean ± standard error, unless otherwise stated). The second peak,

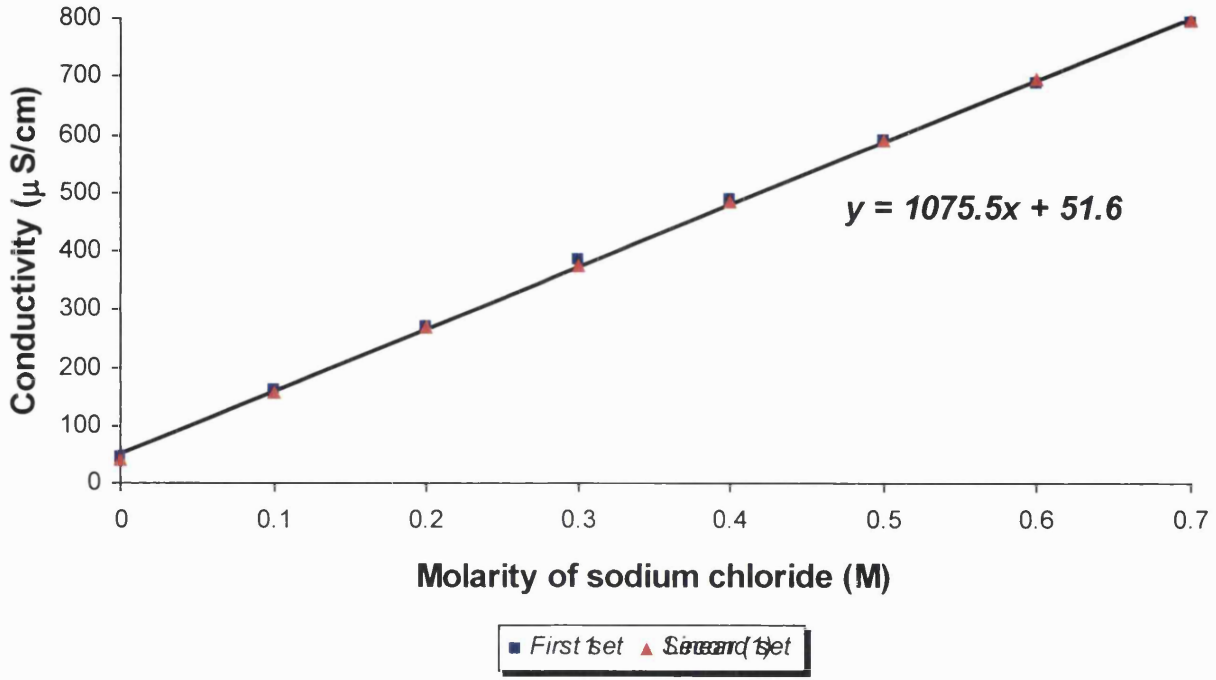


**Figure 5.7 Standard conductivity curve for sodium chloride.** The conductivity ($y$) of known concentrations ($x$) of sodium chloride dissolved in 50 mM Tris buffer was measured in two separate sets of standards. Using linear regression, the line of best fit was found to be described by the equation $y = 1075.5x + 51.6$. The coefficient of determination, $r^2$, was 0.9994. Due to the presence of Tris hydrochloride ions in the buffer solution, the conductivity was 51.6 μS/cm rather than zero when no sodium chloride was present.

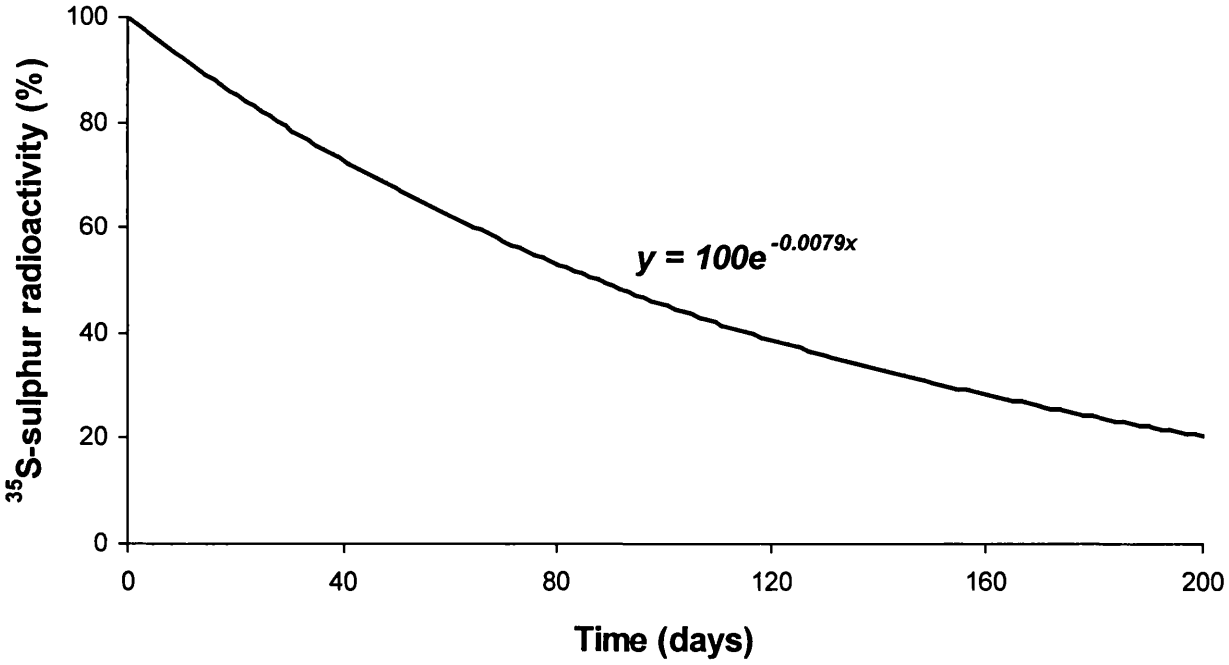


**Figure 5.8 Radioactive decay curve of $^{35}$S-sulphur.** The half life of $^{35}$S-sulphur is 87.4 days The radioactivity level is 100% at Day 0. The percentage ($y$) of $^{35}$S-sulphur radioactivity remaining after time $x$ (in days) is given by the equation $y = 100e^{-0.0079x}$.

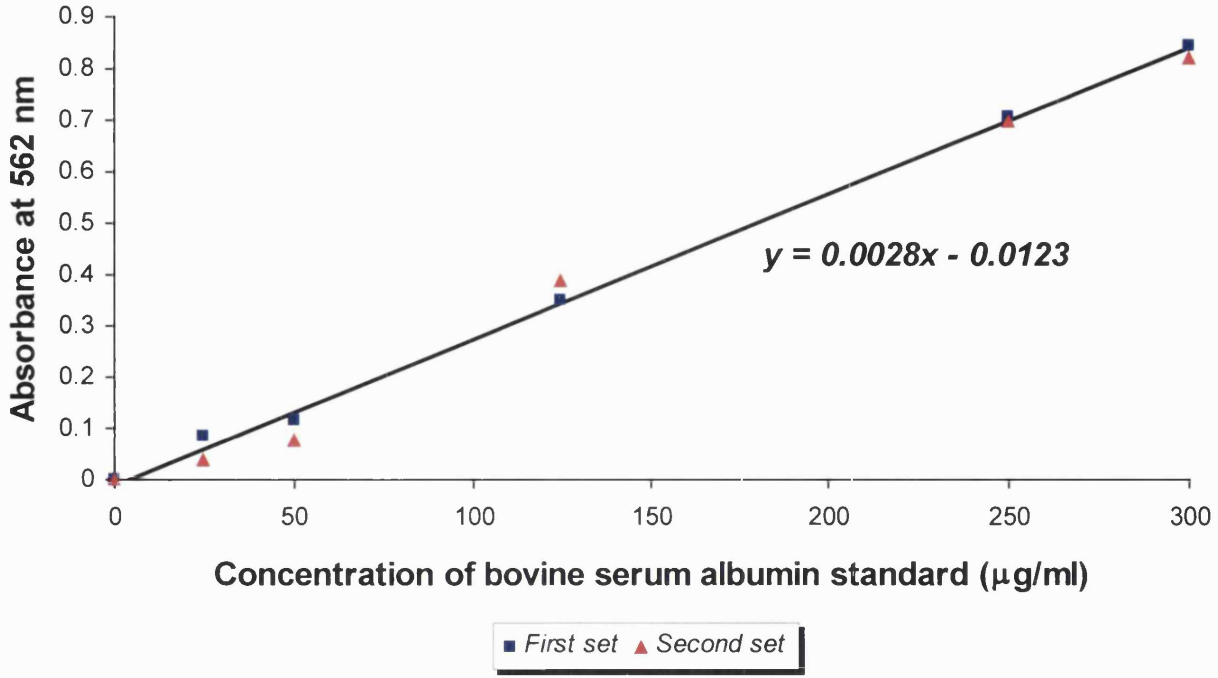


**Figure 5.9 Standard curve for quantification of protein content using the BCA Protein Assay Kit.** The absorbance ($y$) at 562 nm of known concentrations ($x$) of bovine serum albumin was measured in two separate sets of standards. Using linear regression, the line of best fit was found to be described by the equation $y = 0.0028x - 0.0123$. The coefficient of determination, $r^2$, was 0.9944.

**Figure 5.10 Anion exchange chromatography of $^{35}$S-labelled glycosaminoglycans extracted from cultured *CD1* embryos.** A typical elution profile (red line) of $^{35}$S-labelled sulphated glycosaminoglycans separated by anion exchange chromatography shows two peaks representing heparan sulphate (Peak HS) and chondroitin sulphate (Peak CS). The green profile shows the result of pre-treating the glycosaminoglycan sample with chondroitinase, and the blue line shows the result of pre-digestion using heparitinase. The linearly increasing concentration of sodium chloride used for elution is shown by the brown line. Abbreviation: PBS, phosphate buffered saline.

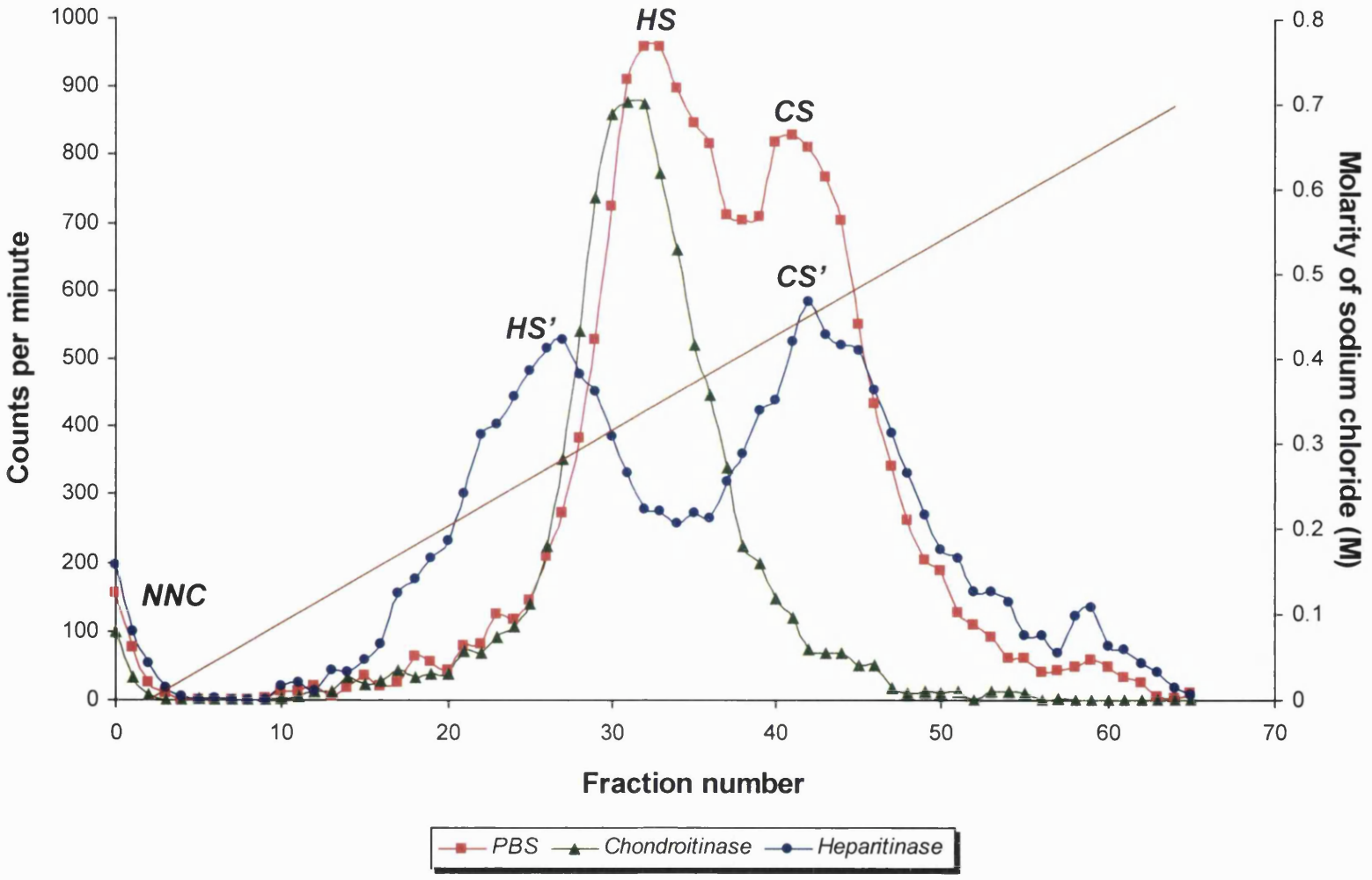
HS
CS
CS'
HS'
NNC
Counts per minute
Molarity of sodium chloride (M)
Fraction number
0
100
200
300
400
500
600
700
800
900
1000
0.1
0.2
0.3
0.4
0.5
0.6
0.7
0.8
10
20
30
40
50
60
70
PBS
Chondroitinase
Heparitinase

Peak CS, eluted at a sodium chloride concentration of 0.43 M ± 0.01. Non-negatively charged $^{35}$S-labelled material in Peak NNC was removed from the chromatography column in the buffer wash before starting the elution. Recovery from the anion exchange column was 99.3% ± 0.4. The efficiency of the scintillation counter was 87.1% ± 0.0.

To determine the identity of Peaks HS and CS, $^{35}$S-labelled glycosaminoglycans extracted from the cultured embryos were pre-treated with heparitinase, chondroitinase or phosphate buffered saline before separation by anion exchange chromatography (Figure 5.10). The commercial preparation of heparitinase used in this experiment contains a small amount of chondroitin lyase activity (Seikagaku data sheet; Linhardt, 1995). Thus, only a minimal amount of heparitinase was used in the digestion. In addition, 'cold' chondroitin sulphate was added to the sample before heparitinase treatment. Chondroitinase treatment completely abolished Peak CS and did not significantly affect Peak HS, suggesting that Peak CS represents chondroitin sulphate. Peak HS was reduced in height by 45.1% after heparitinase treatment. This gives rise to Peak HS' and suggests that Peak HS represents heparan sulphate. There was an accompanying reduction in the height of Peak CS to form Peak CS', probably due to the chondroitin lyase activity in the sample of heparitinase used. Peak NNC was unaffected by either heparitinase or chondroitinase treatment, suggesting that it does not contain heparan sulphate or chondroitin sulphate. Since almost all the $^{35}$S-label is accounted for in Peaks HS, CS and NNC, this suggests that heparan sulphate and chondroitin sulphate are the main sulphated glycosaminoglycans produced by the embryo at this stage of neurulation.

Peak HS could not be further resolved from Peak CS, owing to the inherent limitation on the separation capability of anion exchange chromatography. Several attempts were made to improve the resolution by varying the column height, the type of anion exchange resin and the concentration gradient of sodium chloride used, but these were unsuccessful. Figure 5.11 shows the elution profile from one such attempt.

#### 5.2.3.2 Elution profile of glycosaminoglycans from chlorate-treated embryos

Comparison of the elution profiles of $^{35}S$-labelled sulphated glycosaminoglycans extracted from embryos cultured in the presence of chlorate (treatment group) and in phosphate buffered saline (control group) shows that chlorate inhibited glycosaminoglycan sulphation (Figure 5.12). The elution profile in the control group shows the typical double peaks of heparan sulphate (Peak HS) and chondroitin sulphate (Peak CS). In contrast, only one peak, Peak HS", is present in the treatment group.

To determine the identity of Peak HS", sulphated glycosaminoglycans from the treatment group were pre-treated with heparitinase, chondroitinase or phosphate buffered saline before separation using anion exchange chromatography (Figure 5.13). Chondroitinase treatment had no effect on Peak HS". In contrast, heparitinase significantly reduced the height of Peak HS" to form HS*, suggesting that Peak HS" represents under-sulphated heparan sulphate.

**Figure 5.11 Limitation of anion exchange chromatography in peak resolution.** This elution profile (red line) is the result of one of multiple unsuccessful attempts to improve the resolution of the heparan sulphate (Peak HS) and chondroitin sulphate (Peak CS) peaks. In this case, the anion exchange column length was doubled and the concentration gradient of sodium chloride was reduced by 16.7%, as shown by the brown line. Instead of improving the separation, this set of parameters resulted in further merging of the two peaks.

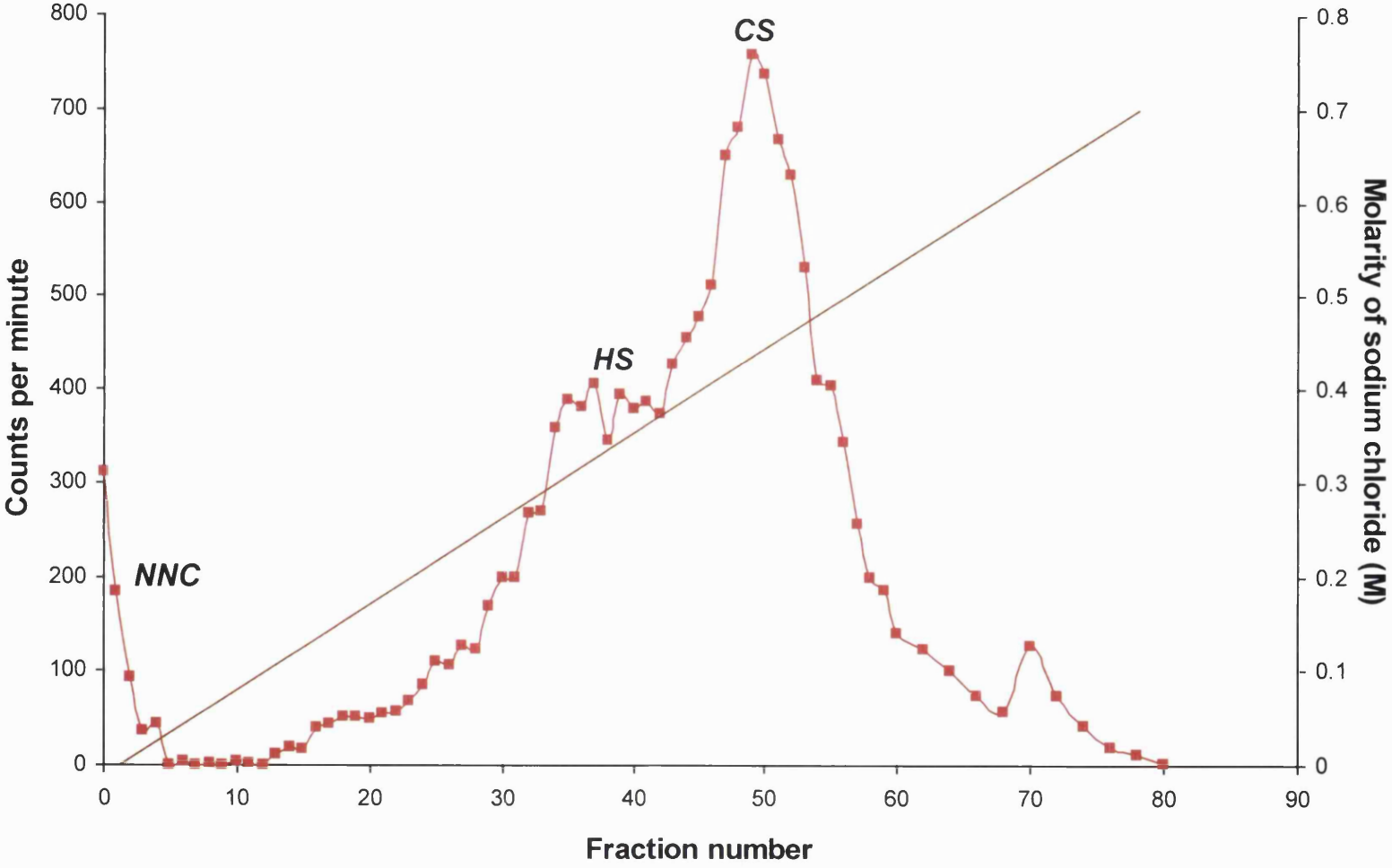
CS
HS
NNC
Counts per minute
Molarity of sodium chloride (M)
Fraction number
800
700
600
500
400
300
200
100
0
0.8
0.7
0.6
0.5
0.4
0.3
0.2
0.1
0
0
10
20
30
40
50
60
70
80
90

**Figure 5.12 Inhibition of sulphation of giycosaminoglycans by chlorate treatment.** The elution profiles of $^{35}S$-labelled sulphated glycosaminoglycans extracted from embryos treated with either phosphate buffered saline (red line) or chlorate (green line) in culture are shown. Radioactivity level of each fraction has been normalised to the protein content of the embryo. The linearly increasing concentration of sodium chloride used for elution is shown by the brown line. Abbreviation: PBS, phosphate buffered saline.

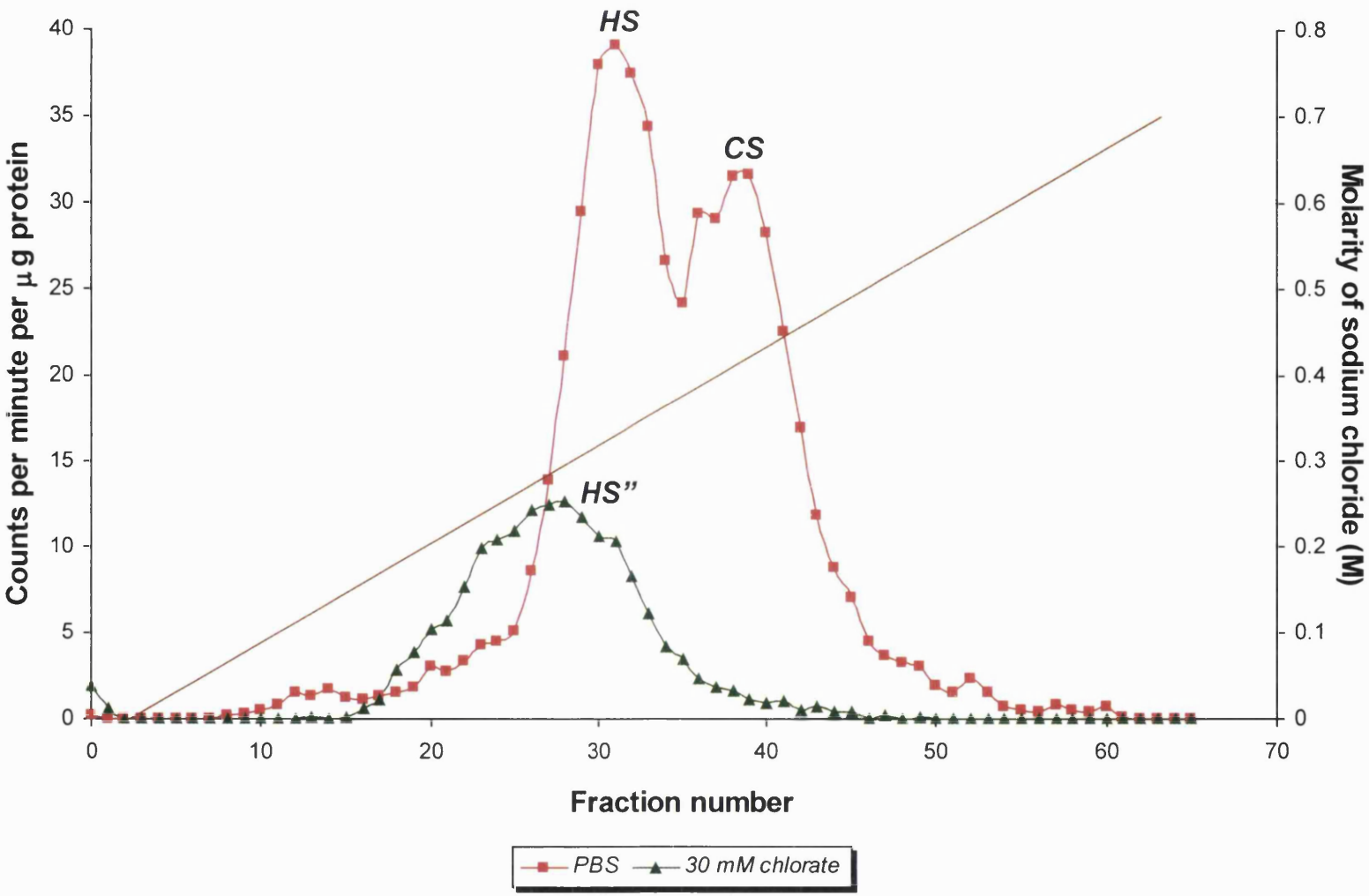
HS
CS
HS"
Counts per minute per µg protein
Molarity of sodium chloride (M)
Fraction number
0
5
10
15
20
25
30
35
40
0
0.1
0.2
0.3
0.4
0.5
0.6
0.7
0.8
0
10
20
30
40
50
60
70
PBS
30 mM chlorate

**Figure 5.13 Identification of the single glycosaminoglycan peak from chlorate-treated *CD1* embryos.** The elution profile (red line) of $^{35}S$-labelled sulphated glycosaminoglycans extracted from embryos treated with chlorate in culture shows only a single glycosaminoglycan peak, Peak HS". This peak was unaffected by pre-treatment with chondroitinase (green line). In contrast, the peak was significantly reduced in height by heparitinase treatment (blue line). Note the expanded scale used for plotting the level of radioactivity compared with that used in previous figures. The linearly increasing concentration of sodium chloride used for elution is shown by the brown line. Abbreviation: PBS, phosphate buffered saline.

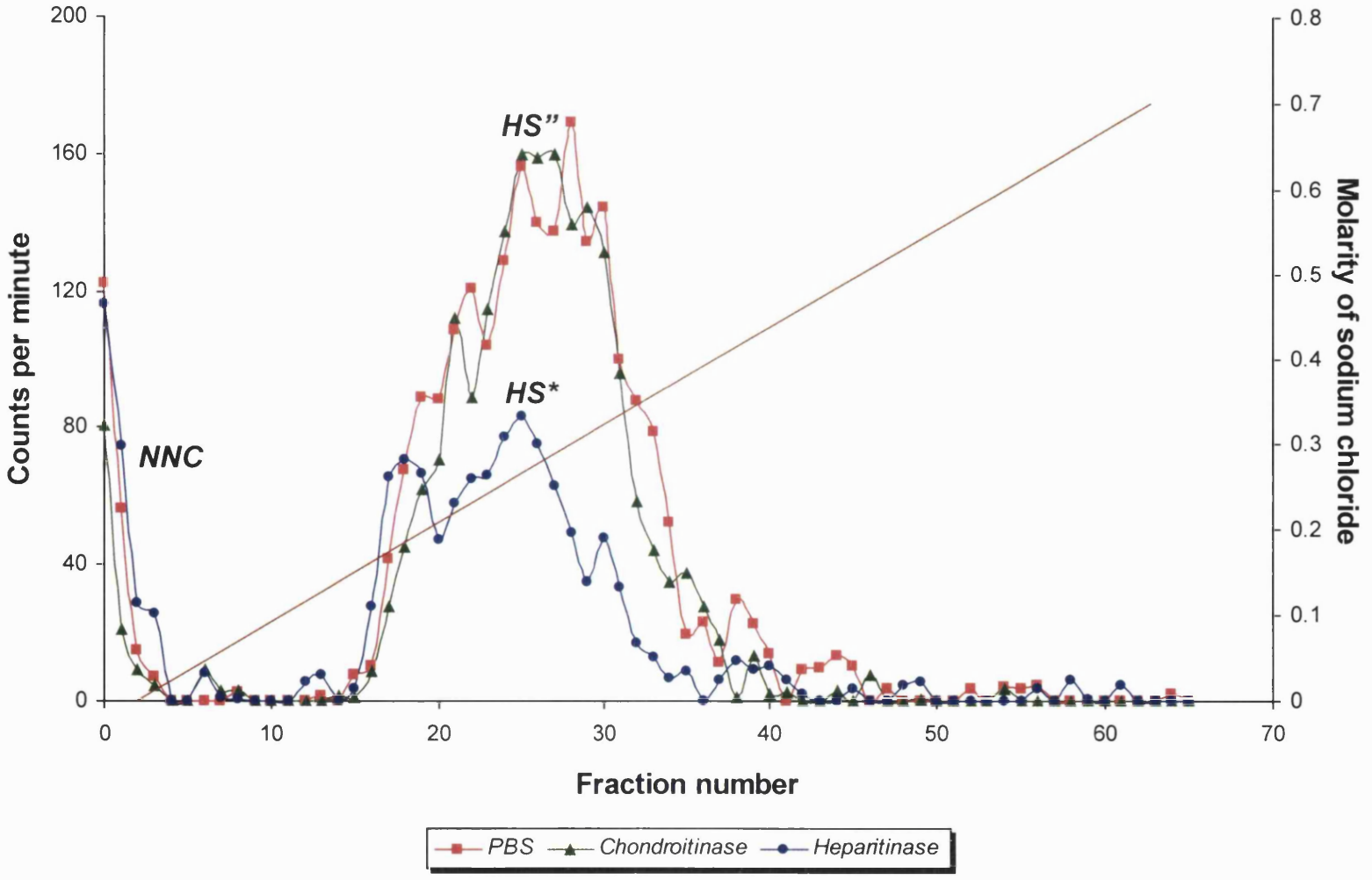
Counts per minute
Molarity of sodium chloride
Fraction number
HS"
HS*
NNC
PBS
Chondroitinase
Heparitinase
0
40
80
120
160
200
0.1
0.2
0.3
0.4
0.5
0.6
0.7
0.8
10
20
30
50
60
70

Chlorate treatment decreased the sulphation of all glycosaminoglycans produced by the embryo by 69.9% (Figure 5.14A). Sulphation of heparan sulphate was reduced by 46.0% (Figure 5.14B). The reduction in sulphation of chondroitin sulphate was complete (Figure 5.12). The amount of $^{35}$S-label incorporated into each glycosaminoglycan species was determined by calculating the area under each peak, details of which are given in Appendix 1.

Chlorate selectively inhibits O-sulphation of heparan sulphate (Safaiyan et al, 1999). At a concentration of 30 mM, N-sulphation is hardly affected by chlorate treatment. This could account for the residual radioactivity seen in Peak HS" after chlorate treatment (Figure 5.12). The sulphate groups in chondroitin sulphate are attached by O-linkages to the glycosaminoglycan chain. This explains the complete abolition of Peak CS after exposure to chlorate (Figure 5.12).

### *5.2.4 Specific requirement for heparan sulphate in posterior neuropore closure*

Both heparan sulphate and chondroitin sulphate are synthesised by the embryo at this stage of neurulation. To determine which of them is required for posterior neuropore closure, embryos were treated with chlorate in culture together with either exogenous heparan sulphate or exogenous chondroitin sulphate. Exogenous heparan sulphate blocked the effect of chlorate on posterior neuropore closure (Figure 5.15). There was no difference in posterior neuropore length between embryos exposed to both chlorate and heparan sulphate and those

**Figure 5.14 Effect of chlorate on degree of glycosaminoglycan sulphation.** Embryos were cultured in the presence of either phosphate buffered saline or 30 mM chlorate. Comparison of the amount of $^{35}S$-label incorporated into all the sulphated glycosaminoglycans (A) and heparan sulphate alone (B) using Student's t-test gives a *p* value of less than 0.0001 and 0.0022 respectively. The level of radioactivity has been normalised to the protein content of each embryo. Line above each bar represents standard error. Values are obtained from three independent assays for each group of embryos. Abbreviations: GAGs, glycosaminoglycans; PBS, phosphate buffered saline.

A

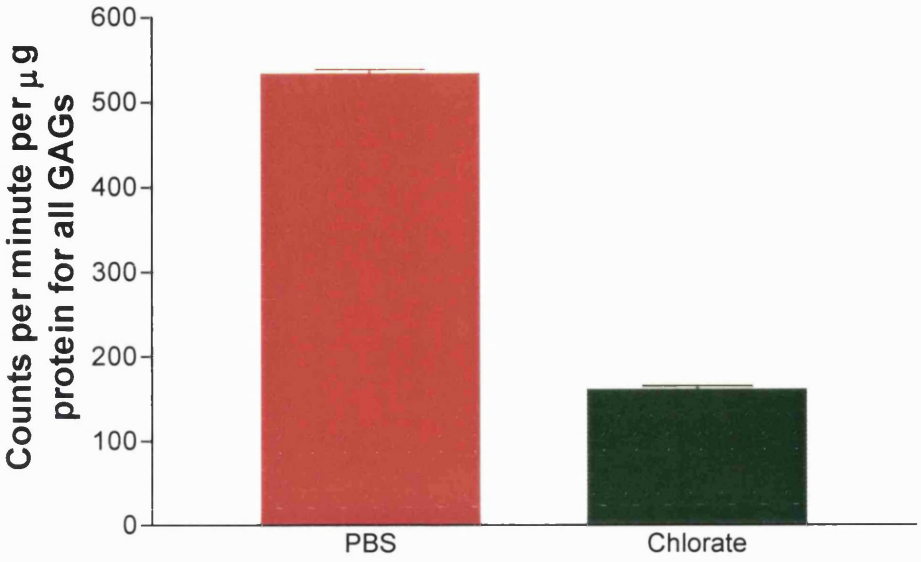
Counts per minute per µg protein for all GAGs
600
500
400
300
200
100
0
PBS
Chlorate

B

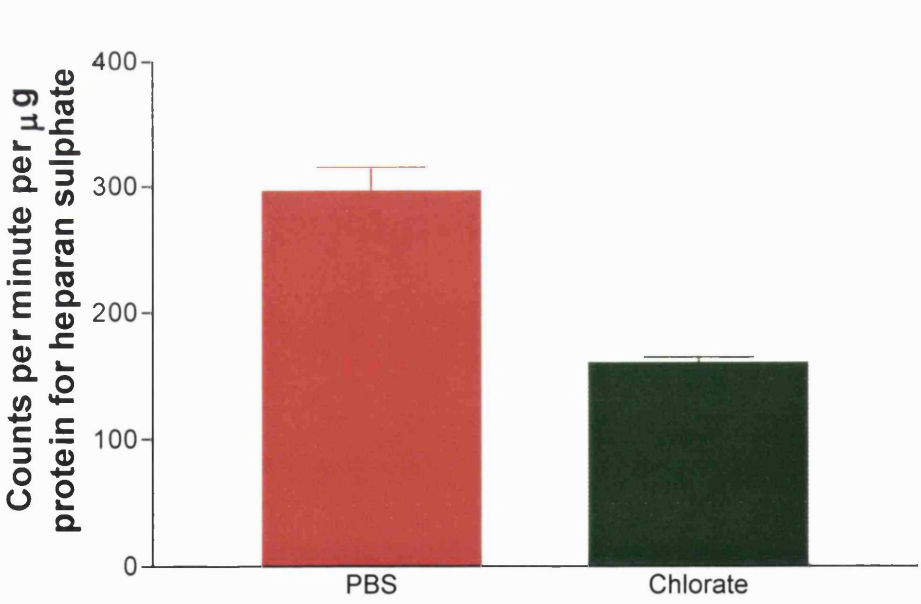
Counts per minute per µg protein for heparan sulphate
400
300
200
100
0
PBS
Chlorate

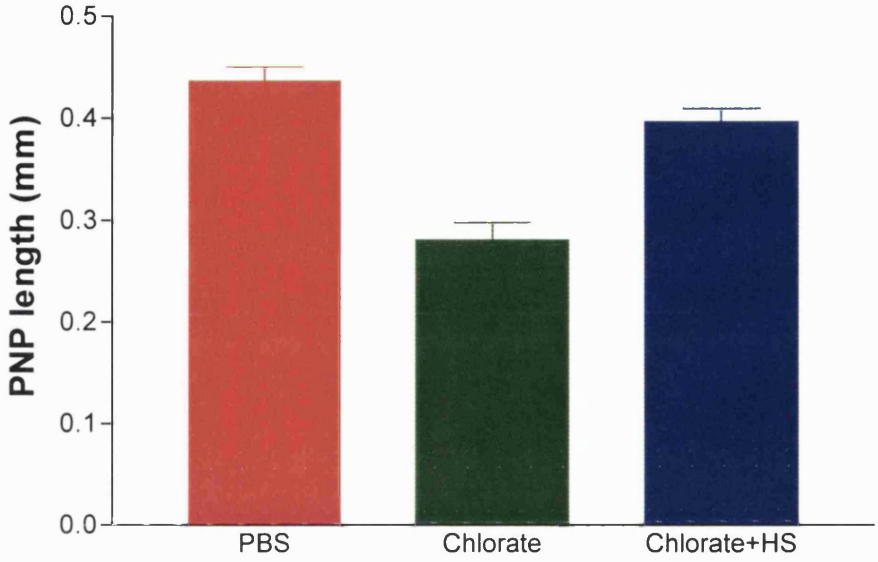


**Figure 5.15 Specific requirement for heparan sulphate in spinal neurulation.** Embryos were cultured in the presence of phosphate buffered saline, 30 mM chlorate, or chlorate and 100 ng/ml exogenous heparan sulphate. Statistical comparison of the posterior neuropore length by one-way ANOVA gives a $p$ value of less than 0.0001. Dunnett's multiple comparison test shows that exposure to chlorate significantly shortened the posterior neuropore length compared with the buffer group ($p < 0.01$). In contrast, embryos treated with both chlorate and exogenous heparan sulphate did not differ significantly from the buffer group in the length of the posterior neuropore ($p > 0.05$). Line above each bar represents standard error. There are at least 12 embryos in each group. Abbreviations: HS, heparan sulphate; PBS, phosphate buffered saline; PNP, posterior neuropore.

exposed to phosphate buffered saline ($p > 0.05$). On the other hand, exogenous chondroitin sulphate did not prevent the chlorate-induced premature posterior neuropore closure (Figure 5.16). This suggests that there is a specific requirement for heparan sulphate in spinal neurulation.

To confirm that heparan sulphate regulates posterior neuropore closure, exogenous heparan sulphate was first degraded by overnight treatment with heparitinase. The enzyme was then heat inactivated, and the degraded heparan sulphate added to embryos cultured in the presence of chlorate. As shown in Figure 5.17, degraded heparan sulphate was unable to block the effect of chlorate in accelerating posterior neuropore closure. This suggests that an intact heparan sulphate chain is required for regulation of spinal neurulation.

To exclude the possibility that exogenous heparan sulphate prevented chlorate from inhibiting glycosaminoglycan sulphation, $^{35}$S-labelled glycosaminoglycans were extracted from embryos cultured in the presence of either chlorate or chlorate and exogenous heparan sulphate. The anion exchange chromatography elution profiles from both groups are similar (Figure 5.18), thus suggesting a genuine requirement for heparan sulphate in spinal neurulation.

### *5.2.5 Importance of N- and O-sulphate groups in heparan sulphate*

Heparan sulphate contains both N-linked and O-linked sulphate groups. To determine which of them is needed for regulating spinal neurulation,

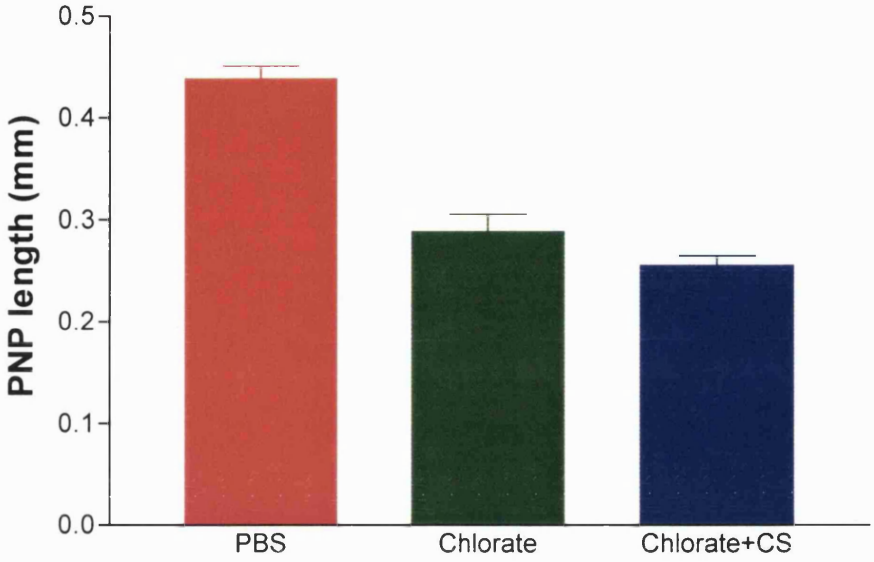


**Figure 5.16 Inability of chondroitin sulphate to prevent effect of chlorate.** Embryos were cultured in the presence of phosphate buffered saline, 30 mM chlorate, or 30 mM chlorate and 100 ng/ml exogenous chondroitin sulphate. Statistical comparison of the posterior neuropore length using one-way ANOVA gives a $p$ value of less than 0.0001. Dunnett's multiple comparison test shows that the posterior neuropore length was significantly shorter in embryos that were treated with either chlorate alone or chlorate and chondroitin sulphate compared with the buffer group ($p < 0.01$ in both cases). The posterior neuropore length was not significantly different between embryos exposed to chlorate alone and those exposed to both chlorate and chondroitin sulphate ($p > 0.05$). Line above each bar represents standard error. There are at least nine embryos in each group. Abbreviations: CS, chondroitin sulphate; PBS, phosphate buffered saline; PNP, posterior neuropore.

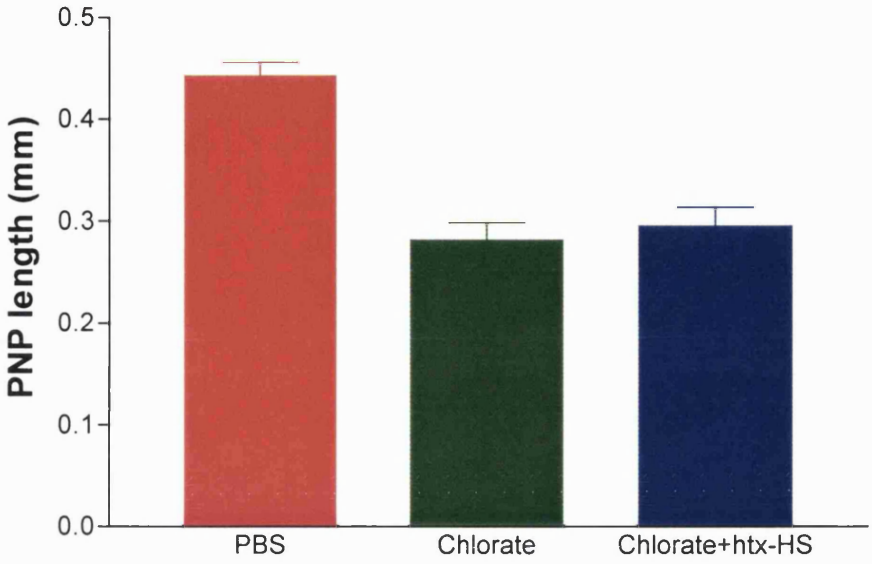


**Figure 5.17 Effect of pre-digestion of heparan sulphate with heparitinase.** Embryos were cultured in the presence of phosphate buffered saline, 30 mM chlorate, or 30 mM chlorate and 100 ng/ml exogenous heparan sulphate that had been pre-digested with heparitinase. Statistical comparison of the posterior neuropore length using one-way ANOVA gives a $p$ value of less than 0.0001. Dunnett's multiple comparison test shows that the posterior neuropore length of the latter two groups was significantly shorter compared with the buffer group ($p < 0.01$ in both cases). The posterior neuropore length of embryos treated with chlorate alone was not significantly different from those exposed to both chlorate and degraded heparan sulphate ($p > 0.05$). Line above each bar represents standard error. There are at least 12 embryos in each group. Abbreviations: htx-HS, heparitinase-treated heparan sulphate; PBS, phosphate buffered saline; PNP, posterior neuropore.

**Figure 5.18 Exogenous heparan sulphate does not prevent inhibition of glycosaminoglycan sulphation by chlorate treatment.** The elution profiles of $^{35}S$-labelled sulphated glycosaminoglycans extracted from embryos treated with either chlorate alone (green line) or chlorate and exogenous heparan sulphate (blue line) in culture are shown. Radioactivity level of each fraction has been normalised to the protein content of the embryo. An expanded scale is used for plotting the standardised radioactivity level. The linearly increasing concentration of sodium chloride used for elution is shown by the brown line.

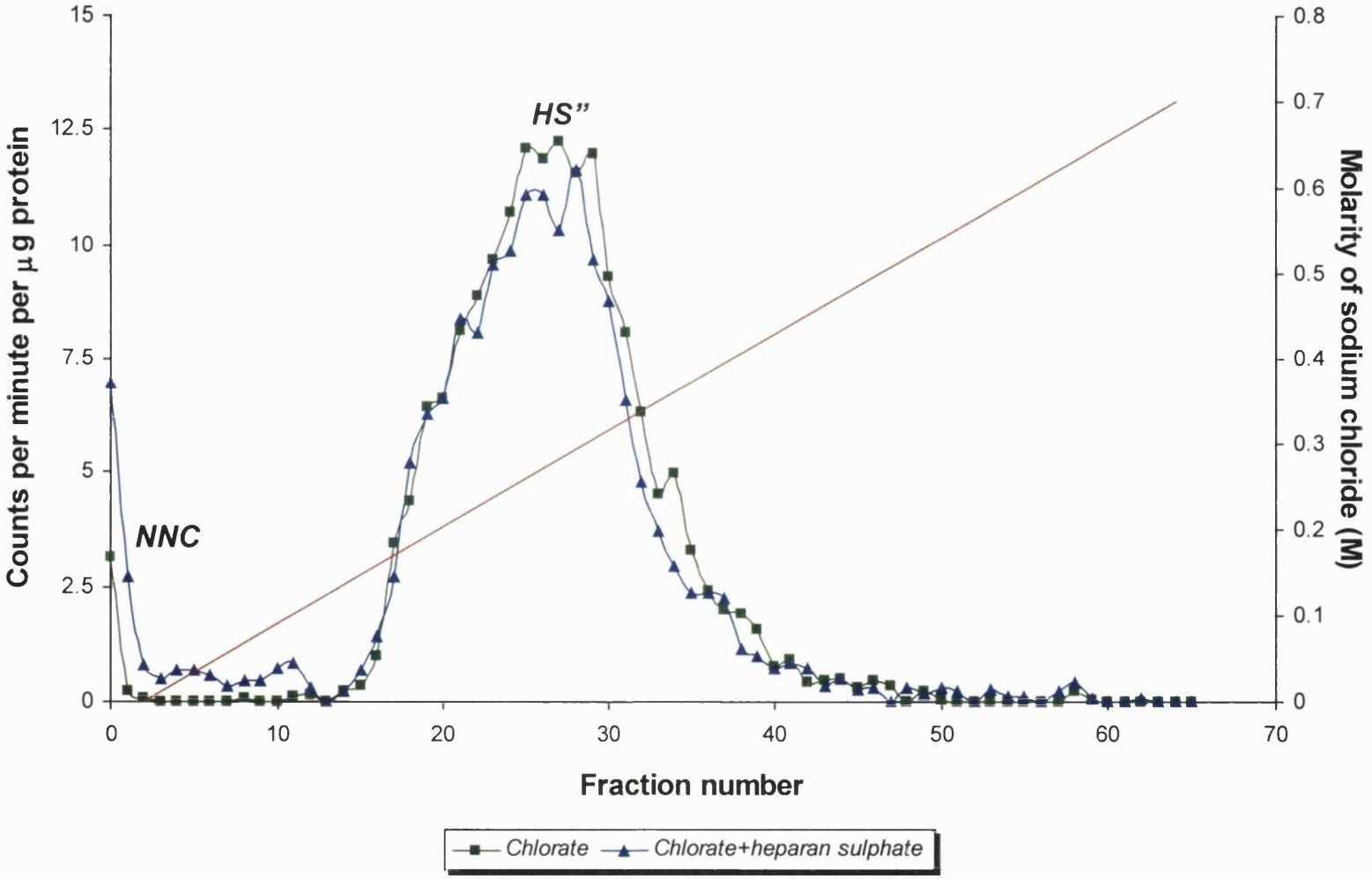
Counts per minute per µg protein
Molarity of sodium chloride (M)
Fraction number
HS"
NNC
15
12.5
10
7.5
5
2.5
0
0.8
0.7
0.6
0.5
0.4
0.3
0.2
0.1
0
0
10
20
30
40
50
60
70
Chlorate
Chlorate+heparan sulphate

embryos were cultured in the presence of chlorate and either de-N-sulphated or de-O-sulphated heparan sulphate. De-N-sulphated heparan sulphate did not block the chlorate-induced premature posterior neuropore closure (Figure 5.19). Similarly, de-O-sulphated heparan sulphate was unable to prevent early closure of the neuropore (Figure 5.20). In both cases, there was no statistically significant difference ($p > 0.05$) in the posterior neuropore length between embryos cultured in the presence of chlorate and those cultured in the presence of chlorate and under-sulphated heparan sulphate (either de-N- or de-O-sulphated heparan sulphate). Thus, neither de-N- nor de-O-sulphated heparan sulphate is able to substitute for 'normally-sulphated' heparan sulphate, suggesting that both N- and O-sulphate groups are needed for heparan sulphate to regulate spinal neurulation.

### *5.2.6 Effect of glycosaminoglycan sulphation on hinge point formation*

To determine if inhibition of glycosaminoglycan sulphation has an effect on the posterior neuropore morphology, transverse sections through the posterior neuropore were prepared from embryos cultured in the presence of chlorate and stained with haematoxylin and eosin. Embryos treated with phosphate buffered saline in culture exhibit Mode 2 pattern of spinal neurulation (Figure 5.21A). A median hinge point overlying the notochord is present, together with paired dorsolateral hinge points in the neural folds. These hinge points help to elevate the neural folds and bring the neural fold apices towards the dorsal midline. The non-bending regions of the neural plate lying between the median and dorsolateral hinge points appear straight and rigid.

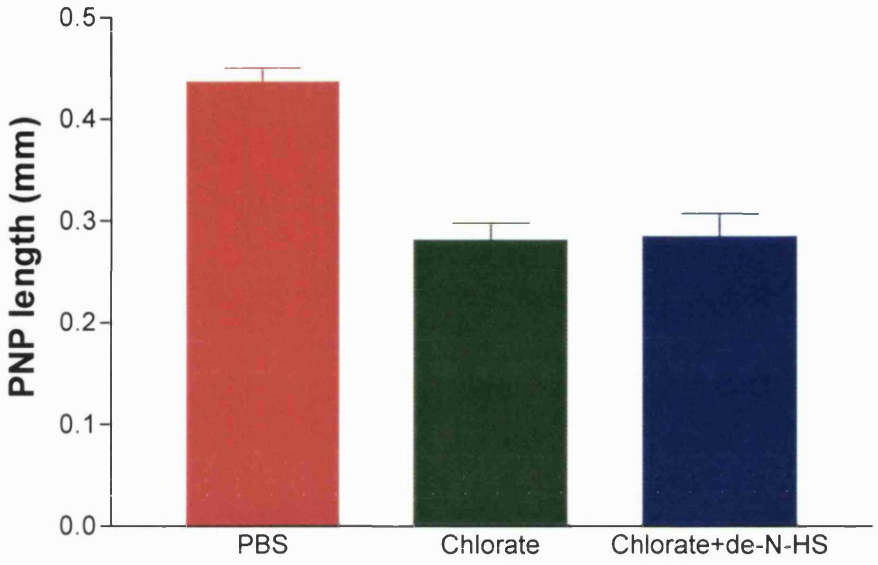


**Figure 5.19 Importance of N-sulphate group in heparan sulphate.** Embryos were cultured in the presence of phosphate buffered saline, 30 mM chlorate or 30 mM chlorate and 100 ng/ml de-N-sulphated heparan sulphate. Statistical comparison of the posterior neuropore length using one-way ANOVA gives a $p$ value of less than 0.0001. Dunnett's multiple comparison test shows that the posterior neuropore length of the latter two groups was significantly shorter compared with the buffer group ($p < 0.01$ in both cases). The posterior neuropore length was not significantly different between embryos treated with chlorate alone and those exposed to both chlorate and de-N-sulphated heparan sulphate ($p > 0.05$). Line above each bar represents standard error. There are at least nine embryos in each group. Abbreviations: de-N-HS, de-N-sulphated heparan sulphate; PBS, phosphate buffered saline; PNP, posterior neuropore.

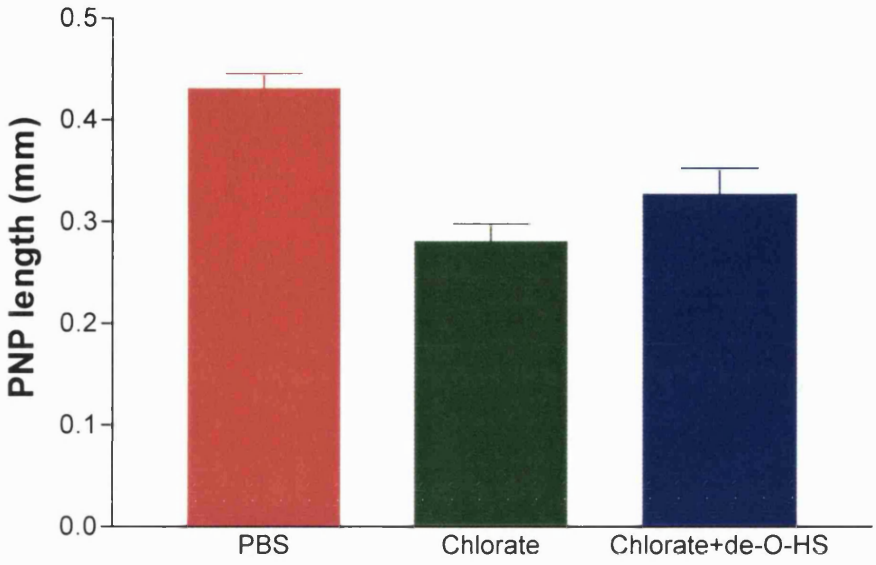


**Figure 5.20 Importance of O-sulphate group in heparan sulphate.** Embryos were cultured in the presence of phosphate buffered saline, 30 mM chlorate or 30 mM chlorate and 100 ng/ml de-O-sulphated heparan sulphate. Statistical comparison of the posterior neuropore length using one-way ANOVA gives a *p* value of less than 0.0001. Dunnett's multiple comparison test shows that the posterior neuropore length of the latter two groups was significantly shorter compared with the buffer group ($p < 0.01$ in both cases). The posterior neuropore length was not significantly different between embryos treated with chlorate alone and those exposed to both chlorate and de-O-sulphated heparan sulphate ($p > 0.05$). Line above each bar represents standard error. There are at least nine embryos in each group. Abbreviations: de-O-HS, de-O-sulphated heparan sulphate; PBS, phosphate buffered saline; PNP, posterior neuropore.

**Figure 5.21 Heparan sulphate is required for median hinge point formation during spinal neurulation.** Haematoxylin and eosin stained transverse sections of the closing posterior neuropore region prepared from embryos cultured in the presence of phosphate buffered saline (A), 30 mM chlorate (B), 30 mM chlorate and 10 mM sulphate (C), 30 mM chlorate and 100 ng/ml heparan sulphate (D), or 30 mM chlorate and 100 ng/ml chondroitin sulphate (E). Arrows, paired dorsolateral hinge points; star, median hinge point. Abbreviations: $ClO_3$, chlorate; CS, chondroitin sulphate; HS, heparan sulphate; PBS, phosphate buffered saline, $SO_4$, sulphate. Scale bar, 100 μm.

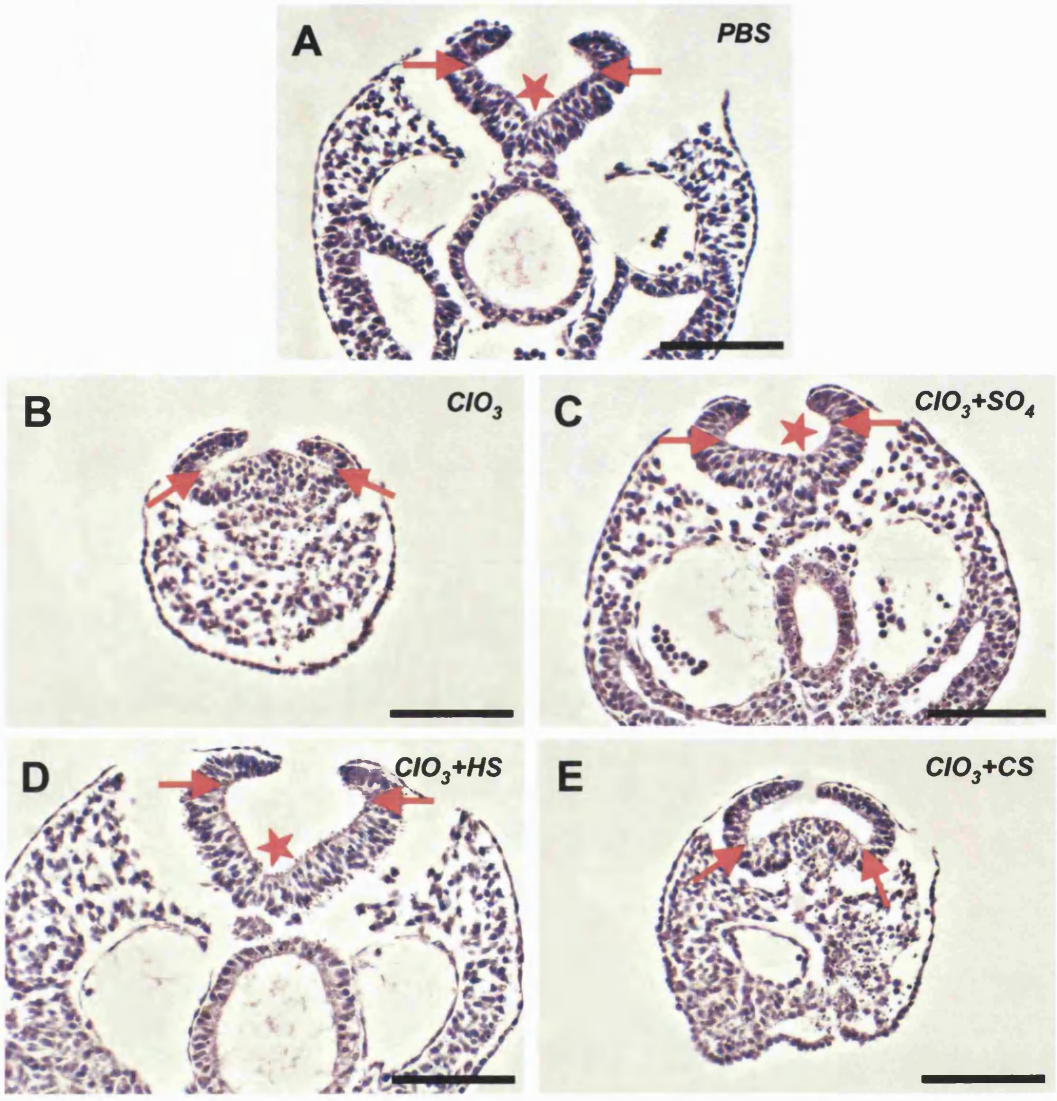
A
PBS
B
ClO3
C
ClO3+SO4
D
ClO3+HS
E
ClO3+CS

In contrast, embryos treated with chlorate do not have a median hinge point (Figure 5.21B). Instead, bending at the paired dorsolateral hinge points is increased, and this compensates for the lack of a median hinge point in bringing the neural fold apices towards the dorsal midline. The region of the neural plate between the paired dorsolateral hinge points appears to have lost its rigidity and buckles. Formation of the chlorate-induced neuroepithelial morphology was blocked by addition of exogenous sulphate to the culture medium (Figure 5.21C). The posterior neuropore morphology of this group of embryos is similar to that seen in embryos that were not exposed to chlorate. Both median and dorsolateral hinge points are present in the neuroepithelium. This result correlates with the finding that exogenous sulphate blocks chlorate-induced premature posterior neuropore closure, and is consistent with competitive inhibition of glycosaminoglycan sulphation by chlorate. Exogenous sulphate works by competing out the effect of chlorate.

Supplementation of the culture medium with exogenous heparan sulphate was also able to prevent the chlorate-induced changes in the posterior neuropore morphology (Figure 5.21D). This group of embryos has both median and dorsolateral hinge points, and appears similar to embryos that had not been exposed to chlorate. This suggests that the exogenous heparan sulphate in the culture medium is an effective substitute for the 'normally-sulphated' heparan sulphate synthesised by the embryo under normal conditions (without chlorate), and correlates with the finding that exogenous heparan sulphate blocks chlorate-induced early closure of the posterior neuropore. In contrast, exogenous chondroitin sulphate in the culture medium was unable to block the change in neuroepithelial morphology produced by chlorate

(Figure 5.21E). The posterior neuropore morphology is similar to that of embryos exposed to chlorate alone (Figure 5.21B), with absence of the median hinge point, increased bending at the paired dorsolateral hinge points, and loss of neuroepithelial rigidity in the region between the dorsolateral hinge points.

To confirm that sulphation of heparan sulphate and chondroitin sulphate is reduced in the posterior neuropore region, transverse sections of the posterior neuropore region were immunostained with anti-heparan sulphate (10E4) and anti-chondroitin sulphate (CS-56) antibodies. As in Chapter 4, embryos that were cultured in the presence of phosphate buffered saline show strong staining for both heparan sulphate (Figure 5.22A) and chondroitin sulphate (Figure 5.22C) in the neuroepithelial basement membrane. Staining is also seen in the basement membrane of the surface ectoderm and gut endoderm, and in the areas around the cells of the mesoderm. There is also non-specific staining of the gut contents. In contrast, the staining for both sulphated glycosaminoglycans is greatly reduced in the chlorate-treated embryos (Figures 5.22B and D). Staining for heparan sulphate is very weak throughout the section in all specimens examined. Staining for chondroitin sulphate is also very much reduced in the neuroepithelium and the neuroepithelial basement membrane, but less so in the underlying mesoderm. This is unlikely to be due to incomplete penetration of chlorate into the mesoderm, since there is a uniform reduction in immunostaining for heparan sulphate. In addition, virtually no $^{35}$S-labelled chondroitin sulphate could be detected by scintillation counting (Figure 5.12). A possible explanation for the immunostaining for chondroitin sulphate in the mesoderm is that the anti-chondroitin

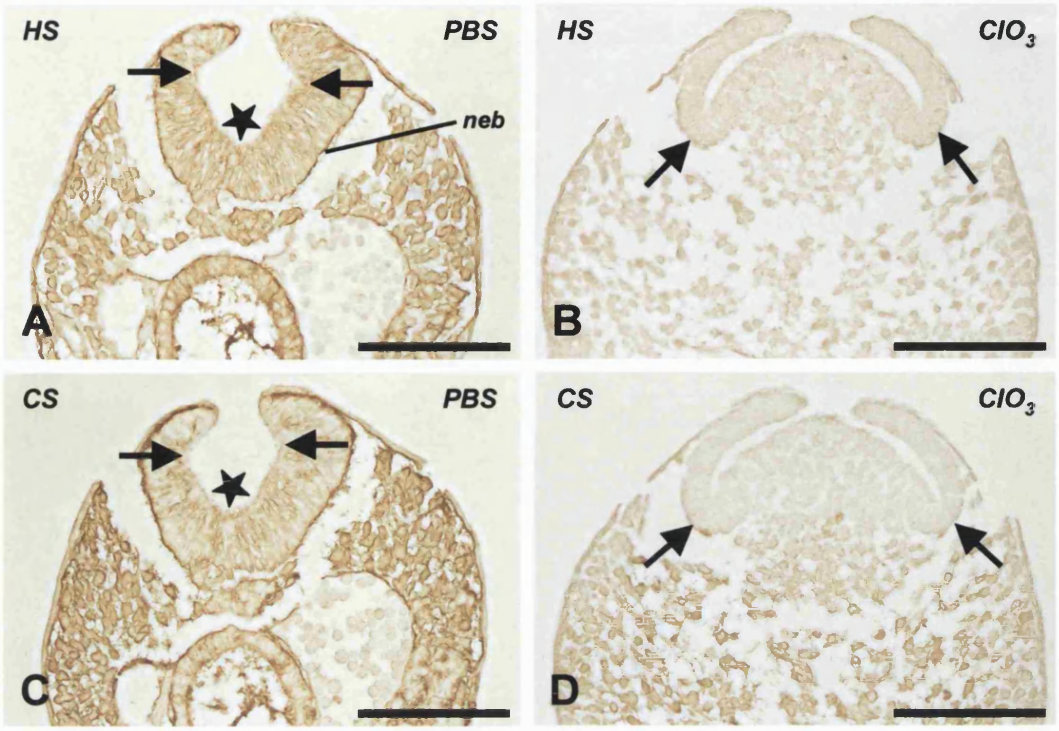


**Figure 5.22 Chlorate reduces the sulphation of glycosaminoglycans in the posterior neuropore region.** Immunohistochemical localisation of heparan sulphate (A, B) and chondroitin sulphate (C, D) on transverse sections through the posterior neuropore region prepared from embryos cultured in the presence of phosphate buffered saline (A, C) or 30 mM chlorate (B, D). Arrows, paired dorsolateral hinge points; star, median hinge point. Abbreviations: $ClO_3$, chlorate; neb, neuroepithelial basement membrane; PBS, phosphate buffered saline. Scale bar, 100 μm.

sulphate antibody is bound to 'normally-sulphated' chondroitin sulphate that was synthesised by the embryo before the addition of chlorate to the culture medium.

### 5.2.7 Effect of glycosaminoglycan sulphation on Sonic hedgehog signalling

Sonic hedgehog (Shh) has been suggested to induce formation of the median hinge point and to inhibit bending of the paired dorsolateral hinge points during spinal neurulation (Ybot-Gonzalez and Copp, unpublished). To determine whether the absence of the median hinge point and the increased bending at the dorsolateral hinge points in chlorate-treated embryos are due to disruption of Sonic hedgehog signalling, the expression patterns of *Sonic hedgehog* and *Patched* (*Ptc*) were compared by *in situ* hybridisation between embryos cultured either with or without chlorate treatment. Sonic hedgehog is a ligand of Patched and upregulates Patched expression (Goodrich et al, 1996; Marigo et al, 1996a). It is thus predicted that there would be an abnormal pattern of *Patched* expression if *Sonic hedgehog* signalling were disrupted. The sizes of the *Shh* and *Ptc* plasmid inserts and the digoxigenin-labelled RNA probes were checked by agarose gel electrophoresis prior to *in situ* hybridisation (Figures 5.23 and 5.24).

In embryos cultured in the presence of phosphate buffered saline, the expression patterns of *Sonic hedgehog* and *Patched* transcripts are essentially as described in the literature (Echelard et al, 1993; Goodrich et al, 1996). *Sonic hedgehog* mRNA is detected in the axial tissues

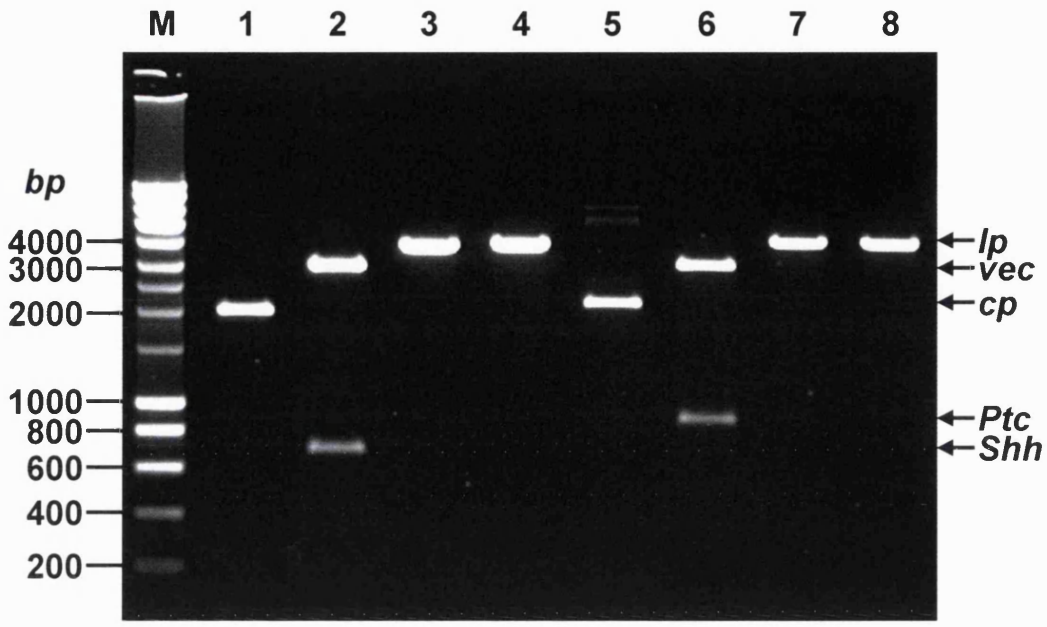


**Figure 5.23 Plasmid linearisation.** Lanes 1 and 5 show the circular plasmids for *Shh* and *Ptc* respectively. The inserts were excised by restriction digestion using *Eco*R I and found to be of the correct sizes (*Shh*, 640 bp in Lane 2; *Ptc*, 841 bp in Lane 6). The upper bands in Lanes 2 and 6 represent the non-circular vector DNA, which migrates more slowly owing to loss of its supercoiled nature. Lanes 3 and 4 show the *Sonic hedgehog* plasmid after linearisation with *Hin*d III (anti-sense orientation) and *Pst* I (sense) respectively. Lanes 7 and 8 show the *Patched* plasmid after digestion with *Bam*H I (anti-sense) and *Hin*d III (sense) respectively. The DNA sizing ladder is seen in Lane M. Abbreviations: *Ptc, Patched; Shh, Sonic hedgehog*; cp, circular plasmid; lp, linearised plasmid; vec, vector.

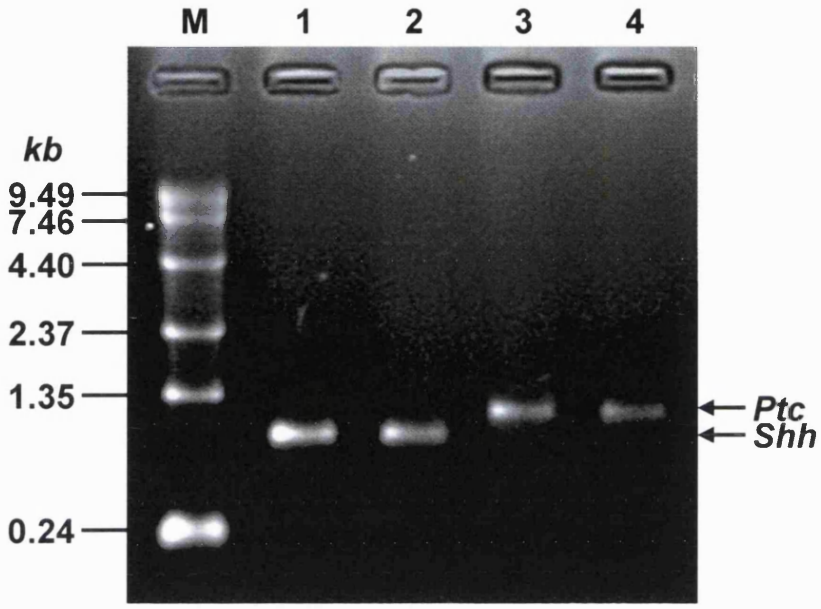


**Figure 5.24 Digoxigenin-labelling of RNA probes.** Lanes 1 and 2 show the respective anti-sense and sense digoxigenin-labelled RNA probes for *Shh* (0.640 kb). Lanes 3 and 4 show the labelled probes (0.841 kb) for *Ptc* (Lane 3, anti-sense probe; Lane 4, sense probe). The RNA sizing ladder is seen in Lane M. Abbreviations: *Ptc, Patched; Shh, Sonic hedgehog.*

(Figures 5.25A and B; Figure 5.26A). In the posterior neuropore region, staining is seen in the notochord and in the ventral part of the hindgut. Staining for *Patched* transcripts is seen near *Sonic hedgehog*-producing cells (Figures 5.25E and F; Figure 5.26C). Strong staining is present in the median hinge point and the staining intensity decreases progressively along the neuroepithelium towards the paired dorsolateral hinge points. The notochord is weakly stained. Staining is also seen in the hindgut (both dorsal and ventral parts) and in the mesodermal tissues lying next to these axial structures. Both *Sonic hedgehog* and *Patched* transcripts are detected along the longitudinal axis of the embryo as far caudally as the rostral part of the posterior neuropore region.

The pattern of expression of *Sonic hedgehog* mRNA in embryos cultured in the presence of chlorate is similar to that seen in the buffer group (Figures 5.25C and D; Figure 5.26B). The expression pattern of *Patched* transcripts is also broadly similar between the two groups (Figures 5.25G and H; Figures 5.26D and E). However, the notochord is more strongly stained for *Patched* mRNA than the overlying neuroepithelium. There is no consistent decrease in staining intensity moving laterally from the midline of the neuroepithelium towards the paired dorsolateral hinge points. Furthermore, there is less restriction of staining to axial and paraxial tissues. Variable amount of punctate staining is detected even in the most lateral regions of the embryo. The difference in staining pattern and intensity is unlikely to be due to a difference in probe penetration between the two groups of embryos. Stronger staining of the notochord is seen in the chlorate-treated group, whereas decapitation of the embryos for the purpose of identification

**Figure 5.25 Whole mount *in situ* hybridisation.** Whole mount *in situ* hybridisation was used to detect *Shh* (A to D) and *Ptc* (E to H) transcripts in embryos cultured in the presence of either phosphate buffered saline (A, B, E, F) or 30 mM chlorate (C, D, G, H). Panels on the right are magnified views of the posterior neuropore region of respective embryos in the left panels. Embryos in the buffer group were decapitated for the purpose of identification prior to starting the *in situ* hybridisation procedure. They were then placed in the same tube as the chlorate-treated group throughout the procedure to ensure uniformity of treatment for both groups. Abbreviations: *Ptc, Patched; Shh, Sonic hedgehog*; $ClO_3$, chlorate; PBS, phosphate buffered saline; PNP, posterior neuropore. Scale bar, 1 mm.

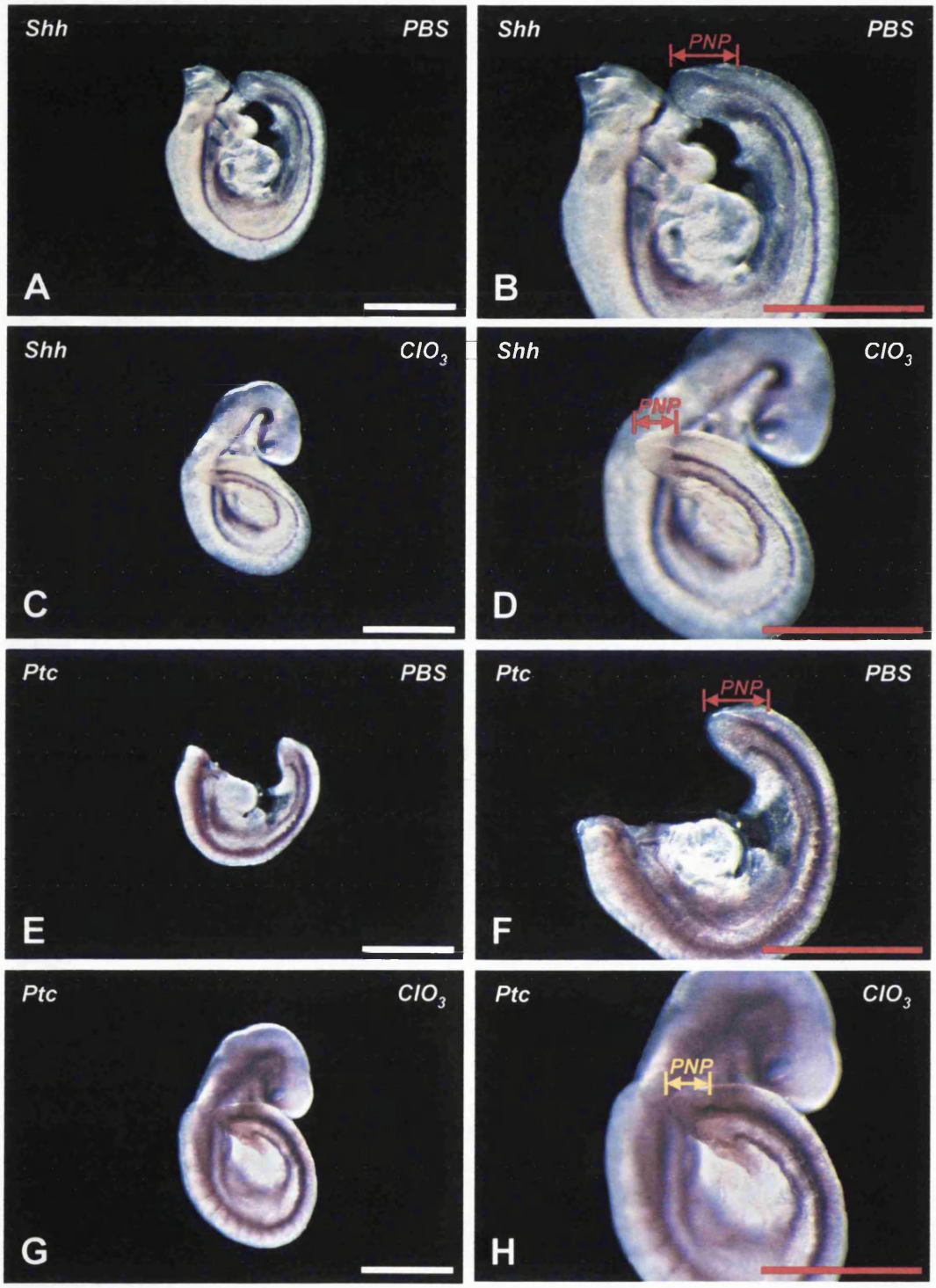
Shh
PBS
A
Shh
PNP
PBS
B
Shh
ClO3
C
Shh
PNP
ClO3
D
Ptc
PBS
E
Ptc
PNP
PBS
F
Ptc
ClO3
G
Ptc
PNP
ClO3
H

**Figure 5.26 Histological localisation of *Sonic hedgehog* and *Patched* transcripts.** Transverse sections through the posterior neuropore region prepared from embryos cultured in the presence of either phosphate buffered saline (A, C) or 30 mM chlorate (B, D and E). *Shh* transcripts are stained in (A) and (B). *Ptc* transcripts are shown in (C), (D) and (E). (E) shows that although the intensity of staining varies between embryos [compare (D) with (E)], the notochord is consistently the most intensely stained structure for *Patched* expression in chlorate-treated embryos. Arrows, paired dorsolateral hinge points; star, median hinge point. Abbreviations: *Ptc, Patched*; *Shh, Sonic hedgehog*; $ClO_3$, chlorate; nc, notochord; PBS, phosphate buffered saline. Scale bar, 100 μm.

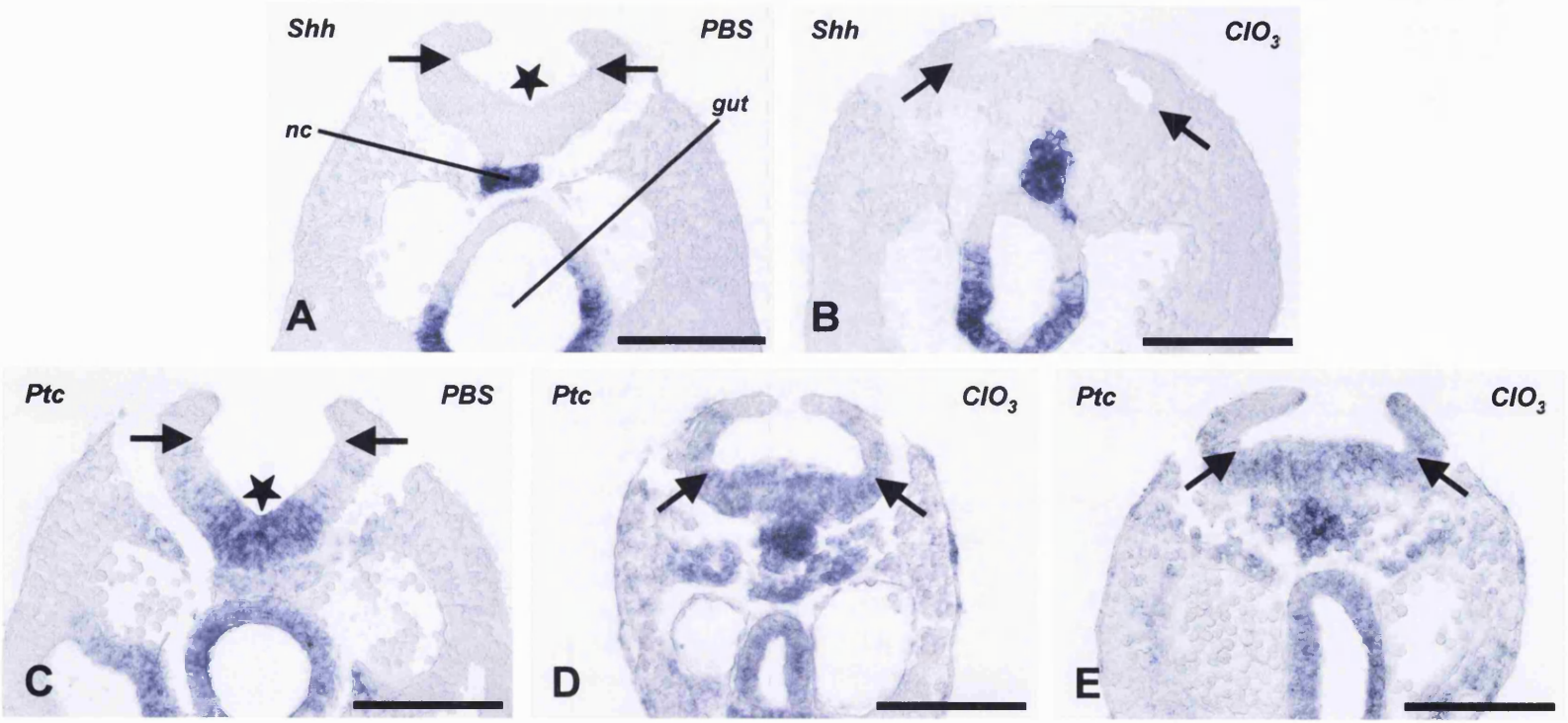
Shh
PBS
nc
gut
A
Shh
ClO3
B
Ptc
PBS
C
Ptc
ClO3
D
Ptc
ClO3
E

(which might improve probe accessibility) was performed on embryos in the buffer group.

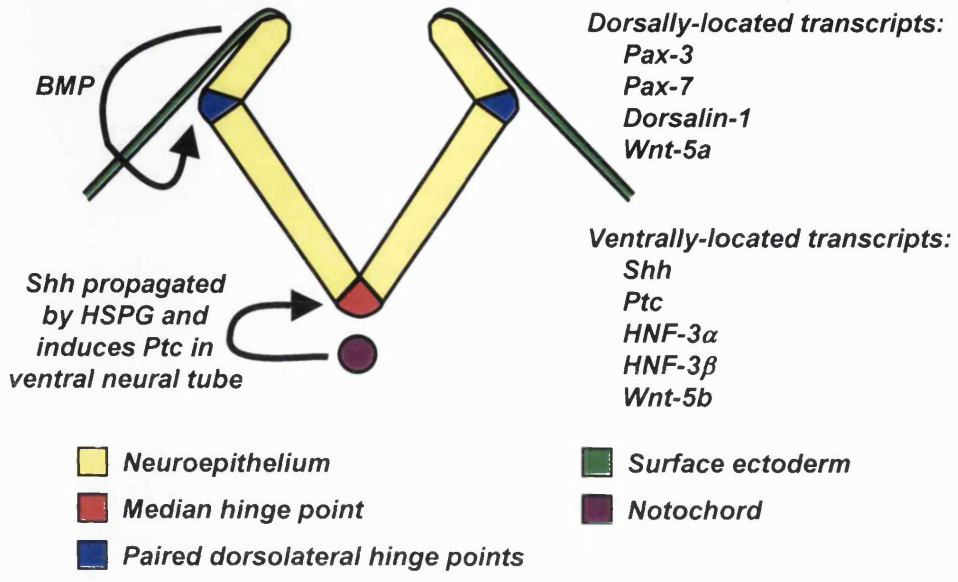


**Figure 5.27 Summary diagram of molecular markers expressed during spinal neurulation.** The notochord produces Shh, which upregulates the expression of *Ptc* in the overlying neuroepithelium and induces median hinge point formation (Ybot-Gonzalez and Copp, unpublished). Propagation of the Shh signal appears to depend on heparan sulphate proteoglycan (HSPG). Usually, minimal amount of *Ptc* transcripts is found in the notochord. However, when sulphation of heparan sulphate is blocked by chlorate treatment, *Ptc* expression in the notochord is increased. Other molecular markers expressed in the notochord and floor plate of the neural tube include *HNF-3α*, *HNF-3β* and *Wnt-5b*. On the other hand, dorsolateral hinge point formation is induced by the surface ectoderm, possibly through BMP signalling. The paired dorsolateral hinge points are absent after removal of the surface ectoderm (Ybot-Gonzalez and Copp, unpublished). Other molecular markers expressed in the dorsal neural tube include *Pax-3*, *Pax-7*, *Dorsalin-1* and *Wnt-5a*. Solid arrow, stimulation.

## 5.3 Discussion

This chapter has examined the role of sulphated glycosaminoglycans in spinal neurulation, using chlorate which competitively inhibits glycosaminoglycan sulphation (Conrad, 1998). Spinal neurulation is found to be specifically regulated by heparan sulphate, an effect that requires both N- and O-linked sulphate groups. Inhibition of sulphation of heparan sulphate blocks median hinge point formation and accelerates closure of the posterior neuropore, the latter effect being mediated by increased bending at the paired dorsolateral hinge points. These chlorate-induced effects can be prevented by supplementation of the culture medium with 'normally-sulphated' heparan sulphate, but not by chondroitin sulphate, heparitinase-treated heparan sulphate or heparan sulphate with either the N- or O-linked sulphate groups removed. These results are summarised in Table 5.1.

### *5.3.1 Mechanism of neural fold elevation and bending*

Closure of the neural tube requires elevation of the neural folds and bending of the neuroepithelium to bring the lateral edges of the neural folds to the dorsal midline (Copp et al, 1990; Smith and Schoenwolf, 1997). Bending at the median and paired dorsolateral hinge points are accompanied by adoption of a wedge shape by neuroepithelial cells at these sites. The forces that drive these changes have been postulated to arise either from the neuroepithelium itself (intrinsic forces) or from the surrounding tissues (extrinsic forces).

**Table 5.1 Effect of under-sulphation of heparan sulphate on the posterior neuropore length**

| CHLORATE | OTHER REAGENT | PNP LENGTH |
|---|---|---|
| - | - | Normal |
| + | - | ↓ |
| + | Carrier-free sulphate | Normal |
| + | Heparan sulphate | Normal |
| + | Chondroitin sulphate | ↓ |
| + | Heparitinase-treated heparan sulphate | ↓ |
| + | De-N-sulphated heparan sulphate | ↓ |
| + | De-O-sulphated heparan sulphate | ↓ |

*Abbreviations: PNP, posterior neuropore; +, present; -, absent; ↓, decreased*

#### 5.3.1.1 Heparan sulphate and actin microfilaments

Heparan sulphate proteoglycans are known to colocalise with and bind to actin and other components of the cytoskeleton in epithelial cells, thus helping to organise the cytoskeleton (Carey et al, 1994; Fernandez-Borja et al, 1995; Carey et al, 1996; Bernfield et al, 1999). Microfilament bundles are found in neuroepithelial cells (Baker and Schroeder, 1967; Karfunkel, 1974; Morriss and New, 1979; Nagele and Lee, 1980; Sadler et al, 1982; Morriss-Kay and Tuckett, 1985; Ybot-Gonzalez and Copp, 1999). Contraction of these microfilaments has been postulated to cause wedging of the cells in the median and dorsolateral hinge points, leading to elevation and bending of the neural folds and bringing the neural fold apices together at the dorsal midline (Karfunkel, 1974). Inhibition of this contraction could theoretically prevent formation of the hinge points and lead to the loss of rigidity of the neural plate seen in the chlorate-treated embryos in this chapter.

Indeed, apical microfilament bundles in the cranial neuroepithelium were found to be poorly organised when cranial neural tube closure was inhibited by β-D-xyloside treatment of cultured rat embryos (Morriss-Kay and Crutch, 1982). The breadth of the apical region of neuroepithelial cells was widened in embryos treated with β-D-xyloside, suggesting that the microfilament bundles were not under tension. β-D-xyloside prevents attachment of glycosaminoglycan chains to their proteoglycan core proteins. In addition, treatment of mouse embryos undergoing spinal neurulation with cytochalasin D in culture resulted in disassembly of the apical microfilaments in the neuroepithelium (Ybot-Gonzalez and Copp, 1999). This led to a loss of rigidity of the neural plate, which was

also seen in the chlorate-treated embryos in this chapter. This suggests that microfilament assembly and contraction in the neuroepithelium require heparan sulphate, and that this heparan sulphate needs to be 'normally' sulphated. However, formation of the median and dorsolateral hinge points in spinal neurulation does not require actin microfilaments (Ybot-Gonzalez and Copp, 1999). Thus, additional factors must be acting to prevent formation of the median hinge point in the chlorate-treated embryos.

#### 5.3.1.2 Heparan sulphate and the cell cycle

Besides apical contraction, wedging of a cell could be achieved by broadening of the cell base. This has been suggested to be an important mechanism for hinge point formation during spinal neurulation, since disassembly of actin microfilaments has no effect on formation of the hinge points (Ybot-Gonzalez and Copp, 1999). Interkinetic nuclear migration results in the cell nucleus occupying a basal position during S- and early $G_2$-phases of the cell cycle, and this is accompanied by wedging of the cell. Indeed, it has been shown that more cells are in $G_2$-phase in the median hinge point than in non-bending regions of the neural plate of the chick embryo, and these cells have a prolonged cell cycle (Smith and Schoenwolf, 1987; Smith and Schoenwolf, 1988). Cells in the median hinge point have been demonstrated to have a lower mitotic index than elsewhere in the neuroepithelium in the mouse embryo (Gerrelli and Copp, 1997).

Nuclear heparan sulphate is known to influence the cell cycle (Fedarko and Conrad, 1986; Fedarko et al, 1989; Ishihara and Conrad, 1989). Heparan sulphate has been localised in the nuclei of hepatoma cells in

culture, and these heparan sulphate molecules have been shown to contain highly sulphated residues (Fedarko and Conrad, 1986). As the hepatoma cells became confluent and stopped dividing, the amount of nuclear heparan sulphate increased up to three fold (Ishihara and Conrad, 1989). When heparan sulphate extracted from confluent cell cultures was added to growing cells, the glycosaminoglycan was taken up and transported to the cell nuclei (Fedarko et al, 1989). This was associated with inhibition of cell division. In contrast, heparan sulphate obtained from cells in the logarithmic phase of growth was less effectively taken up and had no effect on cell division. Thus, it could be postulated that prolongation of the cell cycle in median hinge point cells requires the presence of nuclear heparan sulphate. When biosynthesis of heparan sulphate was perturbed by chlorate treatment, cells in the median hinge point moved on in the cell cycle, resulting in loss of basal localisation of the cell nuclei and loss of cell wedging. The mechanism by which nuclear heparan sulphate affects the cell cycle is unclear.

Heparan sulphate on the cell surface and in the extracellular matrix is also able to regulate cell cycling through its interaction with growth factors (Conrad, 1998). The binding of fibroblast growth factors to heparan sulphate has been extensively studied (Schlessinger et al, 1995). Binding of fibroblast growth factors to high affinity fibroblast growth factor receptors leads to dimerisation and mutual tyrosine phosphorylation of these receptors, resulting in biological effects such as cell proliferation. The growth factor-receptor interaction is facilitated by heparan sulphate. However, heparan sulphate species that inhibits fibroblast growth factor-stimulated cell proliferation has also been described. For example, inhibitory heparan sulphate has been found to prevent the human breast cancer cell line MDA-MB-231 from

responding to fibroblast growth factor-2 (Delehedde et al, 1996). MDA-MB-231 cells do not normally have a mitogenic response to fibroblast growth factor-2. However, blocking sulphation of heparan sulphate by chlorate treatment enabled these cells to respond to fibroblast growth factor-2 and proliferate. Heparan sulphate species that inhibits mitogenic response to fibroblast growth factors-1 and 7 has also been described (Bonneh-Barkay et al, 1997; Pye et al, 2000), and this inhibitory activity has also been correlated with the sulphation pattern of heparan sulphate. Thus, it is possible that cells in the median hinge point have a prolonged cell cycle owing to their inability to respond to growth factors (such as fibroblast growth factors) because of the inhibitory action of heparan sulphate. Blocking sulphation of heparan sulphate by chlorate treatment released these cells from the inhibitory effect of heparan sulphate. These cells were then able to proliferate, leading to the absence of median hinge point formation in the chlorate-treated embryos.

#### 5.3.1.3 Heparan sulphate and Sonic hedgehog signalling

Formation of the median hinge point depends on induction by the notochord (Smith and Schoenwolf, 1989). In the absence of the notochord, the median hinge point does not form. In contrast, implantation of ectopic notochords results in the formation of supernumerary strips of median hinge point cells in the neuroepithelium overlying the extra notochords. Sonic hedgehog is produced by the notochord. The level of expression of *Sonic hedgehog* mRNA has been shown to decrease along the longitudinal axis of the neural tube (Ybot-

Gonzalez and Copp, unpublished). This correlates with the reduction in cell wedging in the median hinge point along the neuraxis, suggesting that Sonic hedgehog induces median hinge point formation. Furthermore, there appears to be a relationship between dorsolateral hinge point formation and the intensity of the Sonic hedgehog signal. The signal is strongest in the notochord and overlying neuroepithelium and decreases towards the neural fold apices. In Mode 1 neurulation, strong Sonic hedgehog signalling from the notochord inhibits formation of the dorsolateral hinge points. In contrast, in Modes 2 and 3 neurulation, reduction in the level of Sonic hedgehog signal allows the dorsolateral hinge points to be formed.

Heparan sulphate has been shown to be required for localisation and propagation of the Hedgehog signal (Bellaiche et al, 1998; The et al, 1999; Lin et al, 2000). Heparan sulphate interacts with the transmembrane protein Dispatched to release Hedgehog from the producing cells and helps to propagate the signal through the tissues to the receiving cells (Burke et al, 1999). Heparan sulphate chain elongation is catalysed by the enzyme heparan sulphate copolymerase (Figure 1.3), which is encoded by the *tout-velu* gene in *Drosophila* and the *EXT* gene family in mammals. Hedgehog signalling is inhibited when either *tout-velu* (in *Drosophila*) or *EXT1* (in mouse) is disrupted (Belaiche et al, 1998; The et al, 1999; Lin et al, 2000). In addition, sulphate groups on heparan sulphate appear to be required for Hedgehog signalling. Disruption of Hedgehog signalling has been reported when sulphation of heparan sulphate is perturbed in the *Drosophila sulfateless* mutant (The et al, 1999). *Sulfateless* encodes the N-deacetylase N-sulphotransferase enzyme, which removes the acetyl group from the glucosamine residue in heparan sulphate and

adds a sulphate group to the residue. Thus, it could be postulated that the lack of a median hinge point and the increased bending at the paired dorsolateral hinge points in the chlorate-treated embryos are due to disruption of Sonic hedgehog signalling.

The expression pattern of *Patched* mRNA is consistent with this hypothesis. In the normal situation, Sonic hedgehog signal from the notochord is restrictively directed by heparan sulphate to the overlying neuroepithelium, where it induces a ventral-dorsal/medial-lateral gradient (higher ventrally and medially) of *Patched* expression in the neuroepithelium. Heparan sulphate is present around the notochord and in the neuroepithelial basement membrane (Figure 5.22A). However, when sulphation of heparan sulphate was inhibited by chlorate treatment, this restrictive distribution of the Sonic hedgehog signal appears to be lost. Instead, *Patched* is strongly induced in the notochord, where Sonic hedgehog is produced, and to a lesser degree in the overlying neuroepithelium and surrounding tissues. The medial-lateral gradient of *Patched* expression in the neuroepithelium is lost. Ectopic induction of *Patched* by mis-expression of *Sonic hedgehog* in the chick limb bud has been previously reported (Marigo et al, 1996b).

However, in the *Drosophila tout-velu* mutant, there is an absence of Patched protein rather than ectopic expression (Bellaiche et al, 1998). This difference between the *tout-velu* mutant and the chlorate-treated embryos could be explained by a quantitative and qualitative difference in heparan sulphate. In the *tout-velu* mutant, heparan sulphate is almost undetectable due to lack of heparan sulphate co-polymerase, which is required for chain elongation (Toyoda et al, 2000b). In contrast, chlorate treatment merely inhibits O-sulphation of heparan

sulphate and does not have a significant effect on chain elongation or other structural modifications of the glycosaminoglycan molecule (Greve et al, 1988; Conrad, 1998; Safaiyan et al, 1999). Thus, although heparan sulphate may be required for binding and propagation of the Hedgehog signal, the O-sulphate group on heparan sulphate may be needed to restrict the direction of signal propagation. The heparan sulphate sequence required for binding and propagating the Sonic hedgehog signal has not been described, but a distinct requirement for the O-sulphate group is known in the interaction of heparan sulphate/heparin with fibroblast growth factor-2 (Guimond et al, 1993; Pye et al, 1998). Full-size native heparin (which carries 6-O-sulphate groups) binds to and promotes the mitogenic activity of fibroblast growth factor-2 in Swiss 3T3 fibroblasts. On the other hand, heparin without the 6-O-sulphate group retains the ability to bind to the growth factor but does not promote the mitogenic activity of the growth factor. The expression pattern of Patched in the *Drosophila sulfateless* mutant and in the EXT1-deficient mouse has not been described.

#### 5.3.1.4 Heparan sulphate and structural support of the neural plate

Heparan sulphate proteoglycans form an integral part of the basement membrane of the neuroepithelium, and help in providing structural support to the neuroepithelium (O'Shea, 1987; Martins-Green, 1988; Iozzo, 1998). Loss of this structural support could, at least partly, account for the abnormalities seen in the chlorate-treated embryos. Indeed, abnormalities in the neuroepithelial basement membrane have been described when proteoglycan synthesis was disrupted by β-D-

xyloside treatment. The neuroepithelial basement membrane was found to be discontinuous under transmission electron microscopy, and parts of the adjacent cells herniated through these discontinuities (Morriss-Kay and Crutch, 1982). Heparan sulphate is known to provide sorting information for localisation of proteoglycans (Mertens et al, 1996). Removal of heparan sulphate chains results in apical transport of the core protein of proteoglycans that would, under normal circumstances, be located on the basolateral surface of epithelial cells.

Although structural support from the extracellular matrix in the mesoderm has been suggested to regulate cranial neurulation (Morriss and Solursh, 1978; Morris-Wiman and Brinkley, 1990), it is unlikely that disruption of this support could account for the abnormalities seen in the chlorate-treated embryos. The major glycosaminoglycan present in the extracellular matrix of the posterior neuropore region is hyaluronan, a non-sulphated molecule, rather than heparan sulphate (Morriss and Solursh, 1978; Copp and Bernfield, 1988a). The intercellular spaces within the paraxial mesoderm do not appear to be reduced in the chlorate-treated group of embryos. Furthermore, closure of the posterior neuropore has been shown to occur independently of adjacent non-neural tissues (van Straaten et al, 1993).

### *5.3.2 Different requirements for heparan suiphate in cranial and spinal neurulation*

The findings in this chapter suggest that heparan sulphate regulates spinal neurulation, although it does not appear to be essential for

closure of the posterior neuropore. This conclusion is in agreement with the result of Tuckett and Morriss-Kay (1989a), who showed that closure of the rat spinal neural tube occurred despite degradation of heparan sulphate by heparitinase treatment. Furthermore, the current study shows that formation of the median hinge point, bending at the paired dorsolateral hinge points, and maintenance of the rigidity of non-bending regions of the neural plate are all affected when heparan sulphate is under-sulphated. The N- and O-linked sulphate groups are both important for heparan sulphate to regulate posterior neuropore closure.

In contrast, heparan sulphate appears to be essential for cranial neurulation (Tuckett and Morriss-Kay, 1989a). In cranial neural tube closure, the two sides of the neural plate initially bulge outwards in a dorsolateral direction to form a biconvex shape (Morriss-Kay, 1981). The neural folds then bend medially to become V-shaped and come together to converge in the midline. Rat embryos that were cultured in the presence of heparitinase had an open neural tube in the cranial region (Tuckett and Morriss-Kay, 1989a). The cranial neural folds failed to transform from biconvex to V-shape morphology. Inhibition of the attachment of sulphated glycosaminoglycans to their proteoglycan core proteins by β-D-xyloside treatment also resulted in a failure of cranial neural tube closure, with a similar loss of the biconvex to V-shape transformation of the neuroepithelium (Morriss-Kay and Crutch, 1982).

There appears to be a different requirement for sulphate groups on heparan sulphate between cranial and spinal neurulation. The current study suggests that 6-O-sulphation of heparan sulphate is not essential for cranial neurulation. The cranial neural tube had closed in all the

chlorate-treated embryos at the end of the culture period. On the other hand, failure of cranial neurulation has been reported when chlorate was administered intraperitoneally to pregnant mice on days 8.5 or 9.0 of gestation, in which day 0 was defined as the day of finding the vaginal plug (Kubota et al, 1999). Chlorate was injected at a dose of 3.2, 10.6 or 40 mg/mouse (average weight of ddY mouse strain used: 39.5 g). Approximately 10% of the embryos that received higher doses of chlorate had incomplete cranial neural tube closure. The conflict between this report and the current study could be explained by the selective inhibition of sulphation of heparan sulphate by chlorate treatment (Safaiyan et al, 1999). At a concentration of 50 mM, chlorate reduces both 6-O and 2-O sulphation with negligible effect on N-sulphation. At a concentration of 20 mM or less, 6-O-sulphation was selectively reduced. Thus, the cranial neural tube defects reported by Kubota and colleagues (1999) could have been due to a lack of both 2-O- and 6-O-sulphate groups on heparan sulphate. Indeed, it has been reported that the 2-O sulphate group is required for the ability of heparin to modulate the mitogenic activity of fibroblast growth factor-2 (Ishihara et al, 1994). However, it is possible that the apparent lack of inhibition of cranial neural tube closure by chlorate treatment in this study is because the embryos had already passed the critical phase for cranial neurulation before chlorate was added to the culture medium.

### *5.3.3 Heparan sulphate and other developmental events*

It is interesting to note that in this study, spinal neurulation is specifically affected by inhibiting sulphation of heparan sulphate. Chlorate

treatment does not appear to have any significant effect on growth of the embryo in general (as measured by the crown-rump length, head length, Brown and Fabro morphological score, and protein synthesis). Furthermore, there is no obvious gross morphological malformation in the embryo after chlorate treatment, although detailed examination of other tissues might reveal subtle abnormalities. One possible reason for this is that the main tissue that requires heparan sulphate at the developmental stage examined is the closing neural tube.

Another possibility is that different tissues might require different heparan sulphate species during development. Indeed, deletion of different sulphate groups on heparan sulphate has led to distinct developmental abnormalities. Mutation of the *Hs2st* gene, which encodes heparan sulphate 2-O-sulphotransferase, results in defects in the kidney, eye and skeletal systems in the mouse (Bullock et al, 1998). This suggests that these organ-systems require heparan sulphate species that contains 2-O sulphate groups during development. In contrast, N-sulphate groups appear to be essential to development of the lungs. *Ndst1* null mice, which lack the enzyme N-deacetylase N-sulphotransferase used in heparan sulphate synthesis, die from severe respiratory distress syndrome as a result of pulmonary hypoplasia and atelectasis (Ringvall et al, 2000; Fan et al, 2000). Thus, it appears that in the case of spinal neural tube closure, the heparan sulphate species that is required is one with both N- and O-linked sulphate groups.

### 5.3.4 Chondroitin sulphate and neurulation

The effects of chlorate on spinal neurulation appear to be mediated mainly by inhibition of sulphation of heparan sulphate. Exogenous

heparan sulphate prevented chlorate-induced premature posterior neuropore closure as well as the morphological abnormalities in the neuroepithelium. In contrast, exogenous chondroitin sulphate had no preventive effect, even though chlorate treatment completely abolished sulphation of chondroitin sulphate. This suggests that the sulphate groups on chondroitin sulphate are not required for spinal neurulation. However, it does not imply that the chondroitin sulphate chain itself has no role in spinal neurulation. This question is examined further in the next chapter.

Sulphation of chondroitin sulphate appears not to be required for cranial neurulation. This is in agreement with the findings of Morriss-Kay and Tuckett (1989b), who showed that degradation of chondroitin sulphate by chondroitinase treatment did not inhibit cranial neurulation. However, there was a delay in closure of the cranial neural tube, which was especially prominent at the midbrain/forebrain apposition point. This delay appears to be due to inhibition of cranial neural crest emigration. Emigration of neural crest cells from the cranial neuroepithelium is facilitated by chondroitin sulphate, and this helps in medial bending of the cranial neural folds. The role of chondroitin sulphate in regulating neural crest cell migration is considered in Chapter 7.

# *Chapter 6*

# CHONDROITIN SULPHATE

# AND

# SPINAL NEURULATION

## 6.1 Introduction

In the previous chapters, it is seen that the main sulphated glycosaminoglycans synthesised by the murine embryo at the time of spinal neurulation are heparan sulphate and chondroitin sulphate. Both molecules are present in the basement membrane of the closing spinal neural tube, as well as in adjacent tissues in the posterior neuropore region. Inhibition of glycosaminoglycan sulphation results in the acceleration of posterior neuropore closure and the absence of median hinge point formation. These effects appear to be mediated primarily by inhibition of sulphation of heparan sulphate, since they could be prevented by supplementation of the culture medium with exogenous heparan sulphate and not by chondroitin sulphate.

Although heparan sulphate has been shown to be important for neurulation (Morriss-Kay and Crutch, 1982; Tuckett and Morriss-Kay, 1989a; Chapter 5), the role of chondroitin sulphate in neurulation is less well understood. Quail embryos with spontaneous spinal neural tube defects were found to have a reduced amount of chondroitin sulphate as detected by immunohistochemistry, suggesting that chondroitin sulphate might be essential for neural tube closure (Newgreen et al, 1997). On the other hand, chondroitinase degradation of chondroitin sulphate in cultured rat embryos retarded, but did not inhibit, cranial neurulation (Morriss-Kay and Tuckett, 1989b). The effect appears to be secondary to inhibition of cranial neural crest emigration from the neural epithelium. Furthermore, an increase in the amount of chondroitin sulphate proteoglycans have been reported in the *splotch* mouse

mutant, which has both cranial and caudal neural tube defects (Trasler and Morriss-Kay, 1991; Henderson et al, 1997).

To examine whether chondroitin sulphate is involved in regulation of spinal neural tube closure, *CD1* mouse embryos were cultured in the presence of chondroitinase, an enzyme that degrades chondroitin sulphate (Yamagata et al, 1968). A complementary study was also performed in which cultured embryos were treated with exogenous chondroitin sulphate to determine whether over-abundance of chondroitin sulphate has an effect on posterior neuropore closure.

## 6.2 Results

### *6.2.1 Degradation of chondroitin sulphate retards posterior neuropore closure*

To determine whether chondroitin sulphate has an effect on posterior neuropore closure, *CD1* mouse embryos were exposed to chondroitinase in culture. Embryos were explanted from the uterus at E8.5 between the 10- and 14-somite stages, stabilised in culture, and then treated with either chondroitinase or phosphate buffered saline for 14 hours. At the end of the culture period, both groups of embryos appeared to be healthy, as judged by the presence of vigorous yolk sac circulation and regular heartbeats of over 100 per minute. All embryos had between 19 and 23 pairs of somites. Comparison of the crown-rump length, head length and Brown and Fabro morphological score between the two groups showed no statistically significant difference (Brown and Fabro, 1981; Table 3.1; Figure 6.1). There was no obvious difference in the gross morphology between embryos treated with chondroitinase and those treated with phosphate buffered saline, except in the posterior neuropore length as measured from the rostral end of the posterior neuropore to the tip of the tail bud (Figures 6.2 and 6.3). Treatment with chondroitinase resulted in an 18.6% increase in the posterior neuropore length ($p = 0.0337$), suggesting that degradation of chondroitin sulphate retards posterior neuropore closure.

In addition to degrading chondroitin sulphate, the *Proteus* chondroitinase ABC enzyme used in this experiment is capable of

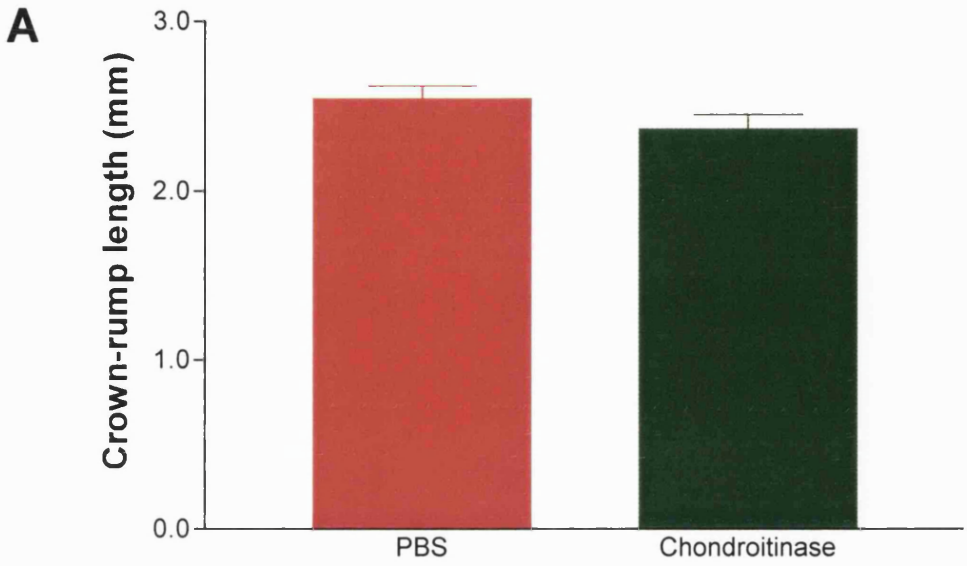
A
Crown-rump length (mm)
3.0
2.0
1.0
0.0
PBS
Chondroitinase

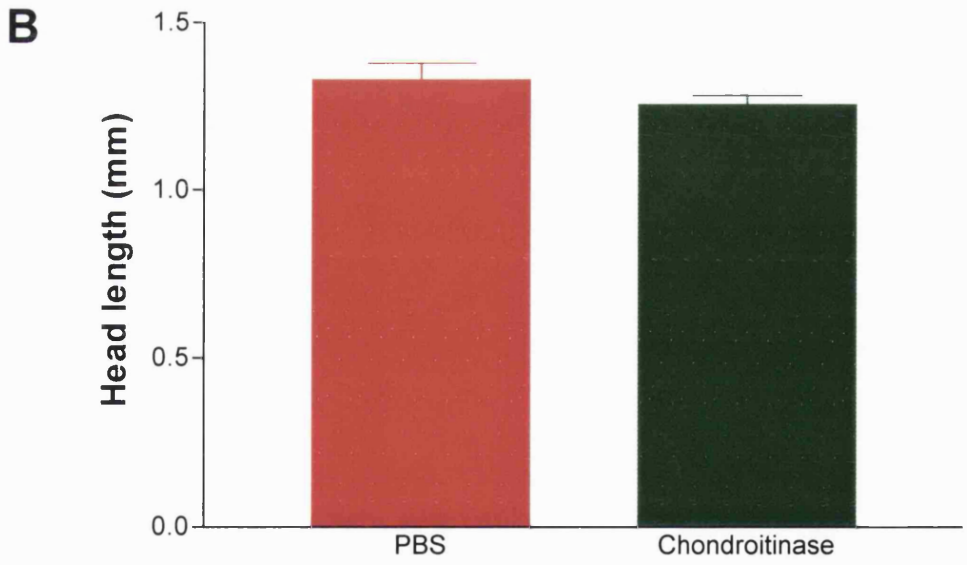
B
Head length (mm)
1.5
1.0
0.5
0.0
PBS
Chondroitinase

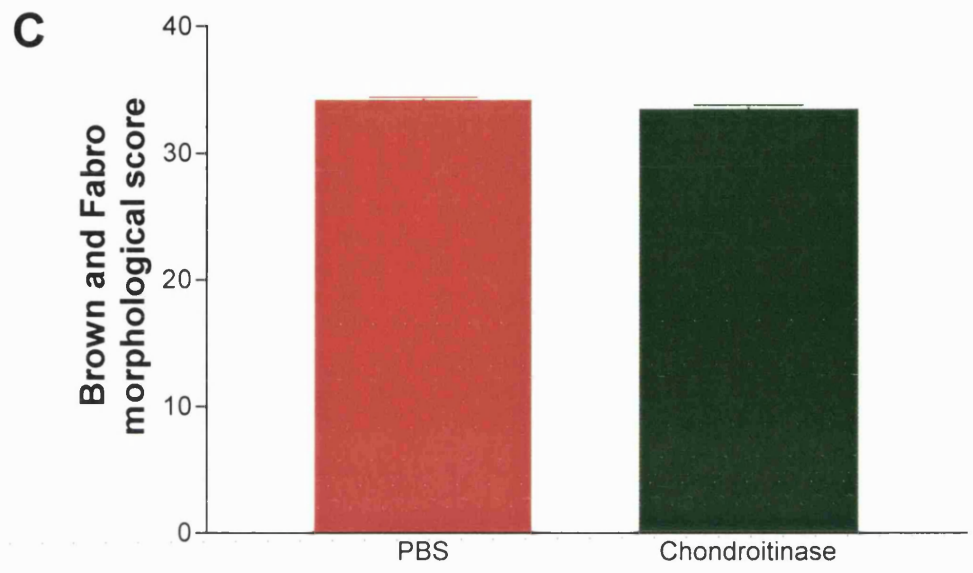


**Figure 6.1 Effect of chondroitinase on embryonic growth parameters.** (A) shows the crown-rump length, (B) shows the head length, and (C) shows the Brown and Fabro morphological score of embryos exposed to either phosphate buffered saline or 0.2 U/ml chondroitinase ABC in culture. Statistical comparison using Student's t-test gives a *p* value of 0.1301, 0.2184 and 0.1233 respectively. Line above each bar represents standard error. There are at least nine embryos in each group. Abbreviation: PBS, phosphate buffered saline.

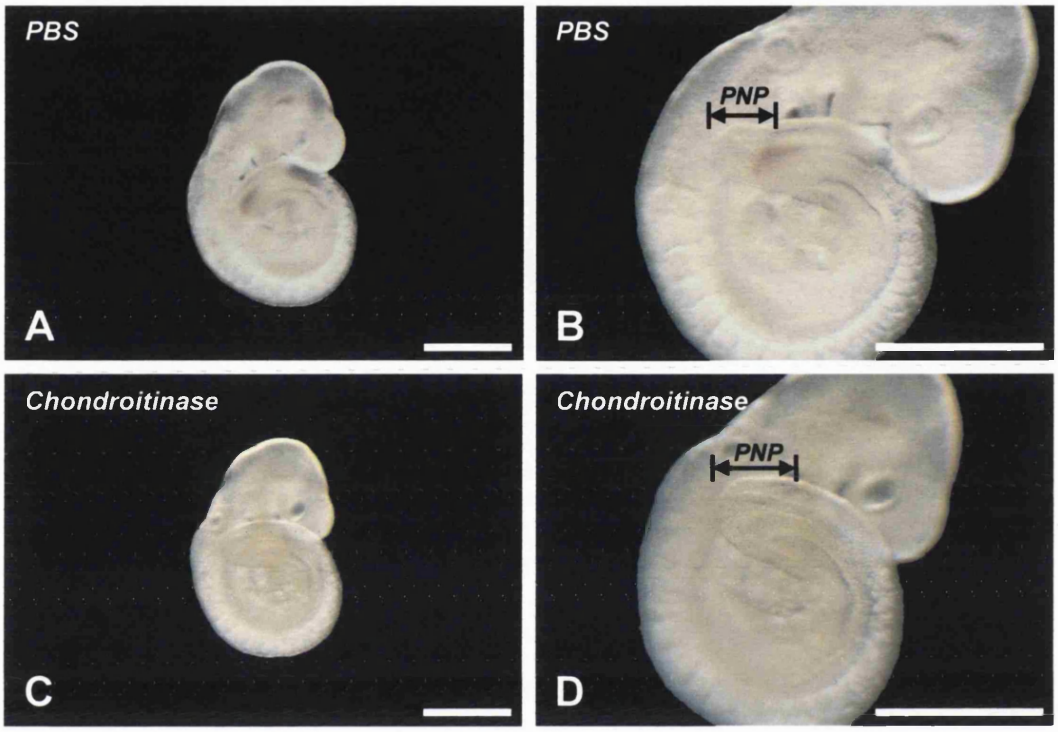


**Figure 6.2 Effect of chondroitinase on embryonic gross morphology.** Embryos were cultured in the presence of either phosphate buffered saline (A, B) or 0.2 U/ml chondroitinase ABC (C, D). (B) and (D) are close-up views of (A) and (C) respectively to illustrate the posterior neuropore. Abbreviation: PBS, phosphate buffered saline; PNP, posterior neuropore. Scale bar, 1 mm.

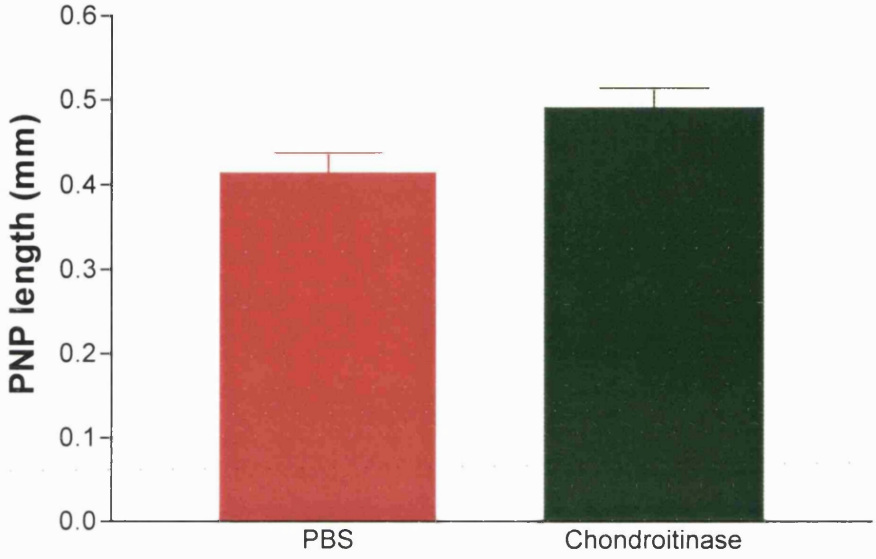


**Figure 6.3 Effect of chondroitinase on posterior neuropore closure.** Embryos were cultured in the presence of either phosphate buffered saline or 0.2 U/ml of chondroitinase ABC. Statistical comparison of the posterior neuropore length using Student's t-test gives a *p* value of 0.0337. Line above each bar represents standard error. There are at least nine embryos in each group. Abbreviation: PBS, phosphate buffered saline; PNP, posterior neuropore.

degrading hyaluronan, although the initial rate of degradation of hyaluronan compared with chondroitin sulphate is only 2% (Yamagata et al, 1968). To exclude the possibility that retardation of posterior neuropore closure by chondroitinase treatment is due to degradation of hyaluronan rather than chondroitin sulphate, embryos were cultured in the presence of either *Streptomyces* hyaluronidase or phosphate-buffered saline. *Streptomyces* hyaluronidase degrades hyaluronan specifically, and has no effect on chondroitin sulphate or heparan sulphate (Ohya and Kaneko, 1970). The enzyme has been previously shown to degrade hyaluronan in cultures of rat embryos (Morriss-Kay et al, 1986). Comparison of the posterior neuropore length between the two groups of embryos revealed no statistically significant difference ($p$ = 0.8729), even when *Streptomyces* hyaluronidase was used at a concentration of 1 U/ml (Figure 6.4). In contrast, *Proteus* chondroitinase was only used at 0.2 U/ml in the previous experiment. This suggests that retardation of posterior neuropore closure after treatment with *Proteus* chondroitinase is unlikely to be secondary to degradation of hyaluronan.

To confirm that the amount of chondroitin sulphate in the posterior neuropore region has been reduced by chondroitinase treatment, transverse sections through the posterior neuropore region were immunostained with CS-56, an anti-chondroitin sulphate antibody (Figure 6.5). In embryos treated with phosphate buffered saline, strong staining is seen in the neuroepithelial and surface ectodermal basement membrane as well as around cells in the mesoderm. The expression pattern is essentially as described in Chapters 4 and 5. However, the intensity of staining is uniformly reduced in embryos that were treated

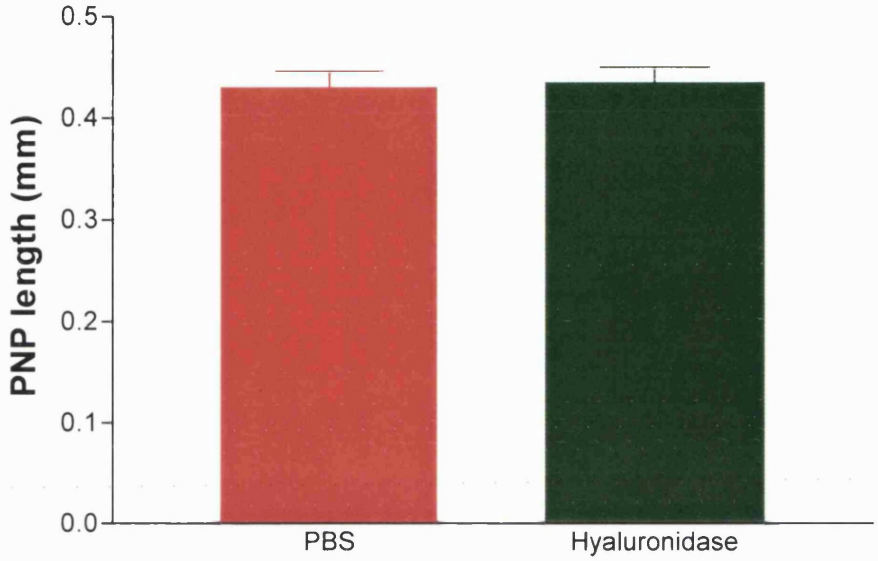


**Figure 6.4 Effect of *Streptomyces* hyaluronidase on posterior neuropore closure.** Embryos were cultured in the presence of either phosphate buffered saline or 1 U/ml of *Streptomyces* hyaluronidase. Statistical comparison of the posterior neuropore length using Student's t-test gives a *p* value of 0.8729. Line above each bar represents standard error. There are at least eight embryos in each group. Abbreviation: PBS, phosphate buffered saline; PNP, posterior neuropore.

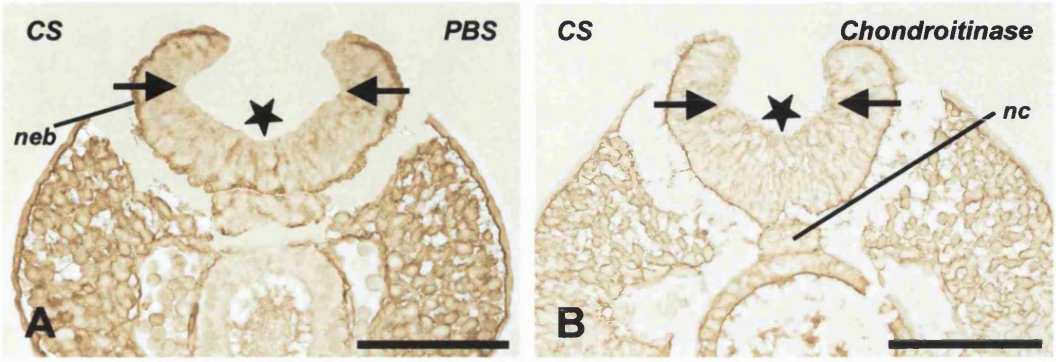


**Figure 6.5 Immunohistochemical localisation of chondroitin sulphate in the posterior neuropore region after chondroitinase treatment.** Immunohistochemical localisation of chondroitin sulphate on transverse sections through the posterior neuropore region prepared from embryos cultured in the presence of either phosphate buffered saline (A) or 0.2 U/ml chondroitinase ABC (B). Arrows, paired dorsolateral hinge points; star, median hinge point. Abbreviations: CS, chondroitin sulphate; neb, neuroepithelial basement membrane; nc, notochord; PBS, phosphate buffered saline. Scale bar, 100 μm.

with chondroitinase. Besides a reduction in staining intensity, there is no apparent difference in tissue morphology between embryos treated with chondroitinase and those treated with buffer (Figures 6.5 and 6.7). The median and paired dorsolateral hinge points are present in both groups, suggesting that loss of chondroitin sulphate does not affect hinge point formation. In addition, there is no obvious loss of intercellular spaces in the mesoderm to suggest that there was significant degradation of hyaluronan by chondroitinase treatment.

### 6.2.2 Chondroitin sulphate accelerates posterior neuropore closure

Since degradation of chondroitin sulphate retarded posterior neuropore closure, exogenous chondroitin sulphate might accelerate posterior neuropore closure in culture. To test this idea, embryos were cultured in the presence of either phosphate buffered saline or exogenous chondroitin sulphate (Figure 6.6). Treatment with exogenous chondroitin sulphate in culture resulted in a 13.8% reduction in posterior neuropore length ($p$ = 0.0392), suggesting that chondroitin sulphate accelerates posterior neuropore closure.

### 6.2.3 Chondroitin sulphate and hinge point formation

To determine whether chondroitin sulphate has an effect on formation of the median and paired dorsolateral hinge points, transverse sections

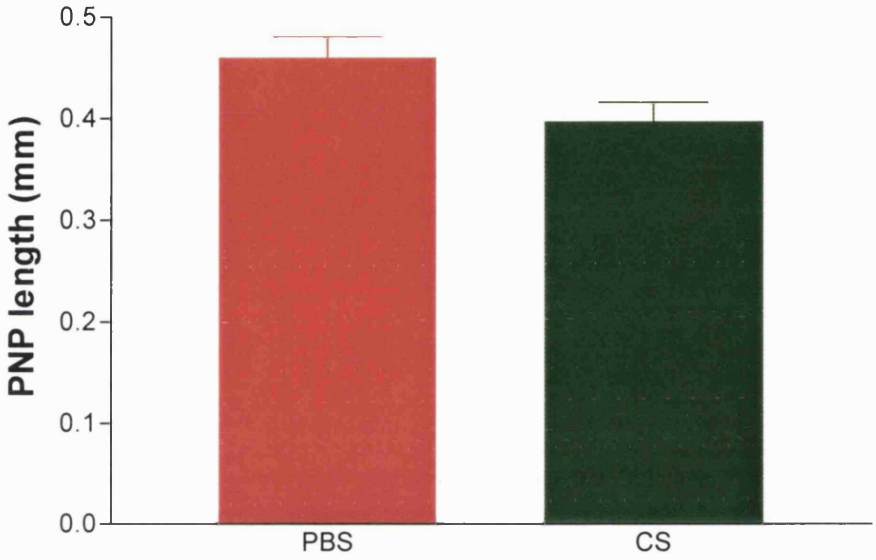


**Figure 6.6 Effect of exogenous chondroitin sulphate on posterior neuropore closure.** Embryos were cultured in the presence of either phosphate buffered saline or 100 ng/ml chondroitin sulphate. Statistical comparison of the posterior neuropore length using Student's t-test gives a *p* value of 0.0392. Lines above each bar represents standard error. There are at least nine embryos in each group. Abbreviations: PBS, phosphate buffered saline; PNP, posterior neuropore.

through the posterior neuropore region were prepared from embryos cultured in the presence of phosphate buffered saline, chondroitinase or exogenous chondroitin sulphate. These sections were stained with haematoxylin and eosin (Figure 6.7). Embryos treated with phosphate buffered saline in culture exhibit Mode 2 pattern of neurulation. Both median and paired dorsolateral hinge points are present, and the non-bending regions of the neural plate lying between these hinge points appear straight and rigid. Degradation of endogenous chondroitin sulphate and exposure to exogenous chondroitin sulphate in culture did not significantly affect the tissue architecture. These two groups of embryos look very similar to the buffer treated embryos, and there is no apparent effect on formation of the median and paired dorsolateral hinge points.

### 6.2.4 Chondroitin sulphate does not regulate posterior neuropore closure by affecting the amount of heparan sulphate

To exclude the possibility that chondroitin sulphate indirectly regulated the speed of posterior neuropore closure by affecting the amount of heparan sulphate, transverse sections through the posterior neuropore region were immunostained with 10E4, an anti-heparan sulphate antibody (Figure 6.8). Embryos cultured in the presence of phosphate buffered saline show strong staining in the basement membrane of the neuroepithelium and surface ectoderm, as described in Chapters 4 and 5. Staining is also present around cells of the mesoderm. A similar pattern of heparan sulphate expression is present in embryos treated


**Figure 6.7 Lack of effect on hinge point formation in the closing neural tube with changes in chondroitin sulphate content.** Haematoxylin and eosin stained transverse sections through the closing posterior neuropore region prepared from embryos cultured in the presence of phosphate buffered saline (A), 0.2 U/ml chondroitinase ABC (B), or 100 ng/ml chondroitin sulphate. Arrows, paired dorsolateral hinge points; star, median hinge point. Abbreviations: CS, chondroitin sulphate; PBS, phosphate buffered saline. Scale bar, 100 μm.

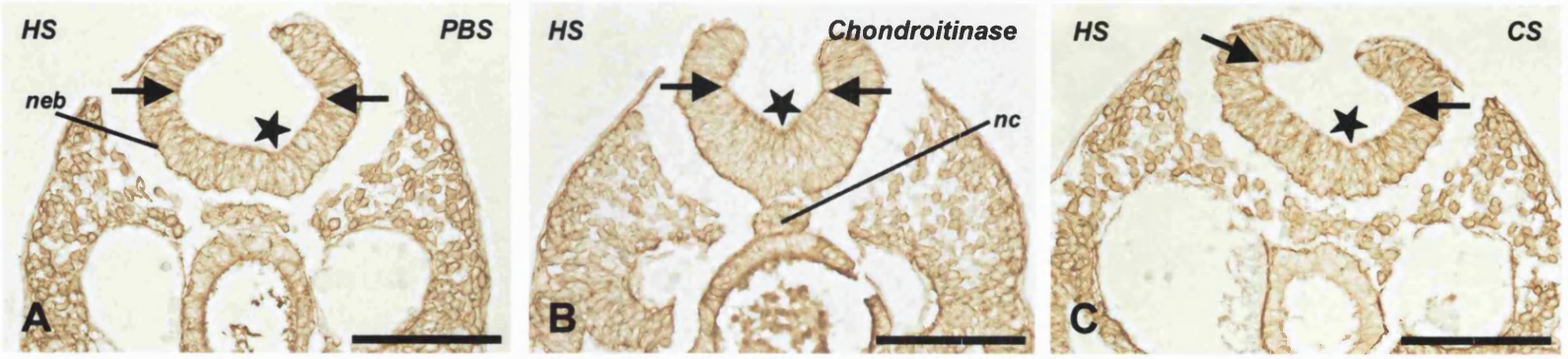




**Figure 6.8 Effect of chondroitin sulphate on posterior neuropore closure is not mediated by changes in heparan sulphate content.** Immunohistochemical localisation of heparan sulphate on transverse sections through the posterior neuropore region prepared from embryos cultured in the presence of phosphate buffered saline (A), 0.2 U/ml chondroitinase ABC (B), or 100 ng/ml chondroitin sulphate (C). Arrows, paired dorsolateral hinge points; star, median hinge point. Abbreviations: CS, chondroitin sulphate; neb, neuroepithelial basement membrane; nc, notochord; PBS, phosphate buffered saline. Scale bar, 100 μm.

with either chondroitinase or exogenous chondroitin sulphate in culture, suggesting that the effect of chondroitin sulphate on posterior neuropore closure is not secondary to alteration in the amount of heparan sulphate. This conclusion is further supported by the presence of the median hinge point in all three groups of embryos. A decrease in heparan sulphate content would be expected to inhibit median hinge point formation (Chapter 5).

## 6.3 Discussion

This chapter has examined the role of chondroitin sulphate in regulating spinal neurulation. Degradation of chondroitin sulphate retards posterior neuropore closure. In contrast, exposure to excess chondroitin sulphate results in premature closure of the posterior neuropore. However, neither median nor dorsolateral hinge point formation appears to be affected by chondroitin sulphate.

### *6.3.1 Cell-matrix interaction in spinal neurulation*

The neural tube is closed by elevation and medial bending of the neural folds to bring the neural fold apices towards each other at the dorsal midline (Copp et al, 1990; Smith and Schoenwolf, 1997). It has been suggested that the forces that drive these morphogenetic changes arise from the interaction between the neuroepithelium/surface ectoderm and the underlying extracellular matrix (Newgreen et al, 1997; Hackett et al, 1997). This results in sliding of the surface ectoderm in the medial direction, which leads to elevation and convergence of the neural folds. The extracellular matrix contains molecules that promote cell adhesion, such as fibronectin and laminin, and those that are anti-adhesive in nature, such as chondroitin sulphate (Tuckett and Morriss-Kay, 1986; O'Shea, 1987; Chapter 4). A decrease in the amount of chondroitin sulphate relative to adhesive molecules could result in greater adhesion of the surface ectoderm/neuroepithelium to the underlying matrix. This would impede sliding of the surface ectoderm over the underlying mesoderm and result in delay of neural tube closure. Indeed, it has

been reported that quail embryos that developed spontaneous spinal neural tube defects had less chondroitin sulphate relative to fibronectin and laminin compared with normal embryos (Newgreen et al, 1997). In contrast, exposure of cultured embryos to exogenous chondroitin sulphate could facilitate neural tube closure by decreasing adhesion between the surface ectoderm/neuroepithelium and the underlying matrix.

### 6.3.2 Cell-cell adhesion in spinal neurulation

It has been proposed that the dorsal third of the neural tube arises from progressive delamination of the surface ectoderm and neuroepithelium (Martins-Green, 1988). This leads to convergence of the neural fold tips in the dorsal midline, resulting in neural fold fusion. Deposition of anti-adhesive molecules such as chondroitin sulphate could contribute to de-adhesion of neuroepithelial cells from the surface ectodermal cells and thus lead to delamination of the two epithelia. This hypothesis is supported by the appearance of proteoglycan granules at the interface between the neuroepithelium and surface ectoderm before delamination begins (Martins-Green, 1988). Thus, degradation of chondroitin sulphate could negatively affect this delamination process, leading to the retardation of spinal neurulation seen in this chapter. Conversely, exogenous chondroitin sulphate could facilitate delamination of the two epithelia and accelerate posterior neuropore closure.

Besides a decrease in adhesion between the neuroepithelium and surface ectoderm, an increase in the strength of intercellular adhesion between adjacent cells in the neural plate has been suggested to contribute to neural fold elevation (Karfunkel et al, 1978; Copp et al,

1990). In this hypothesis, an increase in intercellular adhesive strength would lead to an increase in the area of cell-cell contact. This would result in bending of the neural plate, assuming that there is no change in the volume of each cell and that the basal surface of the cell is tethered to the underlying basement membrane. The cell adhesion molecule N-CAM is expressed in the neuroepithelium at the time of neurulation and, together with N-cadherin, might be involved in this postulated increase in intercellular adhesion (Thiery et al, 1982b; Kintner and Melton, 1987). N-CAM mediates cell-cell adhesion through a homophilic binding mechanism. In addition, N-CAM is able to bind to cell surface heparan sulphate proteoglycans through a heterophilic binding mechanism that increases cell-cell adhesion (Cole et al, 1986). Monoclonal antibodies that recognise the heparin-binding domain on N-CAM inhibit cell-cell adhesion. It has also been shown that chondroitin sulphate promotes heterophilic binding of N-CAM to some heparan sulphate proteoglycans, and that this binding is decreased by chondroitinase treatment (Storms et al, 1996). Thus, chondroitin sulphate could indirectly increase intercellular adhesion between neuroepithelial cells by promoting heterophilic binding of N-CAM to heparan sulphate proteoglycans, and thus promote closure of the spinal neural tube. Conversely, degradation of chondroitin sulphate would lead to a decrease in intercellular adhesion and retardation of posterior neuropore closure.

### 6.3.3 Chondroitin sulphate and fibroblast growth factor-2

Signalling by fibroblast growth factor-receptor interaction appears to be important for neurulation (Deng et al, 1997). Spina bifida has been reported in mouse chimeras that contain fibroblast growth factor receptor-1 null cells. Binding of fibroblast growth factors to their high affinity receptors (such as fibroblast growth factor receptor-1) results in dimerisation and mutual tyrosine phosphorylation of the receptors, leading to biological effects such as cell proliferation. This growth factor-receptor interaction is facilitated by heparan sulphate (Schlessinger et al, 1995; Conrad, 1998). Recently, it has been shown that chondroitin sulphate proteoglycans are also able to bind to fibroblast growth factor-2 and potentiate its mitogenic activity (Milev et al, 1998). These effects appear to be mediated by both the chondroitin sulphate chains and the proteoglycan core protein. Chondroitinase treatment reduced binding of the growth factor to the proteoglycan by 35% and the ability of the proteoglycan to potentiate the mitogenic activity of the growth factor. This suggests that the chondroitin sulphate chain is able to influence, although it is not essential for, fibroblast growth factor signalling. Degradation of chondroitin sulphate could thus reduce fibroblast growth factor signalling during neurulation, leading to the retardation in posterior neuropore closure seen in this chapter.

### 6.3.4 Chondroitin sulphate influences cranial and spinal neuruiation through different mechanisms

Chondroitin sulphate has been shown to indirectly regulate cranial neurulation (Morriss-Kay and Tuckett, 1989b). Rat embryos cultured in the presence of chondroitinase showed a delay in closure of the cranial neural tube. This effect appears to be mediated by inhibition of cranial neural crest emigration from the neuroepithelium. Chondroitin sulphate has been postulated to facilitate emigration of cranial neural crest cells, which leads to increased flexibility of the cranial neural folds for neural tube closure to occur (Morriss and New, 1979; Morriss-Kay and Tuckett, 1989b). Although the current study shows that chondroitin sulphate also has a role in regulating spinal neurulation, this is unlikely to be mediated by the effect of the glycosaminoglycan on trunk neural crest emigration. In the cranial region, neural crest emigration from the neuroepithelium begins before the neural folds have fused. In contrast, in the trunk region, neural crest cells only begin to emigrate after neurulation is completed (Erickson and Weston, 1983).

Taken together, the studies referenced above and the current experimental findings suggest that similar molecules could act through different mechanisms and have different effects in cranial and spinal neurulation. This is also seen in the case of heparan sulphate. Heparan sulphate is essential for cranial neurulation (Morriss-Kay and Crutch, 1982; Tuckett and Morriss-Kay, 1989a; Kubota et al, 1999), but inhibition of sulphation of heparan sulphate results in premature posterior neuropore closure and absence of median hinge point

formation (Chapter 5). Similarly, disassembly of actin microfilaments results in cranial, but not spinal, neural tube defects (Morriss-Kay and Tuckett, 1985; Ybot-Gonzalez and Copp, 1999).

# *Chapter 7*

# SULPHATED GLYCOSAMINOGLYCANS AND THE *SPLOTCH* MUTANT

## 7.1 Introduction

The previous chapters have examined the roles of heparan sulphate and chondroitin sulphate in spinal neurulation, in the context of normal embryonic development. Both molecules are involved in regulating closure of the posterior neuropore. Posterior neuropore closure is accelerated either by inhibiting sulphation of heparan sulphate or by the presence of excess chondroitin sulphate. On the other hand, degradation of endogenous chondroitin sulphate results in delayed spinal neurulation.

In addition to its role in neurulation, chondroitin sulphate helps to regulate neural crest migration. The neural crest arises at the dorsal tips of the neural folds (Le Douarin and Kalcheim, 1999). Neural crest cells migrate extensively to give rise to many different structures, including spinal ganglia, autonomic nervous system, Schwann cells and supporting cells of the peripheral nervous system, pigment cells, and adrenal medulla. They also contribute to formation of the skull bones and connective tissues of the head and neck regions as well as the endocardial cushions of the cardiac outflow tract. Neural crest cell migration is guided by both permissive and non-permissive molecules. Permissive molecules, such as fibronectin, laminin and collagen types I, III, IV and VI, are expressed along the neural crest migratory pathways and support neural crest cell attachment and migration (Tuckett and Morriss-Kay, 1986; Duband et al, 1986; Sternberg and Kimber, 1986; Perris et al, 1991a; Perris, 1997; Henderson and Copp, 1997). On the other hand, non-permissive molecules, such as chondroitin sulphate proteoglycans, F-spondin, collapsin-1, T-cadherin, and ephrins-B1 and

B2, are found in regions avoided by migrating neural crest cells, whereas they are scarce or absent along the migratory pathways (Ranscht and Bronner-Fraser, 1991; Oakley and Tosney, 1991; Oakley et al, 1994; Henderson and Copp, 1997; Wang and Anderson, 1997; Debby-Brafman et al, 1999; Eickholt et al, 1999). These molecules do not sustain significant neural crest cell attachment or movement, and may directly impede migration of these cells. However, recent studies have suggested that not all chondroitin sulphate proteoglycans function as non-permissive molecules to neural crest migration (Perris and Perissinotto, 2000; Perissinotto et al, 2000). Neural crest cells have been shown to migrate towards versican, a chondroitin sulphate proteoglycan, both *in vitro* and *in vivo*.

The *splotch* ($Sp^{2H}$) mouse mutant, so named because of a white belly spot in the heterozygous animal, offers an opportunity to investigate the roles of heparan sulphate and chondroitin sulphate in an organism that has both neural tube and neural crest abnormalities (Auerbach, 1954). The mutation involves a 32-base pair deletion in the *Pax-3* gene (Epstein et al, 1991). Besides cranial and caudal neural tube defects, deficiencies of neural crest derivatives are seen in the mutant embryos. The latter includes reduced or absent dorsal root ganglia, diminished Schwann cell numbers, pigmentation defects, and a persistent truncus arteriosus owing to failure of cardiac neural crest cells to colonise the heart outflow tract (Chalepakis et al, 1993). It has been suggested that the deficiencies of neural crest derivatives could, at least partly, be due to an abnormal environment through which neural crest cells migrate, rather than to an intrinsic migratory defect in the neural crest cells themselves (Trasler and Morriss-Kay, 1991; Henderson et al, 1997). Explants of neural crest cells from *splotch* mutant embryos showed

normal migratory behaviour *in vitro* (Conway et al, 2000; Epstein et al, 2000). *In vivo*, neural crest cells transplanted from *splotch* mutant embryos into chick embryos with a normal extracellular environment demonstrated a normal pattern of migration (Serbedzija and McMahon, 1997; Conway et al, 2000).

*Splotch* mouse mutants appear to have an abnormal increase in the amount of chondroitin sulphate proteoglycans, and this has been postulated to contribute to disruption of neural crest migration (Trasler and Morriss-Kay, 1991; Henderson et al, 1997). Using immunohistochemistry, larger quantities of chondroitin sulphate were detected in the cranial (between 5- and 15-somite stages) and caudal (between 14- and 19-somite stages) regions of *splotch* homozygous embryos (Trasler and Morriss-Kay, 1991). The amount of chondroitin sulphate in older embryos was not examined. Using *in situ* hybridisation, transcripts of the chondroitin sulphate proteoglycan *versican* were found to be over-expressed in *splotch* mutant embryos between E9 to E12.5 (Henderson et al, 1997). However, the question of whether there is a corresponding rise in chondroitin sulphate content was not examined. This chapter aimed to compare the amount of chondroitin sulphate and heparan sulphate between *splotch* homozygous, heterozygous and wild type embryos at the stage of posterior neuropore closure using the Blyscan Assay, a dye binding assay for quantifying sulphated glycosaminoglycans. This is followed by a comparison of the net rate of heparan sulphate and chondroitin sulphate synthesis between the three genotypic groups using $^{35}S$-labelling of sulphated glycosaminoglycans and anion exchange chromatography.

## 7.2 Results

### *7.2.1 Quantification of sulphated glycosaminoglycans*

Sulphated glycosaminoglycans were quantified using the Blyscan Assay, which is based on the binding of these molecules to the cationic dye 1,9-dimethylmethylene blue (Biocolor data sheet; Farndale et al, 1986). Quantities of sulphated glycosaminoglycans as small as 0.2 μg can be measured by this method (Figure 7.1). The main sulphated glycosaminoglycans synthesised by the embryo during spinal neurulation are heparan sulphate and chondroitin sulphate (Solursh and Morriss, 1977; Copp and Bernfield, 1988a; Chapter 5). Before running the Blyscan Assay, samples were pre-treated with either chondroitinase or buffer solution as described in Chapter 3. Briefly, each sample was divided into two equal portions and incubated overnight with either chondroitinase (to completely degrade chondroitin sulphate; see Chapter 5) or buffer solution. The amount of 1,9-dimethylmethylene blue bound to each portion was then determined spectrophotometrically. The absorbance of the buffer-treated portion and the enzyme-treated portion is proportional to the total amount of sulphated glycosaminoglycans and heparan sulphate respectively. The difference in absorbance is proportional to the amount of chondroitin sulphate.

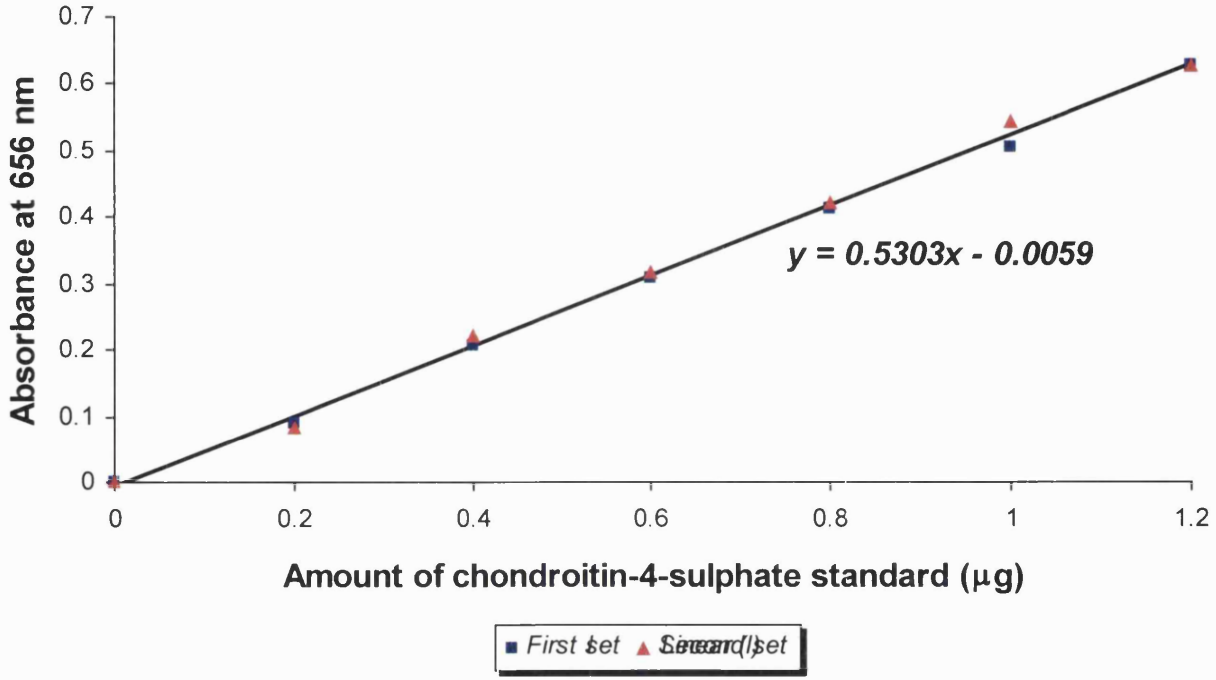


**Figure 7.1 Standard curve for quantification of sulphated glycosaminoglycans using the Blyscan Assay Kit.** The absorbance ($y$) at 656 nm of known amounts ($x$) of chondroitin-4-sulphate was measured in two separate sets of standards. Using linear regression, the line of best fit was found to be described by the equation $y = 0.5303x - 0.0059$. The coefficient of determination, $r^2$, was 0.9975.

*Splotch* ($Sp^{2H}$) embryos were collected at E9.5 and genotyped using the polymerase chain reaction (Figures 7.2 and 7.3). The embryos in all the three genotypic groups (homozygous, heterozygous and wild type) had between 25 and 29 pairs of somites. All the homozygous embryos had cranial and/or caudal neural tube defects. Comparison of the crown-rump length and protein content among the three groups of embryos showed no statistically significant difference ($p$ = 0.3365 and 0.1805 respectively; Figure 7.4). However, the head length of homozygous embryos was 3.7% shorter than wild type embryos ($p$ = 0.0089).

Homozygous and heterozygous *splotch* embryos had almost 15% more chondroitin sulphate, on a per microgram protein basis, than wild type embryos ($p$ = 0.0254; Figure 7.5). The chondroitin sulphate content did not significantly differ between homozygous and heterozygous embryos. In the case of heparan sulphate, although wild type embryos appeared to have, on average, more heparan sulphate than heterozygous embryos, which in turn appeared to have more of this glycosaminoglycan than the homozygous group, this difference was not statistically significant ($p$ = 0.1006; Figure 7.6).

The major glycosaminoglycan produced by the embryo during neurulation is hyaluronan (Solursh and Morriss, 1977; Copp and Bernfield, 1988a). To exclude the possibility that hyaluronan might interfere with the Blyscan Assay, the assay was performed on standard solutions of known quantities ($X_1$) of chondroitin sulphate mixed with large excess (more than 10 times) of hyaluronan. Up to a maximum of 100 μg of hyaluronan was tested. Comparison of the amount of chondroitin sulphate ($X_2$) measured by the assay with $X_1$ using paired

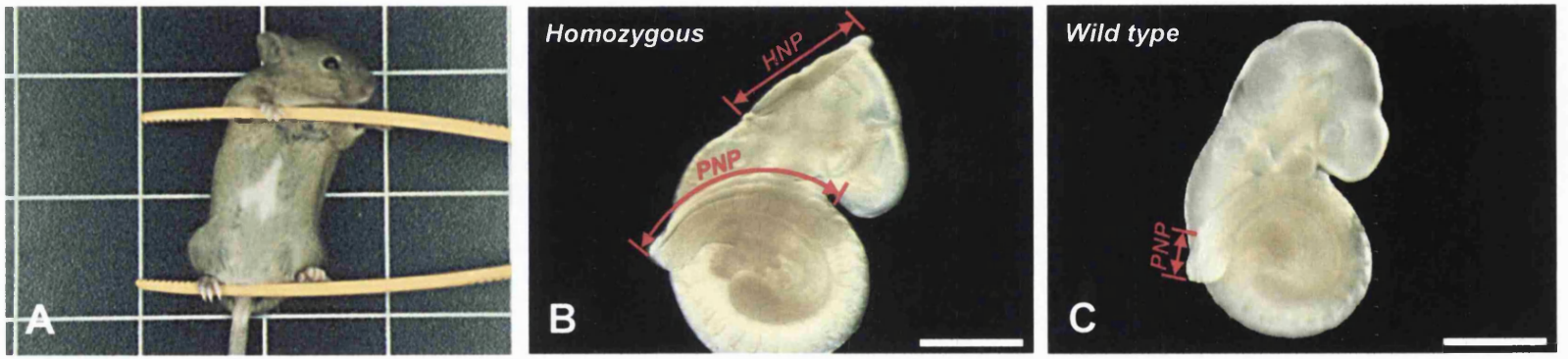


**Figure 7.2 The *splotch* ($Sp^{2H}$) mouse mutant.** (A) Heterozygous adult *splotch* mutant, illustrating the characteristic white belly spot. (B) Homozygous *splotch* mutant at E9.5, with widely separated neural folds both cranially and caudally. (C) Wild type littermate of the mutant embryo in (B). Abbreviations: HNP, hindbrain neuropore; PNP, posterior neuropore. Scale bar, 1 mm.

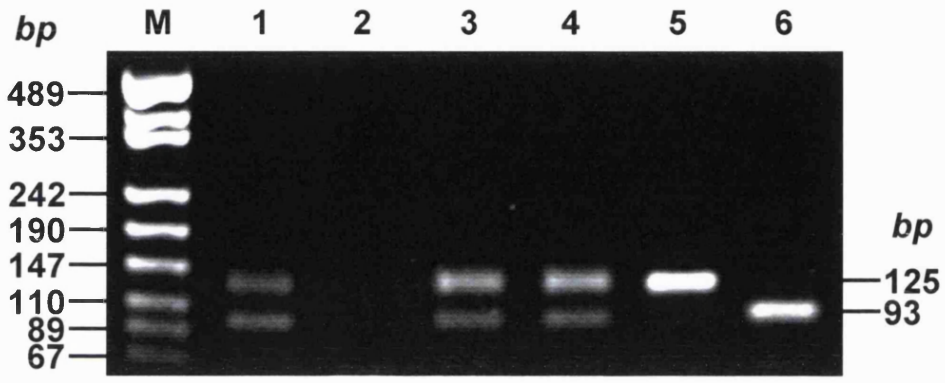


**Figure 7.3 Genotyping of *splotch* ($Sp^{2H}$) embryos using the polymerase chain reaction.** Lanes 1 and 2 show the positive and negative controls respectively. Lanes 3 and 4 (heterozygous embryos) each contains two bands of 93 and 125 base pairs. Lane 5 (wild type embryo) contains a single 125-base pair band. Lane 6 (homozygous embryo) contains a single 93-base pair band. The DNA sizing ladder is seen in Lane M.

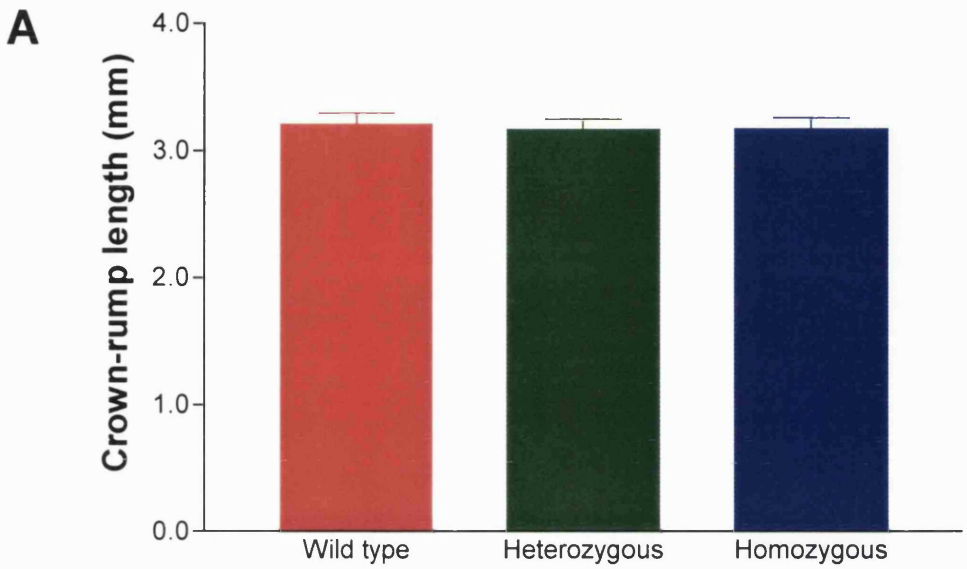
A
Crown-rump length (mm)
4.0
3.0
2.0
1.0
0.0
Wild type
Heterozygous
Homozygous

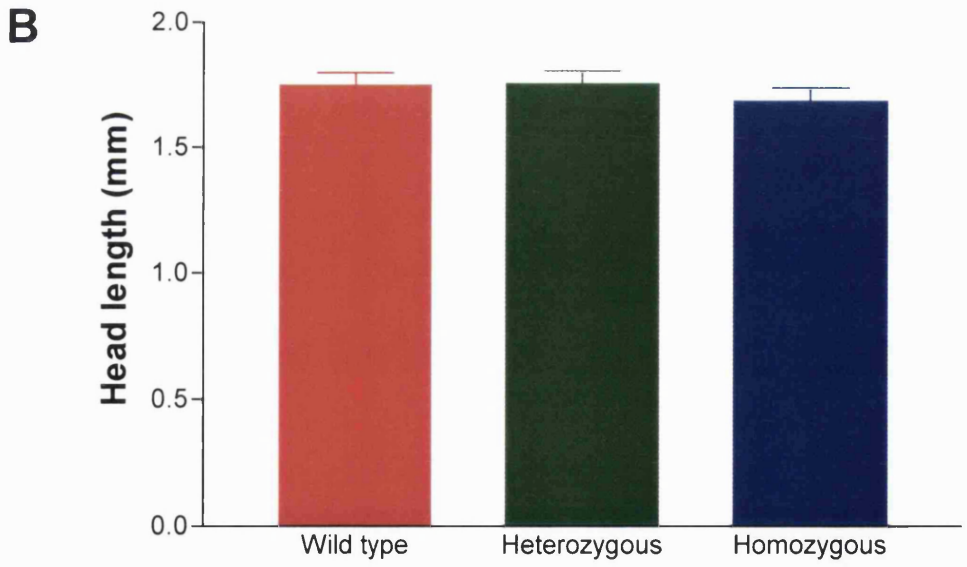
B
Head length (mm)
2.0
1.5
1.0
0.5
0.0
Wild type
Heterozygous
Homozygous

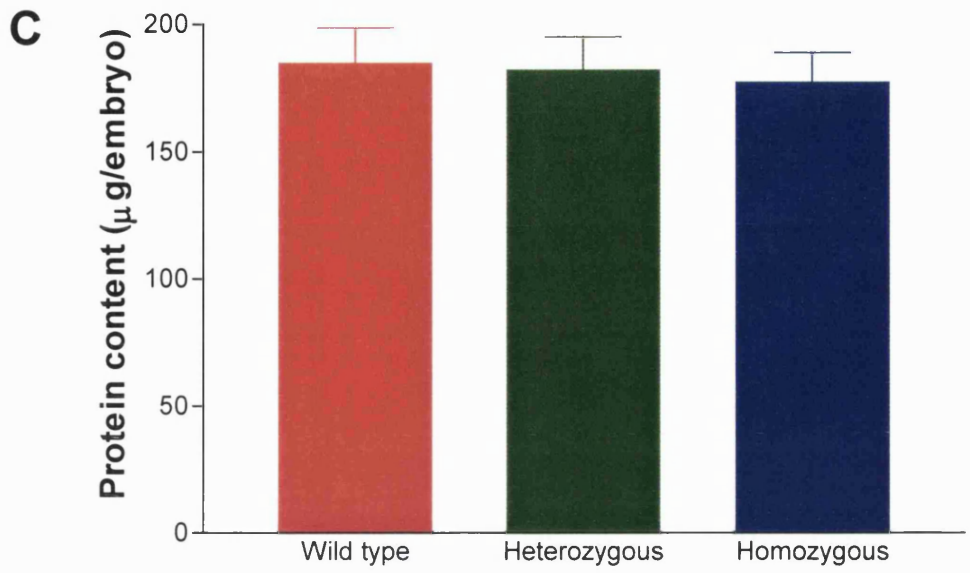


**Figure 7.4 Growth parameters of *splotch* ($Sp^{2H}$) mouse mutant embryos.** (A) shows the crown-rump length, (B) shows the head length, and (C) shows the protein content of *splotch* homozygous, heterozygous and wild type embryos. Statistical comparison using repeated measures ANOVA gives a $p$ value of 0.3365, 0.0089 and 0.1805 respectively. Dunnett's multiple comparison test shows that the head length of *splotch* homozygous embryos is significantly shorter than wild type embryos ($p < 0.05$). The head length of the heterozygous group is not significantly different from wild type embryos ($p > 0.05$). Line above each bar represents standard error. There are 32 embryos in each group.

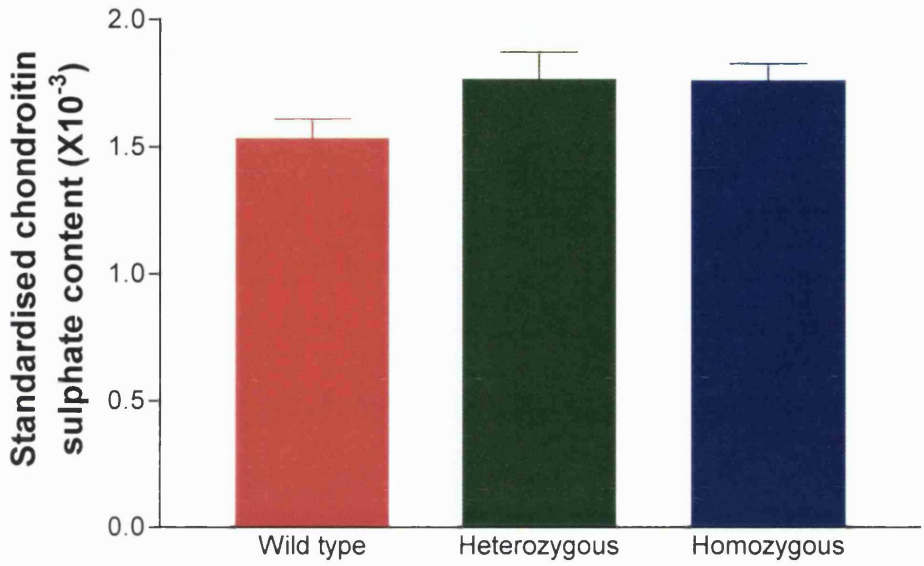


**Figure 7.5 Chondroitin sulphate content of *splotch* ($Sp^{2H}$) mutant embryos.** Statistical comparison of the chondroitin sulphate content, on a per microgram protein basis, among the three genotypes using repeated measures ANOVA gives a $p$ value of 0.0254. Dunnett's multiple comparison test shows that both homozygous and heterozygous embryos had larger amounts of chondroitin sulphate than wild type embryos ($p < 0.05$). Line above each bar represents standard error. There are 32 embryos in each group.

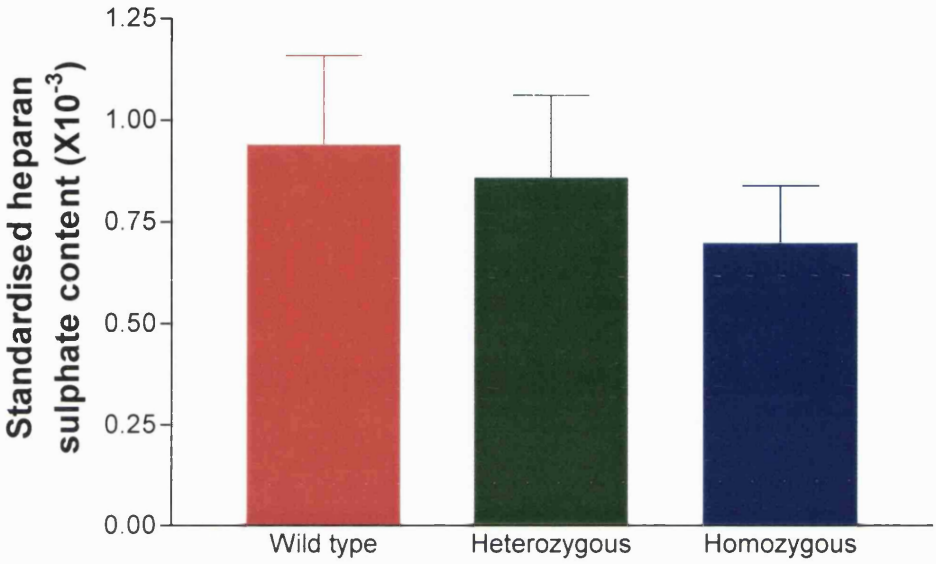


**Figure 7.6 Heparan sulphate content of *splotch* ($Sp^{2H}$) mutant embryos.** Statistical comparison of the heparan sulphate content, on a per microgram protein basis, among the three genotypes using repeated measures ANOVA gives a *p* value of 0.1006. Line above each bar represents standard error. There are 32 embryos in each group.

t-test showed no statistically significant difference ($p$ = 0.6888; $n$ = 3). $X_2/X_1$ gives a value of 1.02, showing that the presence of hyaluronan does not lead to significant over-estimation of the chondroitin sulphate content.

### 7.2.2 Comparison of net rate of synthesis of sulphated glycosaminoglycans

To compare the net rate of synthesis of sulphated glycosaminoglycans between the three genotypes, glycosaminoglycans were labelled by culturing embryos in the presence of $^{35}$S-sulphate for five hours, as described in Chapters 3 and 5. The $^{35}$S-labelled sulphated glycosaminoglycans were then separated into heparan sulphate (Peak HS) and chondroitin sulphate (Peak CS) using anion exchange chromatography (Figure 7.7). The peaks were identified based on their elution positions and confirmed with enzyme digestion assays using heparitinase and chondroitinase (Chapter 5). The amount of $^{35}$S-label incorporated into each glycosaminoglycan species was determined by calculating the area under each peak, as discussed in Appendix 1. This gives the net rate of synthesis of each glycosaminoglycan species, which is equal to the amount of glycosaminoglycan synthesised during the labelling period minus the amount degraded.

The anion exchange chromatography elution profiles of all three genotypes appear very similar to one another (Figure 7.7). Wild type embryo appeared to have a lower average net rate of chondroitin sulphate synthesis among the three genotypes on a per microgram

**Figure 7.7 Anion exchange chromatography of $^{35}$S-labelled glycosaminoglycans extracted from cultured *splotch* (*Sp$^{2H}$*) embryos.** Elution profiles of $^{35}$S-labelled sulphated glycosaminoglycans extracted from *splotch* homozygous (blue line), heterozygous (green line) and wild type (red line) embryos. Radioactivity level of each fraction has been normalised to the protein content of the embryo. The linearly increasing concentration of sodium chloride used for elution is shown by the brown line.

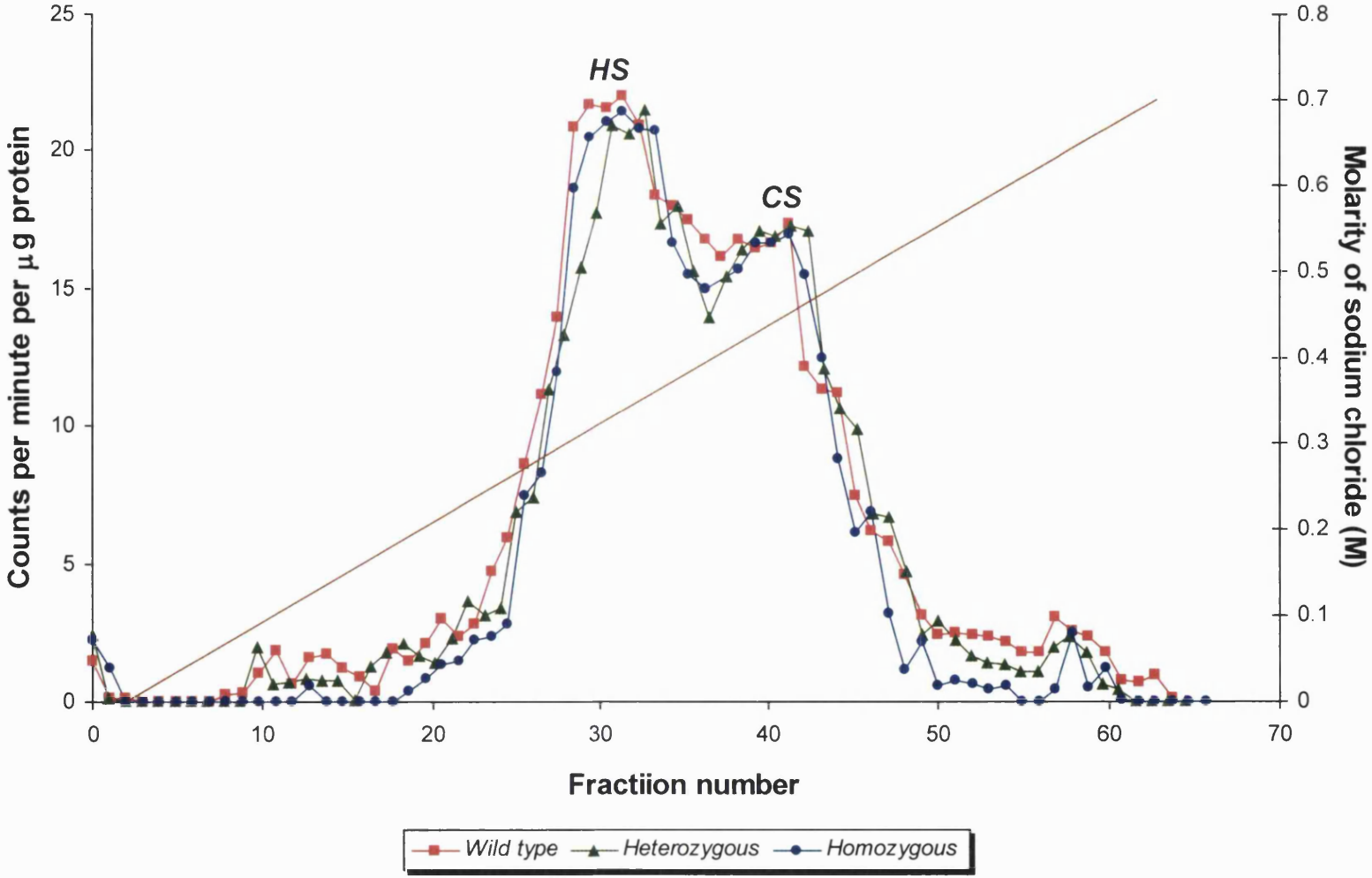
HS
CS
Counts per minute per µg protein
Molarity of sodium chloride (M)
Fractiion number
0
5
10
15
20
25
0
0.1
0.2
0.3
0.4
0.5
0.6
0.7
0.8
0
10
20
30
40
50
60
70
Wild type
Heterozygous
Homozygous

protein basis, although this difference was not statistically significant ($p$ = 0.6267; Figure 7.8). Similarly, comparison of the net rate of heparan sulphate synthesis showed no significant difference among the three groups ($p$ = 0.2886; Figure 7.9). However, homozygous *splotch* embryos synthesised a larger proportion of sulphated glycosaminoglycans as chondroitin sulphate than wild type embryos ($p$ = 0.0439; Figure 7.10). The heterozygous group synthesised an intermediate proportion of sulphated glycosaminoglycans as chondroitin sulphate. In terms of heparan sulphate, a larger proportion of sulphated glycosaminoglycans was synthesised as heparan sulphate in wild type embryos than in homozygous embryos (Figure 7.11).

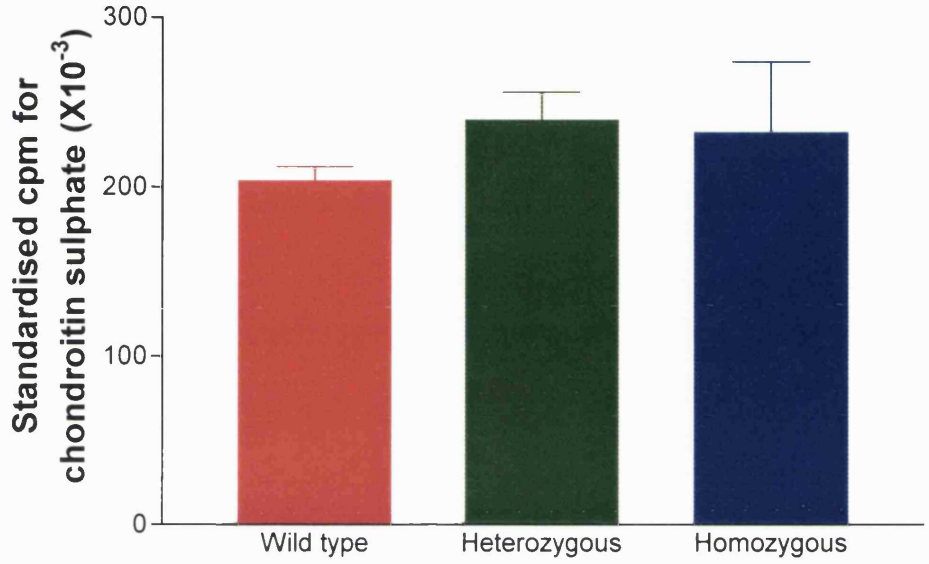


**Figure 7.8 Net rate of chondroitin sulphate synthesis in *splotch* ($Sp^{2H}$) embryos.** Statistical comparison of the net rate of chondroitin sulphate synthesis, on a per microgram protein basis, among the three genotypes using repeated measures ANOVA gives a *p* value of 0.6267. Line above each bar represents standard error. Comparison based on data obtained from 12 independent elution profiles. Abbreviation: cpm, counts per minute.

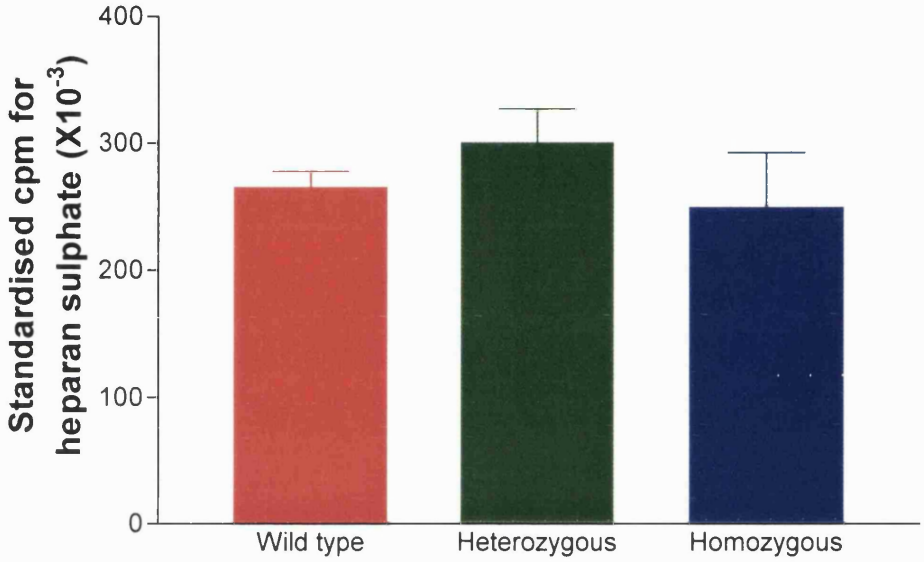


**Figure 7.9 Net rate of heparan sulphate synthesis in *splotch* (*Sp*$^{2H}$) embryos.** Statistical comparison of the net rate of heparan sulphate synthesis, on a per microgram protein basis, among the three genotypes using repeated measures ANOVA gives a *p* value of 0.2886. Line above each bar represents standard error. Comparison based on data obtained from 12 independent elution profiles. Abbreviation: cpm, counts per minute.

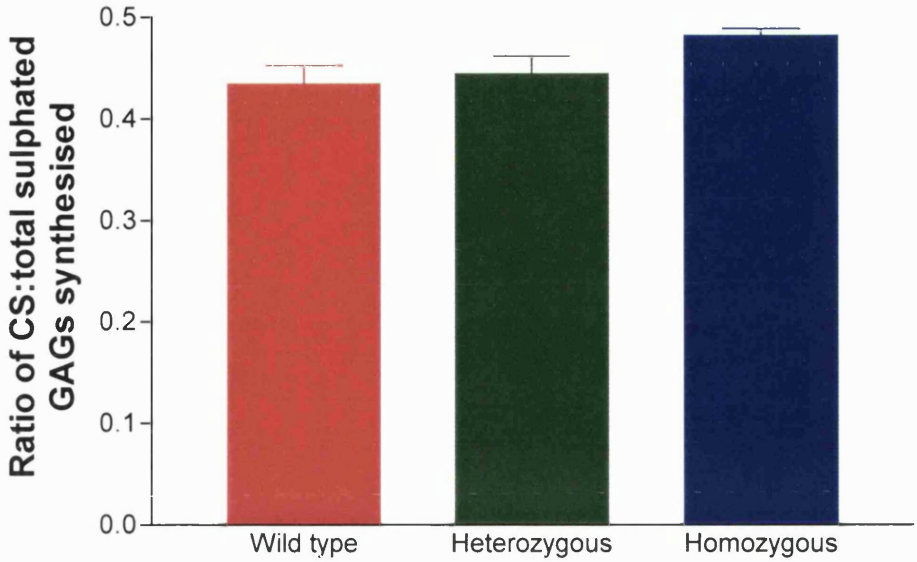


**Figure 7.10 Ratio of chondroitin sulphate:total sulphated glycosaminoglycans synthesised in *splotch* ($Sp^{2H}$) embryos.** Statistical comparison of the proportion of sulphated glycosaminoglycans synthesised as chondroitin sulphate among the three genotypes using repeated measures ANOVA gives a $p$ value of 0.0439. Dunnett's multiple comparison test shows that homozygous embryos synthesised more of its sulphated glycosaminoglycans as chondroitin sulphate than wild type embryos ($p < 0.05$). There is no statistically significant difference between heterozygous and wild type embryos. Line above each bar represents standard error. Comparison based on data obtained from 12 independent elution profiles. Abbreviations: CS, chondroitin sulphate; GAGs, glycosaminoglycans.

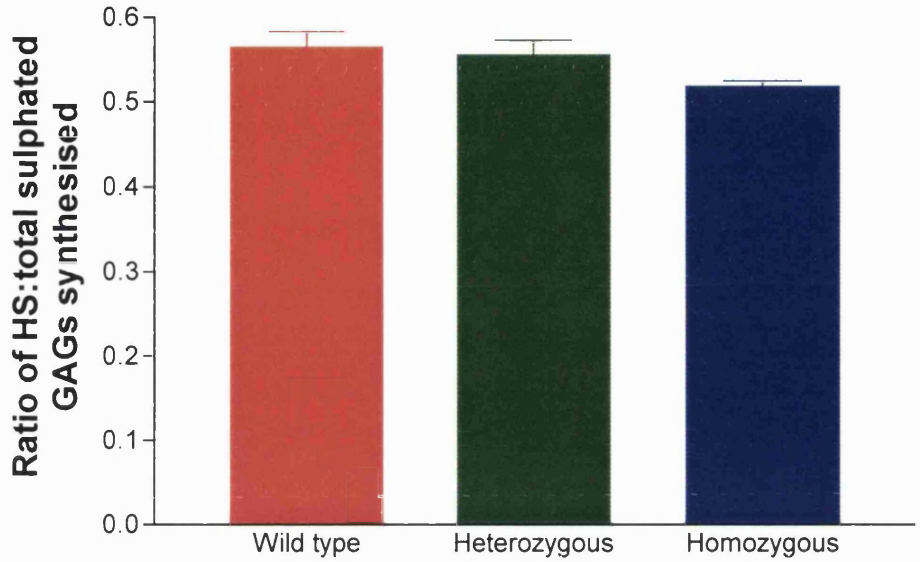


**Figure 7.11 Ratio of heparan sulphate:total sulphated glycosaminoglycans synthesised in *splotch* ($Sp^{2H}$) embryos.** Statistical comparison of the proportion of sulphated glycosaminoglycans synthesised as heparan sulphate among the three genotypes using repeated measures ANOVA gives a *p* value of 0.0439. Dunnett's multiple comparison test shows that the homozygous group synthesised less of its sulphated glycosaminoglycans as heparan sulphate than wild type embryos ($p < 0.05$). There is no statistically significant difference between heterozygous and wild type embryos. Line above each bar represents standard error. Comparison based on data obtained from 12 independent elution profiles. Abbreviations: GAGs, glycosaminoglycans; HS, heparan sulphate.

## 7.3 Discussion

This chapter has quantified the sulphated glycosaminoglycan content in the *splotch* ($Sp^{2H}$) mouse mutant at the stage of posterior neuropore closure. Homozygous and heterozygous embryos were found to contain significantly more chondroitin sulphate than wild type embryos. In contrast, wild type embryos appeared to have more heparan sulphate, although this was not statistically significant. Although no difference in the net rate of synthesis of these two glycosaminoglycans was detected among the three genotypes, homozygous embryos were found to synthesise proportionately more of its sulphated glycosaminoglycans as chondroitin sulphate than wild type embryos. On the other hand, more of the sulphated glycosaminoglycans were synthesised as heparan sulphate in wild type embryos.

### *7.3.1 Chondroitin sulphate proteoglycans and neural crest migration in the splotch mouse mutant*

Chondroitin sulphate proteoglycans have been suggested to act as non-permissive molecules to neural crest migration (Oakley and Tosney, 1991; Oakley et al, 1994; Pettway et al, 1996; Henderson and Copp, 1997). They are found in tissues avoided by migrating neural crest cells, and might help to set up barriers to neural crest migration (Perris et al, 1991b; Oakley et al, 1994). *In vitro*, chondroitin sulphate proteoglycans do not support the attachment and spreading of neural crest cells, and counteract the migration-promoting activities of other

matrix components (Newgreen et al, 1986; Landolt et al, 1995; Perris et al, 1996; Ring et al, 1996; Kerr and Newgreen, 1997). These effects have been attributed to the chondroitin sulphate chains, and are abolished after chondroitinase treatment. *In vivo*, disruption of neural crest migration has been reported after ectopic implantation of chondroitin sulphate or inhibition of chondroitin sulphate proteoglycan synthesis (Pettway et al, 1990; Kubota et al, 1999; Perissinotto et al, 2000). Thus, increased chondroitin sulphate content in the *splotch* mutant could contribute to the lack of neural crest derivatives by inhibiting neural crest migration. Indeed, localised clumps of neural crest cells have been reported to lie adjacent to the neural tube in mutant embryos, suggesting that these cells are able to emigrate from the neural tube but are unable to migrate through the abnormal extracellular environment (Henderson et al, 1997).

Although increased transcription of the gene encoding the chondroitin sulphate proteoglycan *versican* is found in the *splotch* mutant embryo (Henderson et al, 1997), it is possible that over-expression of this proteoglycan does not solely account for the higher chondroitin sulphate content. Indeed, the increase in chondroitin sulphate in the mutant embryo has been reported to be mainly localised to the neuroepithelial basement membrane by immunohistochemistry (Trasler and Morriss-Kay, 1991), whereas the increase in *versican* transcripts are not restricted to cells abutting the neuroepithelial basement membrane (Henderson et al, 1997). It remains to be determined if other basement membrane chondroitin sulphate proteoglycans, such as bamacan, are also over-expressed.

Recent studies have suggested that versican might not be non-permissive to neural crest migration (Perris and Perissinotto, 2000; Perissinotto et al, 2000). Three-dimensional reconstruction of versican distribution in the avian embryo shows that migrating neural crest cells travel from regions that are relatively scarce in versican towards regions that are richer in this proteoglycan. *In vitro*, neural crest cells migrate along an increasing concentration of versican. It is unclear if the cells are attracted to the chondroitin sulphate chains or the core protein of versican. However, rather than refuting the hypothesis that lack of neural crest derivatives in the *splotch* mutant might be due to inhibition of neural crest migration by over-expression of chondroitin sulphate, these studies might offer an additional explanation for this lack of migration. Increased versican transcripts have been reported in the migratory pathway of neural crest cells (Henderson et al, 1997). This could disrupt the normal increasing versican concentration gradient along which neural crest cells migrate. Indeed, it has been found that neural crest cell migration is severely impeded when exposed to a decreasing concentration gradient of versican (Perissinotto et al, 2000).

To summarise, over-expression of versican and possibly other chondroitin sulphate proteoglycans might inhibit neural crest cell migration in the *splotch* mutant by providing excessive non-permissive molecules in the extracellular environment, and by setting up a decreasing concentration gradient of versican along the normal migratory route. However, inhibition of neural crest migration by over-expression of chondroitin sulphate is probably not solely responsible for the lack of neural crest derivatives. A similar increase in chondroitin sulphate content was detected in both homozygous and heterozygous *splotch* mutants, but homozygous embryos suffer from a more severe

lack of neural crest derivatives than do heterozygous embryos. It has been suggested that decreased neural crest stem cell expansion might contribute to the neural crest defects seen in the *splotch* mutant (Conway et al, 2000). In addition, over-expression of *Pax-3* in neural crest cells on a *splotch* background has been shown to rescue the neural crest-related defects (Li et al, 1999). This is suggestive of a cell-autonomous defect in neural crest function in *splotch*, which is independent of environmentally-determined defects.

### 7.3.2 Metabolism of sulphated glycosaminoglycans in the splotch mouse mutant

The present study has shown that the *splotch* mutant over-expresses chondroitin sulphate, and synthesises more of its sulphated glycosaminoglycans as chondroitin sulphate than heparan sulphate. However, no difference in the net rate of chondroitin sulphate synthesis was detected among the three genotypes. One possible explanation could be that the higher chondroitin sulphate content is due to gradual accumulation of the glycosaminoglycan over time. The rate of chondroitin sulphate synthesis in the *splotch* mutant might only be slightly higher than in wild type embryo, and this was not detected in the present study due to the relatively short $^{35}$S-labelling period. Indeed, when sulphation of glycosaminoglycans was inhibited by chlorate treatment of cultured embryos, immunostaining for chondroitin sulphate was greatly reduced in the neuroepithelial and surface ectodermal basement membrane but less so in the underlying mesoderm (Figure 5.22). This suggests that not all the chondroitin sulphate synthesised

before chlorate treatment was degraded during the culture period and that some of the previously synthesised chondroitin sulphate was retained by the embryo.

A second possible explanation for the apparent lack of difference in the net rate of chondroitin sulphate synthesis could be that the chondroitin sulphate synthesised by the *splotch* mutant is under-sulphated. Since the radiolabel used in the present study was $^{35}$S-sulphate, this might not detect over-production of under-sulphated chondroitin sulphate. Indeed, it has been suggested that availability of the sulphate donor, 3'-phosphoadenosine 5'-phosphosulphate, is a limiting condition in the sulphation of glycosaminoglycans during biosynthesis (Conrad, 1998). One difference between heparan sulphate and heparin is that there are many more sulphate groups in heparin (Conrad, 1998; Varki et al, 1999). However, microsomal extracts from mastocytoma cells (which normally produce heparin) and from hepatoma cells (which produce heparan sulphate) both synthesise heparin-like products *in vitro*, where there is an excess of sulphate donor (Conrad, 1998). Thus, over-production of chondroitin sulphate in the *splotch* mutant might lead to an increase in demand for 3'-phosphoadenosine 5'-phosphosulphate that exceeds the available supply, leading to synthesis of under-sulphated chondroitin sulphate. This could further contribute to inhibition of neural crest migration, as partially sulphated chondroitin sulphate retards migration more effectively than does fully sulphated chondroitin sulphate (Newgreen et al, 1982).

A third possibility could be that the higher chondroitin sulphate content in the *splotch* mutant is due to a lower rate of chondroitin sulphate degradation compared with wild type embryos. Although this possibility

cannot be excluded based on the current study, it does not explain the greater proportion of sulphated glycosaminoglycans synthesised as chondroitin sulphate in the *splotch* mutant. In addition, neural tube defects and absence of neural crest derivatives are not associated with mucopolysaccharidoses, a group of inherited human disorders where glycosaminoglycans (including chondroitin sulphate) abnormally accumulate owing to deficiencies in certain lysosomal enzymes needed for degradation of these molecules (Varki et al, 1999).

It is interesting to note that this study, which uses 1,9-dimethylmethylene blue to detect sulphated glycosaminoglycans, found no significant difference in heparan sulphate content among the three genotypes. In contrast, previous studies have reported higher heparan sulphate proteoglycan content using an antibody against the proteoglycan molecule (O'Shea and Liu, 1987; Trasler and Morriss-Kay, 1991). This apparent conflict in findings could be explained on the basis of the different detection methods used and the cellular regulation of proteoglycan biosynthesis. Firstly, glycosaminoglycans are attached to proteoglycan core proteins through a tetrasaccharide linkage region during biosynthesis (Conrad, 1998; Prydz and Dalen, 2000). The same set of enzymes is used for synthesis of this linkage region for both heparan sulphate and chondroitin sulphate proteoglycans (Esko et al, 1985; Esko et al, 1987). Mutant Chinese hamster ovary cells lacking enzymes involved in the production of this linkage region are unable to synthesise both heparan sulphate and chondroitin sulphate. It appears that heparan sulphate and chondroitin sulphate might compete with each other for these enzymes during synthesis of the respective proteoglycans. Mutant cells that are deficient for heparan sulphate copolymerase (encoded by *EXT1*/*EXT2*), which catalyses elongation of

the heparan sulphate chain, have been shown to synthesise excess chondroitin sulphate (Lin et al, 2000). Transfection of these cells with mouse *EXT1* cDNA enables the cells to synthesise heparan sulphate, and this is accompanied by a fall in chondroitin sulphate production (Wei et al, 2000). Secondly, cells appear to regulate heparan sulphate content by changing the amount of proteoglycan core protein produced (Langford et al, 1998). Syndecans have three glycosaminoglycan attachment sites in the extracellular domain of the core protein. Deletion of one, and even two, of these attachment sites does not lead to a substantial drop in the amount of heparan sulphate associated with the cell. This is achieved by increased synthesis of the proteoglycan core protein, thus maintaining the total heparan sulphate content at a relatively constant level at the expense of higher core protein production (Langford et al, 1998). Taken together, it is hypothesised that in the *splotch* mutant, increased chondroitin sulphate synthesis predisposes the embryo to produce less heparan sulphate (Figures 7.6 and 7.11). However, this is opposed by increased production of heparan sulphate proteoglycan core protein, as reflected by the higher immunostaining intensity using an anti-heparan sulphate proteoglycan antibody (O'Shea and Liu, 1987; Trasler and Morriss-Kay, 1991).

### *7.3.3 Sulphated glycosaminoglycans and neural tube defects in the splotch mouse mutant*

Both cranial and caudal neural tube defects are seen in the *splotch* mouse mutant. Although chondroitin sulphate has been shown to regulate neural tube closure (Morriss-Kay and Tuckett, 1989b; Chapter

6), it seems unlikely that these neural tube defects are directly caused by over-expression of chondroitin sulphate. Exposure of mouse embryos to exogenous chondroitin sulphate in culture resulted in premature closure of the posterior neuropore and does not inhibit cranial neural tube closure (Chapter 6). On the other hand, degradation of chondroitin sulphate by chondroitinase treatment retarded both cranial and caudal neural tube closure (Morriss-Kay and Tuckett, 1989b; Chapter 6). Thus, in the *splotch* mutant, the increase in chondroitin sulphate content would have been expected to accelerate neurulation rather than lead to neural tube defects.

On the other hand, heparan sulphate appears to be essential for neurulation. Degradation of heparan suiphate by heparitinase treatment and disruption of heparan sulphate proteoglycan biosynthesis have both been shown to result in cranial neural tube defects (Morriss-Kay and Crutch, 1982; Tuckett and Morriss-Kay, 1989a; Kubota et al, 1999). Although no statistically significant decrease in heparan sulphate content was detected in the *splotch* mutant compared with wild type embryo in the present study, the mutant was shown to produce less of its sulphated glycosaminoglycans as heparan sulphate. As hypothesised above, the relatively unchanged heparan sulphate content could have been due to over-production of heparan sulphate proteoglycan core proteins. If this hypothesis were true, this would imply a reduction in the number of heparan sulphate chains per core protein molecule, which might disrupt the normal biological activity of heparan sulphate proteoglycans and contribute to defective cranial neural tube closure. Indeed, changes in the number of heparan sulphate chains attached to the syndecan core protein have been shown to affect the biological function of the proteoglycan, despite

maintenance of the total amount of cell surface heparan sulphate (Langford et al, 1998). Syndecan-1 on ARH-77 cells (human B lymphoid cells) mediates cell-cell and cell-matrix adhesion and inhibits cell invasion into collagen gels. Deletion of one (or even two) of the glycosaminoglycan attachment sites on the syndecan core protein did not lead to a significant reduction in the total amount of cell surface heparan sulphate, owing to compensatory over-production of the core protein. However, despite maintenance of a relatively unchanged total amount of heparan sulphate, the biological activity of the syndecan molecule was affected by the decrease in number of heparan sulphate chains per core protein (Langford et al, 1998).

Deficiency of normal heparan sulphate species is unlikely to be directly responsible for the occurrence of spina bifida in the *splotch* mouse mutant. Closure of the spinal neural tube was not inhibited after degradation of heparan sulphate by heparitinase treatment of cultured rat embryos (Tuckett and Morriss-Kay, 1989a). Furthermore, inhibiting sulphation of heparan sulphate resulted in premature posterior neuropore closure (Chapter 5). However, it is not known whether heparan sulphate synthesised by the *splotch* mutant has a normal structure. As postulated above, heparan sulphate proteoglycans produced by these mutants might have fewer heparan sulphate chains per core protein molecule. It has been suggested that the fine structure of heparan sulphate is partly dependent on competition between heparan sulphate chains for the available modification enzymes (such as sulphotransferases, deacetylases and epimerases) in a cell (Conrad, 1998). Thus, it is possible that the fine structure of heparan sulphate chains in *splotch* mutants is different from that seen in wild type embryos. Although highly speculative, this would imply that spina bifida

in the mutants is not directly due to a lack of normal heparan sulphate species, but rather it might be partly contributed by the presence of abnormal, biologically active heparan sulphate species that is not synthesised by wild type embryos. It would be interesting to determine the sequence of heparan sulphate extracted from *splotch* mutant embryos and to see if the incidence of spina bifida could be reduced by heparitinase treatment of cultured *splotch* embryos.

# *Chapter 8*

# CONCLUSION

## 8.1 Introduction

This thesis has studied the roles played by the sulphated glycosaminoglycans, heparan sulphate and chondroitin sulphate, in neurulation and neural crest migration. Both molecules are found to be present in the posterior neuropore region at the time of spinal neurulation (Chapter 4). Heparan sulphate and chondroitin sulphate are involved in regulating the speed and mechanism of posterior neuropore closure (Chapters 5 and 6). In heparan sulphate, this regulatory activity appears to depend on sulphation of the glycosaminoglycan molecule. In addition, it is found that *splotch* ($Sp^{2H}$) mutant embryos have a higher chondroitin sulphate content than wild type embryos (Chapter 7). This is accompanied by an increase in the proportion of sulphated glycosaminoglycans synthesised as chondroitin sulphate, and hence relatively less as heparan sulphate. The findings support the hypothesis that over-abundance of chondroitin sulphate could be partly responsible for the deficiency of neural crest derivatives in the *splotch* mouse mutant, and suggest the possibility that qualitative and/or quantitative changes in the sulphated glycosaminoglycans might contribute to the neurulation defects.

## 8.2 Heterogeneity of sulphated glycosaminoglycans

Sulphated glycosaminoglycans, such as heparan sulphate and chondroitin sulphate, are not a homogenous group of molecules. The basic structure of these molecules is relatively simple, consisting of

alternate repeats of a hexosamine and a hexuronic acid (Varki et al, 1999). However, modifications to the basic glycosaminoglycan chain, such as sulphation, acetylation and epimerisation, generate a diverse range of fine structures that possesses different biological activities. For example, heparan sulphate binds to and is capable of potentiating the activity of fibroblast growth factors in general. However, changes in the sulphation pattern of heparan sulphate switches this potentiating activity between different members of the fibroblast growth factor family (Nurcombe et al, 1993; Brickman et al, 1998). Heparan sulphate species that inhibit the activity of fibroblast growth factors have also been described (Delehedde et al, 1996). This thesis has shown that both N- and O-sulphation of heparan sulphate are required for regulating posterior neuropore closure. *In vivo*, absence of 2-O-sulphated heparan sulphate results in renal, eye and skeletal abnormalities whereas the inability to add N-sulphate groups to heparan sulphate results in respiratory distress syndrome (Bullock et al, 1998; Ringvall et al, 2000; Fan et al, 2000). Thus, using a similar argument that not all proteins are alike, it appears that one should not consider that all heparan sulphate or chondroitin sulphate molecules are the same. Instead, it is essential to obtain information on individual sequences and fine structural modifications of sulphated glycosaminoglycans in different biological processes.

Sulphated glycosaminoglycans are synthesised on proteoglycan core proteins. Thus, besides considering the biological actions of different modifications in glycosaminoglycan structure, it may be necessary to examine the various proteoglycan core proteins together with differences in the number and types of attached glycosaminoglycan chains. The glycosaminoglycan chain and core protein could act

synergistically in binding and mediating the biological effects of signalling molecules (Herndon et al, 1999). For example, the number of heparan sulphate chains attached to the syndecan-1 core protein and the sites of linkage influence the ability of this proteoglycan to prevent cultured cells from invading an underlying collagen gel (Langford et al, 1998). The binding of fibroblast growth factor-2 to chondroitin sulphate proteoglycans appears to be dependent on both the glycosaminoglycan chain and the core protein (Milev et al, 1998). Indeed, the presence of cytoplasmic domains in cell surface-associated proteoglycans can help to mediate the biological activity of signalling molecules after they are bound to the proteoglycans (Bernfield et al, 1999; Volk et al, 1999). Furthermore, sulphated glycosaminoglycans appear to influence the localisation of cell surface-associated proteoglycans in polarised cells, thus helping to determine the biological function of the proteoglycans (Mertens et al, 1996; Kolset et al, 1999).

The experiments in Chapter 5 have focussed on the function of the sulphate group in glycosaminoglycans by inhibiting sulphation of these molecules using chlorate treatment. These experiments could be adapted to investigate the role of intact proteoglycans by blocking the attachment of sulphated glycosaminoglycan chains to the core protein backbone. A useful chemical for these experiments is β-D-xyloside. β-D-xyloside acts an a xylose substitute in the attachment of glycosaminoglycan chains to the linkage region of proteoglycans, resulting in the synthesis of core proteins without attached glycosaminoglycans together with free glycosaminoglycan chains that are not linked to core protein molecules (Schwartz, 1977; Conrad, 1998). Chemicals that can affect the ratio of heparan sulphate:chondroitin sulphate synthesised by cells have also been

described (Timár et al, 1995). These chemicals would be useful in determining whether a change in the ratio of heparan sulphate:chondroitin sulphate synthesised could lead to the neurulation defects seen in the *splotch* mouse mutant. Labelling of synthesised glycosaminoglycans with $^{3}$H-glucosamine would allow additional analysis of glycosaminoglycan structures to be made.

## 8.3 Sulphated glycosaminoglycans and human pathology

Since sulphated glycosaminoglycans are involved in neurulation, perturbations in the amount of these molecules might be seen in patients with neural tube defects. However, neural tube defects are not associated with mucopolysaccharidoses, in which sulphated glycosaminoglycans accumulate due to congenital deficiencies of lysosomal enzymes needed for glycosaminoglycan degradation (Varki et al, 1999). Abnormal accumulation of heparan sulphate is seen in patients with Sanfilippo syndrome as well as in the mouse model for this disease (Bhaumik et al, 1999). The inability to degrade heparan sulphate leads to accumulation of this molecule in the body, resulting in mental deterioration and hyperactivity but relatively mild somatic manifestations such as coarse facies and hirsutism. Accumulation of chondroitin sulphate and keratan sulphate is seen in Morquio syndrome in which a deficiency of galactose-6-sulphatase leads to skeletal abnormalities, odontoid hypoplasia and corneal clouding. The absence of neural tube defects in all these patients agrees with the *in vitro* finding that exogenous chondroitin sulphate accelerates posterior neuropore

closure and does not inhibit cranial neurulation (Morriss-Kay and Tuckett, 1989b; Chapter 6).

Human diseases in which sulphated glycosaminoglycan biosynthesis is perturbed have also not been associated with neural tube defects. Mutations of the *GPC3* gene, which codes for glypican-3, leads to the overgrowth and tumour susceptibility syndrome, Simpson-Golabi-Behmel dysmorphia, where affected patients have tissue overgrowth and predisposition to Wilm's tumour and neuroblastomas (Pilia et al, 1996). Mutations of the *EXT1* gene, which codes for heparan sulphate copolymerase, are seen in hereditary multiple exostoses where patients have cartilage-capped exostoses, short stature and an increased risk for chondrosarcoma and osteosarcoma (Ahn et al, 1995; Wicklund et al, 1995). Reduction in heparan sulphate has also been reported in paediatric cases of protein losing enteropathy (Murch et al, 1996). In contrast, *in vitro* studies have suggested that heparan sulphate is essential for cranial neurulation (Morriss-Kay and Crutch, 1982; Tuckett and Morriss-Kay, 1989a). A possible explanation for this apparent conflict could be that heparan sulphate is essential for embryonic development and thus mutations in which heparan sulphate biosynthesis is adversely affected result in abortion of the foetus. Indeed, homozygous mouse embryos that are deficient in EXT1 have gastrulation defects, die by E8.5 and are resorbed (Lin et al, 2000).

Waardenburg syndrome is an autosomal dominant mutation and a major cause of human sensorineural deafness (Tassabehji et al, 1994; Asher et al, 1996). These patients have mutations in the *PAX-3* gene and, like the *splotch* mouse mutant, they have pigmentation defects of the hair, skin and eyes. Hirschsprung disease is seen in patients with

Type IV Waardenburg syndrome, where an absence of intestinal ganglia leads to aganglionic megacolon. Spina bifida is also associated with the syndrome. However, it is not known whether affected patients have an abnormal sulphated glycosaminoglycan content.

## 8.4 Future work

This thesis has shown that the sulphated glycosaminoglycans are involved in neurulation and neural crest migration. It has also raised several interesting questions, some of which have been discussed above and in the previous chapters. A major area of interest is to investigate qualitative and quantitative changes in the fine structure of sulphated glycosaminoglycans during neurulation and neural crest migration, to ascertain whether there is a correlation between these changes and the developmental processes. This analysis might reveal differences in heparan sulphate and/or chondroitin sulphate sequences and fine structures between the different modes of neurulation, or between cranial and spinal neurulation, that might help to unravel the developmental mechanisms involved in these processes. Precedence for such a change has been reported where a correlation was found between neuronal proliferation and differentiation and the fine structure of heparan sulphate (Nurcombe et al, 1993; Brickman et al, 1998).

One approach to this problem is to make use of a series of antibodies that recognises a variety of epitopes on heparan sulphate and chondroitin sulphate. As mentioned above, heparan sulphate and chondroitin sulphate are heterogeneous groups of molecules. It has been discussed in Chapter 4 that the use of, say, a single antibody to heparan sulphate does not allow detection or localisation of all heparan

sulphate species present in a tissue. Indeed, by using phage display technology, a series of anti-heparan sulphate antibodies have been generated (van Kuppevelt et al, 1998). Each of these antibodies shows a characteristic staining pattern in the kidney and skeletal muscle basal lamina, suggesting that heparan sulphate sequences and fine structures might be regulated and that these sequences might play different biological roles (van Kuppevelt et al, 1998; Jenniskens et al, 2000). Heterogeneity of chondroitin sulphate has also been discovered in the embryonic chick heart using a series of different anti-chondroitin sulphate antibodies (Capehart et al, 1999). A disadvantage to this approach is that the epitopes recognised by many of these antibodies have not been fully characterised yet, although this is likely to change in the future.

A complementary approach is to extract the sulphated glycosaminoglycans from the region of interest, say the posterior neuropore region, and analyse the sequence of these molecules. In the past, this would involve the use of mass spectroscopy or nuclear magnetic resonance (Turnbull et al, 1999). Although these provide accurate sequence information, they require specialist experience and equipment and, in some cases, large amounts of material (nanomolar to micromolar quantities). The recent development of relatively simple sequencing techniques is likely to simplify this task (Turnbull et al, 1999; Vivès et al, 1999; Vivès et al, 2001). One such method, called integral glycan sequencing, involves the attachment of a reducing-end fluorescent tag to the glycosaminoglycan to establish a reading frame. The glycosaminoglycan is then chemically cleaved into fragments of various sizes. These fragments are degraded with exosulphatases and exoglycosidases to selectively remove specific sulphate groups and

monosaccharide residues from the non-reducing end. Separation of the products by polyacrylamide gel electrophoresis allows the sequence of the glycosaminoglycan to be read directly.

A third approach is to examine the expression patterns of the various heparan sulphate and chondroitin sulphate biosynthetic enzymes by *in situ* hybridisation and immunohistochemistry, to ascertain if there are changes at different developmental stages. Although the expression patterns of these enzymes do not provide direct evidence for changes in the expression of the various glycosaminoglycans, they do give an idea of the different chain modifications that can potentially take place. It is currently thought that the spatiotemporally regulated expression of different isoforms of these enzymes contributes to the final structures of glycosaminoglycans synthesised by a tissue (Conrad, 1998; Bernfield et al, 1999; Habuchi, 2000).

The possible occurrence of neurulation and neural crest migratory defects in mouse mutants that are defective in glycosaminoglycan synthesis could be investigated. Such an approach can be used for mutants, such as the *Hs2st* and the *Ndst1* mutants, that survive past the stage of neurulation and neural crest migration (Bullock et al, 1998; Ringvall et al, 2000; Fan et al, 2000). Mutants that die before neurulation occurs, such as the *EXT1*$^{-/-}$ mouse embryos (Lin et al, 2000), are not informative, but this problem might be circumvented by generating knockdowns, conditional knockouts or chimaeras with wild type cells. One advantage of using mutants over chemicals that perturb glycosaminoglycan synthesis (such as chlorate and β-D-xyloside) is the avoidance of unwanted side effects of the drugs. However, these chemicals might produce neurulation and/or neural crest abnormalities

that might not be seen in the mutants owing to the presence of multiple enzyme isoforms involved in glycosaminoglycan biosynthesis that might be able to compensate for each other.

A large number of biologically active molecules are known that are capable of binding to proteoglycans (Conrad, 1998; Bernfield et al, 1999; Oohira et al, 2000). However, very few of the binding sequences on the glycosaminoglycan chains are known (Habuchi et al, 1992; Turnbull et al, 1992). Although knowledge of glycosaminoglycan sequences and fine structures will allow better definition of the requirement for these molecules in neurulation and neural crest migration, such knowledge does not currently enable one to tell which signalling molecule is able to bind to a specific glycosaminoglycan sequence. Until more is known about the binding motifs on glycosaminoglycans and the signalling molecules to which they bind, it is not possible to directly infer from the presence of a specific glycosaminoglycan sequence that a particular signalling molecule is involved in a developmental process.

A different angle of investigation into the function of glycosaminoglycans in neurulation and neural crest migration is to examine the effects on glycosaminoglycans after perturbation of other bioactive molecules. For example, the spinal neuroepithelium is buckled in mouse embryos treated with cytochalasin D (Ybot-Gonzalez and Copp, 1999). Buckling is also seen after inhibition of sulphation of heparan sulphate (Chapter 5). Thus, it would be interesting to see if heparan sulphate is affected (indirectly) by cytochalasin D treatment, and vice versa. A similar examination could be made of the *shroom* mouse mutant, since Shroom is a PDZ domain-containing actin-binding protein, and the

syndecan family of heparan sulphate proteoglycans is able to bind to PDZ proteins (Grootjans et al, 1997; Hildebrand and Soriano, 1999). In the *splotch* mutant, it is found that the neurulation defects and the absence of neural crest derivatives are associated with an over-abundance of chondroitin sulphate and that proportionately more sulphated glycosaminoglycans are synthesised as chondroitin sulphate rather than as heparan sulphate (Trasler and Morriss-Kay, 1991; Henderson et al, 1997; Chapter 7). However, such an association does not necessarily imply causation. Chondroitin sulphate is more likely to be the cause of the deficiency of neural crest derivatives if it can be shown that decreasing the amount of chondroitin sulphate to a normal level is able to correct the deficiency. In addition, it would be interesting to see whether folate treatment, which reduces the incidence of neural tube defects in the *splotch* mutant, has an effect on glycosaminoglycans (Fleming and Copp, 1998).

# *Appendix 1*

# AREA UNDER A CURVE

## A1.1 Introduction

In several sections of this thesis, the areas under elution profiles obtained from anion exchange chromatography had to be determined. As a rule, if an equation can be found which describes a curve accurately, the area under the curve can be found using Calculus by mathematical integration of that equation. However, since the elution profiles cannot be described by a simple equation, alternative methods for determination of the areas under the curves were necessary.

## A1.2 Trapezium method

A general technique for estimating the area under any curve is the trapezium method, which also forms the principle behind the calculation of an area by mathematical integration. In this method, vertical lines are drawn to break up the area of interest into multiple segments (Figure A1.1), each of which resembles a trapezium. The area of each trapezium is easily calculated using the formula:

*Area = 0.5 X (sum of width of parallel sides) X height*

By adding up the areas of all the trapezia, an approximate value of the area under the curve is obtained. As would be expected, the larger the number of trapezia that is available by breaking the area up into smaller segments, the closer the approximation would be to the actual value of the area under the curve. Theoretically, by dividing the area into an infinite number of segments, each of which is infinitely narrow, the sum

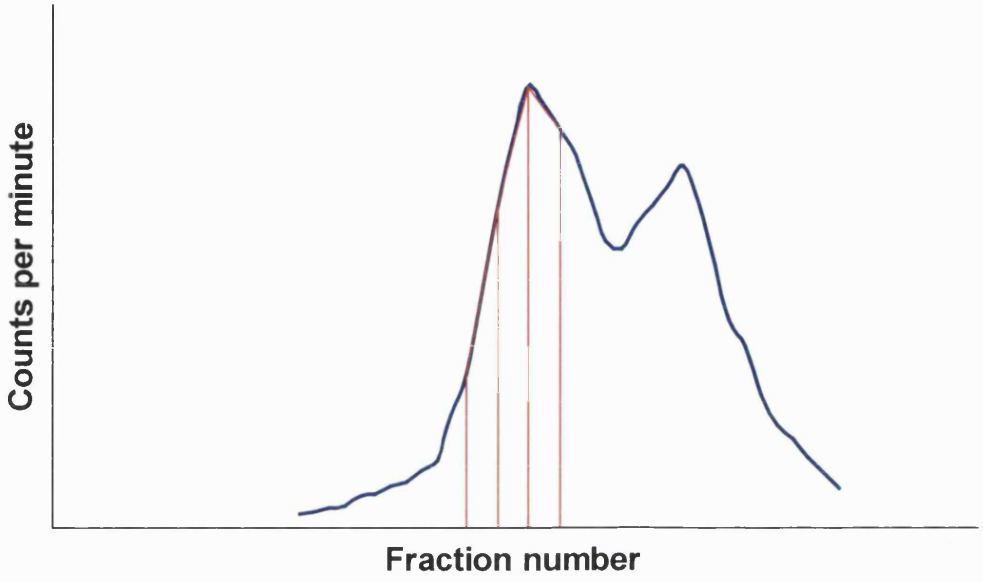


**Figure A1.1 Trapezium method of calculating the area under a curve.** Vertical lines are first drawn under the curve (blue line) to divide the area into multiple segments, each of which resembles a trapezium (red line). Addition of the areas of all the trapezia then provides an approximate value for the area under the curve. The larger the number of trapezia that is obtained by dividing the area into smaller segments, the closer will the estimate be to the actual value of the area under the curve.

of the areas of all the trapezia would exactly be the same as the area under the curve.

The trapezium method was used in this thesis to calculate the areas under the elution profiles, making use of the large number of data points collected for plotting each profile to draw the vertical lines and divide up each area into at least 60 segments. The area under each profile represented the amount of $^{35}$S-radiolabel that had been incorporated into heparan sulphate and chondroitin sulphate during the embryonic culture period.

## A1.3 Incomplete resolution of heparan sulphate and chondroitin sulphate peaks

Although the trapezium method could be used to calculate the total area under an elution profile (representing the sum of the areas under Peaks HS and CS in Figure A1.2), a problem arises when the area under an individual peak has to be determined. Due to the inherent inability of anion exchange chromatography to separate the two peaks completely, the situation arises where the right shoulder of Peak HS overlaps with the left shoulder of Peak CS. A complete outline of neither Peak HS nor Peak CS is available, thus curtailing the direct use of the trapezium method for calculating the area under each peak.

Fortunately, a solution is available that is based upon the symmetrical nature of both Peak HS and Peak CS (Williams and Wilson, 1981). Since each peak is symmetrical about a vertical line that passes

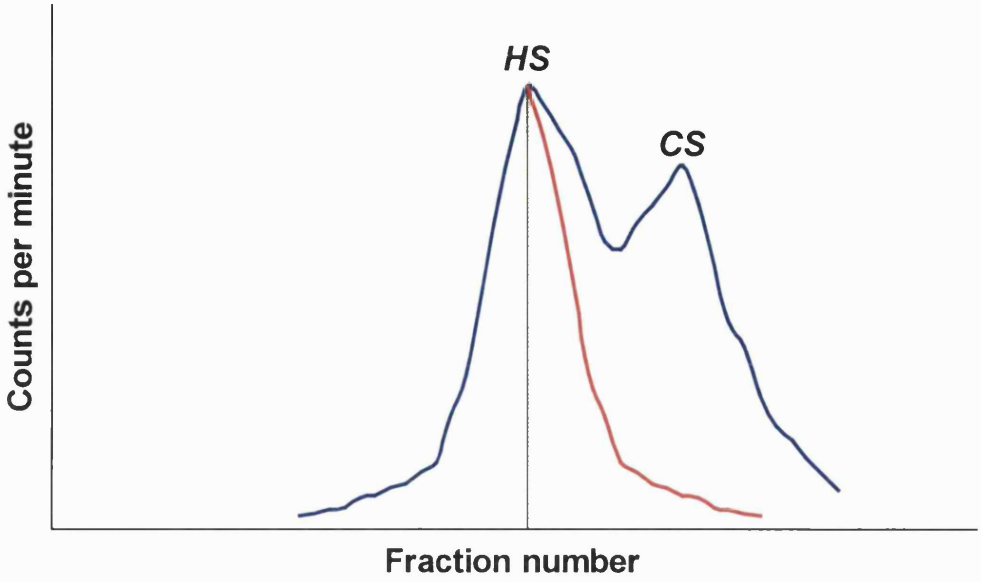


**Figure A1.2 Estimation of area under an incompletely resolved peak.** Due to the inherent inability of anion exchange chromatography to completely separate the heparan sulphate peak (HS) from the chondroitin sulphate peak (CS), an exact value for the area under each peak cannot be obtained. However, an estimate can be made from the elution profile (blue line), as illustrated here for Peak HS where its left shoulder is clearly seen but its right shoulder is lost within the left shoulder of Peak CS. By making use of the symmetrical nature of Peak HS about a vertical line (green line) passing through the summit of the peak, it is possible to trace the outline of the right shoulder (red line) by horizontally reflecting the left shoulder across the line of symmetry. Having thus obtained the contour of the entire peak, the trapezium method can be used to calculate the area under the peak. The area under Peak CS can be similarly determined.

through the summit of the peak, the outline of the right shoulder of Peak HS can be drawn by horizontally reflecting its left shoulder about the line of symmetry (Figure A1.2). The contour of the left shoulder of Peak CS could be similarly obtained. The area under each peak could then be calculated using the trapezium method.

The validity of this argument is shown in Figure A1.3, which is plotted using the experimental data shown in Figure 5.10. Enzymatic removal of Peak CS (chondroitin sulphate) by chondroitinase treatment results in a single peak, Peak HS, that represents heparan sulphate. It can be seen that Peak HS is symmetrical about a vertical line that passes through the apex of the peak.

## A1.4 Accuracy of estimation of the area under an incompletely resolved peak

To test the accuracy of the method described above for calculating the area under an incompletely resolved peak, the individual areas under Peaks HS and CS were first estimated from seven independent elution profiles. For each elution profile, the estimated areas of Peaks HS and CS were added together to give $X_1$, which represented the amount of $^{35}$S-radiolabel that had been incorporated into both heparan sulphate and chondroitin sulphate for that elution profile. $X_1$ was then compared with $X_2$, the area under each profile determined using the trapezium method directly on the entire HS and CS profile. Using the paired t-test, no statistically significant difference was found between $X_1$ and $X_2$ ($p$ = 0.3459). The ratio $X_1$:$X_2$ gives a value of 1.017, showing that the

method used does not lead to over-estimation of the area under each peak.

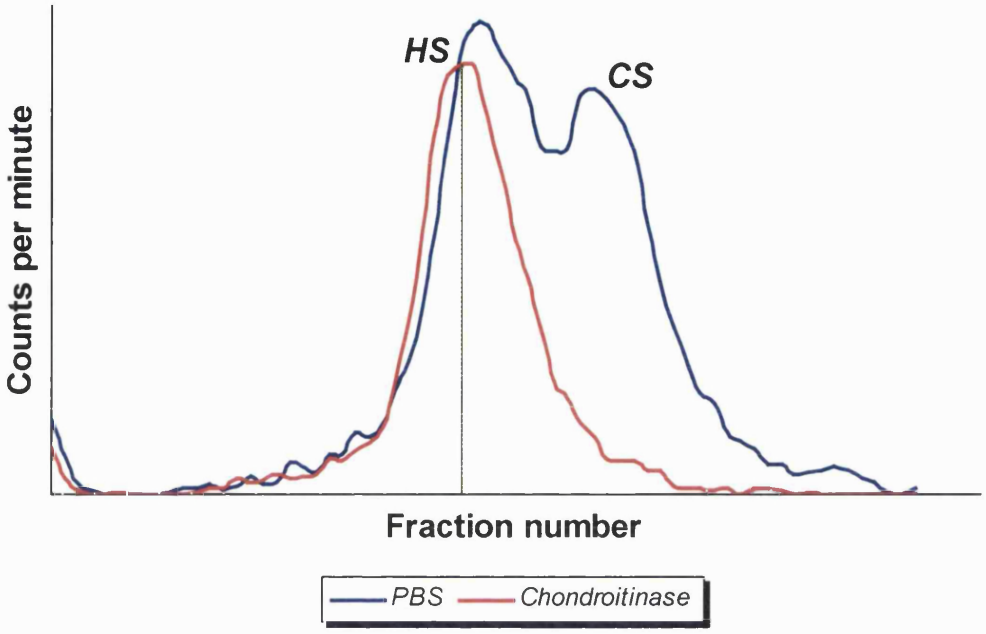


**Figure A1.3 Experimental evidence of peak symmetry.** The blue line shows a typical elution profile of $^{35}S$-labelled sulphated glycosaminoglycans separated by anion exchange chromatography. Peaks HS and CS represent heparan sulphate and chondroitin sulphate respectively. Pre-treatment of the sample with chondroitinase results in degradation of chondroitin sulphate, and only Peak HS is present in the profile (red line). Peak HS is symmetrical about a vertical line (green line) that passes through the apex of the peak.

# REFERENCES


Ahn, J, Ludecke, H J, Lindow, S, Horton, W A, Lee, B, Wagner, M J, Horsthemke, B and Wells, D E (1995) Cloning of the putative tumour suppressor gene for hereditary multiple exostoses (EXT1). *Nat Genet* **11**, 137-143.

Alvarez, I S and Schoenwolf, G C (1992) Expansion of surface epithelium provides the major extrinsic force for bending of the neural plate. *J Exp Zool* **261**, 340-348.

Aruga, J, Nagai, T, Tokuyama, T, Hayashizaki, Y, Okazaki, Y, Chapman, V M and Mikoshiba, K (1996) The mouse *Zic* gene family. Homologues of the *Drosophila* pair-rule gene *odd-paired*. *J Biol Chem* **271**, 1043-1047.

Asher, J H J, Harrison, R W, Morell, R, Carey, M L and Friedman, T B (1996) Effects of Pax3 modifier genes on craniofacial morphology, pigmentation, and viability: a murine model of Waardenburg syndrome variation. *Genomics* **34**, 285-298.

Auerbach, R (1954) Analysis of the developmental effects of a lethal mutation in the house mouse. *J Exp Zool* **127**, 305-329.

Aviezer, D, Hecht, D, Safran, M, Eisinger, M, David, G and Yayon, A (1994) Perlecan, basal lamina proteoglycan, promotes basic fibroblast growth factor-receptor binding, mitogenesis, and angiogenesis. *Cell* **79**, 1005-1013.

Avnur, Z and Geiger, B (1984) Immunocytochemical localization of native chondroitin-sulfate in tissues and cultured cells using specific monoclonal antibody. *Cell* **38**, 811-822.

Baeg, G-H, Lin, X, Khare, N, Baumgartner, S and Perrimon, N (2001) Heparan sulfate proteoglycans are critical for the organization of the extracellular distribution of Wingless. *Development* **128**, 87-94.

Bai, X M, van der Schueren, B, Cassiman, J-J, van den Berghe, H and David, G (1994) Differential expression of multiple cell-surface heparan sulfate proteoglycans during embryonic tooth development. *J Histochem Cytochem* **42**, 1043-1053.

Baker, P C and Schroeder, T E (1967) Cytoplasmic filaments and morphogenetic movement in the amphibian neural tube. *Dev Biol* **15**, 432-450.

Bancroft, J D and Stevens, A (1996) *Theory and practice of histological techniques (4th ed)*. Edinburgh: Churchill Livingstone.

Baynash, A G, Hosoda, K, Giaid, A, Richardson, J A, Emoto, N and Hammer, R E (1994) Interaction of endothelin-3 with endothelin-B receptor is essential for development of epidermal melanocytes and enteric neurons. *Cell* **79**, 1277-1285.

Behar, O, Golden, J A, Mashimo, H, Schoen, F J and Fishman, M C (1996) Semaphorin III is needed for normal patterning and growth of nerves, bones and heart. *Nature* **383**, 525-528.

Bellaiche, Y, The, I and Perrimon, N (1998) *Tout-velu* is a *Drosophila* homologue of the putative tumour suppressor *EXT-1* and is needed for Hh diffusion. *Nature* **394**, 85-88.

Bennett, G D, An, J, Craig, J C, Gefrides, L A, Calvin, J A and Finnell, R H (1998) Neurulation abnormalities secondary to altered gene expression in neural tube defect susceptible *Splotch* embryos. *Teratology* **57**, 17-29.

Bernfield, M, Götte, M, Park, P W, Reizes, O, Fitzgerald, M L, Lincecum, J and Zako, M (1999) Functions of cell surface heparan sulfate proteoglycans. *Annu Rev Biochem* **68**, 729-777.

Bernfield, M, Kokenyesi, R, Kato, M, Hinkes, M T, Spring, J, Gallo, R L and Lose, E J (1992) Biology of the syndecans: a family of transmembrane heparan sulfate proteoglycans. *Annu Rev Cell Biol* **8**, 365-393.

Bhaumik, M, Muller, V J, Rozaklis, T, Johnson, L, Dobrenis, K, Bhattacharyya, R, Wurzelmann, S, Finamore, P, Hopwood, J J, Walkley, S U and Stanley, P (1999) A mouse model for mucopolysaccharidosis type III A (Sanfilippo syndrome). *Glycobiology* **9**, 1389-1396.

Bienkowski, M J and Conrad, H E (1984) Kinetics of proteoheparan sulfate synthesis, secretion, endocytosis, and catabolism by a hepatocyte cell line. *J Biol Chem* **259**, 12989-12996.

Binari, R C, Staveley, B E, Johnson, W A, Godavarti, R, Sasisekharan, R and Manoukian, A S (1997) Genetic evidence that heparin-like

glycosaminoglycans are involved in *wingless* signaling. *Development* **124**, 2623-2632.

Blackshear, P J, Lai, W S, Tuttle, J S, Stumpo, D J, Kennington, E, Nairn, A C and Sulik, K K (1996) Developmental expression of MARCKS and protein kinase C in mice in relation to the exencephaly resulting from MARCKS deficiency. *Dev Brain Res* **96**, 62-75.

Bonneh-Barkay, D, Shlissel, M, Berman, B, Shaoul, E, Admon, A, Vlodavsky, I, Carey, D J, Asundi, V K, Reich-Slotky, R and Ron, D (1997) Identification of glypican as a dual modulator of the biological activity of fibroblast growth factors. *J Biol Chem* **272**, 12415-12421.

Bovolenta, P and Fernaud-Espinosa, I (2000) Nervous system proteoglycans as modulators of neurite outgrowth. *Prog Neurobiol* **61**, 113-132.

Breitschopf, H, Suchanek, G, Gould, R M, Colman, D R and Lassmann, H (1992) *In situ* hybridization with digoxigenin-labeled probes: Sensitive and reliable detection method applied to myelinating rat brain. *Acta Neuropathol* **84**, 581-587.

Breton, M, Berrou, E, Brahimi-Horn, M, Devdon, E and Picard, J (1986) Synthesis of sulfated proteoglycans throughout the cell cycle in smooth muscle cells from pig aorta. *Exp Cell Res* **166**, 416-426.

Brickman, Y G, Ford, M D, Gallagher, J T, Nurcombe, V, Bartlett, P F and Turnbull, J E (1998) Structural modification of fibroblast growth factor-binding heparan sulfate at a determinative stage of neural development. *J Biol Chem* **273**, 4350-4359.

Bronner-Fraser, M (1985) Alterations in neural crest migration by a monoclonal antibody that affects cell adhesion. *J Cell Biol* **101**, 610-617.

Bronner-Fraser, M (1986) An antibody to a receptor for fibronectin and laminin perturbs cranial neural crest development *in vivo*. *Dev Biol* **117**, 528-536.

Bronner-Fraser, M and Stern, C (1991) Effects of mesodermal tissues on avian neural crest cell migration. *Dev Biol* **143**, 213-217.

Bronner-Fraser, M, Wolf, J J and Murray, B A (1992) Effects of antibodies against N-cadherin and N-CAM on the cranial neural crest and neural tube. *Dev Biol* **153**, 291-301.

Brook, F A, Shum, A S W, van Straaten, H W M and Copp, A J (1991) Curvature of the caudal region is responsible for failure of neural tube closure in the curly tail (*ct*) mouse embryo. *Development* **113**, 671-678.

Brown, N A and Fabro, S (1981) Quantitation of rat embryonic development *in vitro*: a morphological scoring system. *Teratology* **24**, 65-78.

Bullock, S L, Fletcher, J M, Beddington, R S P and Wilson, V A (1998) Renal agenesis in mice homozygous for a gene trap mutation in the gene encoding heparan sulfate 2-sulfotransferase. *Genes Dev* **12**, 1894-1906.

Burke, R, Nellen, D, Bellotto, M, Hafen, E, Senti, T A, Dickson, B J and Basler, K (1999) Dispatched, a novel sterol-sensing domain protein

dedicated to the release of cholesterol-modified Hedgehog from signaling cells. *Cell* **99**, 803-815.

Camenisch, T D, Spicer, A P, Brehm-Gibson, T, Biesterfeldt, J, Augustine, M L, Calabro, A Jr, Kubalak, S, Klewer, S E and McDonald, J A (2000) Disruption of hyaluronan synthase-2 abrogates normal cardiac morphogenesis and hyaluronan-mediated transformation of epithelium to mesenchyme. *J Clin Invest* **106**, 349-360.

Canning, D R, Amin, T and Richard, E (2000) Regulation of epiblast cell movements by chondroitin sulfate during gastrulation in the chick. *Dev Dyn* **219**, 545-559.

Cano-Gauci, D F, Song, H H, Yang, H, McKerlie, C, Choo, B, Shi, W, Pullano, R, Piscione, T D, Grisaru, S, Soon, S, Sedlackova, L, Tanswell, A K, Mak, T W, Yeger, H, Lockwood, G A, Rosenblum, N D and Filmus, J (1999) Glypican-3-deficient mice exhibit developmental overgrowth and some of the abnormalities typical of Simpson-Golabi-Behmel syndrome. *J Cell Biol* **146**, 255-264.

Capehart, A A, Mjaatvedt, C H, Hoffman, S and Krug, E L (1999) Dynamic expression of a native chondroitin sulfate epitope reveals microheterogeneity of extracellular matrix organization in the embryonic chick heart. *Anat Rec* **254**, 181-195.

Cardin, A D and Weintraub, H J R (1989) Molecular modeling of protein-glycosaminoglycan interactions. *Atherosclerosis* **9**, 21-32.

Carey, D J, Bendt, K M and Stahl, R C (1996) The cytoplasmic domain of syndecan-1 is required for cytoskeleton association but not detergent insolubility. *J Biol Chem* **271**, 15253-15260.

Carey, D J, Stahl, R C, Tucker, B, Bendt, K A and Cizmeci-Smith, G (1994) Aggregation-induced association of syndecan-1 with microfilaments mediated by the cytoplasmsic domain. *Exp Cell Res* **214**, 12-21.

Carrel, T, Purandare, S M, Harrison, W, Elder, F, Fox, T, Casey, B and Herman, G E (2000) The X-linked mouse mutation Bent tail is associated with a deletion of the *Zic3* locus. *Hum Mol Genet* **9**, 1937-1942.

Chalepakis, G, Stoykova, A, Wijnholds, J, Tremblay, P and Gruss, P (1993) Pax: gene regulators in the developing nervous system. *J Neurobiol* **24**, 1367-1384.

Chen, J, Chang, S, Duncan, S A, Okano, H J, Fishell, G and Aderem, A (1996) Disruption of the MacMARCKS gene prevents cranial neural tube closure and results in anencephaly. *Proc Natl Acad Sci USA* **93**, 6275-6279.

Chen, W-H, Morriss-Kay, G M and Copp, A J (1995) Genesis and prevention of spinal neural tube defects in the *curly tail* mutant mouse: involvement of retinoic acid and its nuclear receptors RAR-β and RAR-γ. *Development* **121**, 681-691.

Chen, W H, Morriss-Kay, G M and Copp, A J (1994) Prevention of spinal neural tube defects in the curly tail mouse mutant by a specific effect of retinoic acid. *Dev Dyn* **199**, 93-102.

Cizmeci-Smith, G, Stahl, R C, Showalter, L J and Carey, D J (1993) Differential expression of transmembrane proteoglycans in vascular smooth muscle cells. *J Biol Chem* **268**, 18740-18747.

Cockroft, D L (1990) Dissection and culture of postimplantation embryos. In *Postimplantation mammalian embryos: A practical approach,* A J Copp and D L Cockroft (eds). Oxford: IRL Press, pp 15-40.

Cole, G J, Loewy, A and Glaser, L (1986) Neuronal cell-cell adhesion depends on interactions of N-CAM with heparin-like molecules. *Nature* **320**, 445-447.

Conrad, H E (1998) *Heparin-binding proteins.* San Diego: Academic Press.

Conway, S J, Bundy, J, Chen, J, Dickman, E, Rogers, R and Will, B M (2000) Decreased neural crest stem cell expansion is responsible for the conotruncal heart defects within the *Splotch* ($Sp^{2H}$)/*Pax3* mouse mutant. *Cardiovasc Res* **47**, 314-328.

Copp, A J and Bernfield, M (1988b) Accumulation of basement membrane-associated hyaluronate is reduced in the posterior neuropore region of mutant (curly tail) mouse embryos developing spinal neural tube defects. *Dev Biol* **130**, 583-590.

Copp, A J and Bernfield, M (1988a) Glycosaminoglycans vary in accumulation along the neuraxis during spinal neurulation in the mouse embryo. *Dev Biol* **130**, 573-582.

Copp, A J, Brook, F A, Estibeiro, P, Shum, A S W and Cockroft, D L (1990) The embryonic development of mammalian neural tube defects. *Prog Neurobiol* **35**, 363-403.

Copp, A J, Brook, F A and Roberts, H J (1988b) A cell-type-specific abnormality of cell proliferation in mutant (curly tail) mouse embryos developing spinal neural tube defects. *Development* **104**, 285-295.

Copp, A J, Cogram, P, Fleming, A, Gerrelli, D, Henderson, D J, Hynes, A, Kolatsi-Joannou, M, Murdoch, J, and Ybot-Gonzalez, P (2000) Neurulation and neural tube closure defects. In *Developmental Biology Protocols, Vol II,* R S Tuan and C W Lo (eds). Totowa: Humana Press, pp 135-160.

Copp, A J, Crolla, J A and Brook, F A (1988a) Prevention of spinal neural tube defects in the mouse embryo by growth retardation during neurulation. *Development* **104**, 297-303.

Copp, A J, Seller, M J and Polani, P E (1982) Neural tube development in mutant (*curly tail*) and normal mouse embryos: the timing of posterior neuropore closure *in vivo* and *in vitro*. *J Embryol Exp Morphol* **69**, 151-167.

Cremer, H, Lange, R, Christoph, A, Plomann, M, Vopper, G, Roes, J, Brown, R, Baldwin, S, Kraemer, P, Scheff, S, Barthels, D, Rajewsky, K and Wille, W (1994) Inactivation of the N-CAM gene in mice results in

size reduction of the olfactory bulb and deficits in spatial learning. *Nature* **367**, 455-459.

Daugaard, S, Strange, L and Schiodt, T (1991) Immunohistochemical staining for chondroitin sulphate and keratan sulphate. An evaluation of two monoclonal antibodies. *Histochemistry* **95**, 585-589.

David, G (1993) Integral membrane heparan sulfate proteoglycans. *FASEB J* **7**, 1023-1030.

David, G, Bai, X M, Van-der, S B, Cassiman, J J and Van-den, B H (1992) Developmental changes in heparan sulfate expression: in situ detection with mAbs. *J Cell Biol* **119**, 961-975.

David, G, Bai, X M, Van-der, S B, Marynen, P, Cassiman, J J and Van-den, B H (1993) Spatial and temporal changes in the expression of fibroglycan (syndecan-2) during mouse embryonic development. *Development* **119**, 841-854.

Davies, J, Lyon, M, Gallagher, J and Garrod, D (1995) Sulphated proteoglycan is required for collecting duct growth and branching but not nephron formation during kidney development. *Development* **121**, 1507-1517.

Debby-Brafman, A, Burstyn-Cohen, T, Klar, A and Kalcheim, C (1999) F-spondin, expressed in somite regions avoided by neural crest cells, mediates inhibition of distinct somite domains to neural crest migration. *Neuron* **22**, 475-488.

Delehedde, M, Deudon, E, Boilly, B and Hondermarck, H (1996) Heparan sulfate proteoglycans play a dual role in regulating fibroblast growth factor-2 mitogenic activity in human breast cancer cells. *Exp Cell Res* **229**, 398-406.

Deng, C-X, Wynshaw-Boris, A, Shen, M M, Daugherty, C, Ornitz, D M and Leder, P (1994) Murine FGFR-1 is required for early postimplantation growth and axial organization. *Genes Dev* **8**, 3045-3057.

Deng, C, Bedford, M, Li, C, Xu, X, Yang, X, Dunmore, J and Leder, P (1997) Fibroblast growth factor receptor-1 (FGFR-1) is essential for normal neural tube and limb development. *Dev Biol* **185**, 42-54.

Detrick, R J, Dickey, D and Kintner, C R (1990) The effects of N-cadherin misexpression on morphogenesis in *Xenopus* embryos. *Neuron* **4**, 493-506.

Domowicz, M, Li, H, Hennig, A, Henry, J, Vertel, B M and Schwartz, N B (1995) The biochemically and immunologically distinct CSPG of notochord is a product of the aggrecan gene. *Dev Biol* **171**, 655-664.

Duband, J L, Rocher, S, Yamada, K M and Thiery, J P (1986) Interactions of migrating neural crest cells with fibronectin. *Prog Clin Biol Res* **226**, 127-139.

Echelard, Y, Epstein, D J, St-Jacques, B, Shen, L, Mohler, J, McMahon, J A and McMahon, A P (1993) Sonic hedgehog, a member of a family of putative signaling molecules, is implicated in the regulation of CNS polarity. *Cell* **75**, 1417-1430.

Edgren, G, Havsmark, B, Jönsson, M and Fransson, L (1997) Glypican (heparan sulfate proteoglycan) is palmitoylated, deglycanated and reglycanated during recycling in skin fibroblasts. *Glycobiology* **7**, 103-112.

Eickholt, B J, Mackenzie, S L, Graham, A, Walsh, F S and Doherty, P (1999) Evidence for collapsin-1 functioning in the control of neural crest migration in both trunk and hindbrain regions. *Development* **126**, 2181-2189.

Elenius, K, Määttä, A, Salmivirta, M and Jalkanen, M (1992) Growth factors induce 3T3 cells to express bFGF-binding syndecan. *J Biol Chem* **267**, 6435-6441.

Embury, S, Seller, M J, Adinolfi, M and Polani, P E (1979) Neural tube defects in curly-tail mice. I. Incidence, expression and similarity to the human condition. *Proc R Soc Lond B* **206**, 85-94.

Epstein, D J, Vekemans, M and Gros, P (1991) *Splotch* ($Sp^{2H}$), a mutation affecting development of the mouse neural tube, shows a deletion within the paired homeodomain of Pax-3. *Cell* **67**, 767-774.

Epstein, J A, Li, J, Lang, D, Chen, F, Brown, C B, Jin, F, Lu, M M, Thomas, M, Liu, E-C J, Wessels, A and Lo, C W (2000) Migration of cardiac neural crest cells in *Splotch* embryos. *Development* **127**, 1869-1878.

Erickson, A C and Couchman, J R (2000) Still more complexity in mammalian basement membranes. *J Histochem Cytochem* **48**, 1291-1306.

Erickson, C (1987) Behavior of neural crest cells on embryonic basal laminae. *Dev Biol* **120**, 38-49.

Erickson, C A and Goins, T L (2000) Sacral neural crest cell migration to the gut is dependent upon the migratory environment and not cell-autonomous migratory properties. *Dev Biol* **219**, 79-97.

Erickson, C A and Weston, J A (1983) An SEM analysis of neural crest migration in the mouse. *J Embryol Exp Morphol* **74**, 97-118.

Esko, J D, Stewart, T E and Taylor, W H (1985) Animal cell mutants defective in glycosaminoglycan biosynthesis. *Proc Natl Acad Sci USA* **82**, 3197-3201.

Esko, J D, Weinke, J L, Taylor, W H, Ekborg, G, Roden, L, Anantharamaiah, G and Gawish, A (1987) Inhibition of chondroitin and heparan sulfate biosynthesis in Chinese hamster ovary cell mutants defective in galactosyltransferase I. *J Biol Chem* **262**, 12189-12195.

Fan, G, Xiao, L, Cheng, L, Wang, X, Sun, B and Hu, G (2000) Targeted disruption of NDST-1 gene leads to pulmonary hypoplasia and neonatal respiratory distress in mice. *FEBS Lett* **467**, 7-11.

Fan, Q-W, Uchimura, K, Yuzawa, Y, Matsuo, S, Mitsuoka, C, Kannagi, R, Muramatsu, H, Kadomatsu, K and Muramatsu, T (1999) Spatially and temporally regulated expression of N-acetylglucosamine-6-O-sulfotransferase during mouse embryogenesis. *Glycobiology* **9**, 947-955.

Farndale, R W, Buttle, D J and Barrett, A J (1986) Improved quantitation and discrimination of sulphated glycosaminoglycans by the use of dimethylmethylene blue. *Biochim Biophys Acta* **883**, 173-177.

Fedarko, N S and Conrad, H E (1986) A unique heparan sulfate in the nuclei of hepatocytes: structural changes with the growth state of the cells. *J Cell Biol* **102**, 587-599.

Fedarko, N S, Ishihara, M and Conrad, H E (1989) Control of cell division in hepatoma cells by exogenous heparan sulfate proteoglycan. *J Cell Physiol* **139**, 287-294.

Fernandez-Borja, M, Bellido, D, Makiya, R, David, G, Olivecrona, G, Reina, M and Vilaró, S (1995) Actin cytoskeleton of fibroblasts organizes surface proteoglycans that bind basic fibroblast growth factor and lipoprotein lipase. *Cell Motil Cytoskel* **30**, 89-107.

Fleming, A and Copp, A J (1998) Embryonic folate metabolism and mouse neural tube defects. *Science* **280**, 2107-2109.

Fleming, A and Copp, A J (2000) A genetic risk factor for mouse neural tube defects: defining the embryonic basis. *Hum Mol Genet* **9**, 575-581.

Forsberg, E, Pejler, G, Ringvall, M, Lunderius, C, Tomasini-Johansson, B, Kusche-Gullberg, M, Eriksson, I, Ledin, J, Hellman, L and Kjellén, L (1999) Abnormal mast cells in mice deficient in a heparin-synthesizing enzyme. *Nature* **400**, 773-776.

Gallagher, J T and Walker, A (1985) Molecular distinctions between heparan sulfate and heparin: analysis of sulphation patterns indicates that heparan sulfate and heparin are separate families of N-sulphated polysaccharides. *Biochem J* **230**, 665-674.

Geelen, J A G and Langman, J (1979) Ultrastructural observations on closure of the neural tube in the mouse. *Anat Embryol* **156**, 73-88.

Gerrelli, D and Copp, A J (1997) Failure of neural tube closure in the *loop-tail* (*Lp*) mutant mouse: analysis of the embryonic mechanism. *Dev Brain Res* **102**, 217-224.

Giger, R L, Wolfer, D P, De Wit, G M and Verhaagen, J (1996) Anatomy of rat semaphorin III/collapsin-1 mRNA expression and relationship to developing nerve tracts during neuroembryogenesis. *J Comp Neurol* **375**, 378-392.

Gofflot, F, Hall, M and Morriss-Kay, G M (1998) Genetic patterning of the posterior neuropore region of *curly tail* mouse embryos: deficiency of *Wnt5a* expression. *Int J Dev Biol* **42**, 637-644.

Golding, J P, Trainor, P, Krumlauf, R and Gassmann, M (2000) Defects in pathfinding by cranial neural crest cells in mice lacking the neuregulin receptor ErbB4. *Nat Cell Biol* **2**, 103-109.

Goodrich, L V, Johnson, R L, Milenkovic, L, McMahon, J A and Scott, M P (1996) Conservation of the *hedgehog/patched* signaling pathway from flies to mice: induction of a mouse *patched* gene by Hedgehog. *Genes Dev* **10**, 301-312.

Gould, S E, Upholt, W B and Kosher, R A (1995) Characterization of chicken syndecan-3 as a heparan sulfate proteoglycan and its expression during embryogenesis. *Dev Biol* **168**, 438-451.

Graham, A, Francis-West, P, Brickell, P and Lumsden, A (1994) The signalling molecule BMP4 mediates apoptosis in the rhombencephalic neural crest. *Nature* **372**, 684-686.

Graham, A, Heyman, I and Lumsden, A (1993) Even-numbered rhombomeres control the apoptotic elimination of neural crest cells from odd-numbered rhombomeres in the chick hindbrain. *Development* **119**, 233-245.

Grässel, S, Cohen, I R, Murdock, A D, Eichsteter, I and Iozzo, R V (1995) The proteoglycan perlecan is expressed in the erythroleukemia cell line K562 and is upregulated by sodium butyrate and phorbol ester. *Mol Cell Biol* **145**, 61-68.

Greenberg, J H, Seppa, S, Seppa, H and Tyl Hewitt, A (1981) Role of collagen and fibronectin in neural crest cell adhesion and migration. *Dev Biol* **87**, 259-266.

Greve, H, Cully, Z, Blumberg, P and Kresse, H (1988) Influence of chlorate on proteoglycan biosynthesis by cultured human fibroblasts. *J Biol Chem* **263**, 12886-12892.

Grootjans, J J, Zimmerman, P, Reekmans, G, Smets, A, Degeest, G, Dürr, J and David, G (1997) Syntenin, a PDZ protein that binds syndecan cytoplasmic domains. *Proc Natl Acad Sci USA* **94** , 13683-13688.

Guimond, S, Maccarana, M, Olwin, B B, Lindahl, U and Rapraeger, A C (1993) Activating and inhibitory heparin sequences for FGF-2 (basic FGF). Distinct requirements for FGF-1, FGF-2, and FGF-4. *J Biol Chem* **268**, 23906-23914.

Habuchi, H, Suzuki, S, Saito, T, Tamura, T, Harada, T, Yoshida, K and Kimata, K (1992) Structure of a heparan sulphate oligosaccharide that binds to basic fibroblast growth factor. *Biochem J* **285**, 805-813.

Habuchi, O (2000) Diversity and functions of glycosaminoglycan sulfotransferases. *Biochim Biophys Acta* **1474**, 115-127.

Hackett, D A, Smith, J L and Schoenwolf, G C (1997) Epidermal ectoderm is required for full elevation and for convergence during bending of the avian neural plate. *Dev Dyn* **210**, 397-406.

Haerry, T E, Heslip, T R, Marsh, J L and O'Connor, M B (1997) Defects in glucuronate biosynthesis disrupt Wingless signaling in *Drosophila*. *Development* **124**, 3055-3064.

Harris, M J and Juriloff, D M (1997) Genetic landmarks for defects in mouse neural tube closure. *Teratology* **56**, 177-187.

Häcker, U, Lin, X and Perrimon, N (1997) The *Drosophila sugarless* gene modulates Wingless signaling and encodes an enzyme involved in polysaccharide biosynthesis. *Development* **124**, 3565-3573.

Henderson, D J and Copp, A J (1997) Role of the extracellular matrix in neural crest cell migration. *J Anat* **191**, 507-515.

Henderson, D J, Ybot-Gonzalez, P and Copp, A J (1997) Over-expression of the chondroitin sulphate proteoglycan *versican* is associated with defective neural crest migration in the *Pax3* mutant mouse (*splotch*). *Mech Dev* **69**, 39-51.

Herndon, M E, Stipp, C S and Lander, A D (1999) Interactions of neural glycosaminoglycans and proteoglycans with protein ligands: assessment of selectivity, heterogeneity and the participation of core proteins in binding. *Glycobiology* **9**, 143-155.

Hildebrand, J D and Soriano, P (1999) Shroom, a PDZ domain-containing actin-binding protein, is required for neural tube morphogenesis in mice. *Cell* **99**, 485-497.

Hosoda, K, Hammer, R E, Richardson, J A, Baynash, A G, Cheung, J C and Giaid, A (1994) Targeted and natural (piebald-lethal) mutations of endothelin-B receptor gene produce megacolon associated with spotted coat color in mice. *Cell* **79**, 1267-1276.

Humphries, D E, Wong, G W, Friend, D S, Gurish, M F, Qiu, W-T, Huang, C, Sharpe, A H and Stevens, R L (1999) Heparin is essential for the storage of specific granule proteases in mast cells. *Nature* **400**, 769-772.

Iozzo, R V (1998) Matrix proteoglycans: from molecular design to cellular function. *Annu Rev Biochem* **67**, 609-652.

Ishihara, M (1994) Structural requirements in heparin for binding and activation of FGF-1 and FGF-4 are different from that for FGF-2. *Glycobiology* **4**, 817-824.

Ishihara, M and Conrad, H E (1989) Correlations between heparan sulfate metabolism and hepatoma growth. *J Cell Physiol* **138**, 467-476.

Ishihara, M, Fedarko, N S and Conrad, H E (1986) Transport of heparan sulfate into the nuclei of hepatocytes. *J Biol Chem* **261**, 13575-13580.

Ishihara, M, Shaklee, P N, Yang, Z, Liang, W, Wei, Z, Stack, R J and Holme, K (1994) Structural features in heparin which modulate specific biological activities mediated by basic fibroblast growth factor. *Glycobiology* **4**, 451-458.

Jackson, S M, Nakato, H, Sugiura, M, Jannuzi, A, Oakes, R, Kaluza, V, Golden, C and Selleck, S B (1997) *dally*, a *Drosophila* glypican, controls cellular responses to the TGF-β-related morphogen, Dpp. *Development* **124**, 4113-4120.

Jacobson, A G and Gordon, R (1976) Changes in the shape of the developing vertebrate nervous system analyzed experimentally, mathematically and by computer simulation. *J Exp Zool* **197**, 191-246.

Jacobson, A G and Tam, P P L (1982) Cephalic neurulation in the mouse embryo analyzed by SEM and morphometry. *Anat Rec* **203**, 375-396.

Jenniskens, G J, Oosterhof, A, Brandwijk, R, Veerkamp, J H and van Kuppevelt, T H (2000) Heparan sulfate heterogeneity in skeletal muscle basal lamina: demonstration by phage display-derived antibodies. *J Neurosci* **20**, 4099-4111.

Johnson, D R (1976) The interfrontal bone and mutant genes in the mouse. *J Anat* **121**, 507-513.

Juriloff, D M and Harris, M J (2000) Mouse models for neural tube closure defects. *Hum Mol Genet* **9**, 993-1000.

Juriloff, D M, Harris, M J, Tom, C and MacDonald, K B (1991) Normal mouse strains differ in the site of initiation of closure of the cranial neural tube. *Teratology* **44**, 225-233.

Kan, M, Wang, F, To, B, Gabriel, J L and McKeehan, W L (1996) Divalent cations and heparin/heparan sulfate cooperate to control assembly and activity of the fibroblast growth factor receptor complex. *J Biol Chem* **271**, 26143-26148.

Karfunkel, P (1974) The mechanisms of neural tube formation. *Int Rev Cytol* **38**, 245-271.

Karfunkel, P, Hoffman, M, Phillips, M and Black, J (1978) Changes in cell adhesiveness in neurulation and optic cup formation. *Zoon* **6**, 23-31.

Kato, M, Turnbull, J, Hooper, K, Gallagher, J T and Bernfield, M (1991) Heparan sulfate chains on syndecan show cell type-specific fine structure. *J Cell Biol* **115**, 125a.

Kato, M, Wang, H, Bernfield, M, Gallagher, J T and Turnbull, J E (1994) Cell surface syndecan-1 on distinct cell types differs in fine structure and ligand binding of its heparan sulfate chains. *J Biol Chem* **269**, 1881-1890.

Kerr, R S E and Newgreen, D F (1997) Isolation and characterization of chondroitin sulfate proteoglycans from embryonic quail that influence neural crest cell behavior. *Dev Biol* **192**, 108-124.

Khare, N and Baumgartner, S (2000) Dally-like protein, a new *Drosophila* glypican with expression overlapping with *wingless*. *Mech Dev* **99**, 199-202.

Kil, S H, Krull, C E, Cann, G, Clegg, D and Bronner-Fraser, M (1998) The $\alpha$4 subunit of integrin is important for neural crest cell migration. *Dev Biol* **202**, 29-42.

Kil, S H, Lallier, T and Bronner-Fraser, M (1996) Inhibition of cranial neural crest adhesion *in vitro* and migration *in vivo* using integrin antisense oligonucleotides. *Dev Biol* **179**, 91-101.

Kim, C W, Goldberger, O A, Gallo, R L and Bernfield, M (1994) Members of the syndecan family of heparan sulfate proteoglycans are expressed in distinct cell-, tissue-, and development-specific patterns. *Mol Biol Cell* **5**, 797-805.

Kintner, C R and Melton, D M (1987) Expression of *Xenopus* N-CAM RNA is an early response of ectoderm to induction. *Development* **99**, 311-325.

Kitagawa, H, Tsutsumi, K, Tone, Y and Sugahara, K (1997) Developmental regulation of the sulfation profile of chondroitin sulfate chains in the chicken embryo brain. *J Biol Chem* **272**, 31377-31381.

Kitsukawa, T, Shimizu, M, Sanbo, M, Hirata, T, Taniguchi, M, Bekku, Y, Yagi, T and Fujisawa, H (1997) Neuropilin-semaphorin III/D-mediated chemorepulsive signals play a crucial role in peripheral nerve projection in mice. *Neuron* **19**, 995-1005.

Kjellen, L and Lindahl, U (1991) Proteoglycans: structures and interactions. *Annu Rev Biochem* **60**, 443-475.

Klootwijk, R, Franke, B, van der Zee, C E E M, De Boer, R T, Wilms, W, Hol, F A and Mariman, E C M (2000) A deletion encompassing *Zic3* in Bent tail, a mouse model for X-linked neural tube defects. *Hum Mol Genet* **9**, 1615-1622.

Kokenyesi, R and Bernfield, M (1994) Core protein structure and sequence determine the site and presence of heparan sulfate and chondroitin sulfate on syndecan-1. *J Biol Chem* **269**, 12304-12309.

Kolset, S O, Vuong, T T and Prydz, K (1999) Apical secretion of chondroitin sulphate in polarized Madin-Darby canine kidney (MDCK) cells. *J Cell Sci* **112**, 1797-1801.

Krotoski, D M, Domingo, C and Bronner-Fraser, M (1986) Distribution of a putative cell surface receptor for fibronectin and laminin in the avian embryo. *J Cell Biol* **103**, 1061-1071.

Krull, C E, Lansford, R, Gale, N W, Collazo, A, Marcelle, C, Yancopoulos, G D, Fraser, S E and Bronner-Fraser, M (1997) Interactions of Eph-related receptors and ligands confer rostrocaudal pattern to trunk neural crest migration. *Curr Biol* **7**, 571-580.

Kubota, Y, Morita, T, Kusakabe, M, Sakakura, T and Ito, K (1999) Spatial and temporal changes in chondroitin sulfate distribution in the sclerotome play an essential role in the formation of migration patterns of mouse neural crest cells. *Dev Dyn* **214**, 55-65.

Kulesa, P M and Fraser, S E (1998) Neural crest cell dynamics revealed by time-lapse video microscopy of whole embryo chick explant cultures. *Dev Biol* **204**, 327-344.

Lallier, T and Bronner-Fraser, M (1991) Avian neural crest cell attachment to laminin: involvement of divalent cation dependent and independent integrins. *Development* **113**, 1069-1084.

Landolt, R M, Vaughan, L, Winterhalter, K H and Zimmermann, D R (1995) Versican is selectively expressed in embryonic tissues that act as barriers to neural crest cell migration and axon outgrowth. *Development* **121**, 2303-2312.

Langford, J K, Stanley, M J, Cao, D and Sanderson, R D (1998) Multiple heparan sulfate chains are required for optimal syndecan-1 function. *J Biol Chem* **273**, 29965-29971.

Le Douarin, N M and Kalcheim, C (1999) *The neural crest (2nd ed)*. Cambridge: Cambridge University Press.

Li, J, Liu, K C, Jin, F, Lu, M M and Epstein, J A (1999) Transgenic rescue of congenital heart disease and spina bifida in *Splotch* mice. *Development* **126**, 2495-2503.

Lin, W, Shuster, S, Maibach, H I and Stern, R (1997) Patterns of hyaluronan staining are modified by fixation techniques. *J Histochem Cytochem* **45**, 1157-1163.

Lin, X, Buff, E M, Perrimon, N and Michelson, A M (1999) Heparan sulfate proteoglycans are essential for FGF receptor signaling during *Drosophila* embryonic development. *Development* **126**, 3715-3723.

Lin, X and Perrimon, N (1999) Dally cooperates with *Drosophila* Frizzled 2 to transduce Wingless signalling. *Nature* **400**, 281-284.

Lin, X, Wei, G, Shi, Z, Dryer, L, Esko, J D, Wells, D E and Matzuk, M M (2000) Disruption of gastrulation and heparan sulfate biosynthesis in EXT1-deficient mice. *Dev Biol* **224**, 299-311.

Linhardt, R J (1995) Analysis of glycosaminoglycans with polysaccharide lyases. In *Current protocols in molecular biology, Vol 3,* F M Ausubel, R Brent, R E Kingston, D D Moore, J G Seidman, J A Smith and K Struhl (eds). New York: John Wiley & Sons, Inc, p 17.13.17-17.13.32.

Litwack, E D, Ivins, J K, Kumbasar, A, Paine, S S, Stipp, C S and Lander, A D (1998) Expression of the heparan sulfate proteoglycan glypican-1 in the developing rodent. *Dev Dyn* **211**, 72-87.

Loring, J F and Erickson, C A (1987) Neural crest cell migratory pathways in the trunk of the chick embryo. *Dev Biol* **121**, 220-236.

Löfberg, J, Perris, R and Epperlein, H H (1989) Timing in the regulation of neural crest cell migration: retarded "maturation" of regional

extracellular matrix inhibits pigment cell migration in embryos of the white axolotl mutant. *Dev Biol* **131**, 168-181.

Lyon, M, Rushton, G and Gallagher, J T (1997) The interaction of the transforming growth factor-βs with heparin/heparan sulfate is isoform-specific. *J Biol Chem* **272**, 18000-18006.

Maddox, P H and Jenkins, D (1987) 3-Aminopropyltriethoxysilane (APES): A new advance in section adhesion. *J Clin Pathol* **40**, 1256-1257.

Margolis, R K, Crockett, C P, Kiang, W L and Margolis, R U (1976) Glycosaminoglycans and glycoproteins associated with rat brain nuclei. *Biochim Biophys Acta* **451**, 465-469.

Marigo, V, Davey, R A, Zuo, Y, Cunningham, J M and Tabin, C J (1996a) Biochemical evidence that Patched is the Hedgehog receptor. *Nature* **384**, 176-179.

Marigo, V, Scott, M P, Johnson, R L, Goodrich, L V and Tabin, C J (1996b) Conservation in *hedgehog* signaling: induction of a chicken *patched* homolog by *Sonic hedgehog* in the developing limb. *Development* **122**, 1225-1233.

Martins-Green, M (1988) Origin of the dorsal surface of the neural tube by progressive delamination of epidermal ectoderm and neuroepithelium: implications for neurulation and neural tube defects. *Development* **103**, 687-706.

Martins-Green, M and Erickson, C A (1986) Development of neural tube basal lamina during neurulation and neural crest cell emigration in the trunk of mouse embryos. *J Embryol Exp Morphol* **98** , 219-236.

Matsumota, R, Sali, A, Ghildyal, N, Karplus, M and Stevens, R L (1995) Packaging of proteases and proteoglycans in the granules of mast cells and other hematopoietic cells: a cluster of histidines on mouse mast cell protease 7 regulates its binding to heparin serglycin proteoglycans. *J Biol Chem* **270**, 19524-19531.

Menoud, P A, Debrot, S and Schowing, J (1989) Mouse neural crest cells secrete both urokinase-type and tissue-type plasminogen activators in vitro. *Development* **106**, 685-690.

Mertens, G, van der Schueren, B, van den Berghe, H and David, G (1996) Heparan sulfate expression in polarized epithelial cells: the apical sorting of glypican (GPI-anchored proteoglycan) is inversely related to its heparan sulfate content. *J Cell Biol* **132**, 487-497.

Miao, H-Q, Ishai-Michaeli, R, Atzmon, R, Peretz, T and Vlodavsky, I (1996) Sulfate moieties in the subendothelial extracellular matrix are involved in basic fibroblast growth factor sequestration, dimerization, and stimulation of cell proliferation. *J Biol Chem* **271**, 4879-4886.

Milev, P, Monnerie, H, Popp, S, Margolis, R K and Margolis, R U (1998) The core protein of the chondroitin sulfate proteoglycan phosphacan is a high-affinity ligand of fibroblast growth factor-2 and potentiates its mitogenic activity. *J Biol Chem* **273**, 21439-21442.

Miner, J H, Cunningham, J and Sanes, J R (1998) Roles for laminin in embryogenesis: exencephaly, syndactyly, and placentopathy in mice lacking the laminin α5 chain. *J Cell Biol* **143**, 1713-1723.

Mjaatvedt, C H, Yamamura, H, Capehart, A A, Turner, D and Markwald, R R (1998) The Cspg2 gene, disrupted in the hdf mutant, is required for right cardiac chamber and endocardial cushion formation. *Dev Biol* **202**, 56-66.

Moase, C E and Trasler, D G (1991) N-CAM alterations in splotch neural tube defect mouse embryos. *Development* **113**, 1049-1058.

Morris-Wiman, J and Brinkley, L L (1990) Changes in mesenchymal cell and hyaluronate distribution correlate with *in vivo* elevation of the mouse mesencephalic neural folds. *Anat Rec* **226**, 383-395.

Morrison-Graham, K, Schatteman, G C, Bork, T, Bowen-Pope, D F and Weston, J A (1992) A PDGF receptor mutation in the mouse (*Patch*) perturbs the development of a non-neuronal subset of neural crest-derived cells. *Development* **115**, 133-142.

Morrison-Graham, K and Weston, J A (1989) Mouse mutants provide new insights into the role of extracellular matrix in cell migration and differentiation. *Trends Genet* **5**, 116-121.

Morriss-Kay, G and Mahmood, R (1992) Morphogenesis-related changes in extracellular matrix induced by retinoic acid. In *Retinoids in normal development and teratogenesis,* G Morriss-Kay (ed). Oxford: Oxford University Press, pp 165-180.

Morriss-Kay, G and Tuckett, F (1985) The role of microfilaments in cranial neurulation in rat embryos: effects of short-term exposure to cytochalasin D. *J Embryol Exp Morphol* **88**, 333-348.

Morriss-Kay, G and Tuckett, F (1989b) Immunohistochemical localisation of chondroitin sulphate proteoglycans and the effects of chondroitinase ABC in 9- to 11-day rat embryos. *Development* **106**, 787-798.

Morriss-Kay, G M (1981) Growth and development of pattern in the cranial neural epithelium of rat embryos during neurulation. *J Embryol Exp Morphol* **65 (Suppl)**, 225-241.

Morriss-Kay, G M and Crutch, B (1982) Culture of rat embryos with β-D-xyloside: evidence of a role for proteoglycans in neurulation. *J Anat* **134**, 491-506.

Morriss-Kay, G M, Tuckett, F and Solursh, M (1986) The effects of Streptomyces hyaluronidase on tissue organization and cell cycle time in rat embryos. *J Embryol Exp Morphol* **98**, 59-70.

Morriss, G M and New, D A T (1979) Effect of oxygen concentration on morphogenesis of cranial neural folds and neural crest in cultured rat embryos. *J Embryol Exp Morphol* **54**, 17-35.

Morriss, G M and Solursh, M (1978) Regional differences in mesenchymal cell morphology and glycosaminoglycans in early neural-fold stage rat embryos. *J Embryol Exp Morphol* **46**, 37-52.

Mourao, P A S, Kato, S and Donnelly, P V (1981) Spondyloepiphyseal dysplasia, chondroitin sulfate type: a possible defect of PAPS-chondroitin sulfate sulfotransferase in humans. *Biochem Biophys Res Commun* **98**, 388-396.

Murch, S H, Winyard, P J, Koletzko, S, Wehner, B, Cheema, H A, Risdon, R A, Phillips, A D, Meadows, N, Klein, N J and Walker-Smith, J A (1996) Congenital enterocyte heparan sulphate deficiency with massive albumin loss, secretory diarrhoea, and malnutrition. *Lancet* **347** , 1299-1301.

Murono, E P, Washburn, A L, Goforth, D P and Wu, N (1993) Evidence that both receptor- and heparan sulfate proteoglycan-bound basic fibroblast growth factor are internalized by cultured immature Leydig cells. *Mol Cell Endocrinol* **98**, 81-90.

Nagai, T, Aruga, J, Minowa, O, Sugimoto, T, Ohno, Y, Noda, T and Mikoshiba, K (2000) Zic2 regulates the kinetics of neurulation. *Proc Natl Acad Sci USA* **97**, 1618-1623.

Nagele, R G and Lee, H (1980) Studies on the mechanisms of neurulation in the chick: microfilament-mediated changes in cell shape during uplifting of neural folds. *J Exp Zool* **213**, 391-398.

Nakato, H, Futch, T A and Selleck, S B (1995) The *division abnormally delayed* (*dally*) gene: a putative integral membrane proteoglycan required for cell division patterning during postembryonic development of the nervous system in *Drosophila*. *Development* **121**, 3687-3702.

Neale, S A and Trasler, D G (1994) Early sialylation on N-CAM in *splotch* neural tube defect mouse embryos. *Teratology* **50**, 118-124.

New, D A T, Coppola, P T and Terry, S (1973) Culture of explanted rat embryos in rotating tubes. *J Reprod Fertil* **35**, 135-138.

Newgreen, D (1984) Spreading of explants of embryonic chick mesenchymes and epithelia on fibronectin and laminin. *Cell Tissue Res* **236**, 265-277.

Newgreen, D and Gibbins, I (1982) Factors controlling the time of onset of the migration of neural crest cells in the fowl embryo. *Cell Tissue Res* **224**, 145-160.

Newgreen, D and Thiery, J P (1980) Fibronectin in early avian embryos: synthesis and distribution along the migration pathways of neural crest cells. *Cell Tissue Res* **211**, 269-291.

Newgreen, D F (1989) Physical influences on neural crest cell migration in avian embryos: contact guidance and spatial restriction. *Dev Biol* **131**, 136-148.

Newgreen, D F, Gibbins, I L, Sauter, J, Wallenfels, B and Wutz, R (1982) Ultrastructural and tissue-culture studies on the role of fibronectin, collagen and glycosaminoglycans in the migration of neural crest cells in the fowl embryo. *Cell Tissue Res* **221**, 521-549.

Newgreen, D F, Kerr, R S, Minichiello, J and Warren, N (1997) Changes in cell adhesion and extracellular matrix molecules in

spontaneous spinal neural tube defects in avian embryos. *Teratology* **55**, 195-207.

Newgreen, D F, Scheel, M and Kastner, V (1986) Morphogenesis of sclerotome and neural crest in avian embryos. In vivo and in vitro studies on the role of notochordal extracellular material. *Cell Tissue Res* **244**, 299-313.

Nurcombe, V, Ford, M D, Wildschut, J A and Bartlett, P F (1993) Developmental regulation of neural response to FGF-1 and FGF-2 by heparan sulfate proteoglycan. *Science* **260**, 103-106.

O'Shea, K S (1987) Differential deposition of basement membrane components during formation of the caudal neural tube in the mouse embryo. *Development* **99**, 509-519.

O'Shea, K S and Kaufman, M H (1980) Phospholipase C-induced neural tube defects in the mouse embryo. *Experientia* **36**, 1217-1219.

O'Shea, K S and Liu, L H (1987) Basal lamina and extracellular matrix alterations in the caudal neural tube of the delayed *splotch* embryo. *Brain Res* **465**, 11-20.

Oakley, R A, Lasky, C J, Erickson, C A and Tosney, K W (1994) Glycoconjugates mark a transient barrier to neural crest migration in the chicken embryo. *Development* **120**, 103-114.

Oakley, R A and Tosney, K W (1991) Peanut agglutinin and chondroitin-6-sulfate are molecular markers for tissues that act as barriers to axon advance in the avian embryo. *Dev Biol* **147**, 187-206.

Ohya, T and Kaneko, Y (1970) Novel hyaluronidase from *Streptomyces*. *Biochim Biophys Acta* **198**, 607-609.

Olsson, L, Svensson, K and Perris, R (1996) Effects of extracellular matrix molecules on subepidermal neural crest cell migration in wild type and white mutant (*dd*) axolotl embryos. *Pigment Cell Res* **9**, 18-27.

Oohira, A, Matsui, F, Tokita, Y, Yamauchi, S and Aono, S (2000) Molecular interactions of neural chondroitin sulfate proteoglycans in the brain development. *Arch Biochem Biophys* **374**, 24-34.

Paine-Saunders, S, Viviano, B L, Zupicich, J, Skarnes, W C and Saunders, S (2000) *glypican-3* controls cellular responses to *Bmp4* in limb patterning and skeletal development. *Dev Biol* **225**, 179-187.

Payette, R F, Tennyson, V M, Pomeranz, H D, Pham, T D, Rothman, T P and Gershon, M D (1988) Accumulation of components of basal laminae: association with the failure of neural crest cells to colonize the presumptive aganglionic bowel of *ls/ls* mutant mice. *Dev Biol* **125**, 341-360.

Peeters, M C E, Schutte, B, Lenders, M-H J N, Hekking, J W M, Drukker, J and van Straaten, H W M (1998) Role of differential cell proliferation in the tail bud in aberrant mouse neurulation. *Dev Dyn* **211**, 382-389.

Peeters, M C E, Shum, A S W, Hekking, J W M, Copp, A J and van Straaten, H W M (1996) Relationship between altered axial curvature and neural tube closure in normal and mutant (*curly tail*) mouse embryos. *Anat Embryol* **193**, 123-130.

Perissinotto, D, Iacopetti, P, Bellina, I, Doliana, R, Colombatti, A, Pettway, Z, Bronner-Fraser, M, Shinomura, T, Kimata, K, Mörgelin, M, Löfberg, J and Perris, R (2000) Avian neural crest cell migration is diversely regulated by the two major hyaluronan-binding proteoglycans PG-M/versican and aggrecan. *Development* **127**, 2823-2842.

Perris, R (1997) The extracellular matrix in neural crest-cell migration. *Trends Neurosci* **20**, 23-31.

Perris, R, Krotoski, D and Bronner-Fraser, M (1991a) Collagens in avian neural crest development: distribution *in vivo* and migration-promoting ability *in vitro*. *Development* **113**, 969-984.

Perris, R, Krotoski, D, Lallier, T, Domingo, C, Sorrell, J M and Bronner-Fraser, M (1991b) Spatial and temporal changes in the distribution of proteoglycans during avian neural crest development. *Development* **111**, 583-599.

Perris, R, Kuo, H-J, Glanville, R W, Leibold, S and Bronner-Fraser, M (1993a) Neural crest cell interaction with type VI collagen is mediated by multiple cooperative binding sites within triple-helix and globular domains. *Exp Cell Res* **209**, 103-117.

Perris, R, Paulsson, M and Bronner-Fraser, M (1989) Molecular mechanisms of avian neural crest cell migration on fibronectin and laminin. *Dev Biol* **136**, 222-238.

Perris, R and Perissinotto, D (2000) Role of the extracellular matrix during neural crest cell migration. *Mech Dev* **95**, 3-21.

Perris, R, Perissinotto, D, Pettway, Z, Bronner-Fraser, M, Morgelin, M and Kimata, K (1996) Inhibitory effects of PG-H/aggrecan and PG-M/versican on avian neural crest cell migration. *FASEB J* **10**, 293-301.

Perris, R, Syfrig, J, Paulsson, M and Bronner-Fraser, M (1993b) Molecular mechanisms of neural crest cell attachment and migration on types I and IV collagen. *J Cell Sci* **106**, 1357-1368.

Pettway, Z, Domowicz, M, Schwartz, N B and Bronner-Fraser, M (1996) Age-dependent inhibition of neural crest migration by the notochord correlates with alterations in the S103L chondroitin sulfate proteoglycan. *Exp Cell Res* **225**, 195-206.

Pettway, Z, Guillory, G and Bronner-Fraser, M (1990) Absence of neural crest cells from the region surrounding implanted notochords *in situ*. *Dev Biol* **142**, 335-345.

Pilia, G, Hughes, B R, MacKenzie, A, Baybayan, P, Chen, E Y, Huber, R, Neri, G, Cao, A, Forabosco, A and Schlessinger, D (1996) Mutations in GPC3, a glypican gene, cause the Simpson-Golabi-Behmel overgrowth syndrome. *Nat Genet* **12**, 241-247.

Poole, T J and Thiery, J P (1986) Antibodies and a synthetic peptide that block cell-fibronectin adhesion arrest neural crest cell migration *in vivo*. *Prog Clin Biol Res* **217B**, 235-238.

Preston, S F, Regula, C S, Sager, P R, Pearson, C B, Brown, L S and Berlin, R D (1985) Glycosaminoglycan synthesis is depressed during mitosis and elevated during early G1. *J Cell Biol* **101**, 1086-1093.

Prydz, K and Dalen, K T (2000) Synthesis and sorting of proteoglycans. *J Cell Sci* **113**, 193-205.

Pye, D A, Vives, R R, Turnbull, J E, Hyde, P and Gallagher, J T (1998) Heparan sulfate oligosaccharides require 6-O-sulfation for promotion of basic fibroblast growth factor mitogenic activity. *J Biol Chem* **273**, 22936-22942.

Pye, D A, Vivès, R R, Hyde, P and Gallagher, J T (2000) Regulation of FGF-1 mitogenic activity by heparan sulfate oligosaccharides is dependent on specific structural features: differential requirements for the modulation of FGF-1 and FGF-2. *Glycobiology* **10**, 1183-1192.

Radice, G L, Rayburn, H, Matsunami, H, Knudsen, K A, Takeichi, M and Hynes, R O (1997) Developmental defects in mouse embryos lacking N-cadherin. *Dev Biol* **181**, 64-78.

Ranscht, B and Bronner-Fraser, M (1991) T-cadherin expression alternates with migrating neural crest cells in the trunk of the avian embryo. *Development* **111**, 15-22.

Reilly, C F, Kindy, M S, Brown, K E, Rosenberg, R D and Sonenshein, G E (1989) Heparin prevents vascular smooth muscle cells progression through the G1 phase of the cell cycle. *J Biol Chem* **264**, 6990-6995.

Rickmann, M, Fawcett, J W and Keynes, R J (1985) The migration of neural crest cells and the growth of motor axons through the rostral half of the chick somite. *J Embryol Exp Morphol* **90**, 437-455.

Ring, C, Hassell, J and Halfter, W (1996) Expression pattern of collagen IX and potential role in the segmentation of the peripheral nervous system. *Dev Biol* **180**, 41-53.

Ringvall, M, Ledin, J, Holmborn, K, van Kuppevelt, T, Ellin, F, Eriksson, I, Olofsson, A, Kjellen, L and Forsberg, E (2000) Defective heparan sulfate biosynthesis and neonatal lethality in mice lacking N-deacetylase/N-sulfotransferase-1. *J Biol Chem* **275**, 25926-25930.

Rogers, S L, Bernard, L and Weston, J A (1990) Substratum effects on cell dispersal, morphology, and differentiation in cultures of avian neural crest cells. *Dev Biol* **141**, 173-182.

Rosengart, T K, Johnson, W V, Friesel, R, Clark, R and Maciag, T (1988) Heparin protects heparin-binding growth factor-1 from proteolytic inactivation *in vitro*. *Biochem Biophys Res Commun* **152**, 432-440.

Rovasio, R A, Delouvée, A, Yamada, K M, Timpl, R and Thiery, J P (1983) Neural crest cell migration: requirements for exogenous fibronectin and high cell density. *J Cell Biol* **96**, 462-473.

Sadler, T W (1978) Distribution of surface coat material on fusing neural folds of mouse embryos during neurulation. *Anat Rec* **191**, 345-349.

Sadler, T W, Burridge, K and Yonker, J (1986) A potential role for spectrin during neurulation. *J Embryol Exp Morphol* **94**, 73-82.

Sadler, T W, Greenberg, D, Coughlin, P and Lessard, J L (1982) Actin distribution patterns in the mouse neural tube during neurulation. *Science* **215**, 172-174.

Sadler, T W and New, D A T (1981) Culture of mouse embryos during neurulation. *J Embryol Exp Morphol* **66**, 109-116.

Safaiyan, F, Kolset, S O, Prydz, K, Gottfridsson, E, Lindahl, U and Salmivirta, M (1999) Selective effects of sodium chlorate treatment on the sulfation of heparan sulfate. *J Biol Chem* **274**, 36267-36273.

Saiki, R K, Scharf, S, Faloona, F, Mullis, K B, Horn, G T, Erlich, H A and Arnheim, N (1985) Enzymatic amplification of β-globin genomic sequences and restriction site analysis for diagnosis of sickle cell anemia. *Science* **230**, 1350-1354.

Salmivirta, M and Jalkanen, M (1995) Syndecan family of cell surface proteoglycans: developmentally regulated receptors for extracellular effector molecules. *Experientia* **51**, 863-872.

Sambrook, J, Fritsch, E F, and Maniatis, T (1989) *Molecular cloning: A laboratory manual*. Cold Spring Harbor: Cold Spring Harbor Laboratory Press.

Saunders, S, Paine, S S and Lander, A D (1997) Expression of the cell surface proteoglycan glypican-5 is developmentally regulated in kidney, limb, and brain. *Dev Biol* **190**, 78-93.

Sausedo, R A, Smith, J L and Schoenwolf, G C (1997) Role of nonrandomly oriented cell division in shaping and bending of the neural plate. *J Comp Neurol* **381**, 473-488.

Schlessinger, J, Lax, I and Lemmon, M (1995) Regulation of growth factor activation by proteoglycans: what is the role of the low affinity receptors? *Cell* **83**, 357-360.

Schmidt, A, Skaletz-Rorowski, A and Buddecke, E (1995) Basic fibroblast growth factor controls the expression and molecular structure of heparan sulfate in corneal endothelial cells. *Eur J Biochem* **234**, 479-484.

Schoenwolf, G C (1984) Histological and ultrastructural studies of secondary neurulation of mouse embryos. *Am J Anat* **169**, 361-374.

Schoenwolf, G C (1985) Shaping and bending of the avian neuroepithelium: morphometric analyses. *Dev Biol* **109** , 127-139.

Schoenwolf, G C (1988) Microsurgical analyses of avian neurulation: separation of medial and lateral tissues. *J Comp Neurol* **276**, 498-507.

Schoenwolf, G C and Alvarez, I S (1989) Roles of neuroepithelial cell rearrangement and division in shaping of the avian neural plate. *Development* **106**, 427-439.

Schoenwolf, G C and Alvarez, I S (1991) Specification of neurepithelium and surface epithelium in avian transplantation chimeras. *Development* **112**, 713-722.

Schoenwolf, G C and Franks, M V (1984) Quantitative analyses of changes in cell shapes during bending of the avian neural plate. *Dev Biol* **105**, 257-272.

Schwartz, N B (1977) Regulation of chondroitin sulfate synthesis. Effect of β-xylosides on synthesis of chondroitin sulfate proteoglycan, chondroitin sulfate chains, and core protein. *J Biol Chem* **252**, 6316-6321.

Seller, M J and Perkins, K J (1982) Prevention of neural tube defects in curly-tail mice by maternal administration of vitamin A. *Prenat Diagn* **2**, 297-300.

Serbedzija, G N and McMahon, A P (1997) Analysis of neural crest cell migration in splotch mice using a neural crest-specific LacZ reporter. *Dev Biol* **185**, 139-147.

Shi, Z R, Itzkowitz, S H and Kim, Y S (1988) A comparison of three immunoperoxidase techniques for antigen detection in colorectal carcinoma tissues. *J Histochem Cytochem* **36**, 317-322.

Shin, M K, Levorse, J M, Ingram, R S and Tilghman, S M (1999) The temporal requirement for endothelin receptor-B signalling during neural crest development. *Nature* **402**, 496-501.

Shum, A S W and Copp, A J (1996) Regional differences in morphogenesis of the neuroepithelium suggest multiple mechanisms of spinal neurulation in the mouse. *Anat Embryol (Berl)* **194**, 65-73.

Smith, J L and Schoenwolf, G C (1987) Cell cycle and neuroepithelial cell shape during bending of the chick neural plate. *Anat Rec* **218**, 196-206.

Smith, J L and Schoenwolf, G C (1988) Role of cell-cycle in regulating neuroepithelial cell shape during bending of the chick neural plate. *Cell Tissue Res* **252**, 491-500.

Smith, J L and Schoenwolf, G C (1989) Notochordal induction of cell wedging in the chick neural plate and its role in neural tube formation. *J Exp Zool* **250**, 49-62.

Smith, J L and Schoenwolf, G C (1991) Further evidence of extrinsic forces in bending of the neural plate. *J Comp Neurol* **307**, 225-236.

Smith, J L and Schoenwolf, G C (1997) Neurulation: coming to closure. *Trends Neurosci* **20**, 510-517.

Smith, J L, Schoenwolf, G C and Quan, J (1994) Quantitative analyses of neuroepithelial cell shapes during bending of the mouse neural plate. *J Comp Neurol* **342**, 144-151.

Smith, P K, Krohn, R I, Hermanson, G T, Mallia, A K, Gartner, F H, Provenzano, M D, Fujimoto, E K, Goeke, N M, Olson, B J and Klenk, D C (1985) Measurement of protein using bicinchoninic acid. *Anal Biochem* **150**, 76-85.

Solursh, M and Morriss, G (1977) Glycosaminoglycan synthesis in rat embryos during the formation of the primary mesenchyme and neural folds. *Dev Biol* **57**, 75-86.

Sorrell, J M, Carrino, D A and Caplan, A I (1996) Regulated expression of chondroitin sulfates at sites of epithelial-mesenchymal interaction:

spatio-temporal patterning identified with anti-chondroitin sulfate monoclonal antibodies. *Int J Devl Neuroscience* **14**, 233-248.

Spivak, K T, Lemmon, M A, Dikic, I, Ladbury, J E, Pinchasi, D, Huang, J, Jaye, M, Crumley, G, Schlessinger, J and Lax, I (1994) Heparin-induced oligomerization of FGF molecules is responsible for FGF receptor dimerization, activation, and cell proliferation. *Cell* **79**, 1015-1024.

Stern, C D, Artinger, K B and Bronner-Fraser, M (1991) Tissue interactions affecting the migration and differentiation of neural crest cells in the chick embryo. *Development* **113**, 207-216.

Sternberg, J and Kimber, S J (1986) Distribution of fibronectin, laminin and entactin in the environment of migrating neural crest cells in early mouse embryos. *J Embryol Exp Morphol* **91**, 267-282.

Stickens, D, Brown, D and Evans, G A (2000) EXT genes are differentially expressed in bone and cartilage during mouse embryogenesis. *Dev Dyn* **218**, 452-464.

Stigson, M, Löfberg, J and Kjellén, L (1997) Reduced epidermal expression of a PG-M/versican-like proteoglycan in embryos of the white mutant axolotl. *Exp Cell Res* **236**, 57-65.

Stipp, C S, Litwack, E D and Lander, A D (1994) Cerebroglycan: an integral membrane heparan sulfate proteoglycan that is unique to the developing nervous system and expressed specifically during neuronal differentiation. *J Cell Biol* **124**, 149-160.

Storms, S D, Anvekar, V M, Adams, L D and Murray, B A (1996) Heterophilic NCAM-mediated cell adhesion to proteoglycans from chick embryonic brain membranes. *Exp Cell Res* **223**, 385-394.

Stringer, S E, Mayer-Proschel, M, Kalyani, A, Rao, M and Gallagher, J T (1999) Heparin is a unique marker of progenitors in the glial cell lineage. *J Biol Chem* **274**, 25455-25460.

Stumpo, D J, Bock, C B, Tuttle, J S and Blackshear, B J (1995) MARCKS deficiency in mice leads to abnormal brain development and perinatal death. *Proc Natl Acad Sci USA* **92**, 944-948.

Taniguchi, M, Yuasa, S, Fujisawa, H, Naruse, I, Saga, S, Mishina, M and Yagi, T (1997) Disruption of *semaphorin III/D* gene causes severe abnormality in peripheral nerve projection. *Neuron* **19**, 519-530.

Tassabehji, M, Newton, V E, Leverton, K, Turnbull, K, Seemanova, E, Kunze, J, Sperling, K, Strachan, T and Read, A P (1994) PAX3 gene structure and mutations: close analogies between Waardenburg syndrome and the Splotch mouse. *Hum Mol Genet* **3**, 1069-1074.

Tautz, D and Pfeiffle, C (1989) A nonradioactive *in situ* hybridization method for the localization of specific RNAs in *Drosophila* embryos reveals a translational control of the segmentation gene hunchback. *Chromosoma (Berl)* **98**, 81-85.

Tennyson, V M, Payette, R F, Rothman, T P and Gershon, M D (1990) Distribution of hyaluronic acid and chondroitin sulfate proteoglycans in the presumptive aganglionic terminal bowel of *ls/ls* fetal mice: an ultrastructural analysis. *J Comp Neurol* **291**, 345-362.

The, I, Bellaiche, Y and Perrimon, N (1999) Hedgehog movement is regulated through *tout velu*-dependent synthesis of a heparan sulfate proteoglycan. *Mol Cell* **4**, 633-639.

Thiery, J P, Duband, J L and Delouvée, A (1982a) Pathways and mechanism of avian trunk neural crest cell migration and localization. *Dev Biol* **93**, 324-343.

Thiery, J P, Duband, J L, Rutishauser, U and Edelman, G M (1982b) Cell adhesion molecules in early chicken embryogenesis. *Proc Natl Acad Sci USA* **79**, 6737-6741.

Thomas, G H (2001) Spectrin: the ghost in the machine. *BioEssays* **23**, 152-160.

Timár, J, Diczházi, C, Bartha, I, Pogány, G, Paku, S, Rásó, E, Tóvári, J, Ladányi, A, Lapis, K, Kopper, L and Jeney, A (1995) Modulation of heparan-sulphate/chondroitin-sulphate ratio by glycosaminoglycan biosynthesis inhibitors affects liver metastatic potential of tumor cells. *Int J Cancer* **62**, 755-761.

Toyoda, H, Kinoshita-Toyoda, A, Fox, B and Selleck, S B (2000b) Structural analysis of glycosaminoglycans in animals bearing mutations in *sugarless*, *sulfateless*, and *tout-velu*, *Drosophila* homologues of vertebrate genes encoding glycosaminoglycan biosynthetic enzymes. *J Biol Chem* **275**, 21856-21861.

Toyoda, H, Kinoshita-Toyoda, A and Selleck, S B (2000a) Structural analysis of glycosaminoglycans in *Drosophila* and *Caenorhabditis elegans* and demonstration that *tout-velu*, a *Drosophila* gene related to

EXT tumor suppressors, affects heparan sulfate *in vivo*. *J Biol Chem* **275**, 2269-2275.

Trasler, D G and Morriss-Kay, G (1991) Immunohistochemical localization of chondroitin and heparan sulfate proteoglycans in pre-spina bifida *splotch* mouse embryos. *Teratology* **44**, 571-579.

Tsuda, M, Kamimura, K, Nakato, H, Archer, M, Staatz, W, Fox, B, Humphrey, M, Olson, S, Futch, T, Kaluza, V, Siegfried, E, Stam, L and Selleck, S B (1999) The cell-surface proteoglycan Dally regulates Wingless signalling in *Drosophila*. *Nature* **400**, 276-280.

Tucker, R P, Hagios, C, Chiquet-Ehrismann, R, Lawler, J, Hall, R J and Erickson, C A (1999) Thrombospondin-1 and neural crest cell migration. *Dev Dyn* **214**, 312-322.

Tuckett, F and Morriss-Kay, G (1988) Alcian blue staining of glycosaminoglycans in embryonic material: effect of different fixatives. *Histochem J* **20**, 174-182.

Tuckett, F and Morriss-Kay, G M (1986) The distribution of fibronectin, laminin and entactin in the neurulating rat embryo studied by indirect immunofluorescence. *J Embryol Exp Morphol* **94**, 95-112.

Tuckett, F and Morriss-Kay, G M (1989a) Heparitinase treatment of rat embryos during cranial neurulation. *Anat Embryol* **180**, 393-400.

Turnbull, J, Powell, A and Guimond, S (2001) Heparan sulfate: decoding a dynamic multifunctional cell regulator. *Trends Cell Biol* **11**, 75-82.

Turnbull, J E, Fernig, D G, Ke, Y, Wilkinson, M C and Gallagher, J T (1992) Identification of the basic fibroblast growth factor binding sequence in fibroblast heparan sulfate. *J Biol Chem* **267**, 10337-10341.

Turnbull, J E, Hopwood, J J and Gallagher, J T (1999) A strategy for rapid sequencing of heparan sulfate and heparin saccharides. *Proc Natl Acad Sci USA* **96**, 2698-2703.

van Allen, M I, Kalousek, D K, Chernoff, G F, Juriloff, D, Harris, M, McGillivray, B C, Yong, S L, Langlois, S, MacLeod, P M, Chitayat, D, Friedman, J M, Wilson, R D, McFadden, D, Pantzar, J, Ritchie, S and Hall, J G (1993) Evidence for multi-site closure of the neural tube in humans. *Am J Med Genet* **47**, 723-743.

van Kuppevelt, T H, Dennissen, M A B A, van Venrooij, W J, Hoet, R M A and Veerkamp, J H (1998) Generation and application of type-specific anti-heparan sulfate antibodies using phage display technology. Further evidence for heparan sulfate heterogeneity in the kidney. *J Biol Chem* **273**, 12960-12966.

van Straaten, H W M, Hekking, J W M, Consten, C and Copp, A J (1993) Intrinsic and extrinsic factors in the mechanism of neurulation: effect of curvature of the body axis on closure of the posterior neuropore. *Development* **117**, 1163-1172.

van Straaten, H W M, Peeters, M C E, Hekking, J W M and van der Lende, T (2000) Neurulation in the pig embryo. *Anat Embryol* **202**, 75-84.

Varki, A, Cummings, R, Esko, J, Freeze, H, Hart, G, and Marth, J (1999) *Essentials of Glycobiology.* New York: Cold Spring Harbor Laboratory Press.

Vivès, R R, Goodger, S and Pye, D A (2001) Combined strong anion-exchange HPLC and PAGE approach for the purification of heparan sulphate oligosaccharides. *Biochem J* **354**, 141-147.

Vivès, R R, Pye, D A, Salmivirta, M, Hopwood, J J, Lindahl, U and Gallagher, J T (1999) Sequence analysis of heparan sulphate and heparin oligosaccharides. *Biochem J* **339**, 767-773.

Volk, R, Schwartz, J J, Li, J, Rosenberg, R D and Simons, M (1999) The role of syndecan cytoplasmic domain in basic fibroblast growth factor-dependent signal transduction. *J Biol Chem* **274**, 24417-24424.

Wang, H U and Anderson, D J (1997) Eph family transmembrane ligands can mediate repulsive guidance of trunk neural crest migration and motor axon outgrowth. *Neuron* **18**, 383-396.

Wang, H U, Chen, Z-F and Anderson, D J (1998) Molecular distinction and angiogenic interaction between embryonic arteries and veins revealed by ephrin-B2 and its receptor Eph-B4. *Cell* **93**, 741-753.

Watanabe, H, Kimata, K, Line, S, Strong, D, Gao, L, Kozak, C A and Yamada, Y (1994) Mouse cartilage matrix deficiency (cmd) caused by a 7 bp deletion in the aggrecan gene. *Nat Genet* **7**, 154-157.

Watanabe, H, Nakata, K, Kimata, K, Nakanishi, I and Yamada, Y (1997) Dwarfism and age-associated spinal degeneration of heterozygote cmd mice defective in aggrecan. *Proc Natl Acad Sci USA* **94**, 6943-6947.

Watanabe, K, Yamada, H and Yamaguchi, Y (1995) K-glypican: a novel GPI-anchored heparan sulfate proteoglycan that is highly expressed in developing brain and kidney. *J Cell Biol* **130**, 1207-1218.

Waterman, R E (1976) Topographical changes along the neural fold associated with neurulation in the hamster and mouse. *Am J Anat* **146**, 151-171.

Wei, G, Bai, X, Gabb, M M G, Bame, K J, Koshy, T I, Spear, P G and Esko, J D (2000) Location of the glucuronosyltransferase domain in the heparan sulfate copolymerase EXT1 by analysis of Chinese hamster ovary cell mutants. *J Biol Chem* **275**, 27733-27740.

Wicklund, C L, Pauli, R M, Johnston, D and Hecht, J T (1995) Natural history study of hereditary multiple exoxtoses. *Am J Med Genet* **55**, 43-46.

Williams, B L and Wilson, K (1981) *A biologist's guide to principles and techniques of practical Biochemistry (2nd ed).* London: Edward Arnold.

Wilson, D B and Finta, L A (1979) Gap junctional vesicles in the neural tube of the *splotch* (*Sp*) mutant mouse. *Teratology* **19**, 337-340.

Wilson, D B and Wyatt, D P (1986) Pathogenesis of neural dysraphism in the mouse mutant vacuolated lens (vl). *J Neuropathol Exp Neurol* **45**, 43-55.

Wilson, D B and Wyatt, D P (1988) Closure of the posterior neuropore in the vl mutant mouse. *Anat Embryol (Berl)* **178**, 559-563.

Wilson, D B and Wyatt, D P (1992) Aberrant convergence of the neural folds in the mouse mutant *vl*. *Teratology* **45**, 105-112.

Wright, D E, White, F A, Gerfen, R W, Silos-Santiago, I and Snider, W D (1995) The guidance molecule semaphorin III is expressed in regions of spinal cord and periphery avoided by growing sensory axons. *J Comp Neurol* **361**, 321-333.

Wu, M, Chen, D F, Sasaoka, T and Tonegawa, S (1996) Neural tube defects and abnormal brain development in F52-deficient mice. *Proc Natl Acad Sci USA* **93**, 2110-2115.

Xu, X, Li, C, Takahashi, K, Slavkin, H C, Shum, L and Deng, C-X (1999) Murine fibroblast growth factor receptor 1α isoforms mediate node regression and are essential for posterior mesoderm development. *Dev Biol* **208**, 293-306.

Yamagata, M, Suzuki, S, Akiyama, S K, Yamada, K M and Kimata, K (1989) Regulation of cell-substrate adhesion by proteoglycans immobilized on extracellular substrates. *J Biol Chem* **264**, 8012-8018.

Yamagata, T, Saito, H, Habuchi, O and Suzuki, S (1968) Purification and properties of bacterial chondroitinases and chondrosulfatases. *J Biol Chem* **243**, 1523-1535.

Yamaguchi, T P, Harpal, K, Henkemeyer, M and Rossant, J (1994) *fgfr-1* is required for embryonic growth and mesodermal patterning during mouse gastrulation. *Genes Dev* **8**, 3032-3044.

Yanagishita, M and Hascall, V C (1992) Cell surface heparan sulfate proteoglycans. *J Biol Chem* **267**, 9451-9454.

Yang, J T, Rayburn, H and Hynes, R O (1995) Cell adhesion events mediated by $\alpha_4$ integrins are essential in placental and cardiac development. *Development* **121**, 549-560.

Yang, X M and Trasler, D G (1988) An ultrastructural study of spinal bifida in the delayed splotch mutant mouse. *Teratology* **37**, 503.

Ybot-Gonzalez, P and Copp, A J (1999) Bending of the neural plate during mouse spinal neurulation is independent of actin microfilaments. *Dev Dyn* **215**, 273-283.

Zhang, L, David, G and Esko, J D (1995) Repetitive Ser-Gly sequences enhance heparan sulfate assembly in proteoglycans. *J Biol Chem* **270**, 27127-27135.

Zhang, L and Esko, J D (1994) Amino acid sequences that drive heparan sulfate assembly in a proteoglycan. *J Biol Chem* **269**, 19295-19299.